Jan-Feb.
1961

SCIENCE

Volume 65D

Number 1

Jan.–Feb. 1961

V.65D.
No.1
Radio-
Propagation

JAN 23 1961

RECEIVED
JAN 25 1961
MIAMI UNIVERSITY
LIBRARY

Radio Propagation

SECTION D

JOURNAL OF RESEARCH

NATIONAL BUREAU OF STANDARDS

MIAMI UNIVERSITY LIBRARY

Journal of Research

of the

National Bureau of Standards

D. RADIO PROPAGATION

JAN.–FEB. • 1961

VOLUME • 65D

NUMBER • 1

Editor: James R. Wait
Central Radio Propagation Laboratory, National Bureau of Standards, Boulder, Colo.

Associate Editors: T. N. Gautier, J. W. Herbstreit, R. C. Kirby, C. G. Little, A. G. McNish, R. A. Helliwell, W. E. Gordon, A. D. Wheelon, S. Silver

IRE Advisors: A. H. Waynick, K. M. Siegel

Publication dates:
Jan. 15, Mar. 15, May 15, July 15, Sept. 15, Nov. 15, 1961

JOURNAL OF RESEARCH

The National Bureau of Standards Journal of Research reports research and development in the fields of activity shown at right. Also included from time to time are survey articles related to the Bureau's scientific and technical program.

The Journal is published in four separate sections as follows:

A. Physics and Chemistry

Contains papers of interest primarily to scientists working in these fields. Issued six times a year. Annual subscription: domestic, $4.00; foreign, $4.75.

B. Mathematics and Mathematical Physics

Presents studies and compilations designed mainly for the mathematician and the theoretical physicist. Issued quarterly. Annual subscription: domestic, $2.25; foreign, $2.75.

C. Engineering and Instrumentation

Reports research and development results of interest chiefly to the engineer and the applied scientist. Issued quarterly. Annual subscription: domestic, $2.25; foreign, $2.75.

D. Radio Propagation

Reports research in radio propagation, upper atmospheric physics, and communications. Issued six times a year. Annual subscription: domestic, $4.00; foreign, $4.75.

Functions and Activities

The functions of the National Bureau of Standards are set forth in the Act of Congress, March 3, 1901, as amended. These include the development and maintenance of the national standards of measurement and the provision of means and methods for making measurements consistent with these standards; the determination of physical constants and properties of materials; the development of methods and instruments for testing materials, devices, and structures; advisory services to government agencies on scientific and technical problems; invention and development of devices to serve special needs of the Government; and the development of standard practices, codes, and specifications. The work includes basic and applied research, development, engineering, instrumentation, testing, evaluation, calibration services, and various consultation and information services. The Bureau also serves as the Federal technical research center in a number of specialized fields. The scope of activities of the National Bureau of Standards is suggested in the following listing of the divisions and sections engaged in technical work.

Washington, D.C.

Electricity. Resistance and Reactance. Electrochemistry. Electrical Instruments. Magnetic Measurements. Dielectrics.

Metrology. Photometry and Colorimetry. Refractometry. Photographic Research. Length. Engineering Metrology. Mass and Scale. Volumetry and Densimetry.

Heat. Temperature Physics. Heat Measurements. Cryogenic Physics. Rheology. Molecular Kinetics. Free Radicals Research. Equation of State. Statistical Physics. Molecular Spectroscopy.

Radiation Physics. X-Ray. Radioactivity. Radiation Theory. High Energy Radiation. Radiological Equipment. Nucleonic Instrumentation. Neutron Physics.

Chemistry. Surface Chemistry. Organic Chemistry. Analytical Chemistry. Inorganic Chemistry. Electrodeposition. Molecular Structure and Properties of Gases. Physical Chemistry. Thermochemistry. Spectrochemistry. Pure Substances.

Mechanics. Sound. Pressure and Vacuum. Fluid Mechanics. Engineering Mechanics. Combustion Controls.

Organic and Fibrous Materials. Rubber. Textiles. Paper. Leather. Testing and Specifications. Polymer Structure. Plastics. Dental Research.

Metallurgy. Thermal Metallurgy. Chemical Metallurgy. Mechanical Metallurgy. Corrosion. Metal Physics.

Mineral Products. Engineering Ceramics. Glass. Refractories. Enameled Metals. Constitution and Microstructure.

Building Research. Structural Engineering. Fire Research. Mechanical Systems. Organic Building Materials. Codes and Safety Standards. Heat Transfer. Inorganic Building Materials.

Applied Mathematics. Numerical Analysis. Computation. Statistical Engineering. Mathematical Physics.

Data Processing Systems. Components and Techniques. Digital Circuitry. Digital Systems. Analog Systems. Applications Engineering.

Atomic Physics. Spectroscopy. Radiometry. Mass Spectrometry. Solid State Physics. Electron Physics. Atomic Physics.

Instrumentation. Engineering Electronics. Electron Devices. Electronic Instrumentation. Mechanical Instruments. Basic Instrumentation.

Office of Weights and Measures

Boulder, Colo.

Cryogenic Engineering. Cryogenic Equipment. Cryogenic Processes. Properties of Materials. Gas Liquefaction.

Ionosphere Research and Propagation. Low Frequency and Very Low Frequency Research. Ionosphere Research. Prediction Services. Sun-Earth Relationships. Field Engineering. Radio Warning Services.

Radio Propagation Engineering. Data Reduction Instrumentation. Radio Noise. Tropospheric Measurements. Tropospheric Analysis. Propagation-Terrain Effects. Radio-Meteorology. Lower Atmosphere Physics.

Radio Standards. High Frequency Electrical Standards. Radio Broadcast Service. Radio and Microwave Materials. Atomic Frequency and Time Standards. Electronic Calibration Center. Millimeter-Wave Research. Microwave Circuit Standards.

Radio Systems. High Frequency and Very High Frequency Research. Modulation Research. Antenna Research. Navigation Systems. Space Telecommunications.

Upper Atmosphere and Space Physics. Upper Atmosphere and Plasma Physics. Ionosphere and Exosphere Scatter. Airglow and Aurora. Ionospheric Radio Astronomy.

U.S. DEPARTMENT OF COMMERCE
Frederick H. Mueller, Secretary

NATIONAL BUREAU OF STANDARDS
A. V. Astin, Director

Order all publications from the Superintendent of Documents, U.S. Government Printing Office, Washington 25, D.C.

Use of funds for printing this publication approved by the Director of the Bureau of the Budget (June 24, 1958).

INDEX

Editorial Notice

Beginning with the January 1961 issues of the NBS Journal of Research, the covers of Journal sections have been redesigned so as to emphasize the subject content of each of the four sections. Thus the name of this section becomes RADIO PROPAGATION, Section D of the JOURNAL OF RESEARCH, National Bureau of Standards. However, it is recommended that the present method of citing the Journal remain the same except for the addition of the section title so that better continuity can be maintained with the referencing of prior issues; see example below.

For the future the Bureau has adopted the following system as the preferred method of referencing. References are to be indicated in the text by the insertion in brackets of the author's name and the year of publication, thus: [Trelease, 1951]. If the author's name is part of the text, only the year is bracketed, thus: ". . . in a paper by Trelease [1951]." If there are two or more references citing different papers published in the same year by the same author, distinguish them by the letters a, b, c, after the year. If two or more references are given in the same brackets they should be given chronologically, thus: [Bean, 1953a and c; Harrison and King, 1955b]. At the end of the paper, list all references alphabetically by the authors' names. Include in each entry the following: name of senior author, followed by his initials; names of junior authors, each preceded by his initials, title of paper (or book); title of publication or journal; volume number (and section title); issue number; inclusive page numbers; month and year of publication, thus:

Bean, B. R., and B. A. Cahoon, The use of surface weather observations to predict the total atmospheric bending of radio waves at small elevation angles, Proc. IRE **45,** No. 11, 1545–1546 (Nov. 1957).

Brite, C. O., C. W. Tolbert, and A. W. Straiton, Radio wave absorption of several gases in the 100 to 118 kMc/s frequency range, J. Research NBS **65D,** (Radio Prop.), No. 1, 17–22 (Jan. 1961).

Slater, J. C., Microwave transmission, first ed., p. 24 (McGraw-Hill Book Co., Inc., New York, N.Y., 1942).

The provision of this complete information should be helpful to the reader in the following ways: the complete title provides a brief indication of the expected content of the reference; the beginning and ending pages indicate the length of the reference; and the volume number, issue number, month and year will assist the reader in locating the reference in libraries even in those cases where the cited reference contains a typographical or other errors.

The above described preferred method of referencing has been adopted primarily to aid the reader by providing directly in the text information relative to the author and year of the reference. This method also is most convenient for the author in preparing his original manuscript since it provides a simple and unambiguous means of relating the references in the text to the bibliography at the end, and also facilitates the introduction of additional references in later drafts.

In the case of papers in which all references are referred to only once and which also do not require a bibliography at the end, the literature references may be given as footnotes on the same page.

Footnote references are to be designated by superscript numbers. In the case of short papers involving only a single literature reference, and in such cases as those described above, the literature references may be given as footnotes.

KENNETH A. NORTON, *Guest Editor.*

November 18, 1960.

Additional Comments on

IMPEDANCE MEASUREMENTS AND STANDARDS*

G. A. Deschamps

Investigations of magnified and squared SWR responses and the use of auxiliary tuners with directional couplers both led to a modified reflectometer technique permitting accuracies of better than 0.1 percent in SWR measurements [Beatty, 1958].

The use of auxiliary tuners with a directional coupler also permits the construction of a highly accurate phase shifter. Combination of this with the above modified reflectometer yields an impedance meter similar to a bridge and both magnitude and phase of the reflection coefficient may be independently determined to high accuracy [Engen, 1959].

Possible errors in the use of a sliding short-circuit as a phase shift standard have been discussed and a method for avoiding them described. Accuracies of 0.3 degree have been obtained [Magid, 1958].

Techniques for the measurement of the equivalent network parameters of discontinuities coupling two or more modes in multimode waveguides have been described [Felsen et al., 1959; Lewis, 1959].

Measurement of standing waves in a specially constructed line was used to evaluate high dielectric constants at UHF [Williams and Foster, 1957].

Rapid measurement of impedance or transmission properties over a wide range of frequencies continues to be of great interest. A system for measuring phase and attenuation through a component [Linker and Grimm, 1958] from 8.7 to 9.6 kMc/s and an automatic impedance plotter [Watts and Alford, 1957] covering the frequency ranges 180 to 900 Mc/s and 50 to 250 Mc/s were developed.

Automatic continuous measurement of phase at microwave can be done by shifting the frequency to audiofrequency [Mittra, 1957]. A broadband direct reading measuring device has been constructed where the LO tracts the RF in order to produce a fixed intermediary frequency [Dropkin, 1958].

*This material belongs after the fourth paragraph of the published report (p. 598, J. Research NBS, **64D**, 6,) and must be used with the references on that page.

JOURNAL OF RESEARCH of the National Bureau of Standards—D. Radio Propagation
Vol. 65D, No. 1, January-February 1961

Incoherent Scattering by Free Electrons as a Technique For Studying the Ionosphere and Exosphere: Some Observations and Theoretical Considerations[1]

Kenneth L. Bowles

(September 1, 1960)

Incoherent scattering by the free electrons of the ionosphere has been suggested as a technique for measuring the electron density profile both below and above the F region maximum. This paper reports observations which confirm the existence of the incoherent scatter and show that its intensity is essentially the predicted value. The observed Doppler broadening is considerably smaller than originally predicted. In the second part of the paper, an explanation for the reduced Doppler broadening is offered. The scatter is explained as arising from statistical fluctuations of electron density, the distribution of which is controlled by the positive ions.

Introduction

The ability of a random distribution of free electrons to exhibit weak scattering of radio waves has been cited by Gordon [1] as a possible means of measuring electron densities and temperatures continuously to heights of several thousand kilometers above the earth's surface. Gordon's prediction is based upon the assumption that the free electrons may be considered to scatter mutually independently. His development is essentially a combination of the Thompson scattering property of the free electron with Lord Rayleigh's theory of the scattering of light by the particles of a gas [2].

Use of such incoherent scatter to study the ionized regions of the outer atmosphere should have the great virtues of theoretical simplicity, and the ability to observe a complete vertical cross section of electron density and other parameters continuously for long periods of time with ground-based equipment. With these considerations as motivation, and having available a large high-power pulse transmitter, the National Bureau of Standards undertook experiments to test the existence of the predicted scatter and to verify its utility. Results of the first preliminary observation were reported by the writer in a short communication [3]. Since then, more sensitive observations have been made that are described in this paper, along with a theoretical interpretation. Much the same material was originally circulated among a limited number of workers in this field as an unpublished report of the National Bureau of Standards [16].

Part I of the paper is devoted to the experimental observations. The characteristics and special features of the equipment are outlined. Observations in which the incoherent scatter may be identified are illustrated using original oscillograph records. The incoherent scattered power is found to be within a factor of two of the value predicted using Gordon's approach. Representative electron density-versus-height profiles are given for two of the oscillograms, and shown to agree reasonably well with profiles for the lower part of the F region obtained from conventional ionograms. The possibility that any one of several other well-known propagation modes might have resulted in ambiguous observations is examined and rejected.

In spite of the apparent verification of Gordon's prediction for echo *power*, a distinct departure is found in terms of the observed echo *spectrum*. The spectral broadening of the scattered echoes is found to be considerably less than the Doppler broadening predicted using Gordon's approach. While a spectral width of approximately 100 kc/s might have been expected for F region echoes, the observation is that the transmitted bandwidth of about 9 kc/s must be broadened only slightly by the scatter process.

In *Part II* we propose that the scatter should be regarded as arising from random fluctuations of *electron density*, rather than from electrons scattering individually. In this way we develop a simple explanation for the slight echo broadening, based upon Coulomb interactions between ions and electrons.

In the past the density fluctuation approach has been used successfully to predict the intensity of scatter from aggregates of gas particles even in cases where the distributions of particle density were not entirely random. However, little attention appears to have been paid to the question of spectral broaden-

[1] Contribution from Central Radio Propagation Laboratory, National Bureau of Standards, Boulder, Colo.

ing using density fluctuations. It is generally assumed that when plasma oscillations can be neglected, as in the case of high frequency "reflections" from the ionosphere, the spectrum of scatter from aggregates of free particles must be directly proportional to the distribution of line-of-sight velocities of the several particles. We offer a simple illustration to show that this proportionality may not necessarily hold true when there is a degree of mutual correlation among the positions of the particles. We argue that such correlation is automatically introduced if there are many particles within a zone whose depth corresponds to approximately 180 degrees of phase or less. This zone defines a preferred "scale" among the density fluctuations, and the rate at which irregularities of this scale change from one state of fluctuation to another provides a means of estimating the spectral breadth of the scatter.

Obviously the picture of density fluctuations breaks down when the individual scattering particles are so sparsely distributed that only one can be found in a volume large relative to the characteristic scale. Such a case is found with radar "chaff," where there is every indication that the chaff particles contribute to the scatter independently. Evidently some criterion must be established to determine when it is better to consider the scatter as arising from density fluctuations, and when from independent particles. Two possible "independence criteria" are examined—one based on mean spacing between neighboring particles, the other based on mean-free-path as proposed by Gordon. The present experiment offers an opportunity to distinguish between these criteria.

It is shown that, apart from a proportionality factor close to unity, the spectral width of radiation scattered from a randomly distributed gas is the same, using either density fluctuations or independent particles. From the experimental results, we draw the conclusion that the distribution of free electrons in the ionosphere is not entirely random (even within a volume small enough that the mean density gradient can be regarded as negligible).

We examine the effect of Coulomb interactions between ions and electrons on the fluctuations of electron density. For scales of irregularities large compared with the Debye shielding distance, λ_D, we find that the fluctuations of ion density and those of the electrons are strongly correlated. The *magnitude* of the fluctuations is close to that of a neutral gas whose density is equal to the electron density. Because the ions have so much more momentum, the *rate of change* from one state of fluctuation to another is controlled almost exclusively by the ions. We therefore estimate, for example, that a spectral broadening of the order of 500 c/s would be correct for echoes from the *F* region at our 41-Mc/s operating frequency. Since the results of recent experiments indicate that this estimate is correct, we infer that the density fluctuation approach is correct in the *F* region. This suggests that the correct independence criterion may be based upon the mean spacing between neighboring particles.

The predicted effects of the earth's magnetic field on the observations are discussed briefly. It is pointed out that these effects may permit one to identify the ionic constituents and to measure the magnetic field strength in the earth's outer atmosphere.

Part I. Experimental Observations

1. Equipment

Except for the dimensions involved, the equipment is in most respects a conventional radar directed vertically. Operating parameters are summarized in table 1.

TABLE 1. *Parameters of radar equipment used*

Operating frequency	40.92 Mc/s
Peak pulse power	(4 to 6)$\times 10^6$ w or 1×10^6 w (see text)
Pulse duration	3 to 150×10^{-6} sec available 120×10^{-6} sec for all data shown in this paper
Average power	4×10^4 w maximum
Pulse repetition frequency	Flexible within above limitations. 25 to 40 p.p.s. used for most work shown in this paper (see text)
Receiver noise (power) bandwidth	9, 13, or 35 kc/s
Receiver noise factor	2
Signal/noise improvement by averaging	Up to approximate factor 100 (20 db) (see text)
Antenna cross section	116 by 140 m (1.6×10^4m^2)
Antenna polarization	Linear north-south
Antenna gain, efficiency, etc.	See text
Location	NBS Long Branch, Illinois transmitting station—WWI Latitude 40.2° N. Longitude 90.0° W.

The transmitter is a newly built unit of a hitherto untried design. Not all malfunctions in its operation had been removed at the time the experiments here reported were carried out. Absolute measurements of the incoherent scatter intensity made during February 1959 (described in detail later in the paper) make it clear that the transmitter was generating roughly 1-Mw peak power at the operating frequency, rather than 4 to 6 Mw, during the work reported in reference 3. The difficulties responsible for this malfunctioning have been corrected, but a new problem appeared before the February tests. Due to damage from a severe frost, the transmitter could only be operated using its driver amplifier with an output power of 1.0 Mw. This power was carefully calibrated using a probe technique for comparison with the known output of a lower power amplifier. Approximately 1 db of attenuation was experienced in the temporary connection of the driver amplifier to the antenna, and this is reported below as part of the total loss of antenna efficiency.

The receiver is a communications unit of conventional design, modified to permit pulse operation.

A preamplifier and converter provide low noise features not available in the commercial receiver. Bandwidths suitable for pulse work were obtained by loading the IF transformers. The switching arrangement of the receiver then permitted the 9-kc/s band to have the characteristic of 6 cascaded L-C circuits. The 35-kc/s band had a flat top, with skirts roughly the same as those of the 9-kc/s band. The bandwidths quoted were measured by comparing and equating the output of the receiver for calibrated inputs from a noise diode source, then from a cw standard signal generator, taking the noise statistics and detector operation into account. The bandwidths, between frequencies at which the response is down 6 db from the maximum, differ only slightly from the noise bandwidths.

Averaging of the receiver output was used to improve the quality of the scatter measurements. The averaging device, or "integrator," is built around a multiple-deck mercury-jet commutator. Each of 240 independent capacitors is connected to the receiver output through a large resistor only during an assigned time interval following the transmitter pulse. Thus the voltage appearing across each capacitor represents the RC running average of receiver output corresponding to a specific range interval—usually 15 to 25 km wide. The vertical d-c amplifier of an oscilloscope having high input impedance is also connected to the capacitors in sequence. The presentation on the oscilloscope is therefore a histogram representing the running average of many conventional A-'scope sweeps. The limitations of the device are such that a maximum improvement in effective signal-to-noise ratio of about 20 db (a factor of 100) can be obtained. Several different time constants were used in taking the photographs presented in this report, in each case the signal-to-noise ratio improvement being somewhat less than 20 db.

The antenna is a simple broadside array of 1,024 half-wave dipoles located 0.16 wavelength above ground. The dipoles are situated in approximately a square array and fed in phase through open wire transmission lines. By attaching the half-wave elements to the transmission line at one wavelength intervals, transposition of the lines is avoided. A total of 32 elements are connected effectively in parallel and fed at the center of each such arrangement. Those elements located at alternate half wavelength intervals are fed by the adjacent transmission line. There are a total of 32 such transmission lines spaced at half wavelength intervals. The neighboring combinations are then connected by pairing successively through equal length feeders until the whole array is connected to one pair of terminals. The reflection coefficient of the ground has been increased and stabilized by placing copper wires on the ground, parallel to the dipoles. The T-R and A-T-R switches are built in open wire line, using open tungsten spark gaps in the conventional configuration.

By a fortunate coincidence, a very suitable celestial radio source is available as a check on antenna performance. The station is located at latitude 40.2° while the radio source known as Cygnus-A is at 40.5° [4]. For practical purposes Cygnus-A can therefore be considered as passing through the center of the main beam of the antenna. A number of total power records of the Cygnus source as it transits the beam were taken as a means of measuring the east-west antenna pattern and calibrating the gain. One such record is shown in figure 1.

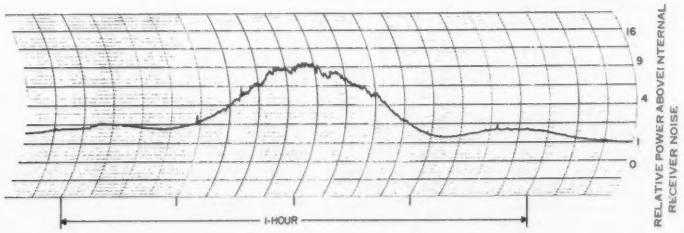

FIGURE 1. *Example of the kind of total-power record obtained using the large dipole-array during transit of the radio source Cygnus-A.*

Although scintillations were often quite severe, several passes were obtained when scintillations were less than 10 percent of the total power received. Hence, a good estimate of the maximum power could be made. As may be seen from figure 1, the antenna exhibits the behavior expected in the main lobe and lowest order side lobes for a uniformly illuminated aperture. The measured beam width between half-power points is 3.1°, and between first nulls is 7.2°, agreeing with the values expected for an aperture 16 wavelengths wide [5]. It may be noted that there appears to be little or no broadening of the trace of Cygnus due to the broad angular component known as Cygnus-X. Using the best available measurements of the flux of power from Cygnus-A, those of H. W. Wells [6], it is estimated that 1.75×10^{-18} w per c/s should be available at the antenna terminals at the peak of the Cygnus trace, assuming perfect efficiency on one polarization. It was found that an equivalent noise diode current of 110 ma through 50 ohms gives a comparable deflection. Since this current generates an input power of approximately 4.4×10^{-19} w per c/s, the antenna is estimated to be 25 percent efficient or to have a degradation in gain of about 6 db. The accuracy of the measurements is certainly not better than 1 db. The loss in efficiency may be explained by the following three factors: 1 db. is lost in coaxial lines and matching networks connecting the T–R system to the receiver input terminal (or transmitter output terminal). Perhaps half of the remainder is represented by resistance losses in the poorly screened ground, and in the transmission lines, matching networks, etc. The remaining efficiency is presumably lost through spurious radiation from portions of the open-wire transmission lines on which matching was not attempted, portions of wires and guys only partially removed from the circuit by quarter-wavelength shorted stubs, etc. This radiation must appear as energy in sidelobes randomly distributed over the hemisphere illuminated by the antenna.

2. Scatter Observations Identified

The kind of observations obtainable using the conventional "A'scope" display is illustrated in figure 2. Cosmic noise is represented by the constant "grass" level, peaking at about one-third of the vertical scale. The apparent rise in the grass level, peaking broadly at about 350 km, is due to the incoherent scatter echo. The sharp peak at about 80 km appears to arise from the same kind of scatter responsible for at least part of oblique path VHF scatter propagation [7]. Further observations of this D region scatter have been made and it is hoped will be discussed in a separate paper.

The kind of record obtainable using an A'scope presentation of the "integrator" output is illustrated in figure 3, a direct photograph of the oscilloscope-screen. The cosmic noise level in this case is just under the first horizontal line above the lower border of the photograph. In this record, and others on the same presentation shown below, the broad features of the electron-density profile of the F region of the ionosphere may be clearly seen. Note that while the E region electron density must be close to one-tenth the F region maximum, the echo intensity varies only slightly between the heights of 100 and 350 km. This results from the decay of system power sensitivity with the inverse square of the height.

Before positively identifying the observed echoes as incoherent scatter, one must reject the possibility that they might arise from sidelobe response to some other known mode of propagation. Overlapping meteor echoes observed via the sidelobes are an obvious possibility. Figure 4 illustrates the appearance of a typical meteor echo. The sharp spike in the midst of the broader but weaker rise in the grass level is a meteor echo which lasted a fraction of a second compared with the 4-sec exposure time. Figure 5 shows the integrator presentation for a time close to 0600 hours local time. As would be expected for the F region, the main features of the broad trace are considerably reduced in amplitude compared with the midday record of figure 3. Between 100- and 200-km range, however, there appears to be stronger echo intensity with a much rougher distribution, due to the greatly increased meteor activity typical of times near 0600. Adjacent integrator intervals show intensities which vary randomly in an uncorrelated fashion. Rejection of meteor echoes as a serious contributing factor therefore seems justified, if allowance is made for their occasional appearance on the records, particularly at ranges less than 700 km.

Long-range F layer-propagated ground-backscatter occasionally produces strong interfering echoes in the system. Examples of such echoes are shown in figures 6a and 6b, where slightly more than one complete radar cycle is displayed. A second transmitted pulse occurs in 6a and 6b at about 5,000-km indicated range. Figure 6a is a record obtained in the customary manner using the large broadside antenna both for transmitting and receiving. Figure 6b was obtained by substituting, for reception, a simple half-wave dipole antenna located one-half wavelength above ground. Since the illumination of the scattering medium was the same for both examples, it is clear that the response of the large antenna at low radiation angles approximates the response of the dipole within a few decibels. Figures 6c and 6d were taken using expanded range and intensity scales for making the same comparison. Figure 6c, taken with the large antenna used for both transmitting and receiving, shows the usual F region profile. Figure 6d, taken with the large antenna used for transmitting, and the dipole for receiving, shows no sign of the F region profile. By utilizing this comparison, and by taking continual care to adjust the spacing between successive transmitter pulses, it has been possible to detect and eliminate any contribution to the interesting part of the records due to long-range backscatter. A similar comparison of the dipole with the large antenna has permitted the rejection of the possibility of important echo contributions due to magnetic field alined irregularities, such as from the aurora.

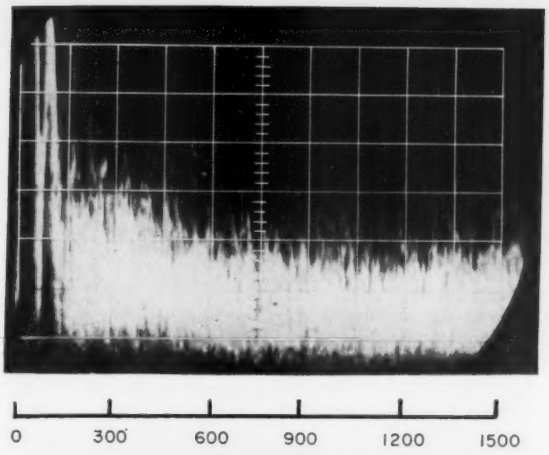

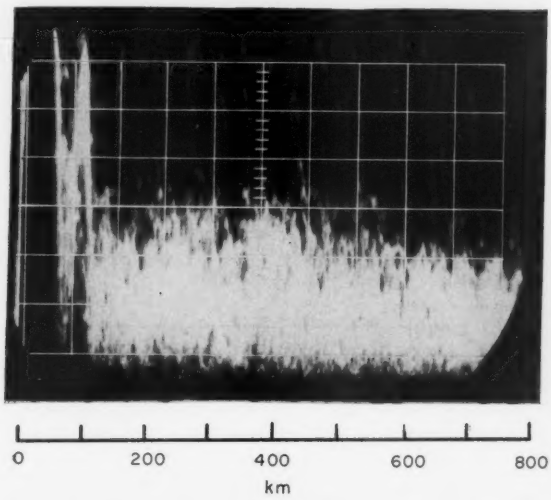

FIGURE 2. *A'scope photographs obtained using 4-sec exposure.*
Near midday, October 22, 1958.

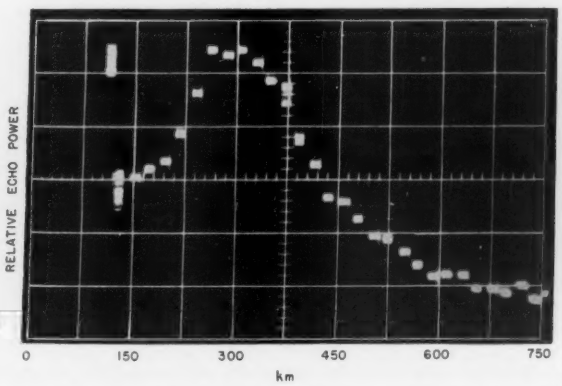

FIGURE 3. *A'scope photograph using the "integrator" display.*
1135 l.t., February 27, 1959.

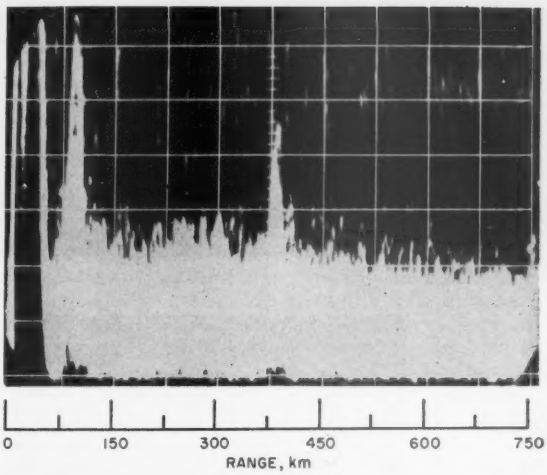

FIGURE 4. *A'scope photograph showing transient trace due to a meteor echo, in addition to incoherent scatter.*

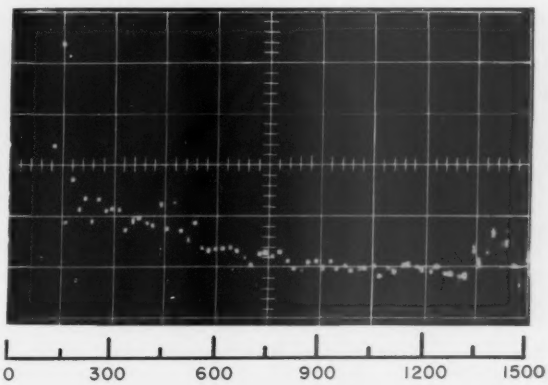

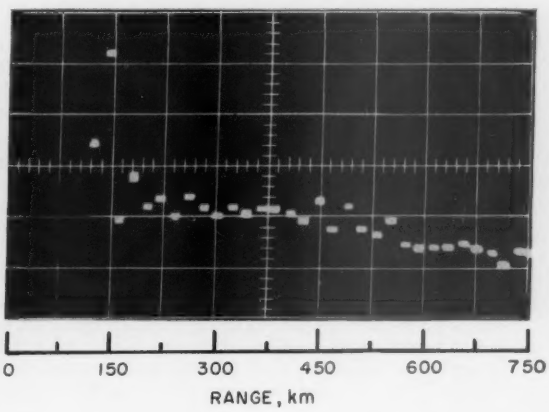

FIGURE 5. *Integrator A'scope photographs taken at about 0600 l.t., February 28, 1959.*

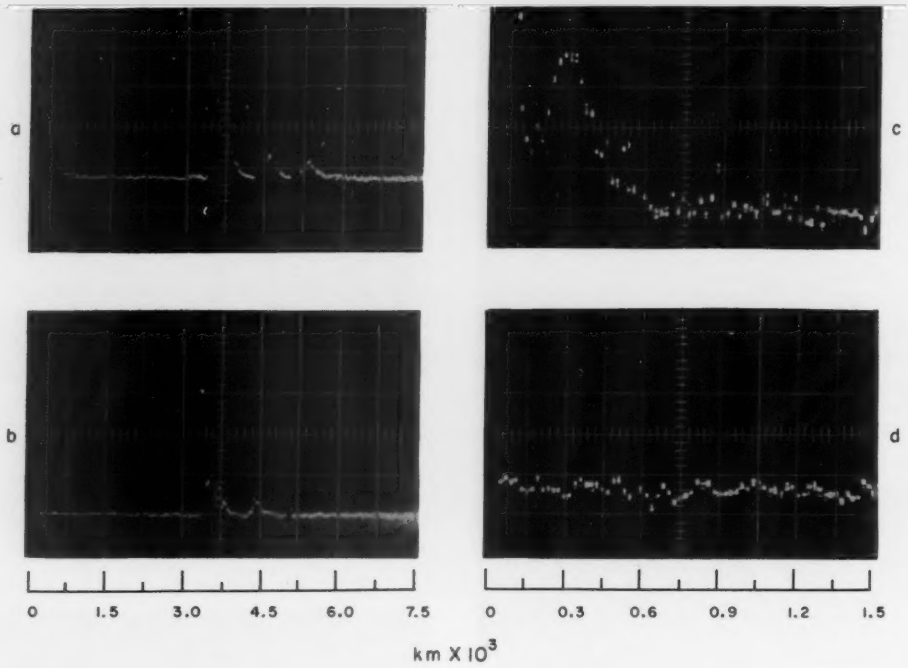

FIGURE 6. *Long-range backscatter records obtained using: (a) Large array, (b) single dipole—for reception. Short range, high gain records using: (c) Large array, single dipole—for reception.*

While it is possible that other interfering modes of propagation might appear, a convincing final argument for the identification of the echoes as incoherent scatter is provided by a comparison with known *F* region characteristics. Assuming the height of the *F* region maximum electron density to remain roughly constant, the maximum scatter intensity should be proportional to the square of the *F*2 region critical frequency observed on a conventional vertical incidence sweep frequency sounder. Unfortunately, such a sounder had not been installed at the Long Branch, Illinois station at the time of this experiment. The scatter records were compared with critical frequencies observed on the sweep frequency sounder at Fort Belvoir, which is located at about the same latitude. Critical frequencies were estimated from the scatter records by normalizing the system sensitivity such that at one particular hour the maximum indicated electron density corresponded with the Fort Belvoir critical frequency for that hour. The Fort Belvoir critical frequencies were then found to lie within one-half megacycle of the values calculated from the scatter records, on the several days in February 1959 when comparisons were made. Figure 7 is a replot of figure 3 to account for the height variation of sensitivity, and should be proportional to the electron density versus height profile. The dotted curves superimposed on this profile are computed from the Fort Monmouth and Boulder ionograms for the same day and local time using the NBS

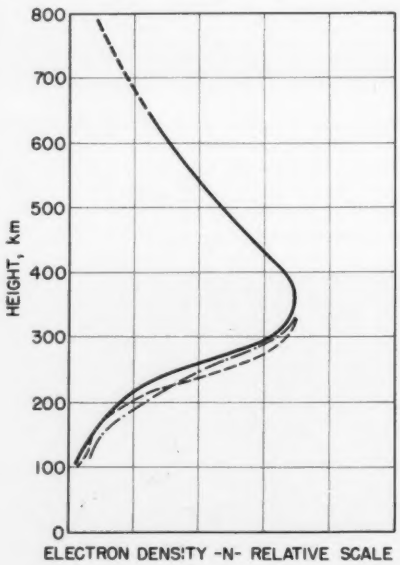

FIGURE 7. *Electron density profile obtained from A'scope display of figure 3.*

Dotted curves are "true height" profiles computed from Fort Monmouth and Boulder ionograms normalized to the same f_0F2.

"true height" technique [8]. A second pair of observations, made in the same way, are shown in figures 8 and 9, respectively. This pair, made shortly after sundown, shows the rapid decay of ionization below F max compared with figures 3 and 7. Although neither the agreement of the scatter profile with the ionograms, nor the ionograms with each other, is exact, the results exhibit a convincing similarity. A more precise comparison has since been made utilizing a conventional sounder at the Long Branch station [26].

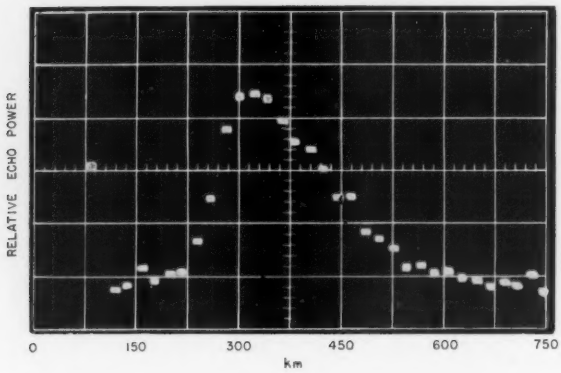

FIGURE 8. *Integrator A'scope photograph taken at 1940 l.t., February 27, 1959.*

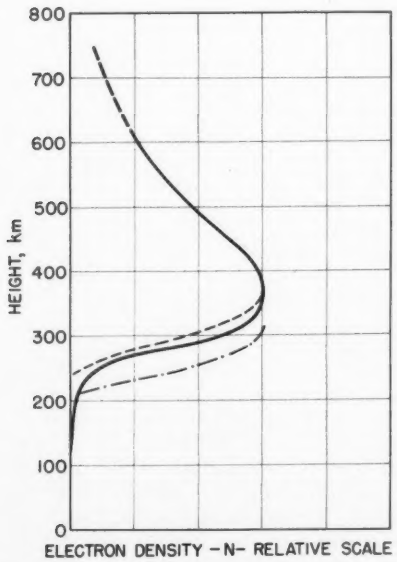

FIGURE 9. *Electron density profile obtained from A'scope display of figure 8.*

Dotted curves are "true height" profiles computed from Fort Monmouth and Boulder ionograms, normalized to the same f_0F2.

3. Comparison of Experimental Observations With Theoretical Predictions

Comparison of the observed scatter power with the values predicted theoretically using Gordon's method [1] is possible, using the system parameters as outlined above. Magneto-ionic effects in the ionosphere, which produce Faraday rotation of polarization [9], degrade the system sensitivity by 3 db. This may be seen as follows: Somewhat over 50 complete rotations of polarization would be expected for a 41-Mc/s wave passing twice through the entire daytime ionosphere. Thus more than one-half revolution can be expected over any given interval of 18-km height corresponding to the transmitted pulse length. The net effect is similar to a randomization of polarization so that on reception the linearly polarized antenna can extract only half of the energy in the incident scattered wave.

Based on all these considerations, the peak scatter power at the receiver terminals corresponding to an $F2$ region critical frequency of 12.8 Mc/s (2×10^6 electrons/cm^3) should be 3.5×10^{-16} w. The height of the $F2$ region maximum electron density is here assumed to be 330 km, in good agreement with the observed height. The observed scatter power at the receiver terminals, corresponding with the $F2$ region maximum, was 4.3×10^{-16} w when the critical frequency was about 13 Mc/s. This must be considered as excellent agreement between experiment and theory, inasmuch as the overall accuracy of the computation cannot be better than plus or minus 3 db. For receiver bandwidths of both 9 and 35 kc/s the observed scatter power was the same.

In spite of the agreement of the observed echo intensity with the prediction, one major difference is apparent from the equality of the echo strength for 9- and 35-kc/s bandwidths. Doppler broadening of the echo due to independent scattering from free electrons should be about 100 kc/s at F region heights. The F region temperature is here assumed to be approximately 1500 degrees Kelvin [10]. Since the 9-kc/s bandwidth apparently admits as much echo power as the 35-kc/s bandwidth, the echo must be no broader than about 9 kc/s. The spectrum of the received energy must be at least 9 kc/s wide since that is the spectral width of the transmitted energy. One must therefore conclude that the spectral broadening due to the scattering process must be considerably less than 9 kc/s, otherwise the received spectrum would be considerably wider. To further test this conclusion, observations were made with the receiver slightly detuned from the transmitted frequency. One such sequence is shown in figure 10. Figure 10a was obtained in the same manner as the records shown above with the receiver correctly tuned. Figures 10b and 10c were obtained with the receiver tuned 15 kc/s above and 15 kc/s below the transmitter frequency, respectively. The latter two records show no sign of an echo from the F region, leading to the conclusion that the bandwidth of the echo power must be considerably less than half the receiver pass band of 9 kc/s. Since the average ve-

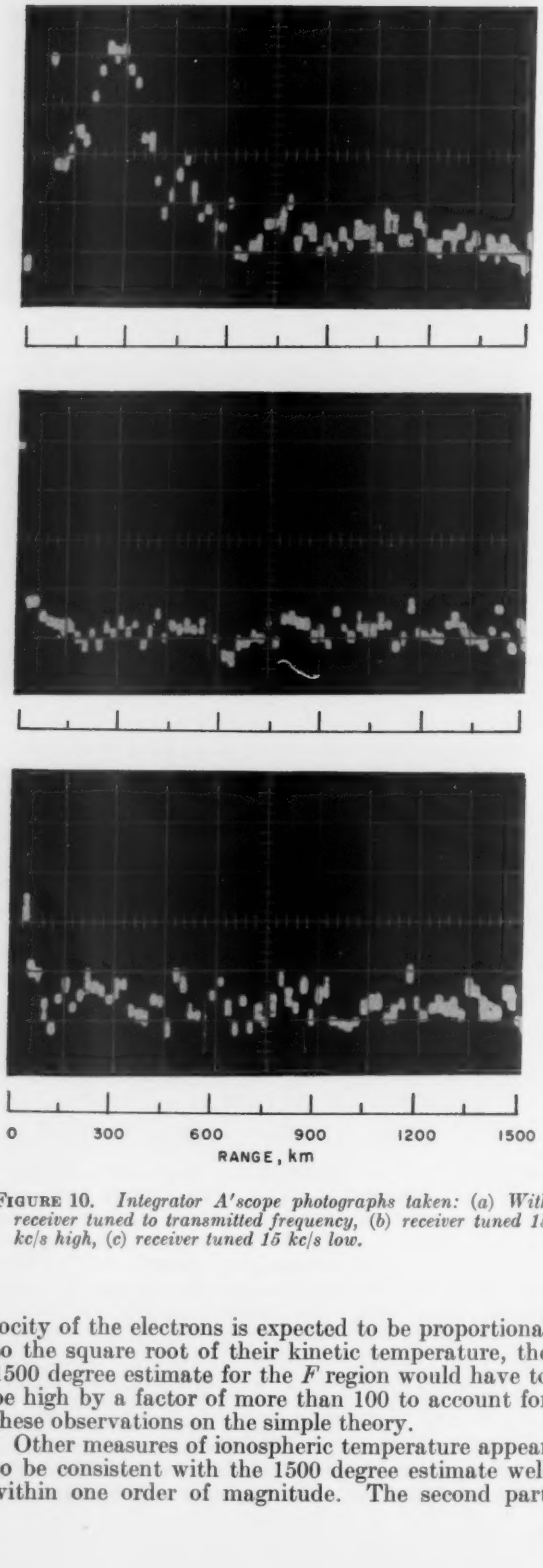

FIGURE 10. *Integrator A'scope photographs taken: (a) With receiver tuned to transmitted frequency, (b) receiver tuned 15 kc/s high, (c) receiver tuned 15 kc/s low.*

locity of the electrons is expected to be proportional to the square root of their kinetic temperature, the 1500 degree estimate for the *F* region would have to be high by a factor of more than 100 to account for these observations on the simple theory.

Other measures of ionospheric temperature appear to be consistent with the 1500 degree estimate well within one order of magnitude. The second part of this paper is a discussion of the observed echo bandwidth.

Recently several theoretical papers have appeared which predict that the intensity of the scatter from the ionosphere should be half that predicted by Gordon's method [11, 12, 13, 14, 15]. The reduced scatter power predicted by these theories is within the experimental accuracy of the present experiment and no disagreement can be inferred. Another experiment has also been performed by Pineo and others [17] at 440 Mc/s, and results very similar to ours have been obtained. Their measurement of the spectrum of the echoes was much more precise than possible with our equipment, and is discussed further in Part II, 3.

Part II. Modified Theory

1. Independent Particles Versus Density Fluctuations

There is a considerable body of literature on the subject of scattering of electromagnetic radiation by small particles. Following the early work of Lord Rayleigh [2], attention has been given to the criterion by which individual particles can be considered to scatter *independently* or, using Rayleigh's term, in *arbitrary phase*. The word "independence" is used in this paper in the statistical sense and implies a lack of statistical correlation.

For particle densities greater than those for which such independence is correct, calculation of the scatter properties has been found to depend upon an understanding and description of the statistical fluctuations of particle density. The reader is referred to Rocard [18] for a comprehensive summary and bibliography of the early developments in this field. A better statistical description as well as a bibliography of more recent work are given by De Boer [19]. Using the De Boer approach, the writer suggests the following arguments as a basis for a modified theory of the incoherent scatter.

The density fluctuation theory begins with a statistical description of the spatial distribution of the scattering particles. When *neutral* particles are separated by many particle diameters so that interparticle forces are small, a random distribution of locations is established. (This is strictly true, of course, only when the gas has no strong gradient of density in a distance comparable with the scale size under consideration.) The statistical fluctuations of particle density create a region containing weak irregularities of refractive index which are capable of scattering radio waves. *When the particle distribution can be considered random over all scale sizes comparable with the wavelength of the incident radiation, De Boer* [19] *finds the scattered intensity to be equal to that of the simple independent scattering case.* De Boer implies that the scattered *intensity* would not depend upon the scale size chosen for the irregularities. On the other hand, we shall see that a specification of scale size is important to an understanding of the *spectral broadening* of the scattered radiation.

On the other hand, when the spatial distribution of the electrons is such that the phases of their respective contributions cannot be considered mutually independent, the simple Doppler profile of the previous paragraph is no longer correct. This conclusion is supported by the fact that the observed frequency broadening of the incoherent scatter echo is much smaller than that implied by the above Doppler profile when any reasonable kinetic temperature is assumed for the ionosphere. (As in the previous section, we have assumed that the temperature in the F region is of the order of 1500 degrees Kelvin.) Assuming that the correct explanation of the discrepancy is to be found in terms of a collective description of the spatial distribution of the electrons —the fluctuation in density of the electrons due to the Brownian motion—an estimate of Doppler broadening which is consistent with the observations is obtained below.

A simple illustration will serve to show how a group of particles, having a Maxwellian distribution of thermal velocities, could under the proper conditions produce a resultant having little or no Doppler shift by comparison with the broadening which the particles would produce, were they independent. Figure 11a is an idealized sketch of a radar system intended for study of the ionosphere. The antenna beam is approximated by a uniform response within the sector, and zero response outside this range.

We now consider the relation between the concept of density fluctuations as scattering centers and the concept of individual electrons as scattering centers. In all cases of interest, the incident electromagnetic field is modified so slightly by scattering that as a first approximation the individual electrons must give rise only to single scattering of the incident energy. That is, each electron is considered to be coupled electromagnetically only to the radar system and not to other free electrons. Hence, a detailed summation of the contributions of all the free electrons individually would lead to the correct description of the scattered field. Such a summation would have to account for the phase of the contribution from each electron individually—an enormous computational problem. By taking advantage of ways in which large groups of electrons—and their individual contributions—exhibit collective behavior, it is possible to simplify the problem considerably. If the phase of the contribution from each free electron is uniformly distributed throughout a range of at least several times 2π radians and is statistically independent of the phase of the individual contribution from each other free electron, the approach used by Rayleigh [2] and Gordon [1] is correct. In this case the scatter due to each particle appears in the resultant signal at the Doppler-shifted frequency corresponding to its line of sight velocity, $f-f_0=2v/\lambda$. The spectrum of the scattered energy (arising from a monochromatic source) would have the functional form of the probability density function describing the number of electrons found at each line of sight velocity. Ordinarily this would reduce to the usual Gaussian, or Maxwellian [12], form

$$S(f)=S(0)\exp\left[-\left(\frac{f-f_0}{\frac{\pi^{\frac{1}{2}}\bar{v}}{\lambda}}\right)^2\right]$$

$$=S(0)\exp\left[-\left(\frac{f-f_0}{\frac{2}{\lambda}\left(\frac{2kT}{m_e}\right)^{\frac{1}{2}}}\right)^2\right], \qquad (1)$$

where $S(f)$ is the power spectrum function of the scattered energy in terms of the spectral frequency, f. The transmitted frequency is f_0, $\bar{v}$ is the mean speed of flight of the electrons, λ is the free space wavelength of the radio energy, T is the kinetic temperature, k is Boltzmann's constant, and m_e is the mass of the electron.

As shown by the phase vector, or phasor, diagrams in figure 11(b), the phase $P(A)$ of an echo arising from from a scatterer at a distance A from T is 360 degrees advanced relative to the phase $P(B)$ of the echo from another scatterer lying a distance $B=A+\lambda/2$ from T. In three dimensions A and B are the radii of the spherical surfaces of constant phase with centers at T.

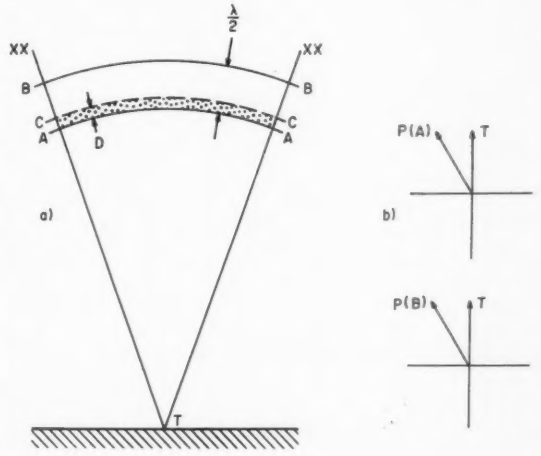

FIGURE 11. *Schematic sketch of radar system.*
Phasors are referred to the transmitted phase—T.

We now consider our group of particles to be initially located at points within the slab AA–CC which has thickness $d \ll \lambda/2$. The phasor resultant signal due to this group of particles is shown in figure 12 along with the individual components, for representative initial particle locations.

We allow enough time to pass that the particles have diffused into a slab of somewhat greater thickness than AA–CC. Figure 13 is a phasor diagram illustrating how the individual components and the

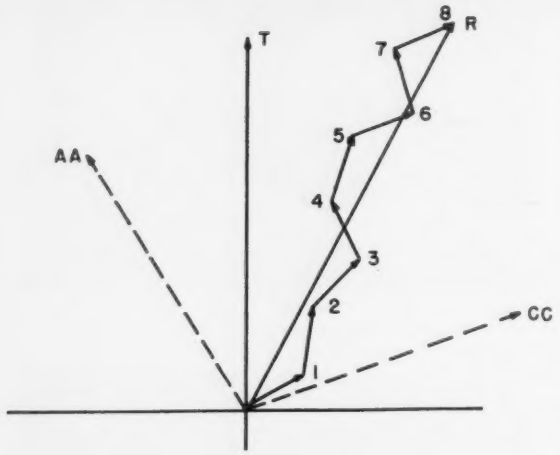

FIGURE 12. *Phasor diagram illustrating the initial distribution of contributions due to particles within the slab* AA-CC.

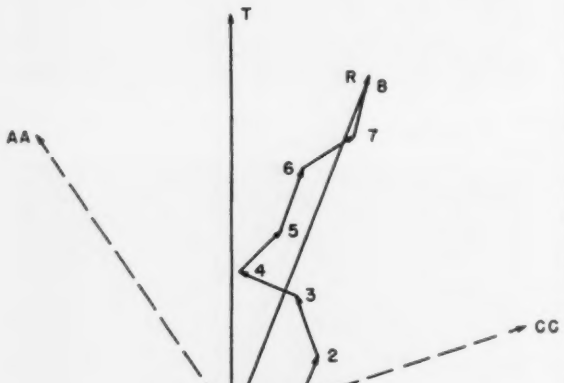

FIGURE 13. *Phasor diagram illustrating how the distribution of electron contributions of figure 12 may have changed after a short time has elapsed.*

resultant phasor might have changed during that time. We see that the phases of the individual components have rotated considerably in the new picture, but the phase and amplitude of the resultant have changed only slightly. Of course, the degree to which the resultant changes is a function of the distribution of rates of change of the components. In the simple illustration above, the reduced rate of change of phase of the resultant can be viewed as an average of the rates of change of the components. The reason for discussing rates of rotation of phasor components is, of course, that the shift of frequency of any component relative to the transmitted frequency is directly proportional to the rate of phase rotation of that component. In the simple illustration the phases of the components would rapidly become randomized as diffusion set in. Until this happened, the probability density function describing the equivalent spectrum of the resultant signal would be markedly reduced in width relative to the spectrum of the individual components. This simple illustration is analogous to the scatter by free electrons in an underdense meteor trail. The echo from a short length of such a trail is not Doppler broadened by thermal motions of the electrons.

We now ignore, temporarily, the continuous motion of the electrons and consider the statistics of the signal scattered from a portion of the ionosphere in which the electrons are suddenly rendered motionless. We consider for two limiting cases the distribution of signal strength arising from a slab *AA–CC*, as in figure 11 above, on a number of successive such instants, or "realizations." In both cases we consider that the particles are randomly distributed within the slab, all positions having equal probability. When, as above, the thickness, d, of the slab is taken to be small relative to $\lambda/2$, or more specifically when $d \lesssim \lambda/4\pi$, the resultant *amplitude*, R, is almost equal to the arithmetic sum ot the contributions from the individual particles. That is, the resultant echo power, $P \approx n^2 r_e$, where r_e is the scattered echo power arising from one electron and n is the total number of electrons within the slab. The phase ot the resultant is somewhere between the phase corresponding to *AA* and that corresponding to *CC*, depending upon the distribution of particle density within the slab. The distribution of the resultant signal amplitude over a large number of realizations is simply proportional to the distribution of n. By virtue of their close spacing in phase, the particles in this case contribute to the resultant collectively, i.e., coherently.

The other limiting case is for $d \gg \lambda/2$. This is the two-dimensional random walk case considered by Rayleigh [2], in which $R_{avg} = nr_e$ and the resultant for any given realization is Rayleigh distributed.

$$P(R)\,dR = \frac{2}{nr_e^2} R \exp\left[-\frac{R^2}{nr_e^2}\right]$$

where $P(R)dR$ denotes the probability that R lies within the range R to $R+dR$. In this case the phase of the resultant is uniformly distributed throughout 2π radians, and without some detailed knowledge of the positions of the individual components the phase cannot be specified within that range. Judging from the result of the argument for a thin slab above, we can satisfactorily describe the properties of the signal from a thick slab by dividing it into components having $d \lesssim \lambda/4\pi$ i.e., knowledge of the position of every particle is not necessary. This is the import of the arguments given by Rocard [18] and De Boer [19] which were referred to above.

Evidently the transition from the collective behavior of the thin slab, to the incoherent behavior

which describes the thick slab, is by no means sudden. As d increases from $\lambda/4\pi$ to larger values there is a transition region in which the coherent aspects of the thin slab are gradually lost. It should suffice to say that there should be some maximum d for a thin slab to exhibit essentially coherent behavior, and some minimum d for a thick slab to exhibit essentially incoherent behavior. We make the approximation that for some intermediate value of d, the electrons within each slab contribute coherently to the scatter, while the contribution from adjacent slabs is uncorrelated statistically in phase or in amplitude. This intermediate value of d will be termed the *scale* of the irregularities of electron density and designated by the letter L. We note, for the case of a radar, that L is of order $\lambda/4$.

A much more precise handling of these concepts is embodied in the theoretical work done in recent years with specific application to the problem of radio wave scattering from irregularities arising in ionospheric or tropospheric turbulence [20, 21, 22]. Here the intensity of the scatter is found to be proportional to the integral over the scattering volume of the spatial autocorrelation function of refractive index, taking phase into account. For a more precise account of this development the reader is referred to the papers cited. What is important to our present problem is that this integral is formally equal to the *spectrum* of the irregularities evaluated at the wavenumber k for the case of direct backscattering as observed by radar. The reciprocal of this wavenumber, $1/k$, is identified with the scale L multiplied by a constant close to unity.

As noted by Balser [13], the spectrum of scatter from a large volume containing independent scattering centers is simply the sum of the spectra associated with the individual centers. In other words, in our approximation the spectrum of incoherent scatter arising from a large volume of the ionosphere should have the form of the spectrum arising from any given slab of scale L (provided the mean characteristics of the volume are uniform throughout—temperature, density etc.). Since we have approximated the contents of such a slab as scattering coherently, the instantaneous field strength arising due to the slab is represented as proportional to the total electron content found at any instant within the confines of the slab.

2. Role of the Ions in Determining the Criterion for Independence

We now face the problem of deciding under what conditions the scattering is best considered to arise from independent particles, and under what conditions the representation using irregularities of particle density gives a more accurate result. We shall see that the ionosphere, being a partially ionized gas, provides a unique opportunity to answer this question.

Gordon [1] made the assumption that the characteristic scale L is meaningful only when the mean free path, l, of the scattering particles is small compared with L. He uses the converse of this assumption as the criterion for independent scattering from individual particles—i.e., when $L \ll l$. We shall refer to this as the "l criterion." An alternate and very different assumption is that the criterion could be set by the relationship of the scale L to the mean separation of neighboring particles. This says that when $L \gg n^{-1/3}$, one must use density fluctuations of scale L to calculate the scattering properties. Here $n^{-1/3}$ is the approximate mean separation between neighboring scattering particles and n is the number of particles per cubic centimeter. We shall refer to this as the "$n^{-1/3}$ criterion." We note that, in the F region and above, l is of order 1 km or greater, while a typical F region electron density of 10^6 per cm^3 corresponds to $n^{-1/3}=0.01$ cm. The scale L, for the experiments reported in the first part of this paper, is of order 2 m. Thus we have $n^{-1/3} \ll L \ll l$, i.e., both criteria are satisfied. However, since the independent particle approach suggests that a Doppler broadening much greater than actually observed should be found, we are led to inspect the consequences of the density fluctuation approach for the ionosphere.

We now offer a crude argument which demonstrates that the distribution of the free electrons cannot be entirely random. We consider the case of scattering from a randomly distributed gas of neutral particles having approximately the same total particle density as that of the F region of the ionosphere. Long-range forces among the particles are considered to be negligible so that only during collisions do the particles affect the motions of each other. Referring to figure 11 we consider the contents of a scattering slab AA–CC the thickness of which is equal to L. Since we have approximated that all particles located within this slab scatter coherently, the amplitude of the scattered contribution from the slab is proportional to its total content of particles. Beginning at a time t_0 we note that at a time $t_0+\tau$, the content of the slab has almost completely changed due to the line-of-sight motions of the particles. Those particles which had been within the slab at t_0 have almost all moved to new locations and have been replaced within AA–CC by other particles. The time τ is therefore given approximately by the time taken for the average particle to move a line-of-sight distance equal to L, or $\tau=L/\bar{v}_z$, where $\bar{v}_z$ is the root mean square line-of-sight velocity of the particles. Another way of saying this is that the content, or state of fluctuation, in the slab AA–CC loses *correlation* with its state at a previous time, if at least τ seconds have elapsed since that previous time. Using the well-known relation between the autocorrelation function and the power spectrum [23], we therefore estimate that the bandwidth of the scattering from the slab of thickness L is approximately $\Delta f=1/\tau=\bar{v}_z/L$. This corresponds to a bandwidth of $\Delta f=4/\lambda \times 0.96\bar{v}_z=0.96\bar{v}_z/L$ from eq (1), noting that $\bar{v}_z=1.085\bar{v}$ (see reference [12]), for the case of independent scattering from the particles. We see that the broadening expected for the two approaches is the same. Turning to the actual case of

incoherent scatter from the F region of the ionosphere, we believe that the velocities of the free electrons are equivalent to the supposed kinetic temperature of about 1,500 degrees Kelvin. Since the observed frequency broadening of the scatter is much smaller than expected for a fully random distribution of electrons at this temperature, we look for an explanation in which some mutual correlation among the electron positions and velocities is found.

We now explain the observed echo spectrum through the use of the density fluctuation approach. Insight regarding the distribution of the free electrons can be gained from a paper published by Pines and Bohm [24]. These authors considered the case of an electron gas embedded in a uniform smear of positive charge. Since the mobilities of electrons are so much greater than the mobilities of ions, this case is a good approximation to the situation in the ionosphere. Pines and Bohm found that the mean square intensity of fluctuations of electron density of scale size L is *reduced*, compared with that for the case of random motions, by a factor $(2\pi)^2\lambda^2_D/L^2$, for all $L \gg \lambda_D$. In this relation λ_D is the so-called Debye shielding distance, $\lambda_D=(kT/4\pi ne^2)^{1/2}$ and T is the temperature in degrees Kelvin, k is Boltzmann's constant, n is the electron density and e is the charge on the electron. Only for the condition $L \ll \lambda_D$ do the free electrons behave as though randomly distributed. Since L is of the order of one or more meters for the present and other proposed radar experiments, and λ_D is less than a few centimeters at all heights of interest, the *independent* random fluctuations in electron density of scale L must be viewed as negligible. The intensity of scatter arising from such fluctuations must also be negligible.

Similar considerations hold for the case of a gas of positive ions embedded in a uniform smear of negative charge. In both cases the mutual repulsion of charges of like sign causes the reduction of fluctuations. However, Spitzer [25] has shown that in a real plasma, the mobility of the electrons is so great as to cause their equilibrium distribution to balance the fluctuations of positive charge density nearly completely. Once the fluctuations of positive charge density are balanced by equal and opposite fluctuations of negative charge density, the ions may be distributed nearly randomly, as they would be distributed if they were neutral particles. The fluctuations of the free electrons from their equilibrium distribution are strongly reduced, in accordance with the argument of Pines and Bohm, inasmuch as the positive ion distribution departs only slightly from the approximation of a uniform smear of charge. Thus one is left with a picture of scattering from fluctuations of free electron density of scale L such that the *magnitude* of the scatter is the same as for a randomly distributed neutral gas, and its *rate of change* is appropriate to particles having the mean mass of the ions. The rate of fading must therefore be computed as if the positive ions, rather than the electrons, produced the scattered echo. This should not be taken to imply that the ions make a direct contribution to the scatter, since the free electrons have a considerably greater radar cross section.

For example, if we assume that the ionized constituent of the F layer is atomic oxygen, we estimate the Doppler broadening

$$\Delta f=\frac{v_z}{L}\approx 540 \text{ c/s}$$

for an operating frequency of 41 Mc/s and a temperature of 1,500 degrees Kelvin.

The result of the arguments given in this section is that the characteristics of incoherent scattering at VHF, for $n^{-1/3} \ll L$, if also $\lambda_D \ll L$, may be estimated by substituting for the ionosphere a fictitious gas of randomly distributed neutral particles with special characteristics. These particles would have the radar cross section of the free electron, and the mass (and consequent velocity distribution) of the ions. For $n^{-1/3} < L < \lambda_D$ the Doppler broadening should approach that of independent electron scatter. For both cases, the scattering is best described in terms of fluctuations of particle density. Only when $n^{-1/3} \gg L$ do we expect to find that the simple independent particle description of the scattering is correct.

3. The Echo Spectrum

In an informal report [16] and in the present paper, approximate calculations for the fading spectrum are presented. Two more rigorous theories have been developed by other workers [11, 12] which, although using different approaches, predict the same spectral distribution. This theoretical spectrum has been experimentally confirmed by Pineo et al., at 440 Mc/s [17]. Two other theoretical papers dealing primarily with the intensity of the scatter have also appeared [13, 14].

At 41 Mc/s, the bandwidth of the spectrum predicted by these authors is about 1,000 c/s for echoes from the F region. Recent statistical studies, of the fading of echoes observed on the equipment described in this paper, show that the bandwidth of 41 Mc/s echoes from the F region is certainly greater than about 600 c/s. This observation agrees with the results of Pineo et al. [17], and with the above mentioned theories.

The author's approximate calculation of spectral width differs from the precise theories by more than a factor of two. The difficulty apparently resulted from the assumption that echo contributions from adjacent volumes of scale L can be considered to be statistically independent. It is true that the fluctuations in density of such adjacent volumes are independently distributed. However the electrons, found in a given volume at one instant, move into adjacent volumes while the phase of the individual contribution of each electron various continuously. This continuous variation of phase implies a sort of long term correlation among many irregularities of scale L. The assumption basic to the approximate calculation was therefore not correct. None of the

theoretical treatments mentioned above suffer from this difficulty. In spite of this difficulty with the author's treatment, the heuristic arguments of the foregoing sections offer an approximately correct explanation of the physical principles involved. The rate of rotation of the resultant phasor representing the contribution of the volume V must be related to the average of the rates of rotation of its component phasors. Since the individual components must have rates of rotation distributed in both advancing and receding senses relative to the reference, the average must be less than the mean absolute rate of phase rotation of the components.

4. Magnetic Field Effects

In the foregoing sections it has been assumed that the effects of the earth's magnetic field can be ignored. In regions where the mean free path is large compared with the wavelength this can only be true for propagation parallel with the lines of force of the earth's field, and for frequencies large compared with the gyrofrequency. The latter condition will always be satisfied in the earth's ionosphere and exosphere at practical operating frequencies. The quantity $\bar{v}$ used in section 2 is related to the Maxwellian distribution of particle velocities and to the components of that distribution in the line of sight. If the magnetic field does not seriously alter the Maxwellian components of velocity parallel to the field, then the results of the preceding sections will be approximately correct for a vertical incidence radar in temperate or arctic zones.

If the propagation is nearly perpendicular to the lines of force of the earth's field, magnetic control of the particles can be serious. The ions now execute paths with a circular component of motion the plane of which includes the line of sight. If L is large compared with the radius of this circular motion, the particles are restricted to paths nearly parallel to the surfaces of constant phase. In this case the fading spectrum should be calculated as in the case of short mean free path [11] using an equivalent coefficient of diffusion, D_m, at right angles to the magnetic field. When L is small compared with the gyroradius, there should be little effect on the main spectrum of fading.

An interesting case arises when L is of the same order of magnitude as the average gyroradius of the ions. All ions of the same mass must have the same gyrofrequency within a volume of scale L. The rate of migration of the center of rotation of any given particle out of the volume, L thick and bounded by surfaces of constant phase, is given approximately by

$$\left[\frac{\bar{v}}{\left(\frac{R\lambda}{2}\right)^{1/2}}\right]$$

where R is the range to the volume in meters and the expression in brackets is the length of the first Fresnel Zone. The fading due to this component of motion would be only a few cycles per second at an operating frequency of 50 Mc/s. The gyrofrequency of the largest ion expected, 0_2^+, is of the order of 10 c/s at F region heights over the magnetic equator. The gyrofrequency for protons, likely to be encountered in the exosphere, is of the order of 250 c/s. Thus each ion may be expected to execute a minimum of several turns during the period taken for its center of rotation to move a small fraction of 360° phase from the radar station. We may therefore expect that the scatter echo will exhibit a tendency toward periodicity having a frequency equal to the ion gyrofrequency. This periodicity should be easily measurable using autocorrelation analysis of sequences of pulse echoes.

From the approximate frequency of the periodic component one may infer the mass of gyrating ions. If several ionic constituents are present, several periodic components should appear, the relative power in each being proportional to the number of ions of the appropriate constituent. In this way the scatter radar can be used as a sort of mass spectrometer to determine the variation of ionic constituents with height. Once the ionic constituents have been identified, precise determination of the gyrofrequency should provide a measure of the profile of the magnetic field intensity as a function of height. At the same time, the thermal broadening of the echo spectrum will be only slightly reduced by the magnetic field when L is of the order of magnitude of the gyroradius. Knowing the mass of the ionic constituents, it should be possible to make a precise determination of temperature. A more refined theory to take the magnetic effects into account is under development.

The author acknowledges the material contributions to this work and the encouragement given by many of his colleagues at the Central Radio Propagation Laboratory, although space permits naming only a few. Of special note were the efforts of John L. Green and his staff at the Long Branch field station to place and keep the transmitter in operation. P. P. Viezbicke did the detail design of the antenna and supervised its construction. T. N. Gautier, R. M. Gallet, R. S. Cohen, and C. G. Little have contributed to development of the theoretical model and have aided in preparation of the manuscript. The writer also appreciates the cooperative exchange of ideas and information provided by the Cornell University group, notably W. E. Gordon, H. G. Booker, and B. N. Nichols; by J. A. Fejer, by J. P. Dougherty and D. T. Farley, by J. Renau by V. C. Pineo, and by many others.

References

[1] W. E. Gordon, Incoherent scattering of radio waves by free electrons with applications to space exploration by radar, Proc. IRE **46,** 1824–1829 (1958).

[2] Lord Rayleigh, On the light from the sky, its polarization and color, Phil. Mag. Ser. 4 **41,** 107–120 (1871).

[3] K. L. Bowles, Observations of vertical incidence scatter from the ionosphere at 41 Mc/sec, Phys. Rev. Letters **1,** 454–455 (Dec. 15, 1958).

[4] J. L. Pawsey, R. N. Bracewell, Radio astronomy, 234 ff. (Oxford Univ. Press, Oxford, England, 1955).

[5] See for example, J. D. Kraus, Antennas, ch. 4 (McGraw-Hill Book Co., Inc., New York, N. Y., 1950).

[6] H. W. Wells, Flux measurements of Cassiopeia-A and Cygnus-A between 18.5 Mc/s and 107 Mc/s, Proc. IRE **46,** 205–208 (1958); also recent private communication of information to be published.

[7] See for example, K. L. Bowles, in Ann. Intern. Geophys. Year **3,** pt. 4, 346–360 (Pergamon Press Inc., London, England, 1957).

[8] J. W. Wright, The NBS electron density profile program—Some features and early results, Proc. URSI/AGI Conf. Brussels, Sept. 1959 (Pergamon Press Inc., New York, N.Y., 1960).

[9] S. J. Bauer, F. B. Daniels, Ionospheric parameters deduced from the Faraday rotation of lunar radio reflections, J. Geophys. Research **63,** 439–442 (1958).

[10] J. W. Siry, Satellite orbits and atmospheric densities at altitudes up to 750 km obtained from the Vanguard orbit determination program, Planet. Space Science **1,** 184–192 (1959); I. Harris, R. Jastrow, An interim atmosphere derived from rocket and satellite data, Planet. Space Science **1,** 20–26 (1959).

[11] J. A. Fejer, Scattering of radio waves by an ionized gas in thermal equilibrium, Can. J. Phys. **38,** 1114–1133 (1960).

[12] J. P. Dougherty, D. T. Farley, A theory of incoherent scattering of radio waves by a plasma, unpublished manuscript, Cavendish Lab., Cambridge, England, to be submitted for publication.

[13] E. E. Salpeter, Scattering of radio waves by electrons above the ionosphere, J. Geophys. Research **65,** 1851–1852 (1960).

[14] J. Renau, Scattering of electromagnetic waves from a non-degenerate ionized gas, unpublished manuscript, submitted for publication by Cornell Aeronaut. Lab., Buffalo, N.Y.

[15] F. D. Kahn, Long range interactions in ionized gases in thermal equilibrium, Astrophys. J. **129,** 205–216 (1959).

[16] An early version of the present paper appeared as an unpublished report of the National Bureau of Standards, dated 18 Sept. 1959.

[17] V. C. Pineo, L. G. Kraft, H. W. Briscoe, Ionospheric backscatter at 440 Mc/s, J. Geophys. Research **65,** 1620–1621 (1960); also unpublished report, Some characteristics of ionospheric backscatter observed at 440 Mc/s, MIT Lincoln Lab. rept. 30G–0008 (6 July 1960).

[18] M. Y. Rocard, Théorie moléculaire de la diffusion de la lumière par les fluides, Ann. Phys. **10,** 117–231 (1928).

[19] J. De Boer, Molecular distribution and equation of state of gases, Repts. Progr. in Phys. **12,** 305–374 (1949), see particularly p. 364 ff.

[20] See for instance, F. Villars, V. F. Weisskopf, On the scattering of radio waves by turbulent fluctuations of the atmosphere, Proc. IRE **43,** 1232–1239 (1955).

[21] H. G. Booker, W. E. Gordon, A theory of radio scattering in the troposphere, Proc. IRE **38,** 401–412 (1950).

[22] A. D. Wheelon, Radio wave scattering by tropospheric irregularities, J. Research NBS **63D,** 205–233 (1959).

[23] See for example, J. S. Bendat, Principles and applications of random noise theory, especially sec. 2.7 (John Wiley & Sons, Inc., New York, N.Y., 1958).

[24] D. Pines, D. Bohm, A collective description of electron interactions: II. Collective vs individual particle aspects of the interactions, Phys. Rev. **85,** 338–353 (1952).

[25] L. Spitzer, Physics of fully ionized gases, see particularly sec. 4.3., p. 62 (Interscience Publishers, Inc., New York, N.Y., 1956).

[26] T. E. Van Zandt, K. L. Bowles, Use of the incoherent scatter technique to obtain ionospheric temperatures, J. Geophys. Research **65,** 2627–2628 (1960).

(Paper 65D1–97)

JOURNAL OF RESEARCH of the National Bureau of Standards—D. Radio Propagation
Vol. 65D, No. 1, January–February 1961

Radio Wave Absorption of Several Gases in the 100 to 117 kMc/s Frequency Range[1]

C. O. Britt, C. W. Tolbert, and A. W. Straiton

(May 16, 1960; revised June 23, 1960)

This paper describes a technique for the measurement of the absorption characteristics of millimeter radio waves over a wide pressure range and presents the results of measurements made with this technique for four gases in the frequency band from 100,000 to 117,000 megacycles per second. The four gases investigated in near pure state were carbon monoxide, nitrous oxide, sulfur dioxide, and nitrogen dioxide. The results of these tests are as follows:

Gas	Predicted or previously measured frequency	New measurement of frequency	Measured absorption coefficient (α)	Measured line width
	Mc/s	*Mc/s*	$\frac{cm^{-1}}{2}$	*Mc/s per mm Hg*
Carbon monoxide	115,270.56		8.75×10^{-5}	4.25
Nitrous oxide	100,491.76		1.25×10^{-4}	4.25
Sulfur dioxide	104,911.75	104,042 and 104,046.		13.75
	105,333.94	105,189	9×10^{-6}	17.0
Nitrogen dioxide	105,158.4	No line detected		

1. Introduction

The Electrical Engineering Research Laboratory of the University of Texas has made a number of measurements throughout the low-centimeter and millimeter wavelength regions of the absorption of radio waves due to atmospheric gases [1].[2] By repeating these tests, the attenuation was plotted as a function of water vapor content. In almost every instance, it was possible to interpret the losses as being due to absorption by water vapor and oxygen.

In one set of measurements, however, variable losses were noted which were not associated with changes in water vapor concentration. These losses occurred in the frequency range between 100,000 and 118,000 Mc/s and were attributed to some of the rarer gases in the atmosphere [2].

It is the purpose of this present paper to investigate the absorption properties of several gases with measured or predicted absorption lines in the frequency region in question. In order to isolate the effect of each line, the gases were studied in the nearly pure state. The absorption characteristics obtained by measuring the gases individually cannot immediately be used to predict their absorption when diluted with air. Further studies are in progress which, we hope, will assist in making this transition from individual gas loss to loss due to mixtures.

[1] Contribution from Electrical Engineering Research Laboratory, The University of Texas, Austin, Tex. Prepared under Office of Naval Research Contract Nonr 375(01), NR 371032.

[2] Figures in brackets indicate the literature references at the end of this paper.

2. Instrumentation and Measuring Technique

The millimeter wave absorption was measured by the use of a circular tube 500 ft in length and 6⅛ in. in diameter. The cell may be evacuated and then filled with the gas under test. For the measurement of the larger absorption coefficients, a diaphragm was inserted between sections of the pipe and only part of the length was filled with the test gas. The remainder of the tube was filled with nonabsorbing gas.

A Teflon diaphragm at either end permitted the injection and extraction of the electromagnetic energy. Horn antennas spaced back of the ends of the pipe provided proper illumination across the diaphragms. The electric field across the end of the cell was in a vertical direction with the intensity varying horizontally from maximum at the center line to zero at the edges. This field approximates that of the TE_{11} mode. Distortion from higher-order modes was very small since the attenuation in the guide for lossless gases was only ¼ db.

The signal source consisted of a Bell Telephone Laboratories M–1805 klystron operating over a 50,000- to 58,500-Mc/s range, a modified L–5506 "in-guide" crystal harmonic generator to provide the second harmonic for the tests, and the associated power supplies and necessary waveguide components. The maximum signal available was of the order of 10^{-7} w.

The receiver also utilizes an M–1805 klystron, an "in-guide" wafer crystal for harmonic generation and mixing, and the necessary amplifiers and power supplies. The receiver was frequency modulated to reduce the d-c amplifier requirements and to compensate for klystron frequency instability.

The usual measurement procedure was to evacuate the cell and determine the attenuation at the frequencies of interest as the test gas pressure was increased. A continuous frequency scanning technique was used at low pressures in the vicinity of the maximum absorption.

3. Carbon Monoxide

As is the case of each of the various gases studied, the frequencies of the absorption lines of carbon monoxide had been predicted from a study of the infrared molecular energy levels. The various resonant frequencies have been tabulated by Ghosh and Edwards [3]. Gordy and his associates have measured with great accuracy the frequency of the carbon monoxide line in the spectrum of interest in this paper. A comparison of these values is as follows:

Predicted:	115,270.2 Mc/s
Measured (Gordy):	115,270.56 Mc/s.

Equipment was not available at this laboratory for absolute frequency measurements to this precision. The above absorption line at the upper end of the band and one for nitrous oxide at the lower end of the band, which was also measured with accuracy by Gordy, were used as calibration points on the wavemeter. By assuming linear variation between these points, a measure was obtained of the intermediate frequencies.

The absorption versus frequency measurements in the vicinity of the carbon monoxide line are shown in figure 1.[3] Pressures ranging from 4.5 to 27 mm of mercury were used in obtaining these data. The lines drawn on figure 1 were calculated by the use of the Van Vleck-Weisskopf equation [5] with the maximum attenuation in the equation being adjusted to fit the maximum measured value at the pressure in question. A line breadth proportional to pressure with a value of 4.25 Mc/s per mm Hg was obtained from the half power points at very low pressure where continuous sweep of the frequency was used. This line breadth constant provided a fairly good fit of the measured data when the maximum absorption was adjusted to fit the measured maximum at each pressure. This variation of maximum absorption with pressure is not implied in the Van Vleck-Weisskopf equation, but it may possibly be explained by saturation effects [6]. This decrease of absorption at the lower pressures has been attributed to the power saturation of the molecules and the possibility that lines could not be completely resolved due to a small amount of frequency modulation present in the measuring signal. Power variations over a range of several decibels did not, however, seem to alter materially the shape of the maximum absorption-pressure curve.

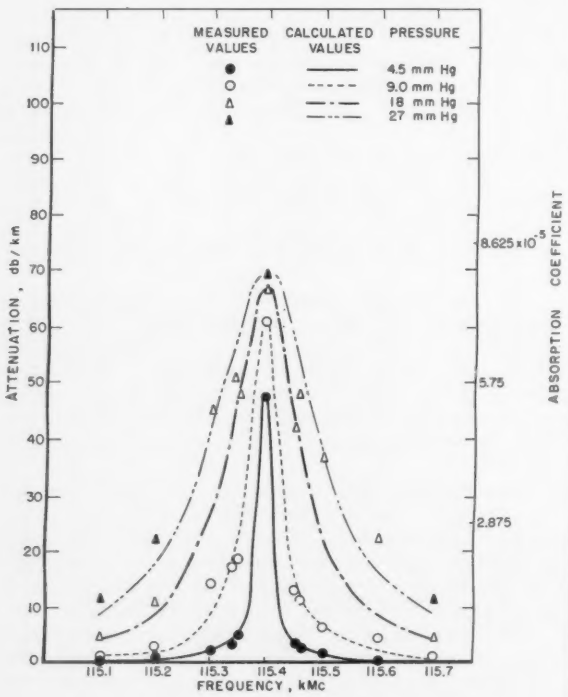

FIGURE 1. *Carbon monoxide absorption spectra.*

Absorption coefficient as used in the figures is in nepers per centimeter.

To further investigate the pressure dependence of the absorption, this peak attenuation was measured over a pressure range from a few millimeters to nearly 1 atm. These data are shown in figure 2. The absorption is seen to increase rapidly at very low pressures and slowly at higher pressures. The higher pressure increase is thought to be due to the "skirts" of higher frequency lines. The absorption coefficient, α, is chosen as the value at which the curvature changes abruptly since the gradual increase with pressure above the knee of the curve is attributed to contributions from other lines. The saturation effect is assumed to be confined to the very low pressures.

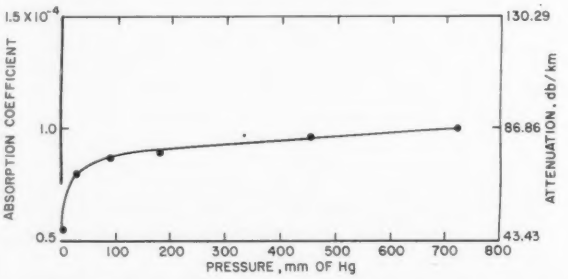

FIGURE 2. *Absorption versus pressure for carbon monoxide.*

Measured values.

4. Nitrous Oxide

Gordy and his associates [4] had measured with precision the frequency of the nitrous oxide line predicted for the spectrum covered by this report. A comparison of the measured and predicted values is as follows:

Predicted:	100,493.0 Mc/s
Measured (Gordy):	100,491.76 Mc/s

As indicated earlier, the frequency of this line was used as a reference in the calibration of the wavemeter for the frequency range in question.

The nitrous oxide absorption spectra for a number of pressures are shown in figure 3. The curves in the figure were drawn using the Van Vleck-Weisskopf equation with a line breadth proportional to pressure for a proportionality constant of 4.25 Mc/s per mm Hg. This line breadth constant was also determined from the half-power width at very low pressures. As in the case of carbon monoxide, it was necessary to adjust the peak absorption for the particular pressure used.

The variation of the peak absorption as a function of pressure for nitrous oxide is shown in figure 4.

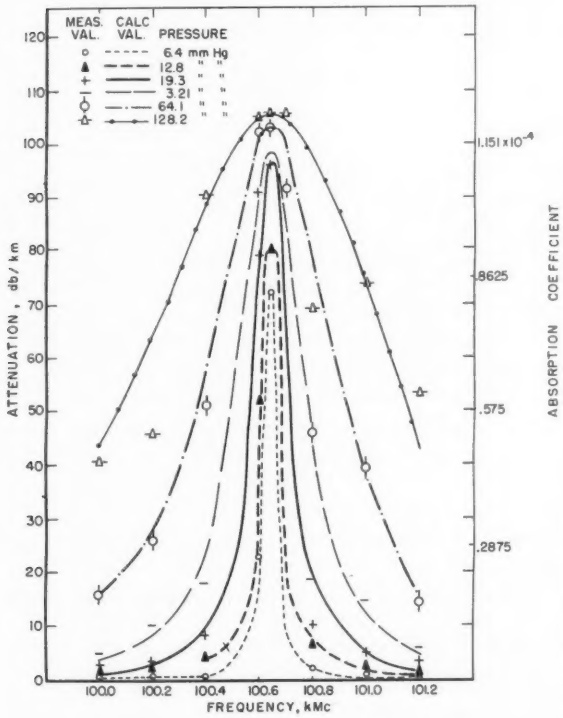

FIGURE 3. *Nitrous oxide absorption spectra.*

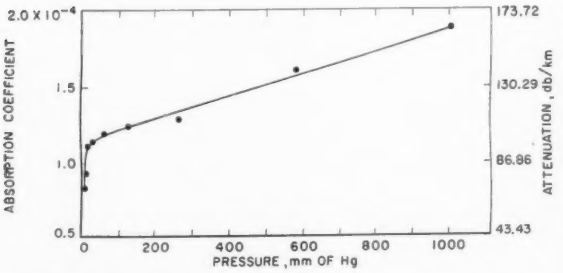

FIGURE 4. *Absorption versus pressure for nitrous oxide.* Measured values.

The low-pressure change may be explained in part by saturation effects and the high-pressure change by the effect of the skirts of other lines. The absorption coefficient applicable to the line is chosen as the value at the point of most rapid change in slope as in the case of carbon monoxide.

5. Sulfur Dioxide

Ghosh and Edwards [3] list four predicted sulfur dioxide lines in the vicinity of the spectrum covered by this report as follows:

100,911.75
104,028.28
105,333.94
116,790.07

plus 40 additional lines between 44,000 and 200,000 Mc/s.

The sulfur dioxide spectra were examined in detail over the range from 102,000 to 106,000 Mc/s and the results are shown in figure 5. The effects of the first three lines listed above are readily seen in this figure. In addition, the complex spectra of sulfur dioxide was evident in the flattening of the absorption spectra over the region investigated.

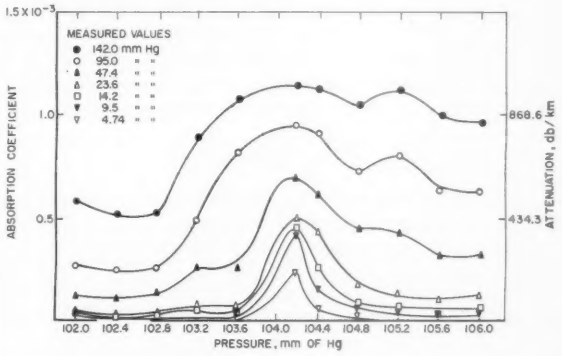

FIGURE 5. *Absorption coefficient of sulfur dioxide versus frequency at different pressures.*

The line in the vicinity of 104,000 Mc/s was examined at low pressures by frequency scanning and was found to consist of two lines with a separation of 4.5 Mc/s centered approximately at 104,042 and 104,046 Mc/s. Each line had a width of 13.7 Mc/s per mm Hg and the absorption of lower frequency component was approximately 1.4 times more intense than the higher frequency one.

The maximum absorption of the combined line as it blended together at increased pressures was measured and is shown in figure 6. The lower line in this figure is the absorption which would be associated with the double line in the vicinity of 104,000 Mc/s. The frequency for which the calculations were made falls between the two lines and therefore goes essentially to zero at very low pressures. The difference in the measured and calculated values is

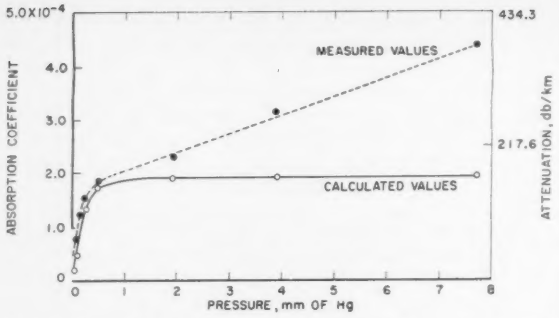

FIGURE 6. *Maximum absorption coefficient for two observed lines of sulfur dioxide versus pressure.*

apparently due to the attenuation caused by the skirts of the many other lines. The absorption of the 105,189 line was so low that it could not be resolved at the lower pressures. Its effect is evident, however, at higher pressures (fig. 5).

6. Nitrogen Dioxide

An absorption line had been predicted at a frequency of 105,158.4 Mc/s for nitrogen dioxide. A continuous search was made from 104,200 to 105,600 Mc/s at very low pressures and spot measurements were made at 104,720, 104,920, and 105,120 Mc/s. In none of the tests was there any indication of appreciable attenuation. It was felt that if a line of nitrogen dioxide exists with significant strength of absorption, its effect would have been noted.

7. Conclusions

The measurements described in this paper have confirmed the presence of absorption lines for carbon monoxide, nitrous oxide, and sulfur dioxide in the frequency range from 100,000 to 117,000 Mc/s. A predicted line for nitrogen dioxide could not be detected. The data can be represented by the Van Vleck-Weisskopf [5] line shape function using a line breadth proportional to pressure and a maximum loss at a given pressure adjusted to fit the measured maximum. One of the predicted lines for sulfur dioxide was found to be a doublet. The numerical results are summarized in the following table:

Gas	Predicted or previously measured frequency	New measurement of frequency	Measured absorption coefficient (α)	Measured line width
	Mc/s	*Mc/s*	$\frac{cm^{-1}}{g}$	*Mc/s per mm Hg*
Carbon monoxide	115,270.56		8.75×10^{-3}	4.25
Nitrous oxide	100,491.76		1.25×10^{-4}	4.25
Sulfur dioxide	104,911.75	104,042 and 104,046.		13.75
	105,333.94	105,189	9×10^{-6}	17.0
Nitrogen dioxide	105,158.4	No line detected		

8. References

[1] A. W. Straiton and C. W. Tolbert, Anomalies in the absorption of radio waves by atmospheric gases, Proc. IRE **48,** 898 (1960).

[2] C. W. Tolbert and A. W. Straiton, Radio propagation measurements in the 100 to 118 Kmcs spectrum, IRE Wescon Conv. Record, Pt. 1, pp. 56–44 (Aug. 1959).

[3] S. N. Ghosh and H. D. Edwards, Rotational frequencies and absorption coefficients of atmospheric gases, Air Force Survey in Geophys., No. 82, Air Force Cambridge Research Center (March 1956).

[4] C. M. Johnson, R. F. Trambarulo, and W. Gordy, Microwave spectroscopy in the region from two to three millimeters, Pt. II, Phys. Rev. **84,** 1178 (1951).

[5] J. H. Van Vleck and V. Weisskopf, On the shape of collision-broadening lines, Rev. Mod. Phys. **17,** 17 (1949).

[6] W. Gordon, W. V. Smith, and R. F. Trambarulo, Microwave spectroscopy, p. 197 (John Wiley & Sons, Inc., New York, N.Y., 1953).

(Paper 65D1—98)

JOURNAL OF RESEARCH of the National Bureau of Standards—D. Radio Propagation
Vol. 65D, No. 1, January–February 1961

On the Theory of Diffraction by a Composite Cylinder [1] [2]

Ralph D. Kodis

(May 31, 1960)

Formulas are developed for the diffracted field around a perfectly conducting cylinder with a dielectric sleeve of arbitrary thickness. These formulas represent the field due to a unit electric line source parallel to the cylinder (either inside or outside the dielectric sleeve) as a spectrum of radial eigenfunctions. It is shown that in each case the field in the region containing the source can be expressed as the sum of two terms, the first of which is a spectral representation of the field when the outer as well as the inner surface of the dielectric is a perfectly conducting boundary. The second term of the sum, which alone involves the properties of the dielectric, is an integral that converges rapidly at high frequencies. Using these general results, perturbation calculations are carried out for three limiting examples of plane wave scattering: (1) Thin dielectric; (2) low-refractive index; (3) very small surface curvature. In the latter approximation the correspondence with optical results is shown.

1. Introduction

The scattering of plane electromagnetic waves by cylindrical obstacles has received detailed theoretical treatment only in the two special cases for which the scalar wave function, Ψ, satisfies either the Dirichlet or the Neumann boundary condition at the cylindrical surface. In electromagnetic terms these problems correspond respectively to the scattering by a perfectly conducting cylinder of a wave whose electric or magnetic vector is parallel to the cylinder axis. For a cylindrical obstacle whose surface is not perfectly conducting a more complicated boundary condition of the type $\Psi+\alpha\partial_n\Psi=0$ is required (sometimes called an impedance boundary condition). In such cases the theory has not been so extensively elaborated.[3]

This paper is concerned with some of the theoretical features of the scattering problem associated with a cylindrical obstacle of this more general kind. In particular we shall examine the scattered wave produced by a dielectric cylinder of circular cross section having a perfectly conducting coaxial core. One aspect of this problem has been investigated experimentally by Tang [1] [4] for an incident wave with electric vector polarized parallel to the cylinder, and in the same paper the Fourier expansion of the wave function has been used for numerical calculations. It seems, however, that no general discussion of the characteristics of the wave solution has been given; it is this task which will now occupy our attention.

2. Derivation of the Green's Function

The cylinder which we shall consider (fig. 1) is composed of a perfectly conducting core of radius a surrounded by a dielectric layer of inner radius a and outer radius b. In the subsequent analysis the relative dielectric constant of the layer will be taken to be a real scalar greater than one, $\epsilon_r=\epsilon/\epsilon_0>1$. That is to say, the refractive index of the dielectric is a real number greater than that which characterizes the surrounding medium (air or vacuum). For a lossy or anisotropic dielectric the theory is unaffected except by the substitution throughout of a complex or tensor dielectric constant for ϵ. Of course, the detailed calculation of field quantities will be much more complicated in such cases.

If the composite cylinder described above is excited by a harmonic line current parallel to its axis (electric line source, $\exp[-i\omega t]$), the task of finding the resultant electric field at

---

[1] Contribution from the Division of Engineering, Brown University, Providence, R.I.

[2] The research reported in this paper has been supported in part by the Office of Naval Research and the David W. Taylor Model Basin under contract Nonr 562(24) and in part by the Electronics Research Directorate of the Air Force Cambridge Research Center under contract AF 19-(604) 4561.

[3] Certain aspects of such problems have been considered by J. R. Wait, Electromagnetic radiation from cylindrical structures, Chapter 16 (Pergamon Press, London, 1959).

[4] Figures in brackets indicate the literature references at the end of this paper.

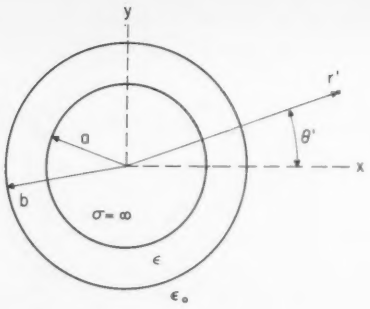

FIGURE 1. *The composite cylinder and coordinate system.*

every point outside the perfect conductor resolves itself into the determination of the Green's functions which satisfy appropriate partial differential equations and boundary conditions. For the moment we shall limit our considerations to the case in which the line source is outside the dielectric. Denoting coplanar position vectors relative to an origin on the cylinder axis by $\mathbf{r}'$ and $\mathbf{r}$ for source and observation points, respectively, we require solutions in the xy-plane for the scalar wave equations

$$(\nabla^2+k_0^2)G_0(\mathbf{r},\mathbf{r}')=-\frac{1}{r}\,\delta(r-r')\delta(\theta-\theta');\ r,r'\geq b \tag{2.1a}$$

$$(\nabla^2+k^2)G_1(\mathbf{r},\mathbf{r}')=0;\ a\leq r\leq b, r'\geq b \tag{2.1b}$$

subject to the following boundary conditions at $r=a$ and $r=b$:

$$G_1(\mathbf{a},\mathbf{r}')=0; \tag{2.2a}$$

$$G_0(\mathbf{b},\mathbf{r}')=G_1(\mathbf{b},\mathbf{r}'); \tag{2.2b}$$

$$\partial_r G_0(\mathbf{b},\mathbf{r}')=\partial_r G_1(\mathbf{b},\mathbf{r}'). \tag{2.2c}$$

Here the wave number, $k=\omega/v$, is related to the dielectric constant and the refractive index, n, of the dielectric according to

$$k=k_0\sqrt{\epsilon_r}=nk_0. \tag{2.3}$$

The mathematical problem defined by eqs (2.1) and (2.2) may be solved in a variety of ways. We shall employ a technique developed and discussed by Titchmarsh [2] and Marcuvitz [3] for separable equations. The procedure consists in constructing so-called characteristic functions which satisfy the related system of ordinary differential equations

$$\left[\frac{d}{dr}\left(r\frac{d}{dr}\right)+rk_0^2-\frac{\lambda}{r}\right]f_0(r,r',\lambda)=-\delta(r-r'), \tag{2.4a}$$

$$\left[\frac{d}{dr}\left(r\frac{d}{dr}\right)+rk^2-\frac{\lambda}{r}\right]f_1(r,r',\lambda)=0, \tag{2.4b}$$

$$\left[\frac{d^2}{d\theta^2}+\lambda\right]g(\theta,\theta',\lambda)=-\delta(\theta-\theta'). \tag{2.4c}$$

These equations are found from (2.1) by separating the polar variables (r, θ) with λ taking the role of separation constant. In addition to (2.4) the functions f_0 and f_1 are required to satisfy boundary conditions corresponding to (2.2), while the angular function g is made unique by certain convergence conditions to be specified. Once the characteristic functions have been explicitly determined from (2.4) and the boundary conditions, the Green's functions required by (2.1) are obtained by an integration in the complex λ-plane. For it can be verified that if

C is a circular contour of infinite radius in this plane, then

$$\frac{1}{2\pi i}\oint_C d\lambda f(r,r',\lambda)=r\delta(r-r'), \tag{2.5a}$$

$$\frac{1}{2\pi i}\oint_C d\lambda g(\theta,\theta'\lambda)=\delta(\theta-\theta'). \tag{2.5b}$$

With the help of (2.4) and (2.5) direct substitution in (2.1) will show that the required Green's function is

$$G(\mathbf{r},\mathbf{r}')=\frac{1}{2\pi i}\int_\Gamma d\lambda f(r,r',\lambda)\,g(\theta,\theta',\lambda), \tag{2.6}$$

where Γ is a contour which encloses the singularities of one of the functions f or g, the sense of the contour being given either by (2.5a) or (2.5b) as the case may be.

In carrying out the procedure outlined above, we shall begin by considering the characteristic function which satisfies (2.4c). It has the form

$$g(\theta,\theta',\lambda)=Ae^{i\nu(\theta_>-\theta_<)}, \tag{2.7}$$

where $\nu^2=\lambda$ and $\theta_>$, $\theta_<$ are respectively the larger and the smaller of the two variables θ and θ'. The positive exponential solution has been chosen to ensure the regularity of g for all values of λ on the principal sheet of the two-sheeted λ surface. On this sheet Im $\nu>0$, and since

$$0<\arg\nu=\arg\sqrt{\lambda}<\pi, \tag{2.8}$$

the region of regularity corresponds to the upper half of the ν-plane. The constant A in (2.7) is determined by the fact that $dg/d\theta$ has unit discontinuity at $\theta=\theta'$ for a delta function source. We thus find from (2.4c) that the characteristic function is

$$g(\theta,\theta',\lambda)=\frac{i}{2\nu}e^{i\nu(\theta_>-\theta_<)}=\frac{i}{2\nu}e^{i\nu|\theta-\theta'|},\quad 0<\arg\nu<\pi. \tag{2.9}$$

It is easy to verify that (2.9) satisfies (2.5b). Since the only singularity of $g(\theta,\theta',\lambda)$ is a branch point at $\lambda=0$, the clockwise contour C may be deformed to an integral around the branch cut which is conveniently taken along the positive real axis of the λ-plane. If the deformed contour is now mapped onto the real axis of the ν-plane by the transformation $\lambda=\nu^2$, the resulting integral is seen to be a representation of the δ-function. Thus

$$\frac{1}{2\pi i}\oint d\lambda g(\theta,\theta',\lambda)=\frac{1}{2\pi}\int_{-\infty}^{\infty}d\nu e^{i\nu|\theta-\theta'|}=\delta(\theta-\theta').$$

The characteristic Green's functions which satisfy (2.4a) and (2.4b) are constructed in a similar fashion but from linear combinations of Bessel functions of order $\nu=\sqrt{\lambda}$. At large distances from the source, $r\gg r'$, they must represent outgoing waves. Furthermore, the interior function must vanish at the conducting surface $r=a$, and the exterior function must behave like a "standing wave" in the region $r'>r\geq b$. In terms of Hankel functions of the first and second kinds the most general expressions which exhibit these characteristics are

$$f_0(r,r',\lambda)=B_0[H_\nu^{(1)}(k_0b)H_\nu^{(2)}(k_0r_<)-DH_\nu^{(2)}(k_0b)H_\nu^{(1)}(k_0r_<)]H_\nu^{(1)}(k_0r_>);\ r,r'\geq b, \tag{2.10}$$

$$f_1(r,r',\lambda)=B_1[H_\nu^{(1)}(ka)H_\nu^{(2)}(kr_<)-H_\nu^{(2)}(ka)H_\nu^{(1)}(kr_<)]H_\nu^{(1)}(k_0r_>);\ a\leq r\leq b,\ r'\geq b. \tag{2.11}$$

Two of the three integration constants appearing in (2.10) and (2.11) are determined by the pair of linear algebraic equations which express the continuity of the radial function and its first derivative at $r=b$. The remaining constant is fixed by the jump in $r\frac{d}{dr}f_0(r,r',\lambda)$ at $r=r'$.

Making use of the Wronskian relation

$$H_\nu^{(1)}(\beta_1)H_\nu^{(2)\prime}(\beta_0)-H_\nu^{(1)\prime}(\beta_0)H_\nu^{(2)}(\beta_0)=-\frac{4i}{\pi\beta_0}, \tag{2.12}$$

and introducing the notation

$$\alpha=ka, \quad \beta=kb, \quad \beta_0=k_0b; \tag{2.13}$$

$$^{5}C_\nu(kr)=H_\nu^{(1)}(\alpha)H_\nu^{(2)}(kr)-H_\nu^{(2)}(\alpha)H_\nu^{(1)}(kr),$$

$$C_\nu'(kr)=H_\nu^{(1)}(\alpha)H_\nu^{(2)\prime}(kr)-H_\nu^{(2)}(\alpha)H_\nu^{(1)\prime}(kr); \tag{2.14}$$

and

$$X_\nu^{(1,2)}=\beta\frac{C_\nu'(\beta)}{C_\nu(\beta)}-\beta_0\frac{H_\nu^{(1,2)\prime}(\beta_0)}{H_\nu^{(1,2)}(\beta_0)}, \tag{2.15}$$

we find that the characteristic function for an exterior source at r' is

$$f_0(r,r',\lambda)=\frac{\pi i}{4}\left[H_\nu^{(2)}(k_0r_<)-\frac{H_\nu^{(2)}(\beta_0)}{H_\nu^{(1)}(\beta_0)}\frac{X_\nu^{(2)}}{X_\nu^{(1)}}H_\nu^{(1)}(k_0r_<)\right]H_\nu^{(1)}(k_0r_>), \quad r\geq b; \tag{2.16}$$

$$f_1(r,r',\lambda)=\frac{C_\nu(kr)H_\nu^{(1)}(k_0r')}{H_\nu^{(1)}(\beta_0)C_\nu(\beta)X_\nu^{(1)}}, \quad r\leq b. \tag{2.17}$$

A direct calculation shows that these functions satisfy (2.5a).

It remains to determine $G(\mathbf{r},\mathbf{r}')$ from (2.6). First we note that the only singularities of f_0 and f_1 in the λ-plane are simple poles at the set of complex values, λ_j, for which

$$X_{\nu_j}^{(1)}=0. \tag{2.18}$$

That these functions have no branch point is easy to verify. With the relations,

$$H_{-\nu}^{(1)}=e^{i\nu\pi}H_\nu^{(1)} \quad \text{and} \quad H_{-\nu}^{(2)}=e^{-i\nu\pi}H_\nu^{(2)},$$

we learn that

$$C_{-\nu}=C_\nu \quad \text{and} \quad X_{-\nu}=X_\nu.$$

It follows that f_0 and f_1 are both single-valued over the entire λ-plane. In accordance with (2.6), we now form the integral

$$G(\mathbf{r},\mathbf{r}')=\frac{1}{2\pi i}\int_\Gamma\frac{id\lambda}{2\nu}f(r,r',\lambda)\,e^{i\nu|\theta-\theta'|}, \tag{2.19}$$

where the contour Γ is chosen to enclose the singularities of f in a positive sense. Since the product function has a branch point at $\lambda=0$, Γ must be indented around the branch cut, which we shall take along the real axis as shown in figure 2. In the ν-plane the resulting contour maps to γ. By virtue of (2.8) and the asymptotic behavior of the Hankel functions, the contribution to (2.19) from the semicircular segment of γ may be made arbitrarily small if the radius of the arc is made large enough. In this way we see that both a discrete and a continuous representation of G are possible,

$$G(\mathbf{r},\mathbf{r}')=\sum \text{Res}\ (\nu=\nu_j)=\frac{1}{2\pi}\int_{-\infty}^{\infty}d\nu\,f(r,r',\lambda)\,e^{i\nu|\theta-\theta'|}. \tag{2.20}$$

---

[5] It would be more explicit to write $C_\nu(\alpha, kr)$, but since subsequent operations on C_ν affect it only as a function of kr, it is perhaps clearer to use the abbreviated notation.

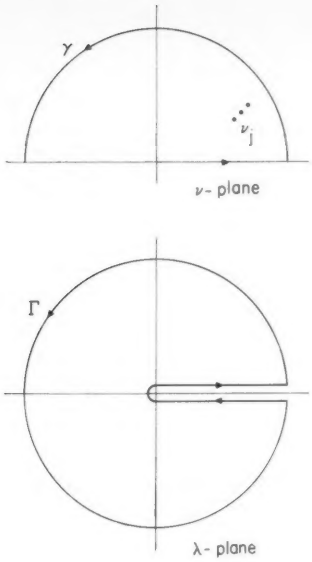

FIGURE 2. *The complex ν and λ planes.*

3. The Discrete Spectrum

The discrete representation of the Green's function is obtained by evaluating the residues of $f(r,r',\lambda)$ from (2.16) and (2.17). A more symmetrical form results if one makes use of the relation

$$X_\nu^{(2)}=X_\nu^{(1)}+\frac{4i}{\pi}\frac{1}{H_\nu^{(1)}(\beta_0)H_\nu^{(2)}(\beta_0)} \tag{3.1}$$

which, at $\nu=\nu_j$, becomes simply

$$X_j^{(2)}=\frac{4i}{\pi}\frac{1}{H_j^{(1)}(\beta_0)H_j^{(2)}(\beta_0)}, \tag{3.2}$$

where the subscript indicates the j^{th} root of (2.18). With this change the residue sums corresponding to (2.19) form discrete spectral representations of the total field due to an exterior line source at $r'\geq b$. They are

$$G_0(\mathbf{r},\mathbf{r}')=i\sum_j \frac{1}{\partial_\nu X_j^{(1)}}\frac{H_j^{(1)}(k_0r)\,H_j^{(1)}(k_0r')}{H_j^{(1)}(\beta_0)\,H_j^{(1)}(\beta_0)}e^{i\nu_j|\theta-\theta'|};\quad r\geq b, \tag{3.3a}$$

$$G_1(\mathbf{r},\mathbf{r}')=i\sum_j \frac{1}{\partial_\nu X_j^{(1)}}\frac{C_j(kr)H_j^{(1)}(k_0r')}{C_j(\beta)H_j^{(1)}(\beta_0)}e^{i\nu_j|\theta-\theta'|};\quad a\leq r\leq b. \tag{3.3b}$$

It is now clear from considerations of symmetry that if the line source is inside the dielectric, $a\leq r'\leq b$, then

$$G_0(\mathbf{r},\mathbf{r}')=i\sum_j \frac{1}{\partial_\nu X_j^{(1)}}\frac{H_j^{(1)}(k_0r)C_j(kr')}{H_j^{(1)}(\beta_0)C_j(\beta)}e^{i\nu_j|\theta-\theta'|};\quad r\geq b, \tag{3.4a}$$

$$G_1(\mathbf{r},\mathbf{r}')=i\sum \frac{1}{\partial_\nu X_j^{(1)}}\frac{C_j(kr)C_j(kr')}{C_j(\beta)C_j(\beta)}e^{i\nu_j|\theta-\theta'|};\quad a\leq r\leq b. \tag{3.4b}$$

It is noteworthy that the representations (3.3a) and (3.4b), with source and observation points

in the same region, are unaffected by an interchange of the variables r and r'. If r and r' are in different regions, however, their interchange turns (3.3b) into (3.4a) and vice versa.

The radial eigenfunction expansions derived above have certain characteristic features which should be mentioned. For fixed r and r' each term of the series represents (in the terminology of Franz) a "creeping wave" propagating in the θ-direction with exponentially damped amplitude. Since θ covers the interval $(-\infty, \infty)$, the total field at any point is the sum of the contributions at $\theta \pm 2m\pi$ for all integral values of m. At high frequencies, however, the imaginary part of ν is a large positive number so that all terms other than the one for which $m=0$ are exponentially small. Asymptotically, (3.3) and (3.4) represent the total field in the range $0<|\theta-\theta'|<2\pi$. It is to be expected, moreover, that the set of ν_j are ordered with increasingly large imaginary parts so that if $|\theta-\theta'|\neq 0$, only the first term of each residue expansion will contribute significantly to the field at high enough frequencies. However, the problem of finding even the first root of (2.18) would seem to be a formidable one.

4. The Continuous Spectrum

An alternative representation of the Green's function as an integral over a continuous spectrum is obtained from (2.19), using (2.16) and (2.17). Since $g(\theta, \theta', \lambda)$ has a branch point singularity at $\lambda=0$, the contour integral becomes

$$G(\mathbf{r},\mathbf{r}')=\frac{1}{4\pi}\int_{\curvearrowright\curvearrowleft}\frac{d\lambda}{\nu}\, e^{i\nu|\theta-\theta'|}\, f(r,r',\lambda), \tag{4.1}$$

where the indicated path is around a branch cut along the real axis of the λ-plane. With the help of (3.1) and the change of variable, $\lambda=\nu^2$, we find from (4.1) that

$$\begin{aligned} G_0(\mathbf{r},\mathbf{r}')=&\frac{i}{8}\int_{-\infty}^{\infty} d\nu[H_\nu^{(1)}(\beta_0)H_\nu^{(2)}(k_0r_<)-H_\nu^{(2)}(\beta_0)H_\nu^{(1)}(k_0r_<)]\,\frac{H_\nu^{(1)}(k_0r_>)}{H_\nu^{(1)}(\beta_0)}\, e^{i\nu|\theta-\theta'} \\ &+\frac{1}{2\pi}\int_{-\infty}^{\infty}\frac{d\nu}{X_\nu^{(1)}}\,\frac{H_\nu^{(1)}(k_0r_<)H_\nu^{(1)}(k_0r_>)}{H_\nu^{(1)}(\beta_0)H_\nu^{(1)}(\beta_0)}\, e^{i\nu|\theta-\theta'|}; \quad r,r'\geq b. \end{aligned} \tag{4.2}$$

Similarly the field inside the dielectric is

$$G_1(\mathbf{r},\mathbf{r}')=\frac{1}{2\pi}\int_{-\infty}^{\infty}\frac{d\nu}{X_\nu^{(1)}}\,\frac{C_\nu(kr)H_\nu^{(1)}(k_0r')}{C_\nu(\beta)H_\nu^{(1)}(\beta_0)}\, e^{i\nu|\theta-\theta'|}; \qquad r'\geq b,\ a\leq r\leq b. \tag{4.3}$$

In this form the Green's function of (4.2) has some interesting features. The first term satisfies all the conditions associated with the field of an electric line source in the vicinity of a perfectly conducting cylinder of radius b when the medium is characterized by the propagation number k_0. One way to see this is to close the integration contour in the upper half of the ν-plane. The residue sum that results is

$$G_c(\mathbf{r},\mathbf{r}')=\frac{\pi}{4}\sum_p\frac{H_p^{(2)}(\beta_0)}{\partial_\nu H_p^{(1)}(\beta_0)}\, H_p^{(1)}(k_0r_<)H_p^{(1)}(k_0r_>)e^{i\nu_p|\theta-\theta'|}, \tag{4.4}$$

where

$$H_p^{(1)}(\beta_0)=H_{\nu_p}^{(1)\prime}(\beta_0)=0. \tag{4.5}$$

From the Wronskian, (2.12), one finds that

$$H_p^{(2)}(\beta_0)=\frac{4i}{\pi\beta_0 H_p^{(1)\prime}(\beta_0)}, \tag{4.6}$$

so that (4.4) can be rearranged in the form

$$G_c(\mathbf{r},\mathbf{r}')=\frac{i}{\beta_0}\sum_p \frac{H_p^{(1)}(k_0 r)\,H_p^{(1)}(k_0 r')}{\partial_\nu H_p^{(1)}(\beta_0)\,H_p^{(1)\prime}(\beta_0)}\,e^{i\nu_p|\theta-\theta'|} \tag{4.7}$$

$$=\frac{1}{2\pi\beta_0}\int_{-\infty}^{\infty} d\nu \frac{H_\nu^{(1)}(k_0 r)\,H_\nu^{(1)}(k_0 r')}{H_\nu^{(1)}(\beta_0)\,H_\nu^{(1)\prime}(\beta_0)}\,e^{i\nu|\theta-\theta'|}. \tag{4.8}$$

These are the results for a conducting cylinder which have been derived in other ways by T. Wu [4] and by the author [5].

We see then that the field of a composite cylinder has as one part the creeping waves of a conducting cylinder. Only the second integral of (4.2) depends upon the parameters of the dielectric (thickness and refraction index) and this dependence resides in the factor $X_\nu^{(1)}$. Indeed as $a\to b$, $X_\nu^{(1)}$ grows without limit and the integral vanishes, leaving the Green's function for a conducting cylinder of radius b. On the other hand, as $k\to k_0$ the limiting value of the second integral of (4.2) is

$$-\frac{i}{8}\int_{-\infty}^{\infty} d\nu\left[\frac{H_\nu^{(2)}(\alpha_0)}{H_\nu^{(1)}(\alpha_0)}-\frac{H_\nu^{(2)}(\beta_0)}{H_\nu^{(1)}(\beta_0)}\right]H_\nu^{(1)}(k_0 r_<)\,H_\nu^{(1)}(k_0 r_>)\,e^{i\nu|\theta-\theta'|},$$

and on substituting we find that the Green's function reduces to that for a conducting cylinder of radius a. These limiting forms will be used later for perturbation calculations.

When the line source is inside the dielectric sleeve, the derivation of the Green's function proceeds in a similar way. We begin with characteristic functions for the radial equations having the form

$$h_0(r,r',\lambda)=A_0 C_\nu(kr_<)\,H_\nu^{(1)}(k_0 r_>);\quad a\le r'\le b,\quad r\ge b, \tag{4.9}$$

$$h_1(r,r',\lambda)=A_1 C_\nu(kr_<)[H_\nu^{(2)}(kr_>)+BH_\nu^{(1)}(kr_>)];\quad a\le r,r'\le b. \tag{4.10}$$

Both functions satisfy the boundary condition at $r_<=a$, and h_0 represents an outgoing cylindrical wave as $r_>\to\infty$. The constants can be evaluated as before, and after a certain amount of manipulation, we find that

$$h_0(r,r',\lambda)=\frac{1}{X_\nu^{(1)}}\frac{C_\nu(kr')\,H_\nu^{(1)}(k_0 r)}{C_\nu(\beta)H_\nu^{(1)}(\beta_0)}; \tag{4.11}$$

$$h_1(r,r',\lambda)=-\frac{\pi i}{4}\frac{C_\nu(kr_<)}{C_\nu(\beta)}\,[H_\nu^{(1)}(\beta)H_\nu^{(2)}(kr_>)-H_\nu^{(2)}(\beta)H_\nu^{(1)}(kr_>)]+\frac{1}{X_\nu^{(1)}}\frac{C_\nu(kr_<)C_\nu(kr_>)}{C_\nu(\beta)C_\nu(\beta)}. \tag{4.12}$$

The exterior function $h_0(r,r',\lambda)$ of (4.11) corresponds exactly to f_1 of (2.17) after an interchange of the variables r and r', so the related Green's function corresponds to (4.3). When both source and observation points are inside the dielectric, the convolution of $h_1(r,r',\lambda)$ with (2.9) around the branch cut of $g(\theta,\theta',\lambda)$ leads to the following integral representation of the Green's function:

$$G_1(\mathbf{r},\mathbf{r}')=-\frac{i}{8}\int_{-\infty}^{\infty} d\nu\frac{C_\nu(kr_<)}{C_\nu(\beta)}\,[H_\nu^{(1)}(\beta)H_\nu^{(2)}(kr_>)-H_\nu^{(2)}(\beta)H_\nu^{(1)}(kr_>)]e^{i\nu|\theta-\theta'|}$$

$$+\frac{1}{2\pi}\int_{-\infty}^{\infty}\frac{d\nu}{X_\nu^{(1)}}\frac{C_\nu(kr_<)C_\nu(kr_>)}{C_\nu(\beta)C_\nu(\beta)}e^{i\nu|\theta-\theta'|}. \tag{4.13}$$

The first term of this Green's function vanishes at $r_<=a$ and $r_>=b$, and one can easily verify that it corresponds exactly to the field of an electric line source inside a dielectric filled coaxial transmission line with perfectly conducting walls. The second term represents the modification of that field due to radiation into the exterior medium.

The residue sum associated with (4.11) has already been given in (3.4). To complete the discussion we shall write down the symmetrical representations for a coaxial line, analogous to (4.7) and (4.8). They follow from the convolution of the first term of (4.12) with $g(\theta,\theta',\lambda)$ around the simple poles located at the points of the λ-plane for which

$$C_{\nu_s}(\beta)=C_s(\beta)=0.$$

It is found that

$$G_{co}(\mathbf{r},\mathbf{r}')=-\frac{i}{\beta}\sum_s \frac{C_s(kr)\,C_s(kr')}{\partial_\nu C_s(\beta)\,C'_s(\beta)}\,e^{i\nu_s|\theta-\theta'|} \tag{4.14}$$

$$=-\frac{1}{2\pi\beta}\int_{-\infty}^{\infty} d\nu\,\frac{C_\nu(kr)\,C_\nu(kr')}{C_\nu(\beta)\,C'_\nu(\beta)}\,e^{i\nu|\theta-\theta'|}, \tag{4.15}$$

where we have made use of the Wronskian relations,

$$H_\nu^{(1,2)}(kr)\,C'_\nu(kr)-H_\nu^{(1,2)'}(kr)\,C_\nu(kr)=-\frac{4i}{\pi kr}H_\nu^{(1,2)}(\alpha). \tag{4.16}$$

5. Plane-Wave Excitation

In order to render more manageable the integrals appearing in (4.2) it is convenient at this stage to turn one's attention to special cases. Since the general class of problems associated with the scattering of a plane wave is of considerable interest, we shall first consider the question of reducing the field to that of an incident plane wave of unit amplitude. This may be done by considering the first term of (4.2), which we shall call G_b,

$$G_b(\mathbf{r},\mathbf{r}')=\frac{i}{8}\int_{-\infty}^{\infty} d\nu\left[H_\nu^{(2)}(k_0r_<)-\frac{H_\nu^{(2)}(\beta_0)}{H_\nu^{(1)}(\beta_0)}H_\nu^{(1)}(k_0r_<)\right]H_\nu^{(1)}(k_0r_>)e^{i\nu|\theta-\theta'|}. \tag{5.1}$$

The Hankel functions, $H_\nu(\rho)$, grow as $\exp\left(\nu\ln\frac{2\nu}{\rho}\right)$ when $\nu\to+\infty$, so the individual terms of this integral diverge and cannot be treated separately. However the divergences may be removed by first putting (5.1) in the form,

$$G_b(\mathbf{r},\mathbf{r}')=\frac{i}{4}\int_0^{\infty} d\nu\left[H_\nu^{(2)}(k_0r_<)-\frac{H_\nu^{(2)}(\beta_0)}{H_\nu^{(1)}(\beta_0)}H_\nu^{(1)}(k_0r_<)\right]H_\nu^{(1)}(k_0r_>)\cos\nu(\theta-\theta'), \tag{5.2}$$

and then making the substitution,

$$H_\nu^{(2)}(\rho)=2J_\nu(\rho)-H_\nu^{(1)}(\rho).$$

With these changes it is found that

$$G_b(\mathbf{r},\mathbf{r}')=\frac{i}{2}\int_0^{\infty} d\nu J_\nu(k_0r_<)H_\nu^{(1)}(k_0r_>)\cos\nu(\theta-\theta')-\frac{i}{2}\int_0^{\infty} d\nu\,\frac{J_\nu(\beta_0)}{H_\nu^{(1)}(\beta_0)}H_\nu^{(1)}(k_0r_<)H_\nu^{(1)}(k_0r_>)\cos\nu(\theta-\theta'). \tag{5.3}$$

Each of these integrals is absolutely convergent.

To establish a correspondence between (5.3) and the required plane wave solution, we follow Wu's procedure and sum the creeping waves for the first term. Then by interchanging the order of summation and integration (or by invoking the Poisson summation formula) it can be shown that

$$\frac{i}{2}\sum_{m=-\infty}^{\infty}\int_0^{\infty} d\nu J_\nu(k_0r_<)H_\nu^{(1)}(k_0r_>)\cos\nu(\theta-\theta'+2m\pi)=\frac{i}{4}H_0^{(1)}(k_0|\mathbf{r}_>-\mathbf{r}_<|), \tag{5.4}$$

where the function on the right is just the free space Green's function representing a unit line source. If we now let $r_> \to \infty$ and make use of the asymptotic form,

$$H_\nu^{(1)}(\rho) \sim \sqrt{\frac{2}{\pi\rho}}\, e^{i\left(\rho-\frac{\pi}{4}\right)}\, e^{-i\nu\frac{\pi}{2}},$$

both sides of (5.4) can be normalized to an incident plane wave of unit amplitude by multiplying with the factor $-4i(2)^{-1/2}(k_0 r_>)\exp -i(k_0 r_> - \pi/4)$. Making these changes in (5.3) and setting $\theta' = 0$ gives the total field, $\psi_b(\mathbf{r})$, when a plane wave from the right is scattered by a conducting cylinder of radius b. This field is

$$\psi_b(\mathbf{r}) = 2\int_0^\infty d\nu J_\nu(k_0 r) e^{-i\nu\frac{\pi}{2}} \cos\nu\theta - 2\int_0^\infty d\nu \frac{J_\nu(\beta_0)}{H_\nu^{(1)}(\beta_0)} H_\nu^{(1)}(k_0 r) e^{-i\nu\frac{\pi}{2}} \cos\nu\theta. \tag{5.5}$$

The procedure that led to (5.4) will also show that

$$2\sum_{m=-\infty}^{\infty} \int_0^\infty d\nu J_\nu(k_0 r) e^{-i\nu\frac{\pi}{2}} \cos\nu(\theta + 2m\pi) = e^{-ik_0 r\cos\theta}. \tag{5.6}$$

When (4.2) has been normalized in accordance with (5.5), the total field outside a dielectric clad cylinder illuminated by a plane wave from the right becomes

$$\psi(\mathbf{r}) = \psi_b(\mathbf{r}) + \frac{2}{\pi i}\int_{-\infty}^{\infty} \frac{d\nu}{X_\nu^{(1)}} \frac{H_\nu^{(1)}(k_0 r)}{[H_\nu^{(1)}(\beta_0)]^2} e^{i\nu\left(\theta-\frac{\pi}{2}\right)}. \tag{5.7}$$

The last term is the modification of the scattered field introduced by the dielectric. It can also be put into the form,

$$\psi_D^{SC}(\mathbf{r}) = \frac{4}{\pi i}\int_0^\infty \frac{d\nu}{X_\nu^{(1)}} \frac{H_\nu^{(1)}(k_0 r)}{[H_\nu^{(1)}(\beta_0)]^2} e^{-i\nu\frac{\pi}{2}} \cos\nu\theta, \tag{5.8}$$

which converges for all values of θ.

6. The Surface Distribution

In this section the distribution of ψ on the dielectric surface will be examined in a number of special cases. This choice of field point does not affect the methods of approximation that will be used, but does simplify the general expression for ψ to a certain extent. For on the circle $r=b$ the first term of (5.7) vanishes, so that the integral to be considered is simply

$$\psi(\mathbf{b}) = \frac{2}{\pi i}\int_{-\infty}^{\infty} \frac{d\nu}{X_\nu^{(1)} H_\nu^{(1)}(\beta_0)} e^{i\nu\left(\theta-\frac{\pi}{2}\right)}. \tag{6.1}$$

In terms of the index of refraction, $n = k/k_0$, and the quantity, $\delta = \beta - \alpha$, the conditions under which approximations to (6.1) will be investigated are (a) $\delta/\beta \ll 1$; (b) $|n-1| \ll 1$; and (c) $k_0 a \gg 1$.

6.1. Thin Dielectric: $\delta/\beta \ll 1$

Since all the dielectric effects are contained in the function,

$$X_\nu^{(1)} = \beta \frac{C_\nu'(\alpha,\beta)}{C_\nu(\alpha,\beta)} - \beta_0 \frac{H_\nu^{(1)\prime}(\beta_0)}{H_\nu^{(1)}(\beta_0)}, \tag{6.2}$$

we require the expansion of $1/X_\nu$ when $a \approx b$. It is clearly advantageous to treat X_ν as a function of the variable α (i. e., the inner radius a) since that parameter appears only in C_ν. Moreover, $H_\nu^{(1)}(\beta_0)$ has no zeros for real ν, so the first term of (6.2) predominates for small δ. We may

therefore put $1/X_\nu \approx F_\nu$, where

$$F_\nu(\alpha)=\frac{1}{\beta}\frac{C_\nu(\alpha,\beta)}{C'_\nu(\alpha,\beta)}=\frac{1}{\beta}\frac{H_\nu^{(1)}(\alpha)H_\nu^{(2)}(\beta)-H_\nu^{(2)}(\alpha)H_\nu^{(1)}(\beta)}{H_\nu^{(1)}(\alpha)H_\nu^{(2)\prime}(\beta)-H_\nu^{(2)}(\alpha)H_\nu^{(1)\prime}(\beta)}. \tag{6.3}$$

Since $\lim_{\alpha\to\beta} F_\nu(\alpha)=0$, the Taylor expansion of (6.3) has the form

$$F_\nu(\beta-\delta)=-\delta F'_\nu(\beta)+\frac{1}{2}\delta^2 F''_\nu(\beta)-\ldots. \tag{6.4}$$

With (6.3) and (6.4) it is a straightforward matter to develop the required series explicitly. We need certain relations of the Wronskian type [6], and up to terms of order δ^4 the result of the calculation turns out to be[6]

$$F_\nu(\alpha)=\frac{\delta}{\beta}+\frac{1}{2}\frac{\delta^2}{\beta^2}+\frac{1}{3}\frac{\delta^3}{\beta^3}+\frac{1}{4}\frac{\delta^4}{\beta^4}+\cdots+\frac{1}{3}\frac{\delta^3}{\beta^3}(\beta^2-\nu^2)+\frac{1}{6}\frac{\delta^4}{\beta^4}(2\beta^2-3\nu^2)+\ldots. \tag{6.5}$$

It is clear that the first group of terms represents the function $-\ln[1-(\delta/\beta)]$, so that

$$\frac{1}{X_\nu^{(1)}}=\ln\frac{b}{a}+\frac{1}{3}\frac{\delta^3}{\beta^3}(\beta^2-\nu^2)+\frac{1}{6}\frac{\delta^4}{\beta^4}(2\beta^2-3\nu^2)+O\left(\frac{\delta^5}{\beta^5}\right). \tag{6.6}$$

On substituting (6.6) in (6.1) a series of integrals is obtained, the first of which is

$$\left(\ln\frac{b}{a}\right)\frac{2}{\pi i}\int_{-\infty}^{\infty}\frac{d\nu}{H_\nu^{(1)}(\beta_0)}e^{i\nu\left(\theta-\frac{\pi}{2}\right)}.$$

The calculation of $\partial_r\psi_b(\mathbf{b})$ from (5.5) shows that except for the constant, $\ln(b/a)$, the last result is just the current distribution on the surface of a perfectly conducting cylinder of radius b. Therefore, to a first approximation for thin dielectric sleeves of any refractive index and radius, the electric field distribution on the dielectric surface is proportional to the magnetic field distribution on a conducting cylinder of the same size when illuminated by a plane wave. The first term involving the refractive index is $O(\delta/\beta)^3$ and is proportional to n^2.

6.2. Low-Refractive Index: $|n-1|\ll 1$

In order to expand the surface distribution,

$$\psi(\mathbf{b})=\frac{2}{\pi i}\int_{-\infty}^{\infty}\frac{d\nu}{X_\nu^{(1)}H_\nu^{(1)}(\beta_0)}e^{i\nu\left(\theta-\frac{\pi}{2}\right)}, \tag{6.1}$$

in the neighborhood of k_0, let us consider the function,

$$G_\nu(k)=[X_\nu^{(1)}H_\nu^{(1)}(\beta_0)]^{-1}. \tag{6.7}$$

Its Taylor expansion may be written in the form

$$G_\nu(k)=G_\nu(k_0)+(n-1)k_0G'_\nu(k_0)+O(n-1)^2, \tag{6.8}$$

where $(n\text{-}1)k_0=k-k_0$. Using (6.2) and the Wronskian (2.12), we find at once that

$$G_\nu(k_0)=\frac{\pi i}{4}\frac{C_\nu(\alpha_0,\beta_0)}{H_\nu^{(1)}(\alpha_0)}=\frac{\pi i}{4}\left[H_\nu^{(2)}(\beta_0)-\frac{H_\nu^{(2)}(\alpha_0)}{H_\nu^{(1)}(\alpha_0)}H_\nu^{(1)}(\beta_0)\right]. \tag{6.9}$$

---

[6] The successive derivatives of $F_\nu(\alpha)$, evaluated at $\alpha=\beta$, are

$$F'_\nu(\beta)=-\frac{1}{\beta} \qquad F'''_\nu(\beta)=-\frac{2}{\beta^3}(1+\beta^2-\nu^2)$$

$$F''_\nu(\beta)=\frac{1}{\beta^2} \qquad F''''_\nu(\beta)=\frac{2}{\beta^4}(3+\tfrac{1}{2}\beta^2-6\nu^2)$$

Thus the first term in the expansion of (6.1) is just $\psi_a(\mathbf{b})$, the total field at $r=b$ when the plane wave is scattered by a conducting cylinder of radius a in the medium k_0.

The second term is found by evaluating

$$G_\nu'(k_0)=-H_\nu^{(1)}(\beta_0)G_\nu^2(k_0)(\partial_k X_\nu^{(1)})_{k=k_0}, \tag{6.10}$$

where ∂_k signifies the differential operator $\partial/\partial k$. Treating C_ν as a function of two dependent variables α, β, and replacing C_ν' by $\partial_\beta C_\nu$, we have

$$\partial_k X_\nu^{(1)}=\partial_k\left[\beta\frac{\partial_\beta C_\nu(\alpha,\beta)}{C_\nu(\alpha,\beta)}\right].$$

It follows, with the help of (6.9), that

$$G_\nu'(k_0)=\frac{\pi^2}{16}\frac{H_\nu^{(1)}(\beta_0)}{[H_\nu^{(1)}(\alpha_0)]^2}\left[bC_\nu\partial_\beta C_\nu+\beta C_\nu\partial_k\partial_\beta C_\nu-\beta\partial_\beta C_\nu\partial_k C_\nu\right]_{k=k_0} \tag{6.11}$$

Since $\partial_k=a\partial_\alpha+b\partial_\beta$, the final bracket of (6.11) becomes, after a little rearrangement,

$$I=kab(C_\nu\partial_\alpha\partial_\beta C_\nu-\partial_\beta C_\nu\partial_\alpha C_\nu)-\beta b(\partial_\beta C_\nu)^2+bC_\nu(\partial_\beta C_\nu+\beta\partial_\beta^2 C_\nu). \tag{6.12}$$

If we now make use of Bessel's differential equation for C_ν, the last parenthesis of (6.12) is seen to be

$$\partial_\beta C_\nu+\beta\partial_\beta^2 C_\nu=\frac{1}{\beta}(\nu^2-\beta^2)C_\nu. \tag{6.13}$$

Moreover, the bracketed expression in the first term of (6.12) can be represented by the Wronskian determinant

$$W(C_\nu,\partial_\beta C_\nu)=\begin{vmatrix} C_\nu & \partial_\beta C_\nu \\ \partial_\alpha C_\nu & \partial_\alpha\partial_\beta C_\nu \end{vmatrix}. \tag{6.14}$$

In the usual way [7] one can show that

$$\partial_\beta(\beta W)=0,$$

which implies that βW is independent of β. To find the value of the constant we let $\beta=\alpha$. Then $C_\nu=0$, and

$$\lim_{\beta\to\alpha}\beta W=-\alpha(\partial_\alpha C_\nu\partial_\beta C_\nu)_{\beta=\alpha}.$$

In the limit the derivatives are ordinary Wronskians like (2.12), and it follows that

$$W=-\frac{16}{\pi^2\alpha\beta}. \tag{6.15}$$

The result of substituting (6.13) and (6.15) into (6.12) is

$$I=-\frac{16}{\pi^2 k}-\frac{1}{k}(\beta\partial_\beta C_\nu)^2-\frac{1}{k}(\beta^2-\nu^2)C_\nu^2.$$

With this result, eq (6.8), (6.9), and (6.11) can be combined into an explicit expression for the first term of the expansion of $G_\nu(k)$ near $k=k_0$. Substitution in (6.1) yields the following perturbed distribution at $r=b$ when $n\approx 1$:

$$\psi(\mathbf{b})\approx\psi_a(\mathbf{b})-(n-1)\left\{\frac{2}{\pi i}\int_{-\infty}^{\infty}\frac{H_\nu^{(1)}(\beta_0)}{[H_\nu^{(1)}(\alpha_0)]^2}e^{i\nu\left(\theta-\frac{\pi}{2}\right)}d\nu+\frac{\pi}{8i}\int_{-\infty}^{\infty}\left[\frac{\beta_0 C_\nu'(\alpha_0,\beta_0)}{H_\nu^{(1)}(\alpha_0)}\right]^2 H_\nu^{(1)}(\beta_0)e^{i\nu\left(\theta-\frac{\pi}{2}\right)}d\nu\right.$$
$$\left.+\frac{\pi}{8i}\int_{-\infty}^{\infty}(\beta_0^2-\nu^2)\left[\frac{C_\nu(\alpha_0,\beta_0)}{H_\nu^{(1)}(\alpha_0)}\right]^2 H_\nu^{(1)}(\beta_0)e^{i\nu\left(\theta-\frac{\pi}{2}\right)}d\nu\right\}. \tag{6.16}$$

If one is interested in the perturbation introduced by the dielectric at points outside the sleeve, it is only necessary to put $H_\nu^{(1)}(k_0 r)$ for $H_\nu^{(1)}(\beta_0)$ wherever that function appears explicitly in (6.16). Whether the field point is on the surface or outside the sleeve, however, it is readily verifiable that all the integrals converge and that the bracket vanishes when $b=a$, leaving only the field of the conducting cylinder. In general, it seems that none of the correction terms in (6.16) can be neglected.

6.3. Very-High Frequencies: $k_0 a \gg 1$

The last method of approximation to be dealt with is useful when both inner and outer cylinders are large compared to the wavelength in either medium. By combining the longer wavelength with the shorter radius these conditions are satisfied by the single relation, $\alpha_0 \gg 1$. When this requirement is met, no further restrictions need be imposed, *a priori*, on either the thickness of the dielectric sleeve or on its refractive index. Since we shall consider only the contribution to (6.1) from that part of the integral for which $|\nu|+3|\nu|^{1/3}<\alpha_0$, it is possible to use the Debye approximation for all Hankel functions. To this order of accuracy we may expect that the integration will yield the optical rays, but no diffraction effects.

For a typical Hankel function the appropriate asymptotic form is

$$H_\nu^{(1)}(\beta_0) \sim 2^{1/2} e^{-i\frac{\pi}{4}} (\pi\beta_0 \sin\eta_0)^{-1/2} \exp i\beta_0 f(\eta_0), \tag{6.17}$$

where η_0 is the real angle

$$\eta_0 = \cos^{-1}(\nu/\beta_0), \tag{6.18}$$

and

$$f(\eta_0) = \sin\eta_0 - \eta_0 \cos\eta_0. \tag{6.19}$$

The corresponding approximation for the derivative with respect to the argument, β_0, is

$$H_\nu^{(1)\prime}(\beta_0) \sim i \sin\eta_0 H_\nu^{(1)}(\beta_0). \tag{6.20}$$

With (6.17) and (6.20) it follows that

$$\beta_0 \frac{H_\nu^{(1)\prime}(\beta_0)}{H_\nu^{(1)}(\beta_0)} \sim i\beta_0 \sin\eta_0. \tag{6.21}$$

In a similar way, by defining the angles

$$\eta = \cos^{-1}(\nu/\beta); \qquad \zeta = \cos^{-1}(\nu/\alpha), \tag{6.22}$$

and the function

$$F(\nu) = \beta f(\eta) - \alpha f(\zeta), \tag{6.23}$$

one can show that

$$\beta \frac{C_\nu'(\beta)}{C_\nu(\beta)} \sim i\beta \sin\eta \frac{e^{iF(\nu)}+e^{-iF(\nu)}}{e^{iF(\nu)}-e^{-iF(\nu)}}. \tag{6.24}$$

If (6.21) and (6.24) are now combined according to (6.2), we find that

$$\frac{1}{X_\nu} \sim \frac{1}{\beta_0 \sin\eta_0} \frac{i\rho}{1+\rho} \frac{1-e^{2iF(\nu)}}{1+\tau e^{2iF(\nu)}}, \tag{6.25}$$

where ρ and τ signify the ratios,

$$\rho = \frac{\beta_0 \sin\eta_0}{\beta \sin\eta}; \qquad \tau = \frac{1-\rho}{1+\rho}. \tag{6.26}$$

Now for all $\nu^2<\beta_0^2$, $\beta \sin\eta > \beta_0 \sin\eta_0$, so that $0>\rho>-1$. Consequently, $0<\tau<1$ and $|\tau \exp 2iF(\nu)|<1$. The denominator of (6.25) can therefore be represented by its Taylor expansion, and it follows that

$$\frac{1}{X_\nu^{(1)}} \sim \frac{1}{\beta_0 \sin\eta_0} \frac{i\rho}{1+\rho} [1-(1+\tau)e^{2iF(\nu)}+(1+\tau)\tau e^{4iF(\nu)}-(1+\tau)\tau^2 e^{6iF(\nu)}+\ldots]. \tag{6.27}$$

This result already makes evident the ray nature of the approximation. Successive terms of the series correspond to the rays which are, (1) reflected by the sleeve, (2) reflected once at the conducting cylinder, (3) reflected once at the conducting cylinder and once internally at the dielectric surface, etc. The phase function of each term corresponds to the number of path segments a ray traverses in the dielectric (with a minus sign added for each reflection at the conducting cylinder), and its amplitude function includes the appropriate transmission and reflection coefficients for each contact with the dielectric surface. Since these quantities are all functions of the integration variable, successive terms can be evaluated in detail only by more and more intricate stationary phase approximations. There is, however, one limiting case for which it is relatively easy to establish the correspondence between the terms of (6.27) and optical rays. When the radii a and b become indefinitely large, while their difference, $d=b-a$, remains constant, the solution for the cylindrical problem at each point $\mathbf{b}=(b,\theta)$ of the dielectric surface approaches that for a plane wave scattered by a conducting plane sheet with a dielectric coating of thickness d, the dielectric surface being tangent to the cylinder at the point in question.

To see how this comes about let us substitute (6.27) and (6.17) in (6.1). The first integral of the resulting asymptotic series becomes

$$\psi^{(1)}(\mathbf{b})=\left(\frac{2}{\pi}\right)^{1/2} e^{i\frac{\pi}{4}}\int_{-A}^{A} d\nu(\beta_0 \sin\eta_0)^{-1/2}\frac{\rho}{1+\rho}\exp ig^{(1)}(\nu), \tag{6.28}$$

where the limits on the integral define the interval within which the Debye approximations are valid and where

$$g^{(1)}(\nu)=-\beta_0 f(\eta_0)+\nu\theta-\frac{1}{2}\nu\pi, \qquad 0<\theta. \tag{6.29}$$

For large β_0 the principal contributions to this integral come from the neighborhood of the stationary points of $g^{(1)}(\nu)$ in $(-A, A)$. Since the asymptotic integrand decays exponentially outside this interval, one may extend its limits to $(-\infty, \infty)$ without appreciable error. Then if a stationary point of $g^{(1)}(\nu)$ is located at $\nu=\nu_1$, the Taylor expansion of (6.28) in the vicinity of this point gives as its first approximation,

$$\psi^{(1)}(\mathbf{b})\sim\left(\frac{2}{\pi\beta_0}\right)^{1/2}(\sin\eta_0)_1^{-1/2}\frac{\rho_1}{1+\rho_1}e^{i\frac{\pi}{4}}\int_{-\infty}^{\infty} d\nu \exp i\left[g^{(1)}(\nu_1)+\frac{\lambda^2}{2}\partial_\nu^2 g^{(1)}(\nu_1)\right], \tag{6.30}$$

where $\lambda=\nu-\nu_1$ and the subscripts indicate functions that are to be evaluated at $\nu=\nu_1$.

The value of ν required in (6.30) is that which reduces $\partial_\nu g^{(1)}(\nu_1)=0$ to an identity. It can be shown that this occurs for the angle $(\eta_0)_1=\frac{1}{2}\pi-\theta$, corresponding to

$$\nu_1=\beta_0\sin\theta \tag{6.31}$$

According to the condition specified prior to (6.17), the angle θ must therefore be such that

$$\sin\theta+3\beta^{-2/3}(\sin\theta)^{1/3}<\frac{\alpha_0}{\beta_0}. \tag{6.32}$$

It is clear that this inequality cannot under any circumstances be satisfied at the shadow boundary where $\theta=\pi/2$. With (6.31) and (6.26) we determine that

$$\partial_\nu^2 g^{(1)}(\nu_1)=-\frac{1}{\beta_0\cos\theta}$$

and

$$\frac{2\rho_1}{1+\rho_1}=\frac{2\beta_0\cos\theta}{\beta_0\cos\theta+\beta\cos\theta_n}=1+R, \tag{6.33}$$

where R is the reflection coefficient for a plane dielectric surface [8] and the angles of incidence

and refraction are related by

$$\frac{\sin\theta}{\sin\theta_n}=n.$$

With these results, we have

$$\psi^{(1)}(\mathbf{b})\sim\frac{1}{2}(1+R)\,e^{-i\beta_0\cos\theta}\left[\frac{2}{\pi\beta_0\cos\theta}\right]^{1/2}e^{i\frac{\pi}{4}}\int_{-\infty}^{\infty}d\lambda\,\exp\left[-i\frac{\lambda^2}{2\beta_0\cos\theta}\right]. \tag{6.34}$$

The value of the infinite integral is given in standard tables, and (6.34) can be reduced to

$$\psi^{(1)}(\mathbf{b})\sim(1+R)\,e^{-i\beta_0\cos\theta}, \tag{6.35}$$

which corresponds in amplitude and phase to the sum of the incident and reflected rays at the dielectric interface for angles $\theta<\frac{\pi}{2}$ (fig. 3). Note that further restrictions on θ, such as (6.32), are no longer required.

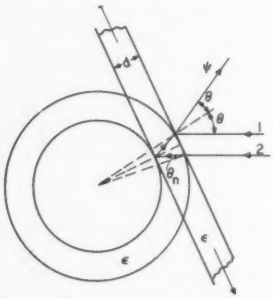

FIGURE 3. *Depicting ray geometry.*

The second term in the expansion of (6.1) is

$$\psi^{(2)}(\mathbf{b})=-\left(\frac{2}{\pi}\right)^{1/2}e^{i\frac{\pi}{4}}\int_{-A}^{A}d\nu(\beta_0\sin\eta_0)^{-1/2}\frac{2\rho}{(1+\rho)^2}\exp\,ig^{(2)}(\nu), \tag{6.36}$$

where

$$g^{(2)}(\nu)=2F(\nu)+g^{(1)}(\nu). \tag{6.37}$$

Again, after finding the point ν_2 at which $\partial_\nu g^{(2)}(\nu_2)$ vanishes, we can approximate (6.36) with

$$\psi^{(2)}(\mathbf{b})\sim-\left(\frac{2}{\pi\beta_0}\right)^{1/2}(\sin\eta_0)_2\frac{2\rho_2}{(1+\rho_2)^2}\,e^{i\frac{\pi}{4}}\int_{-\infty}^{\infty}d\lambda\,\exp\,i\left[g^{(2)}(\nu_2)+\frac{\lambda^2}{2}\partial_\nu^2 g^{(2)}(\nu_2)\right], \tag{6.38}$$

where $\lambda=\nu-\nu_2$ and the subscripts indicate functions that are to be evaluated at $\nu=\nu_2$.

According to (6.37) the required stationary point is the solution of

$$\partial_\nu[2F(\nu)+g^{(1)}(\nu)]=0. \tag{6.39}$$

With the help of (6.23) and (6.29) it may be shown that this equation is equivalent to

$$-2(\eta-\zeta)+\eta_0=\frac{1}{2}\pi-\theta. \tag{6.40}$$

In order to discuss the solution of (6.40) in the plane limit we shall assume that $(\eta-\zeta)$ is small so that sin $(\eta-\zeta)$ is approximately equal to its argument. Then

$$\eta-\zeta\approx\frac{\cos\eta\,\delta}{\sin\eta\,\beta}, \tag{6.41}$$

where $\delta=kd$ and terms of order $(\delta/\beta)^2$ have been neglected. Accordingly, if $(\eta-\zeta)$ is to be a small quantity it is sufficient that $\delta/\beta=d/b<<1$, provided $\eta\neq 0$ or what amounts to the same thing, $\nu^2\neq\beta^2$. This requirement is, of course, the same as that already imposed by the original Debye approximations. With this understanding, (6.40) can be put into the more convenient form

$$\cos\left[\eta_0-2\frac{\cos\eta}{\sin\eta}\frac{\delta}{\beta}\right]=\sin\theta, \tag{6.42}$$

Expanding the left-hand side of this relation up to terms of order δ/β, we obtain

$$\nu_2-\nu_1=-2\rho_1\nu_1\frac{\delta}{\beta}, \tag{6.43}$$

where as before

$$\nu_1=\beta_0\sin\theta; \qquad \rho_1=\frac{\beta_0\cos\theta}{\beta\cos\theta_n}.$$

Since in this limit ν_2 is a perturbation on ν_1, all functions of ν_2 in (6.38) have Taylor expansions in the neighborhood of ν_1. Retaining terms in δ/β if they affect the phase of $\psi^{(2)}$ but not otherwise, we find, for example, that

$$\begin{aligned} g^{(2)}(\nu_2)&=g^{(2)}(\nu_1)+(\nu_2-\nu_1)g^{(2)\prime}(\nu_1)+\ldots \\ &=-\beta_0\cos\theta+2(\beta\cos\theta_n)\frac{\delta}{\beta}+O\left(\frac{\delta}{\beta}\right)^2. \end{aligned} \tag{6.44}$$

To this degree of approximation (6.38) becomes

$$\psi^{(2)}(\mathbf{b})\sim-\frac{1}{2}(1+R)(1-R)\left[\frac{2}{\pi\beta_0\cos\theta}\right]^{\frac{1}{2}}\exp\left[-i\beta_0\cos\theta+2i\delta\cos\theta_n\right]e^{i\frac{\pi}{4}}\int_{-\infty}^{\infty}d\lambda\exp\left[-i\frac{\lambda^2}{2\beta_0\cos\theta}\right),$$

and we finally obtain (6.45)

$$\psi^{(2)}(\mathbf{b})\sim(1+R)(1-R)\exp\left[-i\beta_0\cos\theta+2i\delta\cos\theta_n\right], \tag{6.46}$$

where

$$1-R=\frac{2\beta\cos\theta_n}{\beta_0\cos\theta+\beta\cos\theta_n}=T_n. \tag{6.47}$$

The quantity, T_n, is the transmission coefficient of a ray incident on the dielectric surface from the interior at an angle θ_n with the normal. If the transmission coefficient from the external region is designated by $T=1+R$, then the sum of (6.35) and (6.46) has the form

$$\psi(\mathbf{b})\sim e^{-i\beta_0\cos\theta}\left[T-TT_n e^{2i\delta\cos\theta_n}+\ldots\right]. \tag{6.48}$$

These two rays are depicted in figure 3. It is an elementary exercise in geometry to show that their amplitudes and phases are exactly those predicted by ray optics, provided the dielectric surface is nearly plane over the arc segment illuminated by the bundle included between rays 1 and 2. Additional rays for this quasi-plane example may be written down by inspection from the further terms of (6.27).

7. References

[1] C. C. Tang, J. Appl. Phys. **28**, 628 (1957).
[2] E. C. Titchmarsh, Eigenfunction expansions, p. 113–16 (Oxford University Press, Oxford, England, 1958).
[3] N. Marcuvitz, Commun. Pure Appl. Math. **4**, 284 (1951).
[4] T. T. Wu, Phys. Rev. **104**, 1201 (1956).
[5] R. D. Kodis, Brown Univ. Sci. Rpt. 1391/8, AFCRC-TN-57-957 (October 1957).
[6] G. N. Watson, Bessel functions, p. 76, 2d ed. (Cambridge University Press, New York 22, N.Y., 1945).
[7] G. N. Watson, Bessel functions, p. 42, 2d ed. (Cambridge University Press, New York 22, N.Y., 1945).
[8] J. A. Stratton, Electromagnetic theory, p. 492–4, 1st ed. (McGraw-Hill Book Co., Inc., New York, N.Y., 1941).

(Paper 65D1–99)

JOURNAL OF RESEARCH of the National Bureau of Standards—D. Radio Propagation
Vol. 65D, No. 1, January-February 1961

An Atlas of Oblique-Incidence Ionograms (A Digest)[1]

Vaughn Agy, Kenneth Davies, and Roger Salaman

(June 24, 1960)

A brief description is given of an atlas (published separately) of oblique-incidence ionograms obtained on two paths, 1,150 and 2,370 kilometers.

The purpose of this note is to describe an atlas of oblique-incidence ionograms recently compiled by the authors [1].[2] The atlas is intended to serve a twofold purpose: First, to provide a reasonably comprehensive introduction to this type of ionogram for those workers who are not now familiar with them, and second, to present records which illustrate the various propagation characteristics of the specific paths used by the National Bureau of Standards. An analytical study of the technique and the experimental results was given by Agy and Davies [2]. To date, NBS sweep-frequency experiments have been carried out over two approximately east-west paths [2]: Washington, D.C.—St. Louis, Mo. (about 1,150 km) [3, 4], and Washington, D.C.—Boulder, Colo. (about 2,370 km) [5]. A vertical incidence ionosonde was operated at the path midpoint in each case.

The atlas is divided into four parts, namely: 1. Introduction; 2. Washington—St. Louis routine records; 3. Washington—Boulder routine records; and 4. Washington—Boulder experimental records.

The introduction contains a discussion of the equipment together with charts necessary for the identification of certain modes of propagation and a brief description of the records.

The next two sections illustrate diurnal and seasonal variations, layer formation and disappearance, spread echo, MUF extension and several other phenomena of interest. The magnetic K figures are included to provide a basis for judging the effect of magnetic disturbance. The accompanying figure is a sample page from the section dealing with the Washington—Boulder path.

The final section is devoted to various short term experiments over the Washington—Boulder path. Expanded time-delay and frequency scales were used as well as shorter pulse durations than in the previous cases. Equipment effects such as pulse width and receiver gain are considered. Detailed sequences of oblique ionograms during magnetic storms are shown together with the midpoint vertical-incidence ionograms. A sequence of A-scan records is presented which shows how the field strength varied near the MUF during one sweep.

References

[1] V. Agy, K. Davies, and R. Salaman, An atlas of oblique-incidence ionograms, NBS Technical Note No. 31 (1959). Distributed by United States Department of Commerce, Office of Technical Services, Washington 25, D.C. Price $2.25.

[2] V. Agy and K. Davies, Ionospheric investigations using the sweep-frequency pulse technique at oblique-incidence, J. Research NBS **63D**, 151 (1959).

[3] P. G. Sulzer and E. E. Ferguson, Sweep-frequency oblique-incidence ionospheric measurements over an 1,150 km path, Proc. IRE **40**, 1124 (1952).

[4] B. Wieder, Some results of a sweep-frequency propagation experiment over an 1,150 km east-west path, J. Geophys. Research **60**, 395 (1955).

[5] P. G. Sulzer, Sweep-frequency pulse-transmission measurements over a 2,400 km path, J. Geophys. Research **60**, 411 (1955).

[1] Contribution from Central Radio Propagation Laboratory, National Bureau of Standards, Boulder, Colo.

[2] Figures in brackets indicate the literature references at the end of this paper.

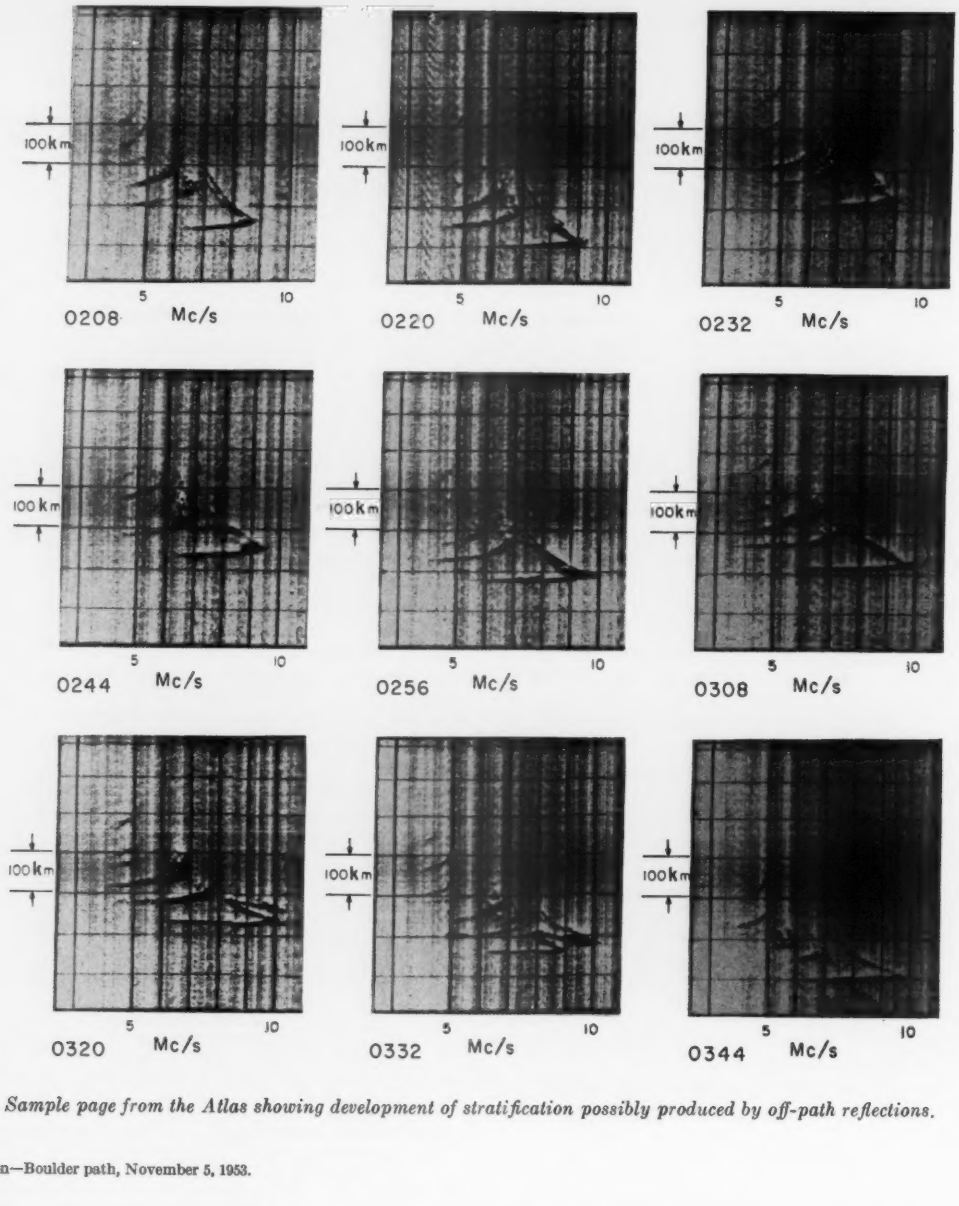

Sample page from the Atlas showing development of stratification possibly produced by off-path reflections.

Washington—Boulder path, November 5, 1953.

(Paper 65D1–100)

JOURNAL OF RESEARCH of the National Bureau of Standards—D. Radio Propagation
Vol. 65D, No. 1, January-February 1961

A New Approach to the Mode Theory of VLF Propagation[1]

James R. Wait

(July 14, 1960)

An attempt is made in this paper to present a concise derivation of the mode theory of VLF propagation. Taking note of the fact that the important modes for long-distance propagation are near grazing, suitable approximate forms of the wave functions are introduced at the outset, rather than at the end, of the analysis. It is thus possible to account for the influence of earth curvature in a relatively concise manner. The influence of the earth's magnetic field is also discussed. Finally, numerical results for the attenuation and the phase velocity of the dominant mode are presented.

1. Introduction

Despite the extensive work [1–5] [2] on the waveguide mode theory of VLF propagation, certain aspects of the subject are not yet resolved. The difficulty appears in finding suitable approximations to the spherical wave functions in the rigorous solution. It is the purpose of this paper to discuss this problem in some detail. For a background of the subject the reader is referred to a recent comprehensive paper on the general subject [6]. Here the solutions will be obtained from a somewhat different point of view.

2. The Groundwave Field

We will start by assuming that the source is a vertical electric dipole located on the surface of a smooth spherical earth of radius a, conductivity σ and dielectric constant ϵ. Spherical coordinates (r,θ,ϕ) are chosen with the dipole located at $r=a$ and $\theta=0$. For harmonic time dependence the radial electric field component is written in the form

$$E_r \cong \frac{e^{-ika\theta}}{a(\theta \sin\theta)^{1/2}} V_0 e^{i\omega\tau} \tag{1}$$

apart from a constant factor.[3] In the case of an airless earth, in which the ionosphere is neglected, it is well known that V_0 may be written in the form [7,8]

$$V_0 \cong 2(\pi x)^{1/2} e^{-i\pi/4} \sum_{s=1,2,\ldots}^{\infty} \frac{e^{-ixt_s}}{(t_s-q^2)} \frac{w_1(t_s-y)}{w_1(t_s)}, \tag{2}$$

where

$$x=\left(\frac{ka}{2}\right)^{1/3}\theta,\ y=\left(\frac{2}{ka}\right)^{1/3}k(r-a),\ iq=\left(\frac{ka}{2}\right)^{1/3}\Delta,$$

and

$$\Delta=\left(\frac{i\epsilon_0\omega}{\sigma+i\epsilon\omega}\right)^{1/2}\left[1-\frac{i\epsilon_0\omega}{\sigma+i\epsilon\omega}\right]^{1/2}.$$

The coefficients t_s are solutions of the equation

$$w_1'(t)-qw_1(t)=0, \tag{3}$$

where $w_1(t)$ is an Airy integral and the prime indicates a derivative with respect to t. In terms of Hankel functions of order one third,

$$w_1(t)=\exp(-2\pi i/3)(-\pi t/3)^{1/2}H_{1/3}^{(2)}[(2/3)(-t)^{3/2}]. \tag{4}$$

The above formula for V_0 is usually called the residue series representation for the groundwave field. It is often used as the basis for field strength calculations on a spherical smooth earth on the assumption that the ionosphere may be neglected or separately accounted for. It is valid when $ka>>1$ and $r-a<<a$. It is also required that the values of $|t_s|$ for the important modes are not large compared with unity. Such approximations as these are certainly valid for VLF waves.

For the purposes of the subsequent analysis V_0 is written as a contour integral in the manner

$$V_0=e^{i\pi/4}(x/\pi)^{\frac{1}{2}}\oint \frac{e^{-ixt}w_1(t-y)}{w_1'(t)-qw_1(t)}dt. \tag{5}$$

The contour encloses the poles at $t=t_s$ in a clockwise sense. The equivalence of eq (2) and (5) is easily verified on noting that

$$w_1''(t_s)-qw_1'(t_s)=(t_s-q^2)w_1(t_s)$$

since

$$w_1''(t)=tw_1(t),$$

and

$$w_1'(t_s)=qw_1(t_s).$$

[1] Contribution from Central Radio Propagation Laboratory, National Bureau of Standards, Boulder, Colo.
[2] Figures in brackets indicate the literature references on page 46.
[3] Equation (1) is normalized such that V_0 approaches 2 for $ka\to\infty$ and $\Delta\to 0$.

3. The Sky Waves

We will now enclose the earth by a concentric reflecting shell located at $r=a+h$ as indicated in figure 1. The electrical properties of this layer will not be specified at the moment, but it is assumed that an upgoing wave will be converted to a downgoing wave. Thus after one reflection

$$e^{-ixt}w_1(t-y)$$

is converted to

$$A(t)e^{-ixt}w_2(t-y),$$

where

$$w_2(t)=\exp(2\pi i/3)(-\pi t/3)^{1/2}H^{(1)}_{1/3}[(2/3)(-t)^{3/2}], \quad (6)$$

and $A(t)$ is unknown function of t. The boundary condition at $r=a+h$ is written in the form

$$\left[\frac{dw(t-y)}{dy}-q_i w(t-y)\right]_{y=y_0}=0 \quad (7)$$

where

$$y_0=\left(\frac{2}{ka}\right)^{1/3}kh$$

and $iq_i=\left(\frac{ka}{2}\right)^{1/3}\Delta_i$. The quantity Δ_i involves the properties of the layer beyond $r=a+h$; for the moment it is not given explicitly. Formally $\Delta_i=Z/\eta_0$ where Z is the radial surface impedance at $r=a+h$. Most generally Δ_i (or Z) is a function of t but usually it may be taken as a constant [6]. On identifying $w(t-y)$ with $w_1(t-y)+A(t)w_2(t-y)$, it readily follows from eq (7) that

$$A(t)=-\left[\frac{w_1'(t-y_0)+q_i w_1(t-y_0)}{w_2'(t-y_0)+q_i w_2(t-y_0)}\right]. \quad (8)$$

The downcoming wave characterized by the function $w_2(t-y)$ is now reflected at the ground and thus it generates a new upgoing wave of the form

$$A(t)B(t)w_1(t-y)e^{-ixt}$$

The boundary condition at $r=a$ may be written

$$\left[\frac{dw(t-y)}{dy}+qw(t-y)\right]_{y=0}=0. \quad (9)$$

Then on identifying $w(t-y)$ with the sum of the downcoming and the upgoing wave it follows that

$$B(t)=-\left[\frac{w_2'(t)-qw_2(t)}{w_1'(t)-qw_1(t)}\right]. \quad (10)$$

The process may be repeated any number of times. The resultant field can thus be written as a sum

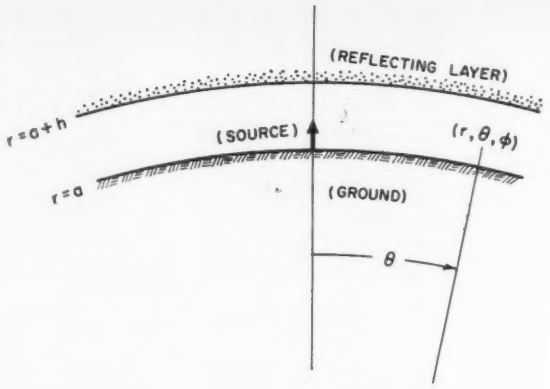

FIGURE 1. *A sketch of the model employed in this paper.*

The surface of the ground and the lower edge of the reflecting layer are concentric spherical surfaces.

$$E_z=\frac{e^{-ika\theta}}{a(\theta\sin\theta)^{1/2}}V, \quad (11)$$

where

$$V=\sum_{j=0,1,2\ldots}V_j, \quad (12)$$

and

$$V_j=e^{i\pi/4}\left(\frac{x}{\pi}\right)^{1/2}\oint\frac{e^{-ixt}w_1(t-y)}{w_1'(t)-qw_1(t)}[A(t)B(t)]^{j/2}dt \quad (13)$$

for j even, while

$$V_j=e^{i\pi/4}\left(\frac{x}{\pi}\right)^{1/2}\oint\frac{e^{-ixt}w_2(t-y)}{w_1'(t)-qw_1(t)}[A(t)]^{\frac{j+1}{2}}[B(t)]^{\frac{j-1}{2}}dt \quad (14)$$

for j odd. Formally these are geometrical progressions so they can be summed. On interchanging the order of integration and summation, this leads to the integral representation

$$V=e^{i\pi/4}\left(\frac{x}{\pi}\right)^{1/2}\oint\frac{e^{-ixt}[w_1(t-y)+A(t)w_2(t-y)]}{[w_1'(t)-qw_1(t)][1-A(t)B(t)]}dt$$

$$=e^{i\pi/4}\left(\frac{x}{\pi}\right)^{1/2}\oint\frac{e^{-ixt}[w_1(t-y)+A(t)w_2(t-y)]}{w_1'(t)-qw_1(t)+A(t)[w_2'(t)-qw_2(t)]}dt. \quad (15)$$

Now the contour is to enclose the complex poles which occur at $t=t_n$ where t_n is a solution of

$$1-A(t)B(t)=0. \quad (16)$$

The residue series representation for the total field is thus given by

$$V=-2(\pi x)^{1/2}e^{-i\pi/4}$$

$$\times\sum_{n=0,1,2\ldots}\frac{e^{-ixt_n}[w_1(t_n-y)+A(t_n)w_2(t_n-y)]}{[w_1(t_n)-qw_1(t_n)]\left[\frac{\partial}{\partial t}A(t)B(t)\right]_{t=t_n}}. \quad (17)$$

As in the residue series formula for the groundwave field, eq (17) is valid for $ka>>1$ and $h<<a$.

The interpretation of the preceding results is now discussed and certain simplifications made to facilitate computation. If $(-t)>>1$, it follows that

$$B(t)=-\left[\frac{w_2'(t)-qw_2(t)}{w_1'(t)-qw_1(t)}\right]$$

$$\cong\left[\frac{-i(-t)^{1/2}-q}{i(-t)^{1/2}-q}\right]e^{-i\pi/2}e^{i\frac{4}{3}(-t)^{3/2}}. \quad (18)$$

On making the substitution $(-t)^{1/2}=\left(\frac{ka}{2}\right)^{1/3}C$ and noting that $iq=\left(\frac{ka}{2}\right)^{1/3}\Delta$, it follows that

$$B(t)\cong\frac{C-\Delta}{C+\Delta}e^{i\pi/2}e^{i\frac{4}{3}\left(\frac{ka}{2}\right)C^3}. \quad (19)$$

If C is identified as the cosine of an angle of incidence, $(C-\Delta)/(C+\Delta)$ can be recognized as a Fresnel reflection coefficient. Similarly, if $(y_0-t)>>1$

$$A(t)\cong\frac{C'-\Delta_i}{C'+\Delta_i}e^{-i\pi/2}e^{-i\frac{4}{3}\left(\frac{ka}{2}\right)(C')^3}, \quad (20)$$

where $\left(\frac{ka}{2}\right)^{1/3}C'=(y_0-t)^{1/2}$. C' may be identified as the cosine of the angle of incidence at the ionosphere. It is also noted that

$$C'=\left(C^2+\frac{2h}{a}\right)^{1/2}. \quad (21)$$

The factor $(C'-\Delta_i)/(C'+\Delta_i)$ is, of course, a Fresnel reflection coefficient referred to the bottom of the layer at $r=a+h$.

The modal eq (16) which determines the coefficients t_n may thus be written in the approximate form

$$R_gR_i\exp(-i\hat{I})=1=e^{-i2\pi n}, \quad (22)$$

where

$$R_g=\frac{C-\Delta}{C+\Delta}\text{ and }R_i=\frac{C'-\Delta_i}{C'+\Delta_i},$$

and

$$\hat{I}=\frac{2ka}{3}[(C')^3-C^3]$$

$$=\frac{2ka}{3}\left[\left(C^2+\frac{2h}{a}\right)^{3/2}-C^3\right],$$

if $\frac{h}{a}<<C^2$, then $R_i=\frac{C-\Delta_i}{C+\Delta_i}$ and $\hat{I}\cong 2khC$ which corresponds to the modal equation for the flat-earth case [5].

4. Evaluation of the Residues

For numerical work it is desirable to express the function

$$\left[\frac{\partial}{\partial t}A(t)B(t)\right]_{t=t_n}$$

explicitly in terms of Airy functions.

First, it is noted that

$$\left[\frac{\partial}{\partial t}\frac{w_2'(t)-qw_2(t)}{w_1'(t)-qw_1(t)}\right]_{t=t_n}=\frac{-2i(t_n-q^2)}{[w_1'(t_n)-qw_1(t_n)]^2}, \quad (23)$$

where use has been made of the relations
(1) $w_1''(t)=tw_1(t)$ and
(2) $w_1(t)w_2'(t)-w_1'(t)w_2(t)=-2i$ which are valid for any value of t. Similarly,

$$\left[\frac{\partial}{\partial t}\frac{w_1'(t-y_0)+q_iw_1(t-y_0)}{w_2'(t-y_0)+q_iw_2(t-y_0)}\right]_{t=t_n}$$

$$=\frac{2i(t_n-y_0-q_i^2)}{[w_2'(t_n-y_0)+q_iw_2(t_n-y_0)]^2}. \quad (24)$$

Thus

$$\left[\frac{\partial}{\partial t}A(t)B(t)\right]_{t=t_n}$$

$$=\frac{-2i(t_n-q^2)}{[w_1'(t_n)-qw_1(t_n)][w_2'(t_n)-qw_2(t_n)]}$$

$$+\frac{2i(t_n-y_0-q_i^2)[w_2'(t_n)-qw_2(t_n)]}{w_1'(t_n)-qw_1(t_n)][w_2'(t_n-y_0)+q_iw_2(t_n-y_0)]^2}. \quad (25)$$

Therefore, the complete residue series may be written

$$V=(\pi x)^{1/2}e^{-i3\pi/4}$$

$$\times\sum_{n=0,1,2}\frac{e^{-ixt_n}[w_1(t_n-y)+A(t_n)w_2(t_n-y)]}{\left[\frac{t_n-q^2}{w_2'(t_n)-qw_2(t_n)}\frac{(t_n-y_0-q_i^2)[w_2'(t_n)-qw_2(t_n)]}{[w_2'(t_n-y_0)+q_iw_2(t_n-y_0)]^2}\right]}. \quad (26)$$

Numerical evaluation of the series is straightforward if tables of the Airy functions of complex argument are used. In the situation where

$$(-t_n)^{1/2}=\left(\frac{ka}{2}\right)^{1/3}C_n\gg 1,$$

the Airy functions may be replaced by the first term of their asymptotic expansions. Under this approximation and after considerable algebraic reduction, it is possible to write, for $y=0$,

$$V=4e^{-i\pi/4}(2\pi ka\theta)^{1/2}\sum_{n=0,1,2\ldots}\frac{e^{ika\theta C_n^2/2}F_n}{\left[\frac{\partial\hat{I}}{\partial C}+\frac{i\frac{\partial}{\partial C}R_gR_i}{R_gR_i}\right]_{C=C_n}},$$

where

$$R_g=\frac{C-\Delta}{C+\Delta}, \qquad R_t=\frac{C'-\Delta_t}{C'+\Delta_t}, \qquad F_n=\frac{C_n^2}{C_n^2-\Delta^2}$$

and

$$\hat{I}=\frac{2ka}{3}[(C')^3-C^3]. \tag{27}$$

If the height of the source dipole is $z_0=r_0-a$ and the observer is $z=r-a$, the F_n in the above expression should be replaced by

$$F_n=f_n(z)f_n(z_0)$$

where

$$2f_n(z)=R_g^{-1/2}\exp\left[ik\int_0^z\left(C_n^2+\frac{2z}{a}\right)^{1/2}dz\right]$$

$$+R_g^{1/2}\exp\left[-ik\int_0^z\left(C_n^2+\frac{2z}{a}\right)^{1/2}dz\right]$$

$$=R_g^{-1/2}\exp\left\{\frac{ika}{3}\left[\left(C_n^2+\frac{2z}{a}\right)^{3/2}-C_n^3\right]\right\}$$

$$+R_g^{1/2}\exp\left\{\frac{ika}{-3}\left[\left(C_n^2+\frac{2z}{a}\right)^{3/2}-C_n^3\right]\right\}. \tag{28}$$

If $2z/a<<C_n^2$ it is permissible to use

$$2f_n(z)\cong R_g^{-1/2}\exp(ikC_nz)+R_g^{1/2}\exp(-ikC_nz)$$

and if $R_g\cong 1$ corresponding to a perfectly conducting ground,

$$f_n(z)\cong\cos kC_nz.$$

The value of C_n to employ in the residue series is related, of course, to t_n by

$$C_n=\left(\frac{2}{ka}\right)^{1/3}(-t_n)^{1/2}.$$

Under the condition that $(-t_n)^{1/2}>>1$, the root-determining equation becomes

$$R_tR_ge^{-i(2kh+V)C_n}=e^{-2\pi in} \tag{29}$$

where V is defined by

$$(2kh+V)C_n=\frac{2ka}{3}[(C_n')^3-C_n^3]=\hat{I}_n. \tag{30}$$

Noting that

$$\frac{\partial\hat{I}_n}{\partial C_n}=2ka\left[\left(C_2^n+\frac{2h}{a}\right)^{1/2}-C_n^2\right] \tag{31}$$

$$\cong 2kh \text{ if } 2h/a\ll C_n^2$$

$$\cong 2k(2ah)^{1/2} \text{ if } 2h/a\gg C_n^2,$$

it is seen that the second term within the square bracket on the right-hand side is small if kh is reasonably large and if the losses are small.

5. Discussion of Various Approximations

As a check on the algebra it may be noted that under the flat-earth approximation (i.e., $2h/a<<C_n^2$), the residue series formula may be written

$$V=\frac{2(\rho/\lambda)^{1/2}}{(h/\lambda)}e^{i\left(\frac{2\pi\rho}{\lambda}-\frac{\pi}{4}\right)}\sum_{n=0,\,1,\,2\ldots}\delta_ne^{-i2\pi\rho S_n/\lambda}f_n(z)f_n(z_0), \tag{32}$$

where

$$\delta_n=\left[1+i\,\frac{\partial[R_tR_g]/\partial C}{2khR_tR_g}\right]^{-1}_{C=C_n},$$

$\rho=a\theta$, and $S_n=(1-C_n^2)^{1/2}\cong 1-C_n^2/2$. For practical purposes, $\delta_0\cong 1/2$ and $\delta_n\cong 1$ for $n=1, 2, 3\ldots$. Equation (32) agrees with an earlier analysis [5,6].

For a first approximation it is probably permissible to neglect the curvature altogether. To improve on this it is important to retain curvature dependent terms in a consistent manner. For example, at VLF, the restriction $C_n^2\gg 2h/a$ is not as stringent as

$$C_n\gg(2/ka)^{1/3}.$$

Thus eq (27) for V is probably not any better (if as good) as eq (32). To effect a real improvement one should retain the Airy functions of argument t_n without approximation, but allow the Airy functions of argument t_n-y_0 to be replaced by the first terms of their asymptotic expansions. This is justified since y_0 is reasonably large compared to unity in the VLF range. With this approach the root-determining equation may be written

$$R_tR_gF_ge^{-i(2kh+V)C}=e^{-2\pi in}=1 \tag{33}$$

where

$$F_g=\frac{\dfrac{w_2'(t)-qw_2(t)}{w_1'(t)-qw_1(t)}}{i\exp\left[i\dfrac{4}{3}(-t)^{3/2}\right]\left[\dfrac{-i(-t)^{1/2}-q}{i(-t)^{1/2}-q}\right]}. \tag{34}$$

If the ground is assumed to be perfectly conducting $R_g=1$ and $q=0$. Then, on writing

$$R_t=-e^{-2\beta C'}$$

the mode equation reduces to

$$2\pi n=\pi-2i\beta C'+[(C')^3-C^3]\frac{2}{3}ka+i\arg F_g, \tag{35}$$

where now

$$F_g=\frac{w_2'(t)}{w_1'(t)}\exp\left[i\frac{\pi}{2}-i\frac{4}{3}(-t)^{3/2}\right]. \tag{36}$$

For long-distance propagation in the VLF range, only the mode corresponding to $n=1$ is of importance.

Furthermore, since C is small, for a first approximation

$$\frac{w_2'(t)}{w_1'(t)} \cong e^{i\pi/6};$$

also, β is essentially a constant and is approximately equal to $1/\Delta_i$. Thus

$$C^2 \cong \frac{\frac{7\pi}{6} - \frac{2}{3}(ka)\left(\frac{2h}{a}\right)^{3/2} + 2i\beta\left(\frac{2h}{a}\right)^{1/2}}{ka\left(\frac{2h}{a}\right)^{1/2} - i\beta\left(\frac{a}{2h}\right)^{1/2}}. \quad (37)$$

This formula should be a fairly good approximation if $|C^2|$ is somewhat less than $2h/a$. For example, if $\beta=0$, corresponding to $R_i=-1$, and if $h/a=10^{-2}$ the above may be written

$$C^2 = \frac{0.041248}{(h/\lambda)} - 0.01334.$$

For h/λ in the region from 2.5 to 5, $|C^2|$ is never greater than 5×10^{-3}.

Using perturbation methods, higher order approximations for the solution of eq (35) may be obtained. Details of such computations will not be described here.

6. Certain Extensions of the Theory

The preceding analysis has referred specifically to a vertical electric dipole. If the source is a vertical magnetic dipole the results derived above are still applicable if the reflection coefficients R_g and R_i are replaced by their counterparts R_g^h and R_i^h for horizontal polarization. The only other change is that q is now defined by

$$iq = \left(\frac{ka}{2}\right)^{1/3}\frac{1}{\Delta_h} \quad \text{where} \quad \frac{1}{\Delta_h} = \left[\frac{\sigma + i\epsilon\omega}{i\epsilon_0\omega} - 1\right]^{1/2}.$$

Since $[q] \gg 1$, under all practical conditions,

$$F_g^h \cong \frac{w_2(t)}{w_1(t)} \exp\left[-i\left(\frac{\pi}{2} + \frac{4}{3}(-t)^{3/2}\right)\right], \quad (38)$$

which is to be used instead of F_g. The modes excited by a magnetic dipole are of a TE (transverse electric) type whereas for an electric dipole they are of a TM (transverse magnetic) type.

7. Application to Specific Ionospheric Models

In the case of a homogeneous isotropic ionosphere with a sharp lower boundary, the Fresnel reflection coefficient for small C' may be written

$$R_i = \frac{C' - \Delta_i}{C' + \Delta_i} \cong -e^{-2\beta C'}, \quad (39)$$

where $\beta \cong \frac{1}{\Delta_i}$. In terms of the plasma frequency ω_0 and the collision frequency ν

$$\beta \cong (1 - i\omega_r/\omega)(-i\omega_r/\omega)^{-1/2}$$

where $\omega_r = \omega_0^2/\nu$ under the condition that $\omega \ll \nu$.

Unfortunately, the presence of the earth's magnetic fields renders the ionosphere anisotropic. The reflection coefficient is thus a matrix of the form [1]

$$[R_i] = \begin{bmatrix} {}_{\parallel}R_{\parallel} & {}_{\parallel}R_{\perp} \\ {}_{\perp}R_{\parallel} & {}_{\perp}R_{\perp} \end{bmatrix},$$

where the coefficients ${}_{\parallel}R_{\parallel}$, ${}_{\parallel}R_{\perp}$, ${}_{\perp}R_{\parallel}$, and ${}_{\perp}R_{\perp}$ indicate the complex ratio of a specified electric field in the wave after reflection to a specified electric field in the wave before reflection. The first subscript denotes whether the electric field in the incident wave is parallel ($\parallel$) or perpendicular ($\perp$) to the plane of incidence and the second subscript refers in the same way to the reflected wave. It is understood, of course, that $[R_i]$ is a function of C', the cosine of the angle of incidence at the ionosphere. Following an earlier analysis [6], the generalization of eq (33), to include the influence of anisotropy, may be expressed in the form

$$\begin{aligned} &[1 - {}_{\parallel}R_{\parallel}R_g F_g e^{-i(2kh+V)C}] \\ &\times [1 - {}_{\perp}R_{\perp}R_g^h F_g^h e^{-i(2kh+V)C}] \\ &- {}_{\parallel}R_{\perp}{}_{\perp}R_{\parallel}R_g F_g R_g^h F_g^h e^{-i2(2kh+V)C} = 0, \end{aligned} \quad (40)$$

where R_g, R_g^h, F_g, F_g^h, and V have been defined. Strictly speaking, equation (40) is only valid when there is perfect azimuthal symmetry about the source dipole.

It may be noted that if the conversion coefficients ${}_{\parallel}R_{\perp}$ and ${}_{\perp}R_{\parallel}$ vanish, the modal equation splits into two parts which are

$$1 - {}_{\parallel}R_{\parallel}R_g F_g e^{-i(2kh+V)C} = 0 \quad (41)$$

and

$$1 - {}_{\perp}R_{\perp}R_g^h F_g^h e^{-i(2kh+V)C} = 0. \quad (42)$$

These two uncoupled equations give the solutions for the TM and TE modes, respectively. In the more general case the modes are coupled. However, for low-order modes and particularly for the dominant mode ($n=1$), the coupling is extremely small and a good first-order approximation is obtained on the assumption that coupling may be neglected. Furthermore, the TE mode is only of academic or secondary interest since it is not excited to any extent by a vertical antenna. Thus the constants of the first-order mode may be obtained from eq (37) with an appropriate value of β.

For propagation in the magnetic meridian or for propagation in polar regions the QL (quasi-longitudinal) approximation [9] to describe conditions within the ionosphere is valid. The refractive index μ, in this case, is given by [1]

$$\mu^2=1-i(\omega_r/\omega)\exp(\pm i\phi_L), \tag{43}$$

where

$$\tan\phi_L=\frac{\omega_L}{\nu}=\frac{\text{longitudinal component of gyrofrequency}}{\text{collision frequency}}$$

and $\omega_r=\omega_0^2(\nu^2+\omega_L^2)^{-1/2}$. Thus for highly oblique incidence (i.e., C is small) it may be shown that [6]

$$R\cong -e^{-2\beta C'} \tag{44}$$

where

$$\beta=\frac{\mu_0\mu_e}{\mu_0+\mu_e}\frac{C_0+C_e}{C_0C_e}$$

where μ_0 and μ_e denote the two values of μ, and

$$C_0=(1-1/\mu_0^2)^{\frac{1}{2}} \text{ and } C_e=(1-1/\mu_e^2)^{\frac{1}{2}}.$$

The QL approximation mentioned above is only valid when [10]

$$\frac{\omega_T^4}{4\omega^2\omega_L^2}<<\left|\left(1-\frac{\omega_0^2}{\omega^2}-\frac{\nu}{\omega}\right)^2\right|$$

where ω_L and ω_T are the longitudinal and transverse components of the (angular) gyrofrequency. As mentioned above, this condition is satisfied for propagation in the magnetic meridian and/or for a steeply dipping field. Clearly, this condition is violated when the transverse component of the earth's magnetic field is large such as for propagation around the magnetic equator. The case of a purely horizontal and transverse field has been considered by Barber and Crombie [11]. Using their results, which are applicable to a sharply bounded ionosphere, it may be readily shown that [6]

$${}_{\parallel}R_{\parallel}\cong -e^{-2\beta C'}, \qquad {}_{\parallel}R_{\perp}=0 \tag{45}$$

where now

$$\beta=\frac{(1+iL)^2-\gamma^2}{(1+iL)^{1/2}(iL-L^2-\gamma^2)^{1/2}-i\gamma} \tag{46}$$

and

$$L=\frac{\omega}{\omega_r}=\frac{\omega\nu}{\omega_0^2} \text{ and } \gamma=\frac{\omega_T\omega}{\omega_0^2}.$$

For east-to-west propagation, γ is positive, while for west-to-east propagation, γ is negative. In the present situation it is convenient to define an angle ϕ_T such that

$$\gamma=+L|\tan\phi_T| \text{ for east-to-west propagation}$$

$$=-L|\tan\phi_T| \text{ for west-to-east propagation.}$$

For propagation at any angle with respect to the earth's magnetic field and for an arbitrary angle of dip I, it is necessary to seek more general solutions. First, one must solve a quartic equation for the refractive indices (ordinary and extraordinary components). Then on matching tangential field components at the air-ionosphere boundary, an explicit expression for the reflection coefficient may be obtained [12]. Using this quite general approach Johler and Walters [13] have obtained extensive numerical results for the coefficients ${}_{\parallel}R_{\parallel}$, ${}_{\parallel}R_{\perp}$, ${}_{\perp}R_{\perp}$, and ${}_{\perp}R_{\parallel}$ for various (real) angles of incidence and range of values for the electron density, N, collision frequency ν, dip-angle I and the azimuthal direction of the wave ϕ_a (measured clockwise from the north). Formally, the expressions for these reflection and conversion coefficients may be substituted in eq (13) which, in principle, can be solved for the modes in the general case. For VLF and at highly oblique angles of incidence (e.g., 82°), the quantity $|{}_{\parallel}R_{\perp}\times{}_{\perp}R_{\parallel}|$ is of the order of 10^{-3} or 10^{-4} and thus coupling between the TE and TM modes is negligible. At least this is true for the range of values of the ionospheric parameters considered here. Thus the uncoupled modal equation may again be used for an adequate first approximation after having determined the appropriate value of β.

8. Presentation of Results

Using the above approaches numerical results have been obtained for the complex values of C for the dominant mode.[4] From this quantity, it is a simple matter to compute the corresponding value of S which describes the propagation in the horizontal direction. For example, the attenuation per unit distance is proportional to the quantity—H Im S and the phase velocity relative to c is 1/Re S. In the present paper, these are the quantities of prime interest since they are adequate to describe the propagation characteristics of VLF radio waves at large distances from the source (i.e., >2,000 km). At shorter distances higher order modes should be considered. Their influence has been discussed elsewhere [5].

In figure 2 the attenuation coefficient, for the dominant mode ($n=1$), is plotted as a function of $H(=h/\lambda)$ for a curved earth where $h/a=0.01$. The upper- and right-hand scales in this figure and in many which follow, are a frequency scale and attenuation scale in decibels per 1,000 km of path length applicable to a height of 70 km. The quasi-longitudinal approximation is employed and ϕ_L is either 60° or 0°; the latter, of course, corresponds to no magnetic field. The constant B on the curves is

[4] For sake of brevity, the subscript 1, to indicate the first mode, is dropped in what follows.

defined by

$$B=\frac{L}{H} \text{ where } \frac{1}{L}=\frac{\omega_r}{\omega}=\frac{\omega_0^2}{\omega(\nu^2+\omega_L^2)^{1/2}}, \qquad (47)$$

or alternately

$$B=\frac{2\pi c}{\omega_r h}.$$

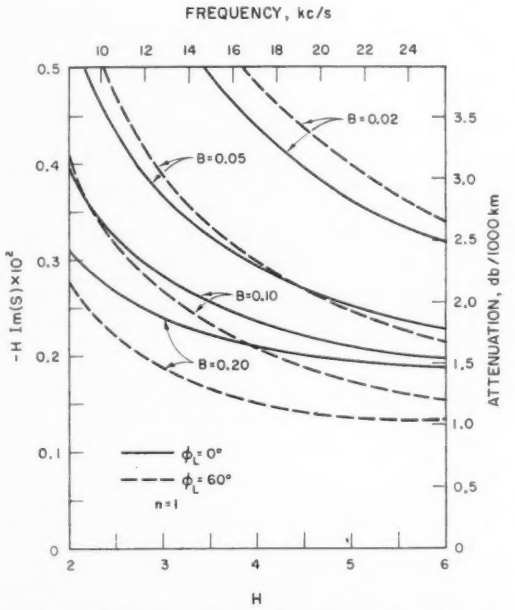

FIGURE 2. *Attenuation coefficient,*—H *Im* S, *as a function of* H (=h/λ) *for the dominant mode.*

The upper and the right-hand scales are for h=70 km.

The four B values on the curves (0.02, 0.05, 0.1, and 0.2) correspond to ω_r values of 13, 5.4, 2.7, and 1.3×10^5, respectively. For a given value of B, it is seen that the attentuation depends on ϕ_L. For large values of B (i.e., poorly conducting ionosphere) the influence of the terrestrial magnetic field is to lower the attenuation whereas the converse is true at smaller values of B. Since B is in the range 0.05 to 0.01 typically for daytime conditions, the influence of the magnetic field is small under the quasi-longitudinal approximation.

The relative phase velocity of the dominant mode is shown in figures 3a and 3b for ϕ_L=0 and 60°, respectively. The (upper) frequency scale is for a height of 70 km. From these it appears that the influence of the magnetic field is quite small. It is rather interesting to note that for a frequency of 14 kc/s the phase velocity is very near, c, the velocity of light.[5] It should be remembered, of course, that the phase velocity is referred to the surface of the ground in this particular analysis.

Since one is interested in relatively small deviations of 1/Re (S) from unity, considerable care is needed in approximating the wavefunctions involved. The results shown in figures 3a and 3b for a curved earth are not expected to be accurate to more than a few parts in 10^4.

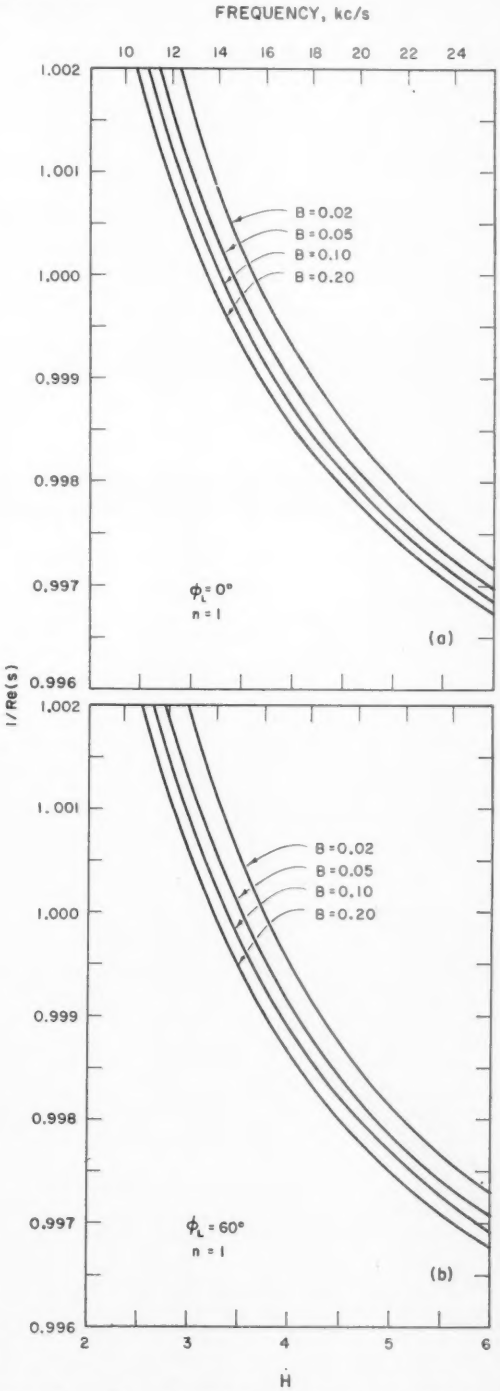

FIGURES 3a and b. *The relative phase velocity, 1/Re* S *as a function of* H *for the dominant mode.*

The upper-frequency scale is for h=70 km.

[5] Recent experimental data appear to confirm this point (M. L. Tibbals, private communication).

The calculation of the mode characteristics for a magnetic field of arbitrary direction is, of course, quite involved. However, approximate results can be obtained if coupling between TE and TM type modes is neglected [6]. Actually, in the case of a purely transverse field, the coupling is zero anyway.

In the following the influence of an arbitary magnetic field is demonstrated by calculating the ratio, P, of the attenuation with a magnetic field to the attenuation without the magnetic field. Various values of the dip-angle I, and the azimuthal direction of propagation, ϕ_a, are chosen. The ratio, Q, of the phase-velocity deviations with and without a magnetic field is also considered. Specifically, these ratios are

$$P=\frac{\text{Attenuation with magnetic field}}{\text{Attenuation without magnetic field}}=\frac{\text{Im } S}{[\text{Im } S]_{H=0}} \tag{48}$$

and

$$Q=\frac{\text{Phase velocity deviation with magnetic field}}{\text{Phase velocity deviation without magnetic field}} \tag{49}$$

$$=\frac{\left[\frac{1}{\text{Re } S}-J\right]}{\left[\frac{1}{\text{Re } S}-J\right]_{H=0}} \text{ where } J\cong\frac{2a}{2a+h}.$$

To obtain numerical values of P and Q, computed data from J. R. Johler [14] were requested for the reflection coefficient ${}_{\|}R_{\|}$ for a real angle of incidence of 82° and at frequencies of 10, 12, 14, 16, 20, and 22 kc/s. The appropriate value of β was then calculated from

$${}_{\|}R_{\|}=-e^{-2\beta C'}, \tag{50}$$

where $C'=\cos 82°$. The electron density values for the sharply bounded model were 10^3 and 3×10^3 electrons/cm^3, respectively. The collision frequency was taken to be 2×10^7 and the strength of the earth's magnetic field was 0.5 gauss. The angle ϕ_a which defined the direction of propagation measured clockwise from north assumed the values 0°, 60°, 120°, 180°, 240°, and 300°. As a check on the method, values of β were calculated directly from eq (40) which is applicable to $\phi_a=90°$ and 180° for $I=0$.

The results for the attenuation ratios are shown in figures 4a and 4b for a dip-angle I of 0°, in figures 5a and 5b for an I of 45°, and in figures 6a and 6b for an I of 84.3°.

These results would indicate that nonreciprocity is most evident in propagation around the geomagnetic equator. North-to-south or south-to-north propagation appears to be almost reciprocal. It is also evident that for this range of electron densities, the nonreciprocity for attenuation is more marked for the smaller densities. It is also apparent from these results that the nonreciprocal effects are

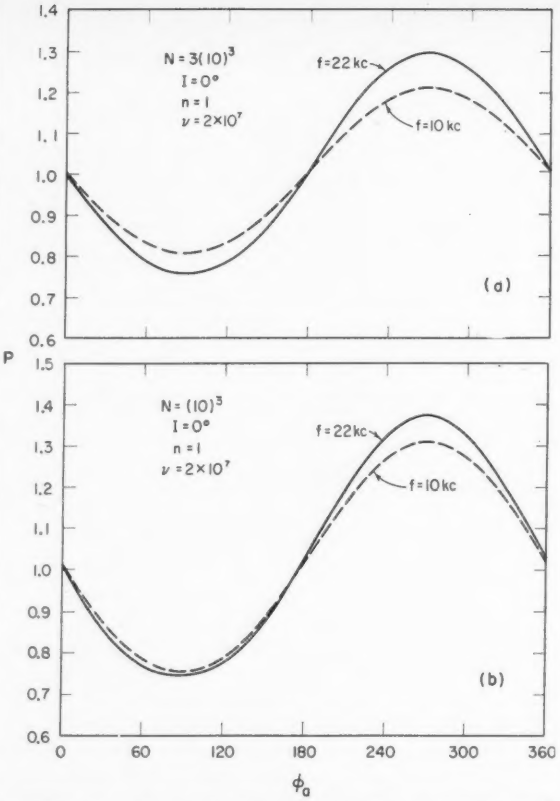

FIGURES 4a and b. *The ratio of the attenuation rates with and without a (transverse) terrestrial magnetic field.* ϕ_a is the direction of propagation with respect to geomagnetic north.

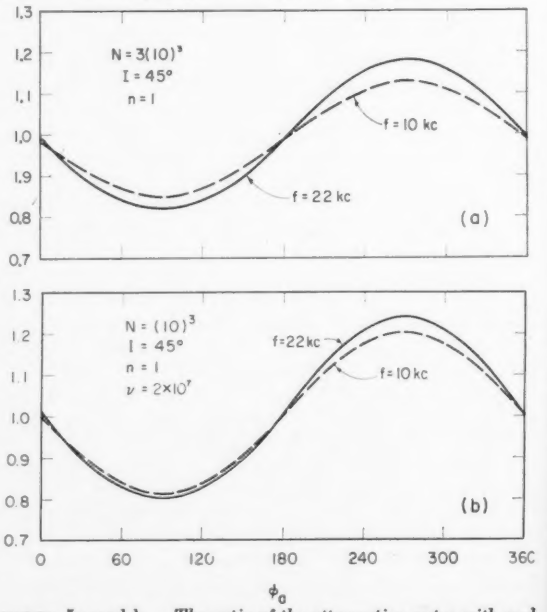

FIGURES 5a and b. *The ratio of the attenuation rates with and without a terrestrial magnetic field for a dip angle of 45°.*

diminished as the magnetic field approaches the vertical. Qualitatively the curves are very similar and there is a strong suggestion that nonreciprocity is proportional to the component of the earth's magnetic field which is horizontal and transverse to the direction of propagation.

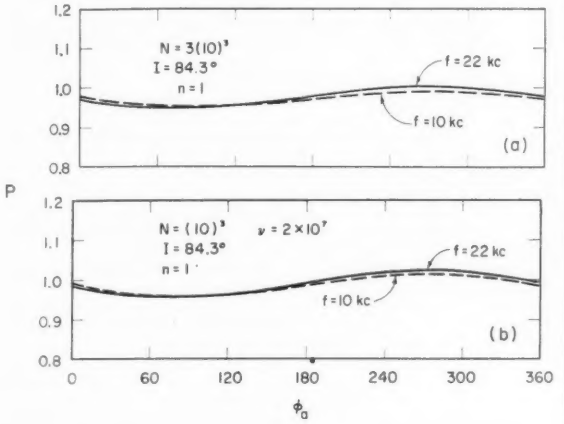

FIGURES 6a and b. *The ratio of the attenuation rates with and without a terrestrial magnetic field for a dip angle of 84.3°.*

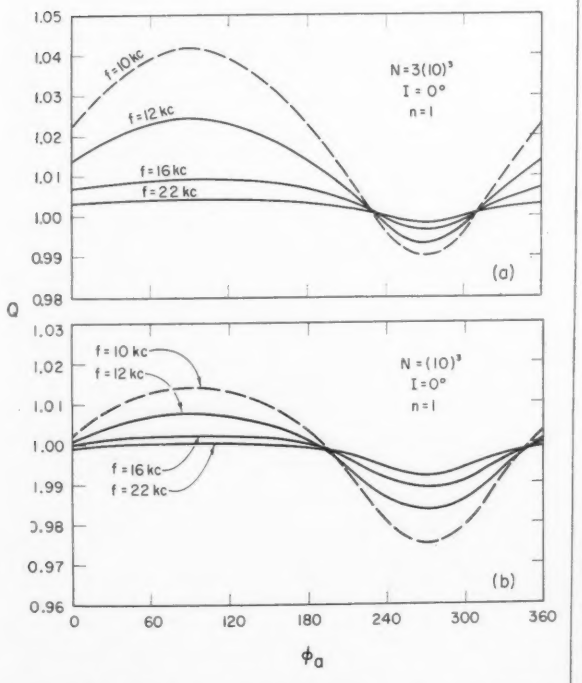

FIGURES 7a and b. *The ratio of the phase-velocity deviations with and without a (transverse) terrestrial magnetic field.*

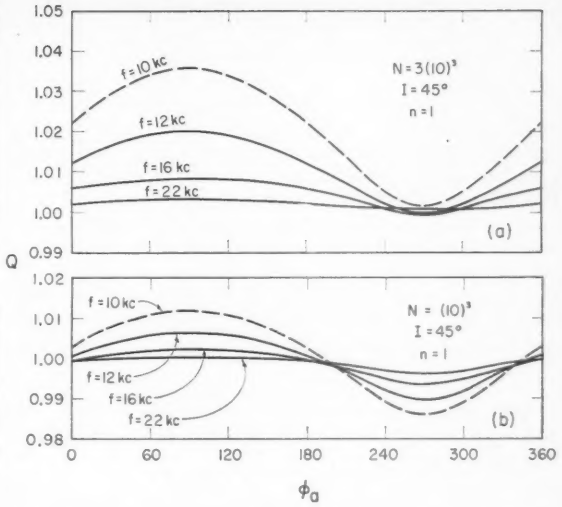

FIGURES 8a and b. *The ratio of the phase-velocity deviations with and without a terrestrial magnetic field for a dip angle of 45°.*

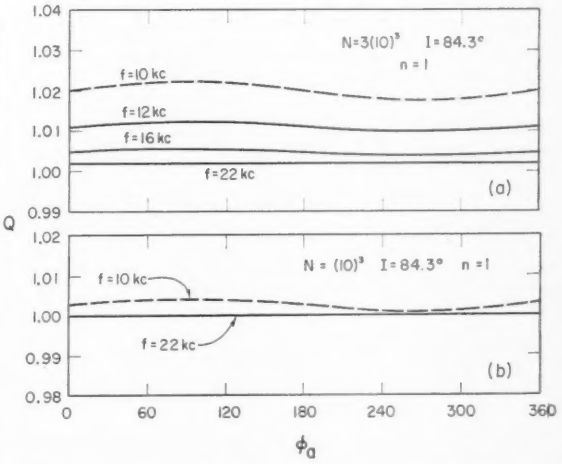

FIGURES 9a and b. *The ratio of the phase-velocity deviations with and without a terrestrial magnetic field for a dip angle of 84.3°.*

The corresponding curves for the ratio Q of the phase velocity deviations are shown in figures 7a and 7b for $I=0$, in figures 8a and 8b for $I=45°$, and in figures 9a and 9b for $I=84.3°$. It is rather interesting to see that these are not symmetrical about the north-south geomagnetic axis. It is also evident that the nonreciprocity in the phase velocity becomes greater at the lower frequencies. It is noticed that Q is never more than 4-percent greater than unity. This corresponds to a change of phase velocity of only a few parts in 10^5.

9. Concluding Remarks

In this paper no direct reference has been made to experimental data. In another paper [15] the experimental data on attenuation rates at VLF in daytime [16] were compared with calculations using formulas from the present paper. The agreement between theory and experiment was quite good and the nature of the nonreciprocity between east-west and west-east propagation was satisfactorily accounted for. Unfortunately, the experimental data on phase velocity is quite sparse. It would be interesting to compare the computed results given in this paper with absolute measurements of phase velocities at various frequencies over a given path.

The author thanks Kenneth Spies for carrying out the calculations and Mrs. Eileen Brackett for her assistance in preparing the manuscript.

10. References

[1] K. G. Budden, The propagation of a radio-atmospheric, Phil. Mag. **43,** 1179 (1952).
[2] K. G. Budden, The "wave-guide mode" theory of the propagation of VLF radio waves, Proc. IRE **45,** 772 (1957).
[3] I. A. Al'pert, The field of long and very long radio waves over the earth under actual conditions, Radiotekh. i Elektron. **1,** 281 (1956).
[4] W. O. Schumann, Über die Oberfelder bei der Ausbreitung langer, elektrischer Wellen im System Erde-Luft-Ionosphäre und 2 Anwendungen, Z. angew. Phys. **6, 34** (1954).
[5] J. R. Wait, The mode theory of VLF ionospheric propagation for finite ground conductivity, Proc. IRE **45,** 760 (1957).
[6] J. R. Wait, Terrestrial propagation of VLF radio waves, a theoretical investigation, J. Research NBS **64D,** 153 (1960). (Note the inequality at the middle of p. 172 should read $(ka/2)^{1/3}\ C>>1$.)
[7] B. van der Pol and H. Bremmer, The diffraction of electromagnetic waves from an electrical point source round a finitely conducting sphere, Phil. Mag., **7, 24,** 141 (1937).
[8] V. A. Fock, Diffraction of radio waves around the earth's surface, J. Phys. U.S.S.R. **9,** 256 (1945).
[9] H. G. Booker, Some general properties of the formulae of the magneto-ionic theory, Proc. Roy. Soc. (London) **A147,** 352 (1934).
[10] J. M. Ratcliffe, Magneto-ionic theory (Cambridge University Press, New York, N.Y., 1959).
[11] N. F. Barber and D. D. Crombie, VLF reflections from the ionosphere in the presence of a transverse magnetic field, J. Atmospheric and Terrest. Phys. **16,** 37 (1959).
[12] H. Bremmer, Terrestrial radio waves (Elsevier Publishing Co., New York, N.Y., 1949).
[13] J. R. Johler and L. Walters, On the theory of reflection of LF and VLF radio waves from the ionosphere, J. Research NBS **64D,** 269 (1960).
[14] J. R. Johler, private communication (1960).
[15] J. R. Wait and K. Spies, Influence of earth curvature and the terrestrial magnetic field on VLF propagation, J. Geophys. Research **65,** 2325 (1960).
[16] W. L. Taylor, Daytime attenuation rates in the VLF band using atmospherics, J. Research NBS **64D,** 349 (1960).

10.1. Additional Reference

D. D. Crombie, Differences between the east-west and west-east propagation of VLF signals over long distances, J. Atmcspheric and Terrest. Phys. **12,** 110 (1958).

10.2. List of Symbols

(r,θ,ϕ) = spherical coordinates of observer,
a = radius of the earth,
h = height of reflecting layer,
$k=2\pi/$wavelength,
θ is central angle,
$x=(ka/2)^{1/3}\,\theta$,
$y=(2/ka)^{1/3}\,(r-a)$,
$iq=(ka/2)^{1/3}\,\Delta$,
$\Delta=\left(\frac{i\epsilon_0\omega}{\sigma+i\epsilon\omega}\right)^{1/2}\left[1-\frac{i\epsilon_0\omega}{\sigma+i\epsilon\omega}\right]^{1/2}$,
$w_1(t)$ is Airy function of first type defined by eq (4),
$w_2(t)$ is Airy function of second type defined by eq (6),
t is argument of Airy function,
$\Delta_i=Z/\eta_0$,
$\eta_0\cong 120\pi$,
Z is surface impedance of ionospheric reflecting layer at $r=a+h$,
$iq_i=(ka/2)^{1/3}\,\Delta_i$,
$y_0=(2/ka)^{1/3}\,kh$,
$w(t)$ is some linear combination of $w_1(t)$ and $w_2(t)$,
$A(t)$ is defined by eq (8); it is related to the ionospheric reflection coefficient,
$B(t)$ is defined by eq (18); it is related to the ground-reflection coefficient,
$C=(2/ka)^{1/3}(-t)^{1/2}$; C may be geometrically interpreted as the cosine of the angle of incidence at the ground,
$C'=(C^2+2h/a)^{1/2}$; C' may be geometrically interpreted as the cosine of the angle of incidence at the ionosphere,
R_g and R_i are reflection coefficients at the ground and the ionosphere, respectively,
$\hat{I}=\frac{2ka}{3}\,[(C')^3-C^3]$,
V is a dimensionless quantity proportional to the vertical electric field,
V_j is defined by eq (13); it may be interpreted loosely as the j'th order skywave,
t_n is the n'th root of eq (16); it determines the attenuation and phase of the n'th mode,
$\rho=a\theta$; it is the great circle distance between source and observer,
δ_n is defined by eq (32); it is a coefficient in the mode sum,
F_g is defined by eq (34); it is a wave correction to the ground-reflection coefficient,
$\omega_r=\omega_0^2/\nu$,
ω_0 is the (angular) plasma frequency,
ν is the collision frequency,
β is defined by eq (39); it characterizes the ionospheric reflection coefficient $\|R\|_i$
$[R_i]=\begin{bmatrix}\|R\|_i & \|R\|_\perp \\ \perp R\|_i & \perp R\|_\perp\end{bmatrix}$; this is a matrix which describes reflection from an anisotropic layer,
μ is defined by eq (43); it is a double-valued index of refraction for the ionosphere subject to the QL approximation,
μ_0 and μ_e are the two components of μ,
ω_L is the longitudinal component of the gyrofrequency,
ω_T is the transverse component of the gyrofrequency,
$B=L/H=\frac{2\pi c}{\omega_r h}$,
$H=h/\lambda$,
$L=\frac{\omega}{\omega_r}=\frac{\omega(\nu^2+\omega_L{}^2)^{1/2}}{\omega_0^2}$,
$\phi_L=\tan^{-1}(\omega_L/\nu)$,
P and Q are defined by eqs (48) and (49),
I = dip angle of the earth's magnetic field,
ϕ_a is the azimuthal direction of propagation of the wave; $\phi_a=0$ corresponds to propagation from south-to-north, $\phi_a=90°$ corresponds to propagation from west-to-east, etc.

(Paper 65D1–101)

JOURNAL OF RESEARCH of the National Bureau of Standards—D. Radio Propagation
Vol. 65D, No. 1, January–February 1961

East-West Effect on VLF Mode Transmission Across the Earth's Magnetic Field [1]

D. Dobrott and A. Ishimaru [2]

(July 5, 1960)

The effect of a constant transverse magnetic field is analyzed for the propagation of VLF electromagnetic waves about the earth. These waves are considered to be propagating by modes in a parallel plate waveguide. The lower boundary of the guide is considered to be a perfect conductor, while the upper boundary is assumed to be a sharply defined, semi-infinite, homogeneous plasma with a constant magnetic field applied. The source of these waves is an infinite number of short, horizontal, cophased dipoles, uniformly spaced parallel to the constant magnetic field vector. Admittance relations are derived for the upper boundary of the guide by considering the waves to be of grazing incidence. It is found that these admittance parameters depend on the direction of propagation. These admittance parameters are plotted versus frequency for various heights. Expressions for eigenvalues and the eigenfunctions are found as functions of the admittance. By employing a two dimensional Green's function, the amplitudes of the various modes due to the dipole source are evaluated. It is noted that the propagation constants differ depending on the direction of propagation, thus offering an explanation of the east-west effect of VLF transmission. A numerical example is calculated and field strength versus distance values are found to correspond to some experimental results.

1. Introduction

The mode theory of VLF radio transmission has evolved from the study of electromagnetic wave propagation between the earth and the ionosphere. Wait [1] [3] and others [2, 3] have solved the VLF electromagnetic problem using mode theory and assuming a sharply bounded ionosphere, while neglecting the earth's magnetic field. Friedman [4, 5] has made a modal analysis which differ in method from that of Wait, but arrives at similar conclusions. Friedman's analysis utilized an upper boundary of scalar impedance Z.

All of these solutions have the same propagation characteristics regardless of the direction of propagation. However, Crombie [6] has noted evidence that VLF propagation differs depending on whether the propagation is from east to west, or from west to east. He also indicated that this so-called "east-west effect" may be partly due to the earth's magnetic field. Recently, Wait [7, 8] and Crombie [6, 9] have shown analytically that the rate of attenuation for east-west propagation behaves as had been indicated by the latter author.

This paper attempts to show analytically the east-west effect on the basis of mode theory and ionosphere-freespace boundary admittance. Because of the presence of the earth's magnetic field, the admittance of the sharply bounded ionosphere is not a scalar, but a tensor. Further, because of these magnetic effects, the tensor depends upon the direction of propagation.

The solution of the radiation from a dipole in this parallel plate waveguide with anisotropic boundary conditions is, in general, difficult. However, one may solve an analogous two-dimensional problem. This simplifies the arithmetic while maintaining the qualitative structure of the three-dimensional case.

The two-dimensional problem corresponds to the source of electromagnetic waves being an infinite number of horizontal, cophased, short dipoles, uniformly spaced parallel to the direction to the earth's magnetic field. This situation is displayed in figure 1.

In the sections that follow, the radiation from these sources are examined in detail. A numerical example is shown also.

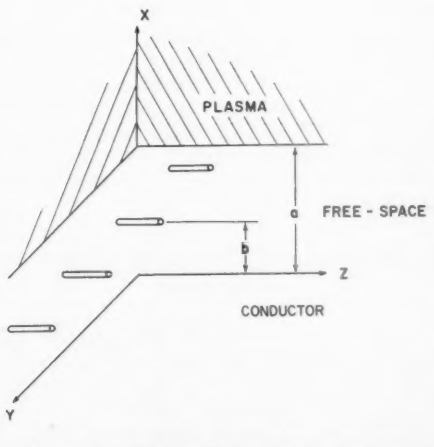

FIGURE 1. *Cophased sources for TM waves.*

[1] Contribution from Boeing Scientific Research Laboratory, Seattle, Wash.
[2] Present address of Professor A. Ishimaru: Department of Electrical Engineering, University of Washington, Seattle, Wash.
[3] Figures in brackets indicate the literature references at the end of this paper.

2. Dielectric Tensor of Magnetically Influenced Plasma

The permittivity of an ionized gas may be determined by examining the ion motion under the influence of electromagnetic waves. Certain restrictions must be placed on this gas if the evaluation of the equation of motion is to remain simple.

For the purpose of this analysis, the gas will be considered to be a homogeneous plasma. That is, the gas is uniform throughout and the number of positive charges is equal to the number of negative charges. The plasma exists in a state where collisions are relatively few. Since the positive and neutral particles have more mass than the electrons, their mobilities are correspondingly smaller and it shall be considered that their velocity is zero. Further, the number of electrons per cubic meter N, does not vary appreciably with time. Thus the behavior of a volume element of gas is the same as that of an "average" electron obeying the laws of classical dynamics. These are the assumptions of the "Magneto-Ionic Theory" [10].

In the special case considered in figure 1, where a magnetic field is considered perpendicular to the direction of propagation, the ionosphere's relative dielectric tensor is given by, [11]

$$\bar{\bar{\epsilon}}=\begin{bmatrix}\epsilon_2 & 0 & -j\eta\\ 0 & \epsilon_1 & 0\\ j\eta & 0 & \epsilon_2\end{bmatrix}, \tag{2.1}$$

$$\epsilon_1=1+\frac{\omega_p^2}{j\omega\nu-\omega^2}, \tag{2.2}$$

$$\epsilon_2=1+\frac{\omega_p^2(j\omega+\nu)}{j\omega[\omega_c^2+(j\omega+\nu)^2]}, \tag{2.3}$$

$$\eta=-\frac{\omega_c\omega_p^2}{\omega[\omega_c^2+(j\omega+\nu)^2]}. \tag{2.4}$$

In expressions 2.2, 2.3 and 2.4 ω_p is the plasma frequency, ν is the collision frequency, ω_c is the cyclotron frequency, and ω is the frequency of the electromagnetic wave propagating in the plasma region.

Using 2.1, one is able to solve for the electromagnetic fields in the plasma region. The solution of the fields is required to examine the conditions at the plasma-freespace interface.

3. Admittance Tensor of Plasma at Interface

In order to solve for the electromagnetic fields for the problem described by section 1, one must first consider the restrictions placed upon the problem by the particular geometry. Since the sources are considered to be uniformly distributed along the y-direction axis, there is no y-variation for the fields. Further, the nature of these sources produces only transverse-magnetic waves. Considering these facts and eq 2.1, Maxwell's equations in the plasma become,

$$\frac{\partial E_z}{\partial x}-\frac{\partial E_x}{\partial z}=j\omega\mu_0 H_y,$$

$$\frac{\partial H_y}{\partial z}=-j\omega\epsilon_0(\epsilon_2 E_x-j\eta E_z),$$

$$\frac{\partial H_y}{\partial x}=j\omega\epsilon_0(j\eta E_x+\epsilon_2 E_z). \tag{3.1}$$

Solving eqs 3.1 in terms of the longitudinal electric field to obtain the following equation

$$\left[\frac{\partial^2}{\partial x^2}+\frac{\partial^2}{\partial z^2}+k^2\frac{(\epsilon_2^2-\eta^2)}{\epsilon_2}\right]E_z=0. \tag{3.2}$$

The solution to this equation is of the form

$$E_z=K_1\epsilon^{-pz}\epsilon^{\pm\Upsilon t} \tag{3.3}$$

where p and γ are, in general, complex and the plus or the minus sign designates a wave traveling in the negative z-direction or positive z-direction respectively.

Substituting eq 3.3. into 3.2 one obtains the characteristic equation of 3.2

$$p^2+\gamma^2+k^2\frac{(\epsilon_2^2-\eta^2)}{\epsilon_2}=0. \tag{3.4}$$

In the free-space region, Maxwell's equations may be solved for the transverse-magnetic case in terms of the longitudinal electric field yielding the following homogeneous wave equation

$$\left[\frac{\partial^2}{\partial x^2}+\frac{\partial^2}{\partial z^2}+k^2\right]E_z=0. \tag{3.5}$$

The solution for the homogeneous wave equation depends upon the boundary conditions, and since the tangential electric field must be zero at a perfect conductor, the solution is of the form,

$$E_z=K_2\sin qx\epsilon^{\pm\Upsilon z} \tag{3.6}$$

where q and γ are complex.

Equation 3.6 has a corresponding characteristic equation given by,

$$-q^2+\gamma^2+k^2=0. \tag{3.7}$$

From eqs 3.1 and 3.3 the fields in the plasma region are related by the following relations
for the $+z$-direction,

$$E_x = \frac{1}{j\omega\epsilon_0} \frac{\epsilon_2\gamma - jp\eta}{\epsilon_2^2 - \eta^2} H_y,$$

$$E_z = \frac{1}{j\omega\epsilon_0} \frac{-j\eta\gamma - \epsilon_2 p}{\epsilon_2^2 - \eta^2} H_y; \qquad (3.8)$$

for the $-z$-direction

$$E_x = \frac{1}{j\omega\epsilon_0} \frac{-\epsilon_2\gamma - jp\eta}{\epsilon_2^2 - \eta^2} H_y,$$

$$E_z = \frac{1}{j\omega\epsilon_0} \frac{j\eta\gamma - \epsilon_2 p}{\epsilon_2^2 - \eta^2} H_p. \qquad (3.8)\ \text{(cont'd)}$$

From the two tangential fields E_z and H_y, an admittance relationship may be defined as

$$Y_0 Y_{12} = -\frac{H_y}{E_z}\bigg|_{z=a}. \qquad (3.9)$$

From the two expressions of eqs 3.8 and relation 3.9, one may obtain two expressions for the admittance of the plasma boundary.

$$Y_{\substack{e-w \\ w-e}} = \frac{jk(\epsilon_2^2 - \eta^2)}{\epsilon_2 p \pm j\eta\gamma} \qquad (3.10)$$

where Y_{e-w} and Y_{w-e} are the relative admittance parameters for east-west and west-east propagation, respectively.

If grazing incidence is considered, upon the plasma-freespace interface, it is found that $\gamma \to jk$, where the sign has already been determined by the form of eq 3.6. This corresponds to the far-field situation. If this condition were not imposed, the admittance would be a function of the free-space eigenvalue q. Thus one obtains the following two expressions for the admittance of the plasma boundary,

$$Y_{\substack{e-w \\ w-e}} = \frac{jk(\epsilon_2^2 - \eta^2)}{\epsilon_2 p \mp \eta k}. \qquad (3.11)$$

The following restriction must be placed upon p,

$$\text{Re } (p) > 0, \text{ Im } (p) > 0. \qquad (3.12)$$

With these restrictions in mind, the final expressions for the admittances in terms of the constituents of equation 2.1 are

$$Y_{\substack{e-w \\ w-e}} = \frac{j(\epsilon_2^2 - \eta^2)}{\epsilon_2\left[1 - \frac{\epsilon_2^2 - \eta^2}{\epsilon_2}\right]^{1/2} \mp \eta}. \qquad (3.13)$$

A numerical solution of these admittance parameters for height versus frequency is shown in figures 2 and 3. The values of collision frequency and electron density have been obtained from papers by M. Nicolet [12] and R. E. Houston [13], respectively.

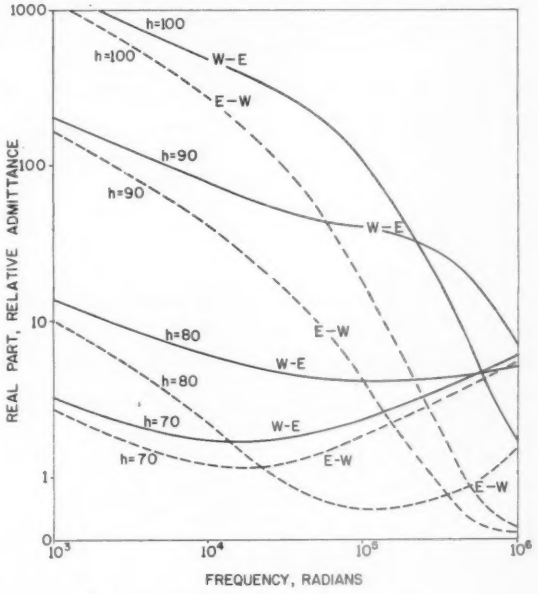

FIGURE 2. *Real part of admittance* (Y_{12}).

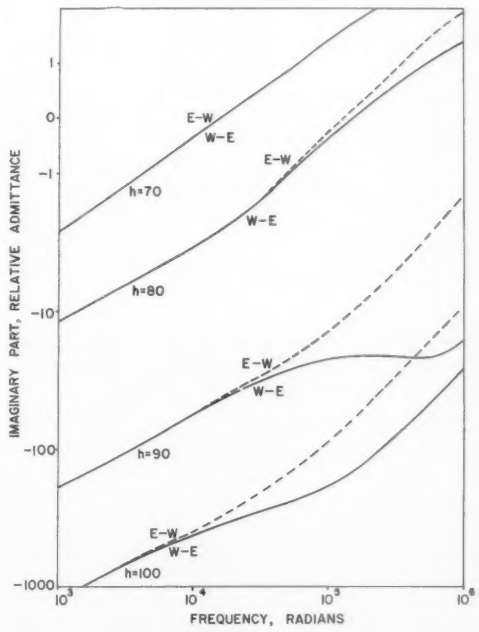

FIGURE 3. *Imaginary part of admittance* (Y_{12}).

4. Eigenvalues and Propagation Constant

In order to solve for a general expression for the eigenvalues in terms of the admittance matrix for all waves, one must also solve Maxwell's equations for the transverse-electric waves. This solution, in terms of the longitudinal magnetic field H_z, is given as

$$H_z=Y_0K_3\epsilon^{\pm\gamma z}\cos qx. \tag{4.1}$$

Recalling eq 3.6 and Maxwell's equations for TM and TE one can obtain,

$$E_y=-\frac{j\omega\mu_0}{q}Y_0K_3\epsilon^{\pm\gamma z}\sin qx \tag{4.2}$$

and

$$H_y=-\frac{j\omega\epsilon_0}{q}K_2\epsilon^{\pm\gamma z}\cos qx. \tag{4.3}$$

Relating these four fields at $x=a$ by the admittance matrix $\overline{\overline{Y}}$,

$$\begin{bmatrix}H_y\\H_z\end{bmatrix}=Y_0\begin{bmatrix}Y_{11}&Y_{12}\\Y_{21}&Y_{22}\end{bmatrix}\begin{bmatrix}E_y\\E_z\end{bmatrix}. \tag{4.4}$$

Substituting the solutions 3.6, 4.1, 4.2, and 4.3 into 4.4 and combining terms

$$\begin{bmatrix}\left(Y_{12}\sin qa-\frac{jk}{q}\cos qa\right)\left(\frac{jk}{q}Y_{11}\sin qa\right)\\(Y_{22}\sin qa)\left(\cos qa+\frac{jk}{q}\sin qa\right)\end{bmatrix}\begin{bmatrix}K_2\\K_3\end{bmatrix}=0. \tag{4.5}$$

For 4.5 to be true, the determinant

$$\begin{vmatrix}\left(Y_{12}\sin qa-\frac{jk}{q}\cos qa\right)\left(\frac{jk}{q}Y_{11}\sin qa\right)\\(Y_{22}\sin qa)\left(\cos qa+\frac{jk}{q}Y_{21}\sin qa\right)\end{vmatrix}=0. \tag{4.6}$$

Evaluating the determinant 4.6, the following general expression for the eigenvalues is obtained in terms of admittance parameters,

$$\Delta_y\tan qa+\cot qa=-j\frac{q^2Y_{12}+k^2Y_{21}}{qk} \tag{4.7}$$

where $\Delta_y=Y_{11}Y_{22}-Y_{12}Y_{21}$.

For the special parallel plate case under consideration, the only admittance parameter needed is Y_{12}. Thus eq 4.7 becomes

$$\cot qa=-j\frac{q}{k}Y_{12}. \tag{4.8}$$

Rewriting relationship 4.8, $q=q_n$, $n=1, 2, 3\ldots$

$$jzq_na=\ln\left(\frac{1-\frac{2}{1+\frac{q_nY_{12}}{k}}}{}\right)+jzn\pi. \tag{4.9}$$

If the term $q_n/k\ Y_{12}$ is large as is the case for the "electric" wall, the following approximation for the eigenvalue q_n may be obtained.

$$q_n=\frac{n\pi}{a}+\frac{jka}{q_na^2Y_{12}}. \tag{4.10}$$

For the "zeroth mode" case, that is $n=0$,

$$q_0=\left(\frac{jk}{aY_{12}}\right)^{1/2}, \tag{4.11}$$

and if n is greater than zero, q_n may be approximated $n\pi$ in the right-hand side of 4.10 yielding,

$$q_n=\frac{n\pi}{a}+\frac{jk}{n\pi Y_{12}}. \tag{4.12}$$

The propagation constant

$$\gamma_n=(q_n^2-k^2)^{1/2} \tag{4.13}$$

may be obtained from the results of 4.11 and 4.12. Restrictions on 4.13 are that

$$\text{Re}\ (\gamma_n)>0, \text{Im}\ (\gamma_n)>0; \tag{4.14}$$

when 4.13 is evaluated for $n=0$, the attenuation constant, $Re(\gamma_n)=\alpha_n$ is very small, and for $n>2$, the phase constant, Im $(\gamma_n)=\beta_n$, is small representing evanescent modes.

One can see that if $Y_{12}\to\infty$, as in the case of a perfect conductor, expression 4.12 reduce to the familiar result, $n\pi/a$. Expressions 4.11 and 4.12 are used, along with the data of Houston and Nicolet, to plot mode decibel loss versus distance on figure 4 for $n=0$, 1, 2. The numerical values for the admittance used were

$$Y_{E-W}=22.5-37.5j, \tag{4.15}$$

$$Y_{W-E}=56.5-41.5j. \tag{4.16}$$

This corresponds to a radian frequency of $\omega=2\times10^4$ and a height of 90 km.

A synopsis of experimental results by Crombie [6] indicates that the ratio of electric field strengths

$$\frac{W-E}{E-W}>1 \tag{4.17}$$

which is certainly true for the numerical case calculated and graphed on figure 4.

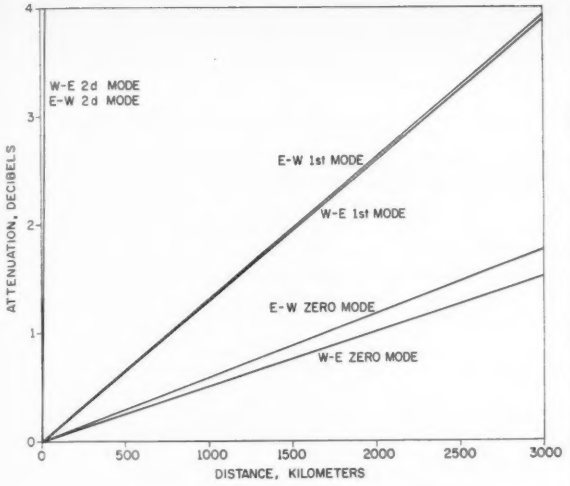

FIGURE 4. *Attenuation versus distance.*

5. Mode Solution—Source Present

With the source of current moment IL eq 3.5 becomes,

$$\left(\frac{\partial^2}{\partial x^2}+\frac{\partial^2}{\partial z^2}+k^2\right)E_z=j\omega\mu_0 IL\delta(x-b)\delta(z) \qquad (5.1)$$

where $\delta\,(x-b)$ and $\delta\,(z)$ are Dirac "delta-functions." This problem is analogous to the Green's function problem if one relates the longitudinal electric field to the Green's function as $E_z=-j\omega\mu_0 ILG$, the corresponding Green's function problem may be solved,

$$\left(\frac{\partial^2}{\partial x^2}+\frac{\partial^2}{\partial z^2}+k^2\right)G=-\delta(x-b)\delta(z). \qquad (5.2)$$

The boundary conditions for the Green's function are the same as for the electric field E_z

$$G|_{x=0}=0$$

$$(G'+YG)|_{x=a}=0. \qquad (5.3)$$

It has been shown in section 4 that the solution to the homogeneous wave equation for the longitudinal electric field and hence the Green's function is of the form

$$G=\sum_0^\infty{}_n A_n\epsilon^{-\gamma_n|z|}\sin\ q_n x. \qquad (5.4)$$

Thus if 5.2 is true we must be able to expand the delta-function in terms of eigenvectors, [14, 15]

$$\delta(x-b)=\sum_0^\infty{}_n B_n\sin\ q_n x. \qquad (5.5)$$

Multiplying through by $\sin\ q_m x$ and integrating over the range of x, an expression for B_n

$$B_n=\frac{4q_n\sin\ q_n b}{(2q_n a-\sin\ 2q_n a)}. \qquad (5.6)$$

Making the substitution

$$r_n=\frac{4q_n}{(2q_n a-\sin\ 2q_n a)} \qquad (5.7)$$

where r_n is often called the normalization factor. Integrating 5.2 over the source with respect to z yields

$$A_n=\frac{r_n\sin\ q_n b}{2\gamma_n} \qquad (5.8)$$

and

$$G=\sum_0^\infty{}_n\frac{2q_n}{\gamma_n(2q_n a-\sin\ 2q_n a)}\epsilon^{-\gamma_n|z|}\sin\ q_n b\sin\ q_n x. \qquad (5.9)$$

Therefore the expression for the electric field is given by

$$E_z=\sum_0^\infty{}_n\frac{j\omega\mu_0 2ILq_n}{\gamma_n(2q_n a-\sin\ 2q_n a)}\epsilon^{-\gamma_n|z|}\sin\ q_n b\sin\ q_n x. \qquad (5.10)$$

The other fields may be evaluated for Maxwell's equations for the TM case.

The expression for the vertical component of the electric field with a "normalized" current is given as

$$E_z=\sum_0^\infty{}_n\frac{\sin\ q_n b}{2q_n a-\sin\ 2q_n a}\epsilon^{-\gamma_n|z|}\cos\ q_n x. \qquad (5.11)$$

If the transmitter is in an airplane at a height of $a/4$ and the receiver is on the ground, 5.11 becomes,

$$E_z=\sum_0^\infty{}_n\frac{\sin\ q_n\left(\frac{a}{4}\right)}{2q_n a-\sin\ 2q_n a}\epsilon^{-\gamma_n|z|} \qquad (5.12)$$

For the first three modes 5.12 is of the form

$$E_z=C_0\epsilon^{-\gamma_0 z}+C_1\epsilon^{-\gamma_1 z}+C_2\epsilon^{-\gamma_2 z} \qquad (5.13)$$

where

$$C_n=\frac{\sin\ q_n\left(\frac{a}{4}\right)}{2q_n a-\sin\ 2q_n a}. \qquad (5.14)$$

The magnitude of the field strength at the receiver is given by the expression,

$$\begin{aligned}|E_x|=\{&|C_0|^2\epsilon^{-\alpha_0 z}+|C_1|^2\epsilon^{-2\alpha_1 z}+|C_2|^2\epsilon^{-2\alpha_2 z}\\&+2|C_0||C_1|\epsilon^{-(\alpha_0+\alpha_1)z}\cos\left[(\beta_0-\beta_1)z+(\bar{C}_0-\bar{C}_1)\right]\\&+2|C_0||C_2|\epsilon^{-(\alpha_0+\alpha_2)z}\cos\left[(\beta_0-\beta_2)z+(\bar{C}_0-\bar{C}_2)\right]\\&+2|C_1||C_2|\epsilon^{-(\alpha_1+\alpha_2)z}\cos\left[(\beta_1-\beta_2)z+(\bar{C}_1-\bar{C}_2)\right]\}^{1/2}\end{aligned} \qquad (5.15)$$

where $|C_n|$ and $\overline{C}_n$ are the magnitude and argument of C_n, respectively.

Equation 5.15 is plotted on figure 5. These results depend not only on attenuation, but also on field strength magnitude which in turn depends on the direction of propagation and the height of the transmitting antenna. This corresponds qualitatively with the far field experimental results mentioned by Crombie [6].

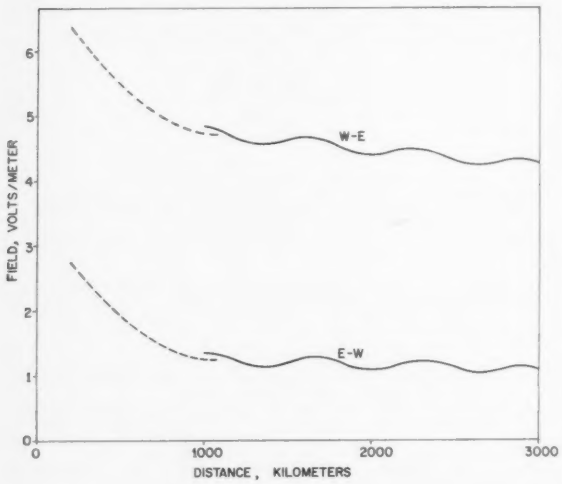

FIGURE 5. *Field strength versus distance.*

6. Conclusion

The effect on east-west, west-east propagation of electromagnetic transverse magnetic waves across the earth's magnetic field has been analyzed as a boundary value problem. Certain idealizations were made to solve this problem. Admittance relationships were derived from field relations existing in a homogeneous anisotropic plasma, and it was found that the admittance parameters depended upon the direction of propagation. These parameters were plotted versus frequency for various heights. Expressions for the eigenvalues were derived. The attenuation over distance was plotted for a special case. It was found that the ratio of the electric field for the individual modes of west-east/east-west propagation was greater than one. This corresponds to some experimental data. A two dimensional Green's function was derived and a numerical calculation of the corresponding electric field strength was plotted versus distance.

The authors express appreciation to the Scientific Research Laboratory and the computer facilities group of the Boeing Airplane Company. Special thanks go to Dr. Bernard Friedman of the University of California for the valuable conversations with the authors while this paper was being written, and to Dr. James R. Wait for his critical and stimulating reviews of this work.

7. References

[1] James R. Wait, The mode theory of VLF ionospheric propagation for finite ground conductivity, Proc. IRE **45,** 760 (1957).

[2] Kenneth Budden, The waveguide mode theory of the propagation of very-low-frequency radio waves, Proc. IRE **45,** 772 (1957).

[3] Irving W. Yabroff, Reflection at a sharply-bounded ionosphere, Proc. IRE **45,** 750 (1957).

[4] Bernard Friedman, Low frequency propagation, Boeing Airplane Co. Document D2-2302 (Nov. 1957).

[5] Bernard Friedman, Low frequency propagation in the ionosphere, Boeing Airplane Co. Document D1-82-0003 (June 1959).

[6] D. D. Crombie, Differences between the east-west and west-east propagation of VLF signals over long distances, J. Atmospheric and Terrest. Phys. **12,** 110 (1958).

[7] James R. Wait, Terrestrial propagation of VLF radio waves—a theoretical investigation, J. Research NBS **64D,** 153 (1960).

[8] James R. Wait and K. Spies, Influence of earth's curvature and terrestrial magnetic field on VLF propagation, J. Geophys. Research (Aug. 1960).

[9] D. D. Crombie, On the mode theory of very-low-frequency propagation in the presence of a transverse magnetic field, J. Research NBS **64D,** 265 (1960).

[10] J. A. Ratcliffe, The magneto-ionic theory and its applications to the ionosphere (Cambridge Univ. Press, Cambridge, England, 1959).

[11] D. R. Dobrott, Effects in VLF mode transmission due to earth's magnetic field, Master's Thesis, University of Washington, Seattle, Wash., (1960).

[12] M. Nicolet, Aeronomic conditions in the mesosphere and lower thermosphere, Penn. State Univ. Ionospheric Research Rept. No. 102 (Apr. 1958).

[13] R. E. Houston, The effect of certain solar radiations in the lower ionosphere, Penn. State Univ. Ionospheric Research Rept. No. 95 (July 1957).

[14] Bernard Friedman, Principles and techniques of applied mathematics (John Wiley and Sons, New York, N.Y., 1957).

[15] Arnold Sommerfeld, Partial differential equations in physics, Lectures on theoretical physics, Vol. VI (Academic Press, Inc., New York, N.Y., 1949).

(Paper 65D1-102)

JOURNAL OF RESEARCH of the National Bureau of Standards—D. Radio Propagation
Vol. 65D, No. 1, January–February 1961

Magneto-Ionic Propagation Phenomena in Low- and Very-Low-Radiofrequency Waves Reflected by the Ionosphere[1]

J. Ralph Johler

(July 8, 1960)

LF–VLF ionosphere reflection coefficients which illustrate the dependence of the amplitude and phase of the reflected wave upon the direction of propagation relative to the direction of the earth's magnetic field are presented. The calculations are based on a plane, sharply bounded, model ionosphere with plane wave excitation, but employ full use of the magneto-ionic formulas for complex directions of propagation in the ionosphere such that the influence of the earth's magnetic field in the different directions of propagation is demonstrated. A special table of values applicable to VLF is presented.

1. Introduction

The classical magneto-ionic theory implies a dependence of the electromagnetic waves on the direction of propagation relative to the direction of the earth's magnetic field.

The application of the classical magneto-ionic theory to the evaluation of low- and very-low-radiofrequency reflection coefficients for a sharply bounded model ionosphere by using an assumed electron equation of motion, together with Maxwell's equations was investigated in a previous paper [1].[2] The importance of the orientation of the earth's magnetic field vector, $\overline{H}_m$, was discussed in considerable detail, and the effect of various orientations of the vector (relative to the direction of propagation) on the precise value of the reflection coefficient was noted. This paper further pursues the subject of "directional effects" at low- and very-low-radiofrequencies. The forces acting on the electron in the ionosphere excited by an electromagnetic field are described by an electron equation of motion, Johler et al. [1] (1960). A particular term of this equation $\mu_o e(\overline{V}\times\overline{H}_m)$ called the "Lorentz force," Lorentz [2] (1906) relates the action of the earth's magnetic induction, $\mu_o\overline{H}_m$, or an electron (charge e) traveling at a velocity, $\overline{V}$, in a medium of permeability μ_o, to the direction of propagation. This dependence upon direction of propagation causes some interesting and predictable phenomena in the low and very low part of the radio spectrum.

The effect of the collision frequency, ν, on the magnitude of abnormal components (i.e., electric-magnetic coupling coefficients, T_{em}, T_{me}) is also investigated. A large angle of incidence, $\phi_i=80°$, 82°, is considered and the resultant intensities of both normal and abnormal components are noted at various directions of propagation.

2. Theory of the Reflection Coefficient

The essential nature of low- and very-low-radiofrequency waves propagated via the ionosphere can be described in terms of a reflection coefficient. Reflection coefficients or propagation constants (complex index of refraction of the ionosphere) for complex angles of incidence, ϕ_i, figure 1, such as would be required for "mode-type" calculations, Wait [3] (1960), can be readily evaluated from the

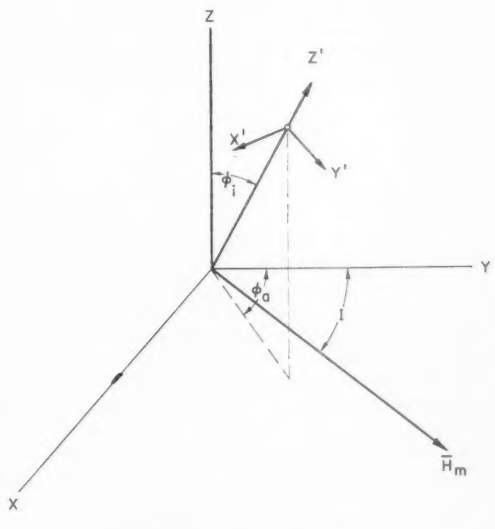

FIGURE 1. *Coordinate systems.*

[1] Contribution from Central Radio Propagation Laboratory, National Bureau of Standards, Boulder, Colo.
[2] Figures in brackets indicate the literature references at the end of this paper.

results of the previous paper, Johler et al. [1] (1960) without analytic modification of the formulas. However, for naive discussion purposes in this paper, a real angle of incidence, ϕ_i, will be employed. It should be noted, however, that the wave normal direction, ψ, relative to the direction of the earth's magnetic field vector, $\overline{H}_m$, in the ionosphere is nevertheless complex [1]. The direction, θ, relative to the vertical, z direction, figure 1, is also a complex number as a consequence of Snell's law: $\sin \phi_i = \eta \sin \theta$. The propagation downward from the ionosphere (i.e., wave traveling from the ionosphere into the negative z, figure 1, region) is defined by four reflection coefficients, T_{ee}, T_{em}, T_{me}, T_{mm}, which relate the reflected radiation to the primary or incident radiation. The reflection coefficient, T_{ee}, refers to the vertical electric polarization of the incident plane wave and a similar vertical electric polarization of the reflected wave. The coefficient, T_{em}, describes the generation of the abnormal component by the incident vertical polarization (vertical electric- magnetic coupling). Similarly, T_{mm}, refers to the incident horizontal electric polarization and the corresponding reflected horizontal electric polarization. Also, the abnormal component generated by horizontal electric polarization (vertical magnetic-electric coupling) is described by the coefficient, T_{me}. The reflection coefficients can therefore be defined (see fig. 1),

$$T_{ee} = \frac{E_{y'r}}{E_{y'i}}, \qquad T_{me} = \frac{E_{y'r}}{E_{x'i}},$$

$$T_{em} = \frac{E_{x'r}}{E_{y'i}}, \qquad T_{mm} = \frac{E_{x'r}}{E_{x'i}},$$

where subscripts i and r refer to incident and reflected waves, respectively. Expressions for these coefficients were developed in the previous paper [1]. In addition to the geometric parameters, figure 1, the reflection coefficient is completely defined by the magnetic intensity $H_m = |\overline{H}_m|$ gauss, the electron density N(el/cm^3), and the collision frequency ν(c/s).

3. Discussion

A comparison of the reflection coefficients of the model ionosphere, $|T_{ee}|$, $|T_{em}|$ and phase, arg T_{ee}, arg T_{em}, figure 2, and amplitude, $|T_{mm}|$, $|T_{me}|$ and phase, arg T_{mm}, arg T_{me}, figure 3, for north-east propagation, magnetic azimuth, $\phi_a = 45°$, with the corresponding reflection coefficients for south-west propagation, magnetic azimuth, $\phi_a = 225°$, is illustrated. It is quite evident that a nonreciprocity exists in the propagation (i.e., the expected value of field intensity would not be the same if transmitter and receiver were interchanged), since neither normal nor abnormal components are precisely the same in both directions except at zero frequency. Indeed, the discrepancy is appreciable not only at LF($<$300 kc/s) but also at VLF($<$30 kc/s).

The effect of the magnetic azimuth, ϕ_a, (reckoned as clockwise angular measurement from magnetic north, fig. 1) is illustrated at a "temperate" magnetic latitude, $I = 45°$, figures 4, 5. Both amplitude, $|T|$, and phase, arg T, are presented, $\phi_a = 0-360°$, at frequencies 10 and 100 kc/s. Note that the component, T_{ee}, is symmetrical about the eastward, $\phi_a = 90°$, and the westward, $\phi_a = 270°$, propagation. Note also that the direction of maximum intensity, $\phi_a = 90°$ (eastward propagation) is considerably greater than the corresponding reverse direction, $\phi_a = 270°$ (westward propagation).

Propagation via the ionosphere at the magnetic equator, $I = 0$, tables [3] 1, 5, 9, 13, 17, exhibit small

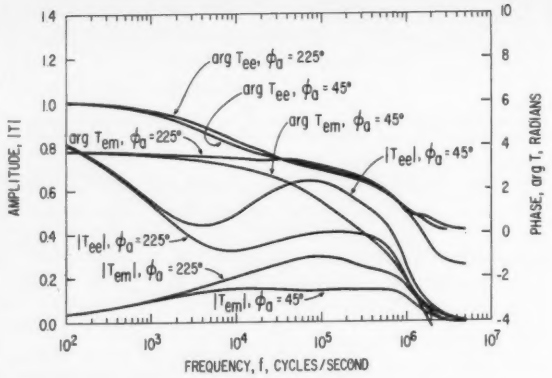
AMPLITUDE, |T|
PHASE, arg T, RADIANS
FREQUENCY, f, CYCLES/SECOND
arg Tee, φa = 225°
arg Tee, φa = 45°
arg Tem, φa = 45°
arg Tem, φa = 225°
|Tee|, φa = 45°
|Tee|, φa = 225°
|Tem|, φa = 225°
|Tem|, φa = 45°

FIGURE 2. *Comparison of north-east propagation with south-west propagation (vertical polarization) illustrating nonreciprocity with the aid of the model ionosphere reflection coefficients, amplitude, |T|, and phase, arg T.*

$N = 870$, $\nu = 4$ (10^6), $\phi_I = 75.08°$, $H_m = 0.5$, $I = 60°$, $\phi_a = 45°$, $225°$.

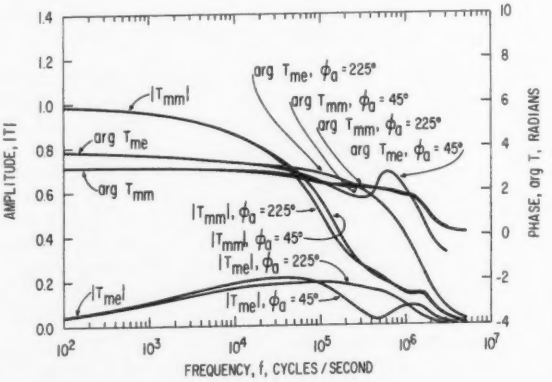

FIGURE 3. *Comparison of north-east propagation with south-west propagation (horizontal polarization) illustrating nonreciprocity with the aid of the model ionosphere reflection coefficients, amplitude, |T|, and phase, arg T.*

$N = 870$, $\nu = 4$ (10^6), $\phi_I = 75.08°$, $H_m = 0.5$, $I = 60°$, $\phi_a = 45°$, $225°$.

[3] The integer to the right of each table entry, if present, indicates the power of the factor ten (10) by which the entry is to be multiplied. Thus, 6.4307−1= 0.64307.

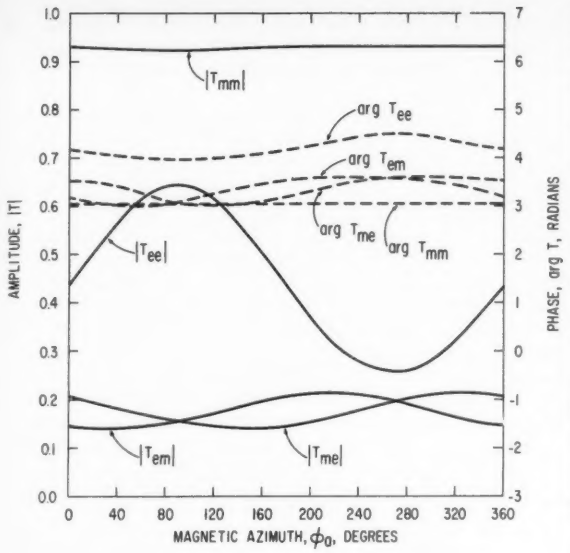

FIGURE 4. *Model ionosphere reflection coefficients, amplitude, |T|, and phase, arg T, illustrating a dependence of the reflected field upon the direction of propagation relative to the direction of the earth's magnetic field vector.*

$N=1.2$ (10^3), $\nu=10^6$, $\phi_i=80.397°$, $H_m=0.5$, $I=45°$, $f=10$ kc/s.

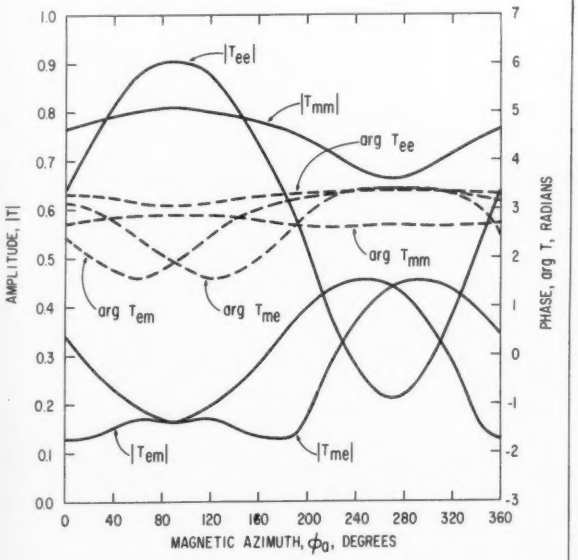

FIGURE 5. *Model ionosphere reflection coefficients, amplitude, |T|, and phase, arg T, illustrating a dependence of the reflected field upon the direction of propagation relative to the direction of the earth's magnetic field vector.*

$N=1.2$ (10^3), $\nu=10^6$, $\phi_i=80.397°$, $H_m=0.5$, $I=45°$, $f=100$ kc/s.

and substantially constant abnormal components ($|T_{em}|$ and $|T_{me}|$ are between 0.01 and 0.04) in all directions, ϕ_a, for a large limiting value of the angle of incidence, $\phi_i=82°$, and a large collision frequency, $\nu=2$ (10^7). It is interesting to note that the components differ in phase by π radians; i.e., arg T_{em}−arg $T_{me}=\pm\pi p$, where p is an odd integer, $p=1, 3, 5 \ldots$. The abnormal components, T_{em} and T_{me}, appear to interchange values abruptly at $\phi_a=90°$ and $\phi_a=270°$ at the magnetic equator. The abruptness of this interchange of values decreases as the magnetic inclination, I, increases. It is of interest to note, tables 9, 13, for example, that north-south propagation, $\phi_a=180°$, and south-north propagation $\phi_a=0$, do not exhibit a precise reciprocity at the magnetic equator, $I=0$. Note (tables 9, 13):

$$\begin{aligned}
\phi_a=0 \qquad & \phi_a=180° \\
|T_{ee}| \quad &= |T_{ee}|, \\
\arg T_{ee} &= \arg T_{ee}, \\
|T_{em}| \quad &= |T_{em}|, \\
\arg T_{em} &= \arg T_{em}-\pi, \\
|T_{mm}| \quad &= |T_{mm}|, \\
\arg T_{mm} &= \arg T_{mm}, \\
|T_{me}| \quad &= |T_{me}|, \\
\arg T_{me} &= \arg T_{me}+\pi.
\end{aligned}$$

Thus, at the "magnetic equator", $I=0$, the only nonreciprocity in the propagation along the magnetic meridian is as might be expected, a phase shift of π in the abnormal components as each abnormal component vanishes at precisely eastward or westward propagation.

Propagation from the model ionosphere at the magnetic north pole, $I=90°$, tables 4, 8, 12, 16, as might be expected, is independent of the magnetic azimuth, ϕ_a. A value, $\phi_a=0$, was computed at all frequencies, $f=10$–22 kc/s and a value, $\phi_a=240°$ at $f=10$ kc/s served as a check on the computation. The behavior of the propagation in the vicinity of the magnetic north pole, $I=84.270°$ is illustrated, tables 3, 7, 11, 15.

Propagation from the model ionosphere in "temperate" magnetic latitudes, $I=45°$, tables 2, 6, 10, 14, figures 4, 5, exhibit abnormal components, T_{em}, T_{me}, which in general differ not only along the magnetic meridian, but also at the various values of magnetic azimuth, ϕ_a (0 to 360°). Although the normal components, T_{ee}, T_{mm}, in the north-south, $\phi_a=180°$, and the south-north, $\phi_a=0$, direction (i.e., along a magnetic meridian) are identical, the propagation does not exhibit a precise reciprocity since the abnormal components, T_{em}, T_{me}, are not identical in these directions. However, reciprocity for propagation along a magnetic meridian can be

considered to be an approximately valid concept if the collision frequency, ν, and angle of incidence, ϕ_i, are sufficiently great such that the abnormal components, T_{em}, T_{me}, become quite small. Indeed, the large values of the angle of incidence, $\phi_i=82°$, employed in the calculations for the tables tended, in conjunction with the high collision frequency, $\nu=2$ (10^7), to reduce greatly the abnormal components.

The intensity of the abnormal component propagated from the ionosphere excited by a vertically polarized transmitter, $|T_{em}|$, has special interest at LF, $f=100$ kc/s, figure 5. The eastward propagation, $\phi_a\sim90°$, from a vertically polarized transmitter provides a dominant vertically polarized field, $|T_{ee}|$, at the receiver; whereas, westward propagation, $\phi_a\sim270°$, from a vertically polarized transmitter can under certain conditions (see fig. 5 specifications) provide a dominant horizontally polarized field, $|T_{em}|$ (abnormal component) at the receiver. In practice, it is necessary to consider the influence of the displacement and conduction currents in the ground which can indeed discriminate between horizontal and vertical polarization in such a manner as to obscure the ionosphere phenomena described.

4. Conclusions

The propagation of low- and very-low-radio-frequency waves reflected by the ionosphere is indeed dependent upon the "Lorentz force" on the electron, and hence is dependent upon the direction of propagation relative to the direction of the earth's magnetic field vector in the region of the ionosphere in which the reflection occurs. The intensity of the abnormal components is dependent upon the values of the various parameters (such as N, ν, H_m, ϕ_a, I, ϕ_i) and in particular, the collision frequency, ν, and the angle of incidence (distance) ϕ_i are especially important in the determination of the precise value of the abnormal components. Precise reciprocity in the LF and VLF propagation (interchange of transmitter and receiver) can occur only at the magnetic north or south pole, $I=\pm90°$. Otherwise, the propagation is dependent upon the direction, ϕ_a, and in general the intensities become greatest in an eastward direction, $\phi_a\sim90°$. Furthermore, it is conceivable at low frequencies, if the influence on the ground can be neglected or separated from this consideration, that the horizontally polarized component excited by a vertically polarized transmitter can approach in magnitude and even exceed the vertically polarized component in the case of westward propagation, whereas it would appear that the corresponding eastward propagation would exhibit a dominant vertical polarization.

Table 1.

$N = 10^3$ $\nu = 2(10^7)$ $\phi_i = 82^\circ$ $H_m = 0.5$ $I = 0$

f, kc	ϕ_a, degrees	$\lvert T_{ee}\rvert$		arg T_{ee}	ϕ_a, degrees	$\lvert T_{em}\rvert$		arg T_{em}	ϕ_a, degrees	$\lvert T_{em}\rvert$		arg T_{em}
10	0, 180	6.4307	- 1	3.3383	0	2.9182	- 2	7.8223	- 1	180	2.9182	- 2	3.9238
12		6.5235	- 1	3.2969		3.1976	- 2	7.5758	- 1		3.1976	- 2	3.8992
14		6.5863	- 1	3.2632		3.4477	- 2	7.3621	- 1		3.4477	- 2	3.8778
16		6.6287	- 1	3.2346		3.6746	- 2	7.1727	- 1		3.6746	- 2	3.8589
18		6.6568	- 1	3.2098		3.8826	- 2	7.0021	- 1		3.8826	- 2	3.8418
20		6.6745	- 1	3.1879		4.0750	- 2	6.8464	- 1		4.0750	- 2	3.8262
22		6.6843	- 1	3.1682		4.2540	- 2	6.7028	- 1		4.2540	- 2	3.8119
10	60, 120	7.1140	- 1	3.3275	60	1.5209	- 2	7.7949	- 1	240	1.3872	- 2	3.9089
12		7.2128	- 1	3.2863		1.6655	- 2	7.5346	- 1		1.5171	- 2	3.8837
14		7.2785	- 1	3.2526		1.7945	- 2	7.3100	- 1		1.6328	- 2	3.8619
16		7.3217	- 1	3.2240		1.9111	- 2	7.1121	- 1		1.7374	- 2	3.8427
18		7.3492	- 1	3.1991		2.0176	- 2	6.9350	- 1		1.8329	- 2	3.8255
20		7.3653	- 1	3.1770		2.1159	- 2	6.7743	- 1		1.9210	- 2	3.8099
22		7.3729	- 1	3.1572		2.2072	- 2	6.6272	- 1		2.0029	- 2	3.7955
10	240, 300	5.7167	- 1	3.3394	120	1.5209	- 2	3.9211		300	1.3872	- 2	7.6730 - 1
12		5.7951	- 1	3.2965		1.6656	- 2	3.8950			1.5170	- 2	7.4211 - 1
14		5.8472	- 1	3.2616		1.7945	- 2	3.8726			1.6328	- 2	7.2033 - 1
16		5.8816	- 1	3.2321		1.9111	- 2	3.8528			1.7374	- 2	7.0112 - 1
18		5.9034	- 1	3.2066		2.0176	- 2	3.8351			1.8329	- 2	6.8391 - 1
20		5.9161	- 1	3.1840		2.1159	- 2	3.8190			1.9210	- 2	6.6828 - 1
22		5.9220	- 1	3.1638		2.2072	- 2	3.8043			2.0029	- 2	6.5396 - 1

Table 2.

$N = 10^3$ $\nu = 2(10^7)$ $\phi_i = 82^\circ$ $H_m = 0.5$ $I = 45^\circ$

f, kc	ϕ_a, degrees	$\lvert T_{ee}\rvert$		arg T_{ee}	ϕ_a, degrees	$\lvert T_{em}\rvert$		arg T_{em}	ϕ_a, degrees	$\lvert T_{em}\rvert$		arg T_{em}
10	0, 180	6.4706	- 1	3.3361	0	2.2933	- 2	2.4742	180	4.9217	- 2	3.4406
12		6.5630	- 1	3.2953		2.2771	- 2	2.3673		5.1006	- 2	3.4343
14		6.6256	- 1	3.2620		2.2720	- 2	2.2697		5.2563	- 2	3.4285
16		6.6679	- 1	3.2339		2.2764	- 2	2.1802		5.3945	- 2	3.4232
18		6.6959	- 1	3.2095		2.2888	- 2	2.0977		5.5189	- 2	3.4181
20		6.7136	- 1	3.1879		2.3079	- 2	2.0216		5.6322	- 2	3.4132
22		6.7234	- 1	3.1685		2.3324	- 2	1.9511		5.7363	- 2	3.4085
10	60, 120	6.9474	- 1	3.3295	60	2.4697	- 2	2.6841	240	4.3756	- 2	3.3903
12		7.0449	- 1	3.2890		2.4266	- 2	2.6032		4.5073	- 2	3.3830
14		7.1102	- 1	3.2558		2.3900	- 2	2.5284		4.6210	- 2	3.3765
16		7.1538	- 1	3.2277		2.3597	- 2	2.4584		4.7212	- 2	3.3705
18		7.1821	- 1	3.2033		2.3352	- 2	2.3925		4.8108	- 2	3.3648
20		7.1993	- 1	3.1816		2.3161	- 2	2.3300		4.8919	- 2	3.3594
22		7.2082	- 1	3.1622		2.3017	- 2	2.2705		4.9659	- 2	3.3542
10	240, 300	5.9784	- 1	3.3379	120	3.7306	- 2	3.2457	300	2.8422	- 2	3.0368
12		6.0618	- 1	3.2962		3.7759	- 2	3.2299		2.8186	- 2	3.0038
14		6.1178	- 1	3.2623		3.8104	- 2	3.2163		2.7927	- 2	2.9744
16		6.1552	- 1	3.2337		3.8375	- 2	3.2042		2.7661	- 2	2.9478
18		6.1796	- 1	3.2088		3.8590	- 2	3.1933		2.7394	- 2	2.9231
20		6.1944	- 1	3.1869		3.8762	- 2	3.1832		2.7130	- 2	2.9001
22		6.2021	- 1	3.1672		3.8900	- 2	3.1739		2.6870	- 2	2.8783

Table 3.

$N = 10^3$ $\nu = 2(10^7)$ $\phi_i = 82^\circ$ $H_m = 0.5$ $I = 84.27^\circ$

f, kc	ϕ_a, degrees	$\lvert T_{ee}\rvert$		arg T_{ee}	ϕ_a, degrees	$\lvert T_{em}\rvert$		arg T_{em}	ϕ_a, degrees	$\lvert T_{em}\rvert$		arg T_{em}
10	0, 180	6.5072	- 1	3.3342	0	4.2815	- 2	3.0972	180	4.6885	- 2	3.1864
12		6.5995	- 1	3.2940		4.2670	- 2	3.0695		4.7133	- 2	3.1669
14		6.6619	- 1	3.2611		4.2459	- 2	3.0451		4.7274	- 2	3.1501
16		6.7041	- 1	3.2334		4.2210	- 2	3.0232		4.7345	- 2	3.1353
18		6.7321	- 1	3.2093		4.1940	- 2	3.0033		4.7368	- 2	3.1219
20		6.7497	- 1	3.1880		4.1657	- 2	2.9848		4.7355	- 2	3.1097
22		6.7596	- 1	3.1689		4.1368	- 2	2.9676		4.7317	- 2	3.0984
10	60, 120	6.5743	- 1	3.3336	60	4.3267	- 2	3.1040	240	4.6400	- 2	3.1808
12		6.6674	- 1	3.2934		4.3149	- 2	3.0768		4.6617	- 2	3.1610
14		6.7304	- 1	3.2606		4.2961	- 2	3.0529		4.6732	- 2	3.1440
16		6.7730	- 1	3.2329		4.2731	- 2	3.0314		4.6780	- 2	3.1289
18		6.8013	- 1	3.2088		4.2478	- 2	3.0119		4.6782	- 2	3.1153
20		6.8190	- 1	3.1876		4.2209	- 2	2.9938		4.6752	- 2	3.1028
22		6.8289	- 1	3.1685		4.1933	- 2	2.9770		4.6698	- 2	3.0913
10	240, 300	6.4399	- 1	3.3347	120	4.5278	- 2	3.1501	300	4.4339	- 2	3.1378
12		6.5311	- 1	3.2944		4.5351	- 2	3.1273		4.4354	- 2	3.1142
14		6.5929	- 1	3.2615		4.5334	- 2	3.1074		4.4287	- 2	3.0936
16		6.6346	- 1	3.2337		4.5259	- 2	3.0898		4.4170	- 2	3.0753
18		6.6623	- 1	3.2097		4.5146	- 2	3.0738		4.4019	- 2	3.0587
20		6.6798	- 1	3.1884		4.5008	- 2	3.0592		4.3848	- 2	3.0435
22		6.6895	- 1	3.1692		4.4851	- 2	3.0456		4.3663	- 2	3.0294

Table 4.

$N = 10^3$ $\nu = 2(10^7)$ $\phi_i = 82^\circ$ $H_m = 0.5$ $I = 90^\circ$

f, kc	ϕ_a	$\lvert T_{ee}\rvert$		arg T_{ee}	$\lvert T_{em}\rvert$		arg T_{em}
10	All	6.5080	- 1	3.3342	4.5011	- 2	3.1438
12	Values	6.6002	- 1	3.2939	4.5054	- 2	3.1206
14		6.6626	- 1	3.2611	4.5011	- 2	3.1004
16		6.7048	- 1	3.2334	4.4913	- 2	3.0824
18		6.7328	- 1	3.2093	4.4780	- 2	3.0661
20		6.7504	- 1	3.1880	4.4623	- 2	3.0512
22		6.7603	- 1	3.1689	4.4450	- 2	3.0373

Table 5.

$N = 10^3$ $\nu = 2(10^7)$ $\phi_i = 82^\circ$ $H_m = 0.5$ $I = 0$

f, kc	ϕ_a, degrees	$\lvert T_{mm}\rvert$		arg T_{mm}	ϕ_a, degrees	$\lvert T_{me}\rvert$		arg T_{me}	ϕ_a, degrees	$\lvert T_{me}\rvert$		arg T_{me}	
10	0, 180	8.8429	- 1	3.0158	0	2.9182	- 2	3.9238	180	2.9182	- 2	7.8223	- 1
12		8.7395	- 1	3.0034		3.1976	- 2	3.8992		3.1976	- 2	7.5758	- 1
14		8.6452	- 1	2.9919		3.4477	- 2	3.8778		3.4477	- 2	7.3621	- 1
16		8.5579	- 1	2.9812		3.6746	- 2	3.8589		3.6746	- 2	7.1727	- 1
18		8.4764	- 1	2.9711		3.8826	- 2	3.8418		3.8826	- 2	7.0021	- 1
20		8.3997	- 1	2.9616		4.0750	- 2	3.8262		4.0750	- 2	6.8464	- 1
22		8.3271	- 1	2.9525		4.2540	- 2	3.8119		4.2540	- 2	6.7028	- 1
10	60, 120	8.8384	- 1	3.0174	60	1.5209	- 2	3.9211	240	1.3872	- 2	7.6731	- 1
12		8.7348	- 1	3.0054		1.6655	- 2	3.8950		1.5171	- 2	7.4211	- 1
14		8.6405	- 1	2.9944		1.7945	- 2	3.8726		1.6328	- 2	7.2033	- 1
16		8.5536	- 1	2.9841		1.9111	- 2	3.8528		1.7374	- 2	7.0112	- 1
18		8.4727	- 1	2.9745		2.0176	- 2	3.8351		1.8329	- 2	6.8391	- 1
20		8.3969	- 1	2.9653		2.1159	- 2	3.8190		1.9210	- 2	6.6829	- 1
22		8.3252	- 1	2.9566		2.2072	- 2	3.8043		2.0029	- 2	6.5395	- 1
10	240, 300	8.8384	- 1	3.0174	120	1.5209	- 2	7.7949	- 1 300	1.3872	- 2	3.9089	
12		8.7349	- 1	3.0054		1.6656	- 2	7.5346	- 1	1.5171	- 2	3.8837	
14		8.6406	- 1	2.9944		1.7945	- 2	7.3100	- 1	1.6328	- 2	3.8619	
16		8.5537	- 1	2.9841		1.9111	- 2	7.1121	- 1	1.7374	- 2	3.8427	
18		8.4728	- 1	2.9745		2.0176	- 2	6.9350	- 1	1.8329	- 2	3.8255	
20		8.3970	- 1	2.9654		2.1159	- 2	6.7743	- 1	1.9210	- 2	3.8099	
22		8.3254	- 1	2.9567		2.2072	- 2	6.6272	- 1	2.0029	- 2	3.7956	

Table 6.

$N = 10^3$ $\nu = 2(10^7)$ $\phi_i = 82^\circ$ $H_m = 0.5$ $I = 45^\circ$

f, kc	ϕ_a, degrees	$\lvert T_{mm}\rvert$		arg T_{mm}	ϕ_a, degrees	$\lvert T_{me}\rvert$		arg T_{me}	ϕ_a, degrees	$\lvert T_{me}\rvert$		arg T_{me}
10	0, 180	8.8103	- 1	3.0119	0	4.9217	- 2	3.4406	180	2.2933	- 2	2.4742
12		8.7037	- 1	2.9992		5.1006	- 2	3.4343		2.2771	- 2	2.3673
14		8.6064	- 1	2.9874		5.2563	- 2	3.4285		2.2720	- 2	2.2697
16		8.5165	- 1	2.9764		5.3945	- 2	3.4232		2.2764	- 2	2.1802
18		8.4325	- 1	2.9661		5.5189	- 2	3.4181		2.2888	- 2	2.0977
20		8.3534	- 1	2.9563		5.6322	- 2	3.4132		2.3079	- 2	2.0216
22		8.2786	- 1	2.9470		5.7363	- 2	3.4085		2.3324	- 2	1.9511
10	60, 120	8.8089	- 1	3.0131	60	3.7306	- 2	3.2457	240	2.8422	- 2	3.0368
12		8.7028	- 1	3.0006		3.7759	- 2	3.2299		2.8186	- 2	3.0038
14		8.6061	- 1	2.9891		3.8104	- 2	3.2163		2.7927	- 2	2.9744
16		8.5169	- 1	2.9784		3.8375	- 2	3.2042		2.7661	- 2	2.9478
18		8.4338	- 1	2.9683		3.8590	- 2	3.1933		2.7394	- 2	2.9231
20		8.3557	- 1	2.9588		3.8762	- 2	3.1832		2.7130	- 2	2.9001
22		8.2819	- 1	2.9496		3.8900	- 2	3.1739		2.6870	- 2	2.8783
10	240, 300	8.8071	- 1	3.0123	120	2.4697	- 2	2.6841	300	4.3756	- 2	3.3903
12		8.6998	- 1	2.9997		2.4267	- 2	2.6032		4.5073	- 2	3.3830
14		8.6019	- 1	2.9882		2.3900	- 2	2.5284		4.6210	- 2	3.3765
16		8.5115	- 1	2.9774		2.3597	- 2	2.4584		4.7212	- 2	3.3705
18		8.4272	- 1	2.9672		2.3352	- 2	2.3925		4.8108	- 2	3.3648
20		8.3480	- 1	2.9577		2.3161	- 2	2.3300		4.8919	- 2	3.3594
22		8.2732	- 1	2.9486		2.3017	- 2	2.2705		4.9659	- 2	3.3542

Table 7.

$N = 10^3$ $\nu = 2(10^7)$ $\phi_i = 82^\circ$ $H_m = 0.5$ $I = 84.27^\circ$

f, kc	ϕ_a, degrees	$\lvert T_{mm}\rvert$		arg T_{mm}	ϕ_a, degrees	$\lvert T_{me}\rvert$		arg T_{me}	ϕ_a, degrees	$\lvert T_{me}\rvert$		arg T_{me}
10	0, 180	8.7806	- 1	3.0082	0	4.6885	- 2	3.1864	180	4.2815	- 2	3.0972
12		8.6710	- 1	2.9952		4.7133	- 2	3.1669		4.2670	- 2	3.0695
14		8.5711	- 1	2.9831		4.7274	- 2	3.1501		4.2459	- 2	3.0451
16		8.4786	- 1	2.9718		4.7345	- 2	3.1353		4.2210	- 2	3.0232
18		8.3923	- 1	2.9612		4.7368	- 2	3.1219		4.1940	- 2	3.0033
20		8.3110	- 1	2.9512		4.7355	- 2	3.1097		4.1657	- 2	2.9848
22		8.2342	- 1	2.9417		4.7317	- 2	3.0984		4.1368	- 2	2.9676
10	60, 120	8.7808	- 1	3.0084	60	4.5278	- 2	3.1501	240	4.4339	- 2	3.1378
12		8.6714	- 1	2.9953		4.5351	- 2	3.1273		4.4354	- 2	3.1142
14		8.5716	- 1	2.9833		4.5334	- 2	3.1074		4.4287	- 2	3.0936
16		8.4793	- 1	2.9720		4.5259	- 2	3.0898		4.4169	- 2	3.0753
18		8.3931	- 1	2.9614		4.5146	- 2	3.0738		4.4019	- 2	3.0587
20		8.3120	- 1	2.9514		4.5008	- 2	3.0592		4.3848	- 2	3.0435
22		8.2353	- 1	2.9419		4.4851	- 2	3.0456		4.3663	- 2	3.0294
10	240, 300	8.7803	- 1	3.0081	120	4.3267	- 2	3.1040	300	4.6400	- 2	3.1808
12		8.6706	- 1	2.9951		4.3149	- 2	3.0768		4.6617	- 2	3.1610
14		8.5705	- 1	2.9830		4.2961	- 2	3.0529		4.6732	- 2	3.1440
16		8.4778	- 1	2.9717		4.2731	- 2	3.0314		4.6780	- 2	3.1289
18		8.3913	- 1	2.9611		4.2478	- 2	3.0119		4.6782	- 2	3.1153
20		8.3100	- 1	2.9511		4.2209	- 2	2.9938		4.6752	- 2	3.1028
22		8.2330	- 1	2.9416		4.1933	- 2	2.9770		4.6698	- 2	3.0913

Table 8.

$N = 10^3$ $\nu = 2(10^7)$ $\phi_i = 82^\circ$ $H_m = 0.5$ $I = 90^\circ$

f, kc	ϕ_a	$\lvert T_{mm}\rvert$		arg T_{mm}	$\lvert T_{me}\rvert$		arg T_{me}
10	All	8.7800	- 1	3.0082	4.5011	- 2	3.1438
12	Values	8.6704	- 1	2.9951	4.5054	- 2	3.1206
14		8.5704	- 1	2.9830	4.5011	- 2	3.1004
16		8.4779	- 1	2.9717	4.4913	- 2	3.0824
18		8.3915	- 1	2.9611	4.4779	- 2	3.0661
20		8.3102	- 1	2.9511	4.4623	- 2	3.0512
22		8.2333	- 1	2.9416	4.4450	- 2	3.0373

Table 9.

$N = 3(10^3)$ $\nu = 2(10^7)$ $\phi_i = 82^o$ $H_m = 0.5$ $I = 0$

f, kc	ϕ_a, degrees	$\lvert T_{ee}\rvert$		arg T_{ee}	ϕ_a, degrees	$\lvert T_{em}\rvert$		arg T_{em}	ϕ_a, degrees	$\lvert T_{em}\rvert$		arg T_{em}
10	0, 180	5.5106	- 1	3.6472	0	1.5969	- 2	9.2038 - 1	180	1.5969	- 2	4.0620
12		5.6996	- 1	3.5862		1.7759	- 2	8.9780 - 1		1.7759	- 2	4.0394
14		5.8509	- 1	3.5384		1.9391	- 2	8.7854 - 1		1.9391	- 2	4.0201
16		5.9744	- 1	3.4994		2.0897	- 2	8.6170 - 1		2.0897	- 2	4.0033
18		6.0769	- 1	3.4667		2.2298	- 2	8.4669 - 1		2.2298	- 2	3.9883
20		6.1629	- 1	3.4386		2.3610	- 2	8.3312 - 1		2.3610	- 2	3.9747
22		6.2360	- 1	3.4140		2.4847	- 2	8.2070 - 1		2.4847	- 2	3.9623
10	60, 120	6.0983	- 1	3.6292	60	8.3103	- 3	9.2518 - 1	240	7.6588	- 3	4.0495
12		6.3099	- 1	3.5702		9.2483	- 3	9.0152 - 1		8.5058	- 3	4.0267
14		6.4783	- 1	3.5238		1.0103	- 2	8.8127 - 1		9.2769	- 3	4.0072
16		6.6151	- 1	3.4857		1.0891	- 2	8.6353 - 1		9.9870	- 3	3.9902
18		6.7280	- 1	3.4536		1.1624	- 2	8.4767 - 1		1.0647	- 2	3.9749
20		6.8225	- 1	3.4260		1.2310	- 2	8.3332 - 1		1.1264	- 2	3.9611
22		6.9024	- 1	3.4019		1.2955	- 2	8.2017 - 1		1.1844	- 2	3.9485
10	240, 300	4.9235	- 1	3.6629	120	8.3103	- 3	4.0668	300	7.6589	- 3	9.0791 - 1
12		5.0865	- 1	3.5988		9.2483	- 3	4.0431		8.5058	- 3	8.8513 - 1
14		5.2173	- 1	3.5486		1.0103	- 2	4.0229		9.2769	- 3	8.6566 - 1
16		5.3243	- 1	3.5077		1.0891	- 2	4.0051		9.9870	- 3	8.4860 - 1
18		5.4129	- 1	3.4735		1.1624	- 2	3.9893		1.0647	- 2	8.3335 - 1
20		5.4873	- 1	3.4442		1.2310	- 2	3.9749		1.1264	- 2	8.1954 - 1
22		5.5503	- 1	3.4187		1.2955	- 2	3.9618		1.1844	- 2	8.0689 - 1

Table 10.

$N = 3(10^3)$ $\nu = 2(10^7)$ $\phi_i = 82^o$ $H_m = 0.5$ $I = 45^o$

f, kc	ϕ_a, degrees	$\lvert T_{ee}\rvert$		arg T_{ee}	ϕ_a, degrees	$\lvert T_{em}\rvert$		arg T_{em}	ϕ_a, degrees	$\lvert T_{em}\rvert$		arg T_{em}
10	0, 180	5.5512	- 1	3.6405	0	2.4175	- 2	2.9446	180	3.9510	- 2	3.4778
12		5.7404	- 1	3.5804		2.4077	- 2	2.8824		4.1017	- 2	3.4702
14		5.8917	- 1	3.5333		2.3944	- 2	2.8254		4.2318	- 2	3.4641
16		6.0151	- 1	3.4948		2.3799	- 2	2.7725		4.3467	- 2	3.4590
18		6.1174	- 1	3.4626		2.3653	- 2	2.7227		4.4500	- 2	3.4547
20		6.2033	- 1	3.4349		2.3515	- 2	2.6756		4.5441	- 2	3.4508
22		6.2761	- 1	3.4107		2.3387	- 2	2.6306		4.6306	- 2	3.4474
10	60, 120	5.9594	- 1	3.6285	60	2.6130	- 2	3.0448	240	3.6347	- 2	3.4348
12		6.1643	- 1	3.5699		2.6096	- 2	2.9953		3.7537	- 2	3.4256
14		6.3277	- 1	3.5237		2.5998	- 2	2.9506		3.8552	- 2	3.4183
16		6.4605	- 1	3.4860		2.5864	- 2	2.9096		3.9439	- 2	3.4122
18		6.5704	- 1	3.4543		2.5709	- 2	2.8713		4.0230	- 2	3.4070
20		6.6624	- 1	3.4269		2.5545	- 2	2.8352		4.0945	- 2	3.4024
22		6.7403	- 1	3.4030		2.5377	- 2	2.8011		4.1599	- 2	3.3983
10	240, 300	5.1430	- 1	3.6513	120	3.3619	- 2	3.3404	300	2.8191	- 2	3.2099
12		5.3147	- 1	3.5892		3.4347	- 2	3.3234		2.8434	- 2	3.1823
14		5.4523	- 1	3.5406		3.4926	- 2	3.3092		2.8579	- 2	3.1585
16		5.5647	- 1	3.5010		3.5401	- 2	3.2971		2.8659	- 2	3.1374
18		5.6578	- 1	3.4678		3.5799	- 2	3.2865		2.8695	- 2	3.1183
20		5.7360	- 1	3.4394		3.6138	- 2	3.2770		2.8700	- 2	3.1010
22		5.8023	- 1	3.4146		3.6433	- 2	3.2685		2.8681	- 2	3.0849

Table 11.

$N = 3(10^3)$ $\nu = 2(10^7)$ $\phi_i = 82^\circ$ $H_m = 0.5$ $I = 84.27^\circ$

f, kc	ϕ_a, degrees	$\lvert T_{ee} \rvert$		arg T_{ee}	ϕ_a, degrees	$\lvert T_{em} \rvert$		arg T_{em}	ϕ_a, degrees	$\lvert T_{em} \rvert$		arg T_{em}
10	0, 180	5.5886	- 1	3.6345	0	4.1384	- 2	3.2478	180	4.3604	- 2	3.2998
12		5.7779	- 1	3.5752		4.1891	- 2	3.2233		4.4359	- 2	3.2802
14		5.9292	- 1	3.5287		4.2240	- 2	3.2022		4.4934	- 2	3.2636
16		6.0525	- 1	3.4908		4.2482	- 2	3.1837		4.5386	- 2	3.2493
18		6.1546	- 1	3.4589		4.2648	- 2	3.1671		4.5747	- 2	3.2367
20		6.2404	- 1	3.4316		4.2759	- 2	3.1520		4.6041	- 2	3.2253
22		6.3131	- 1	3.4077		4.2829	- 2	3.1382		4.6283	- 2	3.2150
10	60, 120	5.6453	- 1	3.6329	60	4.1690	- 2	3.2522	240	4.3284	- 2	3.2958
12		5.8369	- 1	3.5739		4.2218	- 2	3.2280		4.4015	- 2	3.2759
14		5.9899	- 1	3.5275		4.2586	- 2	3.2072		4.4569	- 2	3.2592
16		6.1146	- 1	3.4897		4.2845	- 2	3.1890		4.5002	- 2	3.2447
18		6.2179	- 1	3.4580		4.3027	- 2	3.1726		4.5346	- 2	3.2318
20		6.3045	- 1	3.4307		4.3152	- 2	3.1578		4.5624	- 2	3.2203
22		6.3781	- 1	3.4069		4.3234	- 2	3.1442		4.5851	- 2	3.2098
10	240, 300	5.5319	- 1	3.6360	120	4.2793	- 2	3.2787	300	4.2168	- 2	3.2703
12		5.7189	- 1	3.5765		4.3444	- 2	3.2570		4.2773	- 2	3.2481
14		5.8684	- 1	3.5298		4.3924	- 2	3.2386		4.3212	- 2	3.2292
16		5.9903	- 1	3.4918		4.4286	- 2	3.2226		4.3538	- 2	3.2127
18		6.0913	- 1	3.4598		4.4563	- 2	3.2083		4.3783	- 2	3.1980
20		6.1761	- 1	3.4324		4.4778	- 2	3.1954		4.3967	- 2	3.1847
22		6.2480	- 1	3.4085		4.4944	- 2	3.1837		4.4106	- 2	3.1726

Table 12.

$N = 3(10^3)$ $\nu = 2(10^7)$ $\phi_i = 82^\circ$ $H_m = 0.5$ $I = 90^\circ$

f, kc	ϕ_a	$\lvert T_{ee} \rvert$		arg T_{ee}	$\lvert T_{em} \rvert$		arg T_{em}
10	All	5.5893	- 1	3.6344	4.2676	- 2	3.2745
12	Values	5.7787	- 1	3.5751	4.3307	- 2	3.2525
14		5.9299	- 1	3.5286	4.3768	- 2	3.2338
16		6.0532	- 1	3.4907	4.4113	- 2	3.2175
18		6.1554	- 1	3.4589	4.4375	- 2	3.2030
20		6.2411	- 1	3.4315	4.4575	- 2	3.1900
22		6.3138	- 1	3.4076	4.4728	- 2	3.1780

Table 13.

$N = 3(10^3)$ $\nu = 2(10^7)$ $\phi_i = 82^\circ$ $H_m = 0.5$ $I = 0$

f, kc	ϕ_a, degrees	$\lvert T_{mm}\rvert$		arg T_{mm}	ϕ_a, degrees	$\lvert T_{me}\rvert$		arg T_{me}	ϕ_a, degrees	$\lvert T_{me}\rvert$		arg T_{me}	
10	0, 180	9.3138	- 1	3.0697	0	1.5969	- 2	4.0620	180	1.5969	- 2	9.2038	- 1
12		9.2513	- 1	3.0627		1.7759	- 2	4.0394		1.7759	- 2	8.9780	- 1
14		9.1942	- 1	3.0563		1.9391	- 2	4.0201		1.9391	- 2	8.7854	- 1
16		9.1415	- 1	3.0502		2.0897	- 2	4.0033		2.0897	- 2	8.6170	- 1
18		9.0923	- 1	3.0446		2.2298	- 2	3.9883		2.2298	- 2	8.4669	- 1
20		9.0460	- 1	3.0392		2.3610	- 2	3.9747		2.3610	- 2	8.3312	- 1
22		9.0023	- 1	3.0341		2.4847	- 2	3.9623		2.4847	- 2	8.2070	- 1
10	60, 120	9.3121	- 1	3.0700	60	8.3103	- 3	4.0668	240	7.6588	- 3	9.0791	- 1
12		9.2493	- 1	3.0631		9.2482	- 3	4.0431		8.5058	- 3	8.8513	- 1
14		9.1919	- 1	3.0568		1.0103	- 2	4.0229		9.2769	- 3	8.6566	- 1
16		9.1388	- 1	3.0509		1.0891	- 2	4.0051		9.9870	- 3	8.4859	- 1
18		9.0892	- 1	3.0453		1.1624	- 2	3.9893		1.0647	- 2	8.3334	- 1
20		9.0427	- 1	3.0401		1.2310	- 2	3.9749		1.1264	- 2	8.1953	- 1
22		8.9986	- 1	3.0351		1.2955	- 2	3.9618		1.1844	- 2	8.0689	- 1
10	240, 300	9.3121	- 1	3.0700	120	8.3103	- 3	9.2518	- 1	300	7.6589	- 3	4.0495
12		9.2493	- 1	3.0631		9.2483	- 3	9.0151	- 1		8.5058	- 3	4.0267
14		9.1918	- 1	3.0568		1.0103	- 2	8.8127	- 1		9.2769	- 3	4.0073
16		9.1388	- 1	3.0509		1.0891	- 2	8.6352	- 1		9.9870	- 3	3.9902
18		9.0892	- 1	3.0453		1.1624	- 2	8.4767	- 1		1.0647	- 2	3.9749
20		9.0427	- 1	3.0401		1.2310	- 2	8.3331	- 1		1.1264	- 2	3.9611
22		8.9986	- 1	3.0351		1.2955	- 2	8.2017	- 1		1.1844	- 2	3.9485

Table 14.

$N = 3(10^3)$ $\nu = 2(10^7)$ $\phi_i = 82^\circ$ $H_m = 0.5$ $I = 45^\circ$

f, kc	ϕ_a, degrees	$\lvert T_{mm}\rvert$		arg T_{mm}	ϕ_a, degrees	$\lvert T_{me}\rvert$		arg T_{me}	ϕ_a, degrees	$\lvert T_{me}\rvert$		arg T_{me}
10	0, 180	9.2963	- 1	3.0674	0	3.9510	- 2	3.4778	180	2.4175	- 2	2.9446
12		9.2318	- 1	3.0602		4.1017	- 2	3.4702		2.4077	- 2	2.8824
14		9.1729	- 1	3.0536		4.2318	- 2	3.4641		2.3944	- 2	2.8254
16		9.1184	- 1	3.0474		4.3467	- 2	3.4590		2.3799	- 2	2.7725
18		9.0676	- 1	3.0415		4.4500	- 2	3.4547		2.3653	- 2	2.7227
20		9.0198	- 1	3.0360		4.5441	- 2	3.4508		2.3515	- 2	2.6756
22		8.9745	- 1	3.0307		4.6306	- 2	3.4474		2.3387	- 2	2.6306
10	60, 120	9.2952	- 1	3.0677	60	3.3619	- 2	3.3404	240	2.8191	- 2	3.2099
12		9.2305	- 1	3.0606		3.4347	- 2	3.3234		2.8434	- 2	3.1823
14		9.1715	- 1	3.0540		3.4926	- 2	3.3092		2.8579	- 2	3.1585
16		9.1169	- 1	3.0479		3.5401	- 2	3.2971		2.8659	- 2	3.1374
18		9.0661	- 1	3.0422		3.5799	- 2	3.2865		2.8695	- 2	3.1183
20		9.0182	- 1	3.0367		3.6138	- 2	3.2770		2.8700	- 2	3.1010
22		8.9730	- 1	3.0315		3.6433	- 2	3.2685		2.8681	- 2	3.0849
10	240, 300	9.2957	- 1	3.0674	120	2.6130	- 2	3.0448	300	3.6347	- 2	3.4348
12		9.2309	- 1	3.0603		2.6096	- 2	2.9953		3.7537	- 2	3.4256
14		9.1718	- 1	3.0536		2.5998	- 2	2.9506		3.8552	- 2	3.4183
16		9.1171	- 1	3.0475		2.5864	- 2	2.9096		3.9439	- 2	3.4122
18		9.0660	- 1	3.0417		2.5709	- 2	2.8713		4.0230	- 2	3.4070
20		9.0179	- 1	3.0362		2.5545	- 2	2.8352		4.0945	- 2	3.4024
22		8.9724	- 1	3.0309		2.5377	- 2	2.8011		4.1599	- 2	3.3983

Table 15.

$N = 3(10^3)$ $\nu = 2(10^7)$ $\phi_i = 82^\circ$ $H_m = 0.5$ $I = 84.27^\circ$

f, kc	ϕ_a, degrees	$\lvert T_{mm}\rvert$		arg T_{mm}	ϕ_a, degrees	$\lvert T_{me}\rvert$		arg T_{me}	ϕ_a, degrees	$\lvert T_{me}\rvert$		arg T_{me}
10	0, 180	9.2802	- 1	3.0653	0	4.3604	- 2	3.2998		4.1384	- 2	3.2478
12		9.2138	- 1	3.0579		4.4359	- 2	3.2802	180	4.1891	- 2	3.2233
14		9.1533	- 1	3.0511		4.4934	- 2	3.2636		4.2240	- 2	3.2022
16		9.0972	- 1	3.0447		4.5386	- 2	3.2493		4.2482	- 2	3.1837
18		9.0449	- 1	3.0387		4.5747	- 2	3.2367		4.2648	- 2	3.1671
20		8.9958	- 1	3.0330		4.6041	- 2	3.2253		4.2759	- 2	3.1520
22		8.9492	- 1	3.0276		4.6282	- 2	3.2150		4.2829	- 2	3.1382
10	60, 120	9.2801	- 1	3.0653	60	4.2793	- 2	3.2787		4.2168	- 2	3.2703
12		9.2138	- 1	3.0579		4.3444	- 2	3.2570	240	4.2773	- 2	3.2481
14		9.1532	- 1	3.0511		4.3924	- 2	3.2386		4.3212	- 2	3.2292
16		9.0972	- 1	3.0447		4.4286	- 2	3.2226		4.3538	- 2	3.2127
18		9.0449	- 1	3.0388		4.4563	- 2	3.2083		4.3783	- 2	3.1980
20		8.9958	- 1	3.0331		4.4778	- 2	3.1954		4.3967	- 2	3.1847
22		8.9493	- 1	3.0277		4.4944	- 2	3.1837		4.4106	- 2	3.1726
10	240, 300	9.2803	- 1	3.0652	120	4.1690	- 2	3.2522		4.3284	- 2	3.2958
12		9.2139	- 1	3.0578		4.2218	- 2	3.2280	300	4.4015	- 2	3.2759
14		9.1533	- 1	3.0510		4.2586	- 2	3.2072		4.4569	- 2	3.2592
16		9.0972	- 1	3.0446		4.2845	- 2	3.1890		4.5002	- 2	3.2447
18		9.0449	- 1	3.0386		4.3027	- 2	3.1726		4.5346	- 2	3.2318
20		8.9957	- 1	3.0329		4.3152	- 2	3.1578		4.5624	- 2	3.2203
22		8.9491	- 1	3.0275		4.3234	- 2	3.1442		4.5851	- 2	3.2098

Table 16.

$N = 3(10^3)$ $\nu = 2(10^7)$ $\phi_i = 82^\circ$ $H_m = 0.5$ $i = 90^\circ$

f, kc	ϕ_a	$\lvert T_{mm}\rvert$		arg T_{mm}	$\lvert T_{me}\rvert$		arg T_{me}
10	All	9.2799	- 1	3.0652	4.2676	- 2	3.2745
12	Values	9.2135	- 1	3.0578	4.3307	- 2	3.2525
14		9.1529	- 1	3.0510	4.3768	- 2	3.2338
16		9.0968	- 1	3.0446	4.4113	- 2	3.2175
18		9.0445	- 1	3.0386	4.4375	- 2	3.2030
20		8.9953	- 1	3.0329	4.4575	- 2	3.1900
22		8.9487	- 1	3.0275	4.4728	- 2	3.1780

Table 17

$N = 10^3$ $\phi_i = 82^\circ$ $H_m = 0.5$ $I = 0$ $\phi_a = 0$

f, kc	ν	$\lvert T_{ee}\rvert$		arg T_{ee}	$\lvert T_{em}\rvert$		arg T_{em}	
10	0	9.9841	- 1	5.9879	5.6404	- 2	1.4088	
10	10^6	3.4326	- 1	4.8070	8.0119	- 2	9.3737	- 1
10	$4(10^6)$	4.7778	- 1	3.8325	5.7508	- 2	9.1968	- 1
10	$2(10^7)$	6.4307	- 1	3.3383	2.9182	- 2	7.8223	- 1
10	10^8	6.5471	- 1	3.0070	1.2215	- 2	5.5561	- 1

f, kc	ν	$\lvert T_{mm}\rvert$		arg T_{mm}	$\lvert T_{me}\rvert$		arg T_{me}
10	0	9.9841	- 1	3.1129	5.6404	- 2	4.5504
10	10^6	9.7612	- 1	3.1006	8.0119	- 2	4.0790
10	$4(10^6)$	9.4888	- 1	3.0802	5.7508	- 2	4.0613
10	$2(10^7)$	8.8429	- 1	3.0158	2.9182	- 2	3.9238
10	10^8	7.5707	- 1	2.8653	1.2215	- 2	3.6972

Summary of tables

Table	Polarization	N	ν	ϕ_i	H_m	I	ϕ_a	f
		el/cm^3	*c/s*	*Degrees*	*Gauss*	*Degrees*	*Degrees*	*kc/s*
1	*e*	10^3	$2(10^7)$	82	0.5	0	0–300	10–22
2						45		
3						84.27		
4						90	(a)	
5	*m*					0	0–300	
6						45		
7						84.27		
8						90	(a)	
9	*e*	$3(10^3)$				0	0–300	
10						45		
11						84.27		
12						90	(a)	
13	*m*					0	0–300	
14						45		
15						84.27		
16						90	(a)	
17	*e,m*	10^3	0–10^8			0	0	

[a] Independent of ϕ_a.

5. References

[1] J. R. Johler and L. C. Walters, On the theory of reflection of low- and very-low-radiofrequency waves from the ionosphere, J. Research NBS **64D,** 269 (May 1960).

[2] H. A. Lorentz, The theory of electrons (G. E. Stechert and Co., New York, N.Y., 1906).

[3] J. R. Wait, Terrestrial propagation of very low frequency radio waves, a theoretical investigation, J. Research NBS **64D,** 153 (1960); see also J. R. Wait and K. Spies, Influence of earth curvature and the terrestrial magnetic field on VLF propagation, J. Geophys. Research (Aug. 1960).

(Paper 65 D1–103)

565004—60——6

JOURNAL OF RESEARCH of the National Bureau of Standards—D. Radio Propagation
Vol. 65D, No. 1, January–February 1961

Correlation of Monthly Median Transmission Loss and Refractive Index Profile Characteristics [1]

B. R. Bean and B. A. Cahoon

(July 14, 1960; revised August 5, 1960)

The difference in the monthly mean values of the refractive index at ground level and at one kilometer above the ground level is often used for the purpose of predicting the annual cycle of radio transmission loss. The present study investigates the possibility of utilizing differences to heights other than one kilometer. A comparison of 100 megacycles per second transmission loss recorded over twenty-one paths with various refractivity differences from the surface to three kilometers reveals that the surface value of the refractive index yields as good a correlation as any of the refractive index differences due to the high correlation between the surface values and these differences; therefore the more accessible surface value can be effectively substituted for the differences. Specifying the refractive index profile at two or three additive points and using multiple correlation techniques does not significantly increase the correlation.

The use of radio data over the same path does not significantly improve the correlation over that obtained from only meteorological data, indicating the very practical result that inexpensive meteorological data may be used to predict the seasonal trend of VHF radio field strengths with as much accuracy as expensive radio path measurements.

1. Introduction

Current engineering practice in estimating the level of beyond-the-horizon VHF-UHF radio field strengths [1 to 5] [2] consists of determining an average level for a given distance and then adjusting this average level for climatic and seasonal differences by reference to common meteorological measurements of pressure, temperature, and humidity as expressed by the radio refractive index, n. Although past investigations have principally utilized the difference in n between the earth's surface and 1 km above the earth's surface, better results might be obtained by using differences to heights other than 1 km or between different levels on the profile. It is the purpose of this study to explore this possibility via the correlation of the annual cycles of monthly median radio transmission loss and n gradients obtained over a variety of height increments. The sections that follow deal with the available radio and meteorological data, deriving correlations between the two and discussing their significance on a regional and a statistically-combined basis.

2. Radio and Meteorological Data

The radio data used in the present studies are the 100 Mc/s monthly median transmission losses for the 21 transmission paths listed in table 1. All data correspond to the hours of the 0300 and 1500 G.m.t. radiosonde observations (1000 and 2200 e.s.t.). These data represent climatic conditions ranging from those of New England (path 19) to the central and southeastern seaboard (paths 17 and 21) the Gulf States (paths 1 to 6), Great Lakes (paths 7, 11, and 18), the high plains (paths 16 and 20), and the Pacific Coast (path 15). Examples of annual cycles of monthly median basic transmission loss for four geographically representative radio paths are given on figure 1. It is quite clear that, with but minor variation, the transmission loss from each path follows a rather definite annual cycle, the loss being low in the summer months and high in the winter months. It appears to be quite significant that similar annual cycles are observed in such different climatic regions as the Appalachian Mountains of Pennsylvania and southern California coast.

TABLE 1

Path	Call letters	Transmitter location	Receiver location	Frequency	Distance	θ(mr)
				Mc/s	km	
1	KXYZ	Houston, Tex.	Austin, Tex.	96.5	237.9	20.32
2	KPRC	Houston, Tex.	Austin, Tex.	102.9	237.9	21.00
3	KIXL	Dallas, Tex.	Austin, Tex.	104.5	283.1	32.38
4	KWKH	Shreveport, La.	Austin, Tex.	94.5	446.4	47.36
5	KLTI	Longview, Tex.	Austin, Tex.	105.9	365.6	40.40
6	WFAA	Dallas, Tex.	Austin, Tex.	97.9	280.3	32.54
7	WMBI	Chicago, Ill.	Urbana, Ill.	95.5	202.8	16.13
8	WCSI	Columbus, Ind.	Urbana, Ill.	93.7	223.7	20.88
9	KXOK	St. Louis, Mo.	Urbana, Ill.	93.7	235.8	19.34
10	WHKC	Columbus, Ohio	Hudson, Ohio	98.7	201.0	19.42
11	WCOL	Columbus, Ohio	Hudson, Ohio	92.3	195.1	20.12
12	WJAS	Pittsburgh, Pa.	State College, Pa.	99.7	188.5	30.44
13	WEST	Easton, Pa.	State College, Pa.	107.9	224.2	36.67
14	WTOP	Washington, D.C.	State College, Pa.	96.3	215.8	63.47
15	KFSD	San Diego, Calif.	Santa Ana, Calif.	94.1	136.3	28.97
16	KFOR	Lincoln, Nebr.	Grand Island, Nebr.	102.9	150.0	14.59
17	WCAC	Anderson, S.C.	Powder Springs, Ga.	101.1	205.2	19.81
18	KDKA	Pittsburgh, Pa.	Hudson, Ohio	92.9	155.6	12.15
19	WTIC	Hartford, Conn.	Millis, Mass.	96.5	129.9	16.29
20	NBS-CRPL	Cheyenne Mt. Colo.	Haswell, Colo.	92.0	155.8	6.469
21	WIP-FM	Philadelphia, Pa.	Laurel, Md.	93.3	167.7	12.04

[1] Contribution from Central Radio Propagation Laboratory, National Bureau of Standards, Boulder, Colo.

[2] Figures in brackets indicate the literature references at the end of this paper.

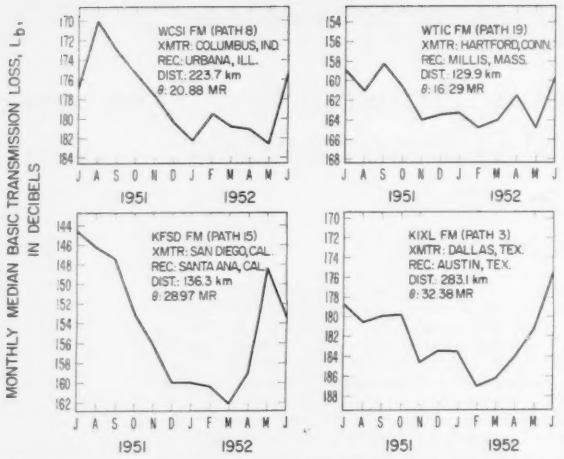

FIGURE 1. *Annual cycles of monthly median basic transmission loss for four geographically diverse radio paths.*

These annual cycles plus the data indicated by table 1 were used as a test of various radio meteorological parameters that might be used in propagation studies. The refractive index gradients were prepared from 6-yr means of temperature, pressure, and humidity as a function of height by the National Weather Records Center of the U.S. Weather Bureau. These data were then converted to

$$N=(n-1)10^6 \tag{1}$$

by means of the Smith-Weintraub relationship [6]. Simple differences of the value of N at the earth's surface, N_s, and its value at 0.1, 0.2, 0.3, 0.5, 0.7, 1.0, 2.0, and 3.0 km above the earth's surface were obtained. This procedure is illustrated for an exponential curve on figure 2. For example, the value of the difference to 500 m, $\Delta N_{0.5}$, is determined by

$$\Delta N_{0.5}=N_s-N_{0.5}. \tag{2}$$

The variations of transmission loss were also compared with those of N_s since it has received such wide engineering applications [1 to 4, 7 to 9].

3. Choice of Statistical Model

When analyzing two variables for a possible interrelation one has available many statistical techniques such as linear, multiple, and polynomial regression. Individual graphs of transmission loss and ΔN_h were prepared for each of the gradient levels on each of the propagation paths to aid in the choice of an appropriate statistical model. Visual investigation of these data, examples of which are shown on figures 3 and 4, reveals the presence of a large random component that masks any obvious nonlinear relation between the variables. On this basis it was decided that use of nonlinear regression techniques was an unnecessary complication at this stage of the analysis, and the simple linear regression model was adopted.

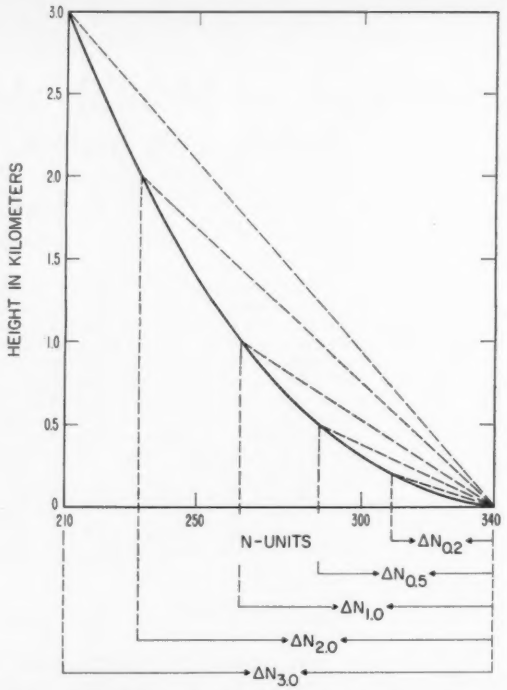

FIGURE 2. *Graphical representation of the determination of various N differences in an average atmosphere.*

4. Statistical Considerations

We are here concerned with the degree to which the annual cycle of radio transmission loss may be predicted from the several ΔN_h values described above under the assumption of a linear regression model. This is done on a quantitative basis by determining the linear correlation coefficient, $r_{y\cdot x}$, between a dependent variable, y, (in this case the transmission loss) and an independent variable x (whichever ΔN_h we are considering). The reason for determining the correlation coefficient can be understood more easily in terms of the standard error of estimate, $(SE)_y$, which is given by

$$(SE)_y=s_y(1-r^2_{y\cdot x})^{1/2}, \tag{3}$$

where s_y is the standard deviation of the dependent variable. Equation (3) allows one to evaluate quantitatively the degree to which one may predict the variations of y by knowing its correlation with x (and the concomitant regression equation). Thus it is seen that if y is completely determined from x, and $r_{y\cdot x}=1$, then $(SE)_y=0$. Conversely, if x and y are totally independent, then $r_{y\cdot x}=0$, and $(SE)_y=s_y$, and there is no advantage gained by attributing variations of y to x. We may define the improvement factor

$$k=100\left[\frac{s_y-(SE)_y}{s_y}\right], \tag{4}$$

TABLE 2. *Coefficient of correlation between monthly median transmission loss and indicated meteorological variable.*

Path	Pieces of data	N_s	$\Delta N_{0.1}$	$\Delta N_{0.2}$	$\Delta N_{0.3}$	$\Delta N_{0.5}$	$\Delta N_{0.7}$	$\Delta N_{1.0}$	$\Delta N_{2.0}$	$\Delta N_{3.0}$
1	38	0.586	0.504	0.517	0.525	0.553	0.589	0.612	0.626	0.624
2	36	.618	.462	.527	.552	.593	.614	.632	.659	.651
3	68	.787	.670	.690	.707	.724	.737	.768	.787	.786
4	41	.774	.619	.623	.640	.654	.657	.706	.714	.732
5	23	.672	.549	.541	.536	.539	.533	.589	.617	.627
6	7	.940	.806	.850	.851	.883	.890	.909	.916	.925
7	22	.714	.539	.559	.567	.645	.695	.711	.727	.718
8	48	.726	.713	.729	.729	.742	.763	.766	.767	.745
9	24	.588	.626	.643	.639	.627	.638	.626	.627	.608
10	74	.506	.527	.540	.540	.550	.540	.556	.532	.518
11	64	.525	.542	.542	.534	.552	.554	.575	.556	.539
12	41	.868	.778	.858	.871	.874	.866	.873	.874	.869
13	26	.785	.590	.724	.734	.725	.743	.778	.802	.800
14	12	.935	.733	.887	.886	.893	.901	.928	.940	.938
15	28	.797	−.128	−.228	−.246	−.134	.731	.802	.787	.814
16	17	.626	.542	.576	.619	.654	.660	.666	.655	.636
17	17	.373	.247	.298	.314	.370	.384	.466	.455	.421
18	30	.803	.809	.830	.836	.832	.797	.791	.787	.799
19	13	.744	.214	.686	.779	.782	.775	.760	.778	.768
20	13	.115	.364	.373	.299	.292	.270	.214	.118	.117
21	38	.652	.579	.806	.781	.761	.722	.688	.655	.647
Mean values (omitting path 20)										
$r(z)$	667	0.694	0.578	0.633	0.640	0.655	0.676	0.702	0.704	0.700
$k[r(\bar{z})]$	667	28.0%	18.4%	22.6%	23.2%	24.4%	26.4%	28.8%	29.0%	28.6%

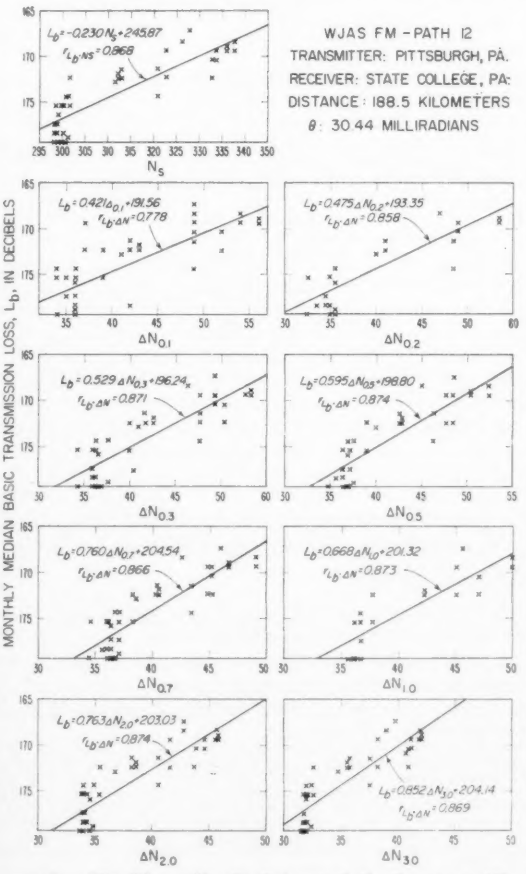

FIGURE 3. *Monthly median basic transmission loss versus* N_s *or* ΔN_h *for Path 12 (Pittsburgh to State College, Pa).*

as the percentage reduction of uncertainty of predicting y from knowledge of its correlation with x.

It is frequently desirable to estimate the average value of the correlation coefficient when dealing with several correlation coefficients between the same variables but derived in different climatic regions. Since r is not normally distributed it is desirable to convert r to Fisher's z,

$$z=\tfrac{1}{2}[\log_e(1+r)-\log_e(1-r)]$$

when is more nearly normally distributed, obtain the average of z, and convert this average $\bar{z}$ to an estimate of $\bar{r}$ [10].

5. Comparison of Annual Cycles

Individual correlation coefficients of the monthly median transmission loss and the mean value of the various refractive index gradients were determined for each path and are listed in table 2. Figure 5 depicts the relative behavior of r versus N difference to various heights for the same four radio paths as those graphed in figure 1. It can be noted from figure 5 and table 2 that the magnitude of the correlation coefficients is generally lowest when determined versus $\Delta N_{0.1}$ and rises with increasing Δh until the maximum value is reached at 1.0 or 2.0 km.

Table 2 also lists the average correlation coefficients [10], indicating that the correlation of radio transmission loss with N_s is as large as those obtained with any value of ΔN_h.

There are some notable exceptions to the above observations. For example, path 18 (Pennsylvania to Ohio) and path 9 (Missouri to Illinois) displayed a fairly uniform correlation for all height increments with a very small range of coefficients. Path 19,

where the 0.5 km level evinced the highest correlation, and path 21, where the maximum correlation appeared at 0.2 km, also had a very low range with the exception of the 0.1-km level where the correlation coefficient was significantly lower.

The low correlations for path 20 might arise from the fact that this path is a borderline knife-edge diffraction case, as indicated by the low value of the angular distance, θ.

Perhaps the most interesting case is that of path 15, San Diego to Santa Ana, California, where the largest correlations are found between the transmission loss and N_s and gradients for height increments in excess of 0.7 km. The correlation coefficients for height increments below 0.7 km are not only relatively small but are negative. This physically unrealistic behavior, shown in more detail in figures 4 and 5, may be explained by the presence of the well-known southern California coastal inversion which occurs at about 0.7 km and is known to exert a dominating influence upon radio field strengths in that region [11, 12]. The interesting conclusion here is that the variations of radio fields follow those of N_s and any of the N differences to heights above the base of the inversion but do not follow the intermediate differences.

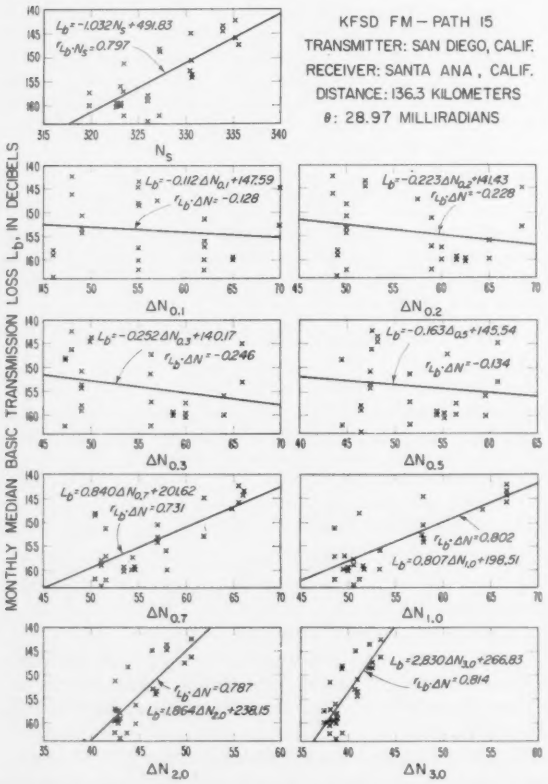

FIGURE 4. *Monthly median basic transmission loss versus* N_s *or* ΔN_h *for Path 15 (San Diego to Santa Ana, Calif.).*

6. Other Measures of the Gradient

The preceding analysis has been concerned with the correlation of transmission loss and ΔN_h when h takes on several different values. It is also profitable to examine the correlation of transmission loss and differences in index taken between various points on the N profile such as has been found useful in Germany by Grosskopf [13]. Another profile measure is Misme's "useful gradient" [14], G, given by [3]

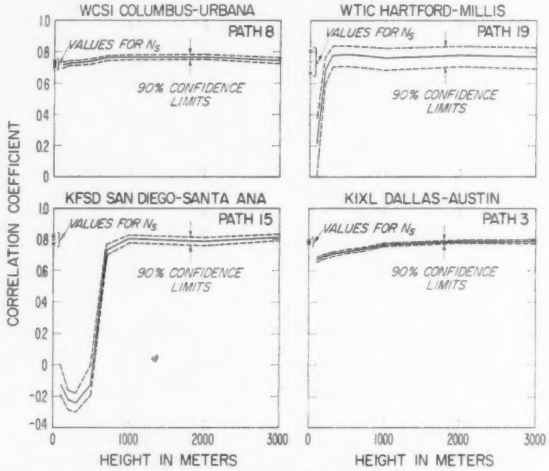

FIGURE 5. *Correlation coefficients of monthly median basic transmission loss versus height in meters of* ΔN_h *for four geographically diverse paths.*

$$G=\frac{2\Delta N_0+\Delta N_c}{3}$$

where ΔN_0 is the initial gradient and ΔN_c is the gradient at the crossover height of the radio horizon rays. The correlation coefficients resulting from such a comparison are tabulated in table 3 and, it is seen that the average correlation coefficients are generally lower than those obtained previously. The general conclusion one reaches here, then, is that none of these other profile measures offers a significant improvement over the widely used N_s and $\Delta N_{1.0}$.

7. Use of Previous or Concurrent Radio Field Strengths to Predict the Annual Cycle of Radio Fields

A perspective on the magnitude and usefulness of the above correlation coefficients may be gained by comparing the correlation of transmission loss recorded over nearly identical paths. Seven of the radio paths on table 1 had sufficient data so that the

[3] In the course of a private conversation, P. Misme has pointed out to the authors that recent studies have led him to adopt a different value for the altitude at which the parameter dN/dh (referred to as ΔN_c in our equation for G) is measured. Furthermore, calculation by layers is in every case preferable as a method of obtaining the value of the "equivalent gradient." Unfortunately, this comment reached the authors too late to be considered in this work. However, a forthcoming article by the authors will compare the variation of the equivalent gradient and other measures of atmospheric refraction with variations of transmission loss.

TABLE 3. *Coefficient of correlation between monthly median transmission loss and indicated meteorological variable*

Path	G	$\Delta N_{0.2-0.5}$*	$\Delta N_{0.5-1.0}$	$\Delta N_{1.0-2.0}$	$\Delta N_{2.0-3.0}$	N_s
1	0.5477	0.04999	−0.2892	0.4042	0.5032	0.586
2	.5273	−.1219	−.2191	.2297	.5519	.618
3	.6959	.4511	.2437	.6747	.7425	.787
4	.6489	.3679	.1349	.5567	.5925	.774
5	.5673	.4166	.1988	.4450	.5455	.672
6	.8383	.5087	.6355	.7893	.8666	.940
7	.5708	.1986	.1543	.3675	.6610	.714
8	.7351	.6248	.5134	.6105	.8102	.726
9	.6369	.6583	.5700	.4834	.6980	.588
10	.5312	.4951	.4531	.5694	.5681	.506
11	.5451	.4933	.4207	.5743	.6074	.525
12	.8178	.6308	.6174	.5985	.7920	.868
13	.6746	.3432	.3610	−.5836	.6850	.785
14	.8400	−.2005	.6165	.8162	.8775	.935
15	−.1262	−.3484	−.4062	.7793	.6321	.797
16	.5636	.3844	.5682	.6797	.6889	.626
17	.2844	−.0350	.0044	.3981	.6309	.373
18	.8213	.7762	.7643	.6950	.6336	.803
19	.5428	−.8087	.7599	.5665	.7712	.744
20	.3636	.4088	.3519	.1786	.1188	.115
21	.7488	−.09026	.8065	.6900	.6566	.652
Mean values (omitting path 20)						
$r(\bar{z})$	0.6224	0.3548	0.3811	0.5461	0.6624	0.694
$k[r(\bar{z})]$	21.7%	6.5%	7.5%	16.2%	25.1%	28.0%

*Note: $N_{0.2-0.5}$ indicates that the transmission loss was correlated with the difference in N taken at $h=0.2$ km and $h=0.5$ km.

first 12 months of record could be used to predict the monthly median radio field strengths in subsequent years. The results of this study, including the mean correlation coefficient and the improvement factor, are given in category 3 of table 4. A comparison of the improvement factor with those of tables 2 and 3 leads one to the conclusion that for any practical prediction problem, where only past radio or meteorological data are available, one obtains at least as good a prediction of the annual cycle of transmission loss from long-term meteorological data as from relatively short-term radio data.

This conclusion arises from the fact that the correlation between paths 1 and 2 is low (0.348) even though the paths are so nearly identical that one would not hesitate to make such a comparison for any

TABLE 4. *Correlation of annual cycles of transmission loss over identical or nearly identical paths*

Category	Paths	Data	j*	r	90% confidence limits
1	1&2	Successive 15-month periods.	30	0.348	0.295 to 0.399.
2	10&11	Coincident months.	58	.838	0.829 to 0.847.
3	3.	First 12 months of record on subsequent years of record.	44	.767	0.750 to 0.783.
	4.		17	.762	0.708 to 0.807.
	8.		24	.764	0.730 to 0.795.
	9.		12	.624	0.500 to 0.723.
	12.		18	.737	0.683 to 0.783.
	15.		16	.656	0.578 to 0.723.
	21.		14	.890	0.859 to 0.917.
		$r(\bar{z})=0.751$			
		$k[r(\bar{z})]=34.0\%$			

*j=pieces of data.

engineering applications. The use of radio data from the same path (category 3) does yield a higher correlation than the use of meteorological data alone; but this type of prediction, running the actual circuit for a year, results in only a slight improvement in prediction at a cost increase of many orders of magnitude over that of procuring the necessary meteorological data. However, any actual radio path strength testing would probably fall into category 1 where data from nearly identical paths are used, and the resulting correlation appears to be less than that obtained from meteorological data alone. Category 2, use of simultaneous radio data, yields the highest correlation but is generally an impractical procedure for engineering applications.

These results have a very important implication for future radio meteorological studies involving monthly median field strengths. It is hard to imagine any predictor of field strength variations that would be more effective than a nearby radio station at nearly the same frequency, recorded over nearly identical paths to the same receiver site. In this case it would seem that the maximum reduction in the uncertainty of predicting fields from monthly mean refractive index data could not exceed about 35 percent. If this is indeed true, then further work along these lines would seem quite futile, and new approaches should be tried. Perhaps a profitable new approach would be to combine the effects of day-to-day variations of refractive index profiles in some manner similar to that suggested in the earlier works of the senior author [15].

8. Multiple Regression

One might wonder if a combination of the above meteorological variables would produce a greater reduction of the uncertainty of prediction. Several combinations of meteorological parameters that might occur in practice were evaluated. These were transmission loss as a function of both N_s and $\Delta N_{1.0}$ (assuming that both N_s and ΔN could be obtained from climatic maps for the United States [1, 16] or the worldwide climatic maps in preparation by the International Consultative Committee for Radio) and also as a function of N_s and $\Delta N_{0.1}$, such as might be obtained from meteorological towers. These data, reported in table 5, indicate that very little improvement may be accomplished by using two meteorological variables determined from radiosonde data. Indeed, even when transmission loss as a function of all three of these meteorological parameters is considered, the augmentation of the correlation coefficient does not appear to be significant. In fact, the examination of the linear relationship involving all three of the meteorological factors,

$$\begin{aligned} -L_b &= b_1N_s+b_2\Delta N_{0.1}+b_3\Delta N_{1.0}+a \\ &= b_1N_s+b_2N_s-b_2N_{0.1}+b_3N_s-b_3N_{1.0}+a \\ &= N_s(b_1+b_2+b_3)-b_2N_{0.1}-b_3N_{1.0}+a, \end{aligned} \qquad (5)$$

TABLE 5.—*Correlation coefficients of transmission loss versus multiple meteorological factors*

Path	$r_{y\cdot x_1x_2}$*	$r_{y\cdot x_1x_3}$*	$r_{y\cdot x_1x_2x_3}$*
1	0.586	0.613	0.622
2	.636	.633	.669
3	.797	.787	.800
4	.794	.812	.814
5	.696	.790	.790
6	.958	.958	.959
7	.758	.716	.782
8	.733	.818	.822
9	.627	.688	.764
10	.528	.607	.610
11	.542	.626	.628
12	.869	.874	.875
13	.787	.785	.787
14	.936	.936	.936
15	.823	.816	.837
16	.690	.730	.798
17	.435	.592	.736
18	.812	.803	.813
19	.749	.766	.770
20	.500	.315	.500
21	.771	.718	.778
Mean values (omitting path 20)			
$r^*(\bar{x})$	0.717	0.742	0.758
$k[r(\bar{x})]$	30.3%	33.0%	34.8%

*For this table $y=L_b$, $x_1=N_s$, $x_2=\Delta N_{0.1}$, $x_3=\Delta N_{1.0}$.

discloses that the attempt to specify the refractive profile by three points apparently does not lead to an appreciable increase in the correlation coefficient. However, the error analysis carried out in the next section indicates that the probable errors associated with radiosonde measurements are sufficient to mask the true correlation value to the extent that this conclusion might well be modified by the use of more accurate meteorological data.

The above correlations do reflect systematic properties of the atmosphere which in themselves present an interesting study. It is not too surprising to note that the mean correlation coefficient between N_s and $\Delta N_{1.0}$ is high (0.9840). This interdependence of N_s and $\Delta N_{1.0}$ is fortunate since it allows the computation of $\Delta N_{1.0}$ from surface data, which is readily available throughout the world.

9. Error Analysis

It is really quite surprising that the initial gradient, $\Delta N_{0.1}$, did not yield larger correlation coefficients since the refraction of radio waves is known to be extremely sensitive to the initial gradient. It is quite possible that this low correlation reflects the difficulty of determining an N difference over a small increment with relatively inaccurate radiosonde sensing elements. We may analyze this error by reference to common meteorological standard atmospheres and standards of measurement set by the International Consultative Committee for Radio (CCIR). By setting

$$\Delta N_{1-2}=\frac{(N_1+\epsilon_1)-(N_2+\epsilon_2)}{(h_1-h_2)} \tag{6}$$

where N_1 and N_2 represent the true value of N at h^1 and h_2 and ϵ_1 and ϵ_2 represent the errors determining N at h_1 and h_2 respectively, then the standard deviation of the error in ΔN_{1-2} is

$$\sigma(\Delta N_{1-2})=\left[\frac{\sigma^2(\epsilon_1)+\sigma^2(\epsilon_2)}{(h_1-h_2)^2}\right]^{1/2} \tag{7}$$

assuming that h_1-h_2 is known exactly and that ϵ_1 and ϵ_2 are uncorrelated. The errors ϵ_1 and ϵ_2 may be determined by noting that [6]

$$N=K_1\frac{P}{T}+K_2\frac{e}{T^2} \tag{8}$$

and that

$$dN=\frac{\partial N}{\partial T}dT+\frac{\partial N}{\partial e}de+\frac{\partial N}{\partial P}dP. \tag{9}$$

The partial derivatives may be evaluated from the ICAO standard atmosphere [17] assuming 60 percent relative humidity to yield approximate relationships

$$\Delta N=-1.27\Delta T+4.50\Delta e+0.27\Delta P \tag{10}$$

for $h=0$ and

$$\Delta N=-1.09\Delta T+4.72\Delta e+0.28\Delta P \tag{11}$$

for $h=1$ km.

By assuming the relatively stringent accuracies in measuring P, T, and e called for by the CCIR [18] one obtains standard errors of 3.5 percent of the mean in determining $\Delta N_{1.0}$, and 22.7 percent of the mean in determining $\Delta N_{0.1}$.

Reference to standard treatment of the effect of measurement errors upon correlation coefficients [19] shows that if y is the dependent variable and the indpendent variable $x^*=x+\epsilon$ where x is the true value and ϵ is the measurement error then the correlation coefficient is

$$\rho_{y\cdot x}{}^*=\frac{\rho_{y.x}}{\sqrt{1+s^2(\epsilon)/s^2(x)}} \tag{12}$$

assuming that ϵ has zero mean and variance $s^2(\epsilon)$ and is uncorrelated with either x or y, the other terms having their usual meaning. It is seen that the effect of measurement error is to reduce the correlation coefficient by the factor

$$\frac{1}{\sqrt{1+s^2(\epsilon)/s^2(x)}}. \tag{13}$$

If we now assume that y (in this case the transmission loss) is correlated with two different measures of the same variable, x_1 and x_2, (in this case $\Delta N_{0.1}$ and $\Delta N_{1.0}$) then from the ratio

$$\frac{\rho_{y.x_1^*}}{\rho_{y.x_2^*}}=\frac{\rho_{y.x_1}}{\rho_{y.x_2}}\left[\frac{1+s^2(\epsilon_2)/s^2(x_2)}{1+s^2(\epsilon_1)/s^2(x_1)}\right]^{1/2}. \tag{14}$$

one may determine the relative size of the measurement errors necessary to yield the same correlation coefficient by setting

$$\frac{\rho_{y.x_1^*}}{\rho_{y.x_2^*}}=\frac{\rho_{y.x_1}}{\rho_{y.x_2}}=1 \tag{15}$$

and obtaining

$$s(\epsilon_1)/s(\epsilon_2)=s(x_1)/s(x_2). \tag{16}$$

Returning to our data we find that this ratio averages about 1.5 for the observed values of $s(\Delta N_{0.1})/s(\Delta N_{1.0})$ while the ratio of the errors determined from the ICAO standard atmosphere and the CCIR standards of measurement is about 10.0. Thus it is seen that the errors of measurement may indeed be the cause of the differences in these correlation coefficients. Although one cannot estimate the actual size of the true correlation coefficients, one can estimate their ratio by reexpressing (14) as

$$\frac{\rho_{y.x_1}}{\rho_{y.x_2}}=\frac{\rho_{y.x_1^*}}{\rho_{y.x_2^*}}\left[\frac{1+s^2(\epsilon_1)/s^2(x_1)}{1+s^2(\epsilon_2)/s^2(x_2)}\right]^{1/2}. \tag{17}$$

When we again use the standard-atmosphere-estimated errors and the actual values of $s^2(x_1)$ and $s^2(x_2)$ for the 21 paths in our analysis, we find that the ratio $\rho_{y.x_1}/\rho_{y.x_2}$ averages about 1.5 which implies, since $r_{L_b.\Delta N_{1.0}}\sim 0.7$, the actual correlation with the surface layer $r_{L_b.\Delta N_{0.1}}$ is near unity, an observation that should guide future experimental research in the quest of more efficient radio-meteorological parameters.

Although it is evident that the errors of measurement do make the choice of a radio climatological parameter based upon this study somewhat indefinite, we may use the present study as an objective criterion of the relative merits of such parameters when determined from radiosonde observations. Perhaps the advent of more accurate measurements will shed more light on the true role of the surface layer in radio meteorology.

10. Extension to Other Regions

Although this study encompasses only a small portion of the United States because of limited radio data, several of the more important climates of the world are represented by the 21 paths. Paths 1 to 6, 14, 17, and 21 lie in the same humid subtropical region which covers parts of Argentina, China, and Yugoslavia; the climate of paths 7 to 13, 16, and 18 is similar to that of Hungary, Romania, and parts of Japan; path 15 represents the Mediterranean regions and includes southern Australia, Africa, and central Chile; path 20 has meteorological conditions which resemble the middle latitude steppes of Canada and southern Russia while path 19 is similar to southern Sweden and central Russia. It is reasonable to assume that the general pattern of the mean profile of a climatic area would repeat itself, regardless of the country in which it was located. Such an assumption would permit the extension of any conclusions reached in this paper regarding the correlative aspects of various meteorological parameters versus transmission loss to other regions. In fact, studies which have been completed of N_s versus transmission loss show good results not only in the Florida-Caribbean [3] area but also with transmission paths from Argentina to Uruguay [3], from Minorca to Sardinia in the Mediterranean [4], and from Tokyo to Osaka in Japan [20].

11. Conclusions

In this study the calculation of the correlation coefficients of recorded transmission loss over 21 radio paths versus various properties of the refractive index profile up to 3 km provides a means of evaluating which radio-meteorological parameter is most efficient to predict average radio transmission loss. The best correlations appeared to be associated with the time-honored values of $\Delta N_{1.0}$ and N_s, indicating that they continue to yield as good a correlation as any other parameter derived from currently available radiosonde observations.

While comparing the interdependence of meteorological parameters, the correlation of surface refractivity, N_s, with a gradient interval of 1 km was found to be high, explaining why the more accessible N_s can be used with significant results in place of the 1-km gradient in the prediction of transmission loss.

An examination of the correlations of transmission loss recorded for 1 year versus that recorded in another year for the same radio path revealed correlations of the same order as those obtained from meteorological data alone, indicating the very practical result that inexpensive meteorological data may be used to predict the seasonal variation of radio fields as accurately as expensive radio path measurements.

The authors acknowledge the assistance of K. A. Norton, G. Richmond, B. J. Weddle, and P. C. Whittaker in this study.

12. References

[1] B. R. Bean and F. M. Meaney, Some applications of the monthly median refractivity gradient in tropospheric propagation, Proc. IRE **43,** 1419 (1955).

[2] K. A. Norton, P. L. Rice, and L. E. Vogler, Use of angular distance in estimating transmission loss and fading range for propagation through a turbulent atmosphere over irregular terrain, Proc. IRE **43,** 1488 (1955).

[3] R. E. Gray, Refractive index of the atmosphere as a factor in tropospheric propagation far beyond the horizon, Elec. Commun. **36,** 60 (1959).

[4] L. Bonavoglia, Correlazione fra fenomeni meteorologici e propagazione oltre l'orizzonte sul Mediterraneo, Alta Frequenza XXVII, 815 (1958).

[5] F. du Castel, Sur la validite de l'hypothese d'une gradient lineaire de l'indice de refraction tropospherique pour le calcul du champ dans la zone de diffraction en ondes metriques en Mediterranee occidentale, Note Prelim. No. 175 (Lab. Natl. Radioelec., France, 1954).

[6] E. K. Smith and S. Weintraub, The constants in the equation for atmospheric refractive index at radio frequencies, Proc. IRE **41,** 1035 (1953).
[7] G. W. Pickard and H. T. Stetson, Comparison of tropospheric reception, J. Atmospheric and Terrest. Phys. **1,** 32 (1950).
[8] G. W. Pickard and H. T. Stetson, Comparison of tropospheric reception at 44.1 Mc with 92.1 Mc over the 167-mile path of Alpine, New Jersey to Needham, Massachusetts, Proc. IRE **38,** 1450 (1950).
[9] K. A. Norton, Point-to-point radio relaying via the scatter mode of tropospheric propagation, IRE Trans. **PGCS-4,** 39 (1956).
[10] G. W. Snedecor, Statistical Methods, p. 152 (Iowa State College Press, Ames, Iowa, 1946).
[11] J. B. Smyth and L. G. Trolese, Propagation of radio waves in the lower atmosphere, Proc. IRE **35,** 1198 (1947).
[12] L. J. Anderson and E. E. Gossard, Prediction of oceanic duct propagation from climatological data, IRE Trans. **AP-3,** 163 (1955).
[13] Untersuchungen uber die Wetterabhangigkeit der Feldstarke im 100-MHz-Band auf der Strecke Bielstein-Darmstadt, Tech. Ber. 5518, Fernmeldetech. Zentralamt der Deutschen Bundespost, 20 Marz 1956.
[14] P. Misme, The correlation between the electric field at a great distance and a new radio-meteorological parameter, Trans. IRE **AP-6,** 289 (1958).
[15] B. R. Bean, Sur L'Utilisation Des Observations Meteorologiques Courantes En Propagation, Radioelectrique, Onde Elec. 37 e Annee, **362**, 411 (1957).
[16] B. R. Bean, and G. D. Thayer, On models of the atmospheric radio refractive index, Proc. IRE **47,** 740 (1959).
[17] U.S. Extension to the ICAO Standard Atmosphere, Tables and data to 300 standard geopotential kilometers, U.S. Weather Bureau, Washington, D.C. (1958).
[18] International Radio Consultative Committee, Documents of the IX Plenary Assembly, Los Angeles (1959); Vol. II, Study Programme No. 138 (v), Tropospheric Wave Propagation, ITU, Geneva (1959).
[19] A. Hald, Statistical theory with engineering applications (John Wiley and Sons, New York, N.Y., 1952).
[20] M. Onoe, M. Hirai, and S. Niwa, Results of experiment of long-distance overland propagation of ultra-short waves, J. Radio Research Labs., Japan **5,** 79 (1958).

(Paper 65D1–104)

JOURNAL OF RESEARCH of the National Bureau of Standards—D. Radio Propagation
Vol. 65D, No. 1, January–February 1961

Characteristics of Waveguides for Long-Distance Transmission[1]

A. E. Karbowiak and L. Solymar

(May 23, 1960)

Discussion of a waveguide communication system is given and the system is compared with existing communication media. The principal properties of waveguide—the medium of communication—are discussed in some detail. The particular significance of helical and coated waveguides is pointed out and the design formulas included. The phenomenon of mode conversion-reconversion, which is peculiar to a waveguide communication system, is discussed in general and the basic theory as applicable to design is also discussed. Design features of components such as bends, transducers, tapers, etc., are analyzed. The effect of waveguide discontinuities is analyzed in some detail and various aspects of signal distortion are also considered.

1. Introduction

Man, in his constant efforts towards progress, finds it necessary to establish better, quicker, and more numerous communication systems. It is even said that complexity of communication systems grows in proportion to the development of civilization. As the conventional means of communication become gradually used to capacity and the traffic continues to increase, one, naturally, turns towards more exotic means of communication. Waveguide is a possible winner [1, 2, 3] [2] and in this connection special acknowledgment should be made of the very important pioneer and continuing work of the Bell Laboratories in this field. Although the final assessment can only be made against the background of economy, a detailed performance assessment must be the first step. For a number of reasons, as we shall see subsequently, such a waveguide is essentially a circular tube about 1 to 3 in. in diameter and the waves involved are in the millimetric band. Such a pipe—the medium of communications—would be laid in the ground or at the bottom of oceans for hundreds and thousands of miles.

In order to bring out any advantages that a waveguide communication system may have over the existing systems, the principal features are shown tabulated in table 1. From this it is evident that the main advantage of a waveguide communication system is its large communication capacity. Provided that very short millimetric waves are used then, in principle, several hundreds of television channels, or the equivalent in speech channels, can be accommodated in a single pipe. The waveguide is also characterized by small attenuation, and in contrast to microwave links it is a screened system. Whether such enormous communication capacities will ever be required is another matter; but, if present statistics are anything to go by, then these capacities will be required in less than 20 years time, if not for telephone communication then for purposes such as data transmission, color and cinema television as well as for purposes not yet conceived.

A waveguide communication system is essentially simple (fig. 1). The video channels are grouped together (say by frequency division) and passed to a coder (C) where, for reasons to be discussed, it is coded in PCM (pulse code modulation). The coded signal is then made to activate an on-off modulator (M) operating on one of the many carriers in the whole spectrum carried by the waveguide. The carriers are combined through a suitable channel insertion filter and passed through a transducer (T) on to the waveguide. At convenient intervals along the waveguide (say every 10 miles) regenerative repeaters are inserted to amplify and restore the quality of the signal.

For effective operation the terminal equipment (modulation/demodulation and coding/decoding) is designed to handle millimicrosecond pulses. This in itself is a complication but it is a necessary one to achieve PCM coding of the wide video band and

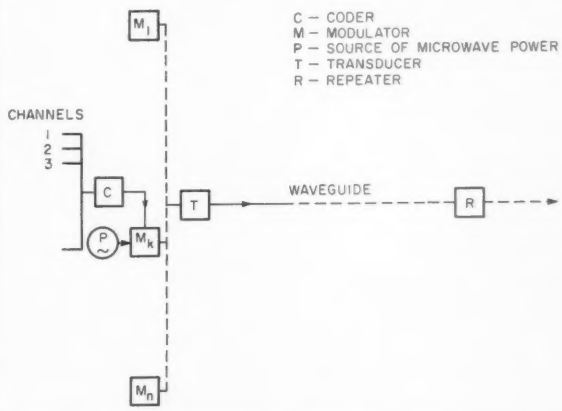

FIGURE 1. *A possible communication system using waveguide.*

[1] Contribution from Standard Telecommunication Laboratories, Ltd., London Road, Harlow, Essex, England.
[2] Figures in brackets indicate the literature references at the this paper

TABLE 1. *Comparison of communication media*

NOTE: One super channel=4 Mc/s.

Type		Operating frequency	Channel capacity	Repeater spacing / attenuation
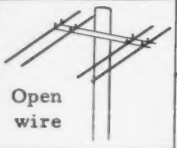 Open wire	One pair	36 to 84 kc/s (go) 92 to 140 kc/s (return)	12 + 3 + (1) = 15 + (1)	60 to 70 miles (0.4 db/mile)
	Maximum 16 pairs	As above	240 + (16)	
Balanced pair	One pair	12 to 252 kc/s	60	12 to 30 miles (4 db/mile)
	Maximum 24 pairs	As above	1440	
Coaxial G.B.		Up to 4 Mc/s	960 (One super channel)	6 miles
		Up to 12 Mc/s	3 super channels	3 miles
Coaxial U.S.		Up to about 3 Mc/s	720	8 miles
		L3 system	1 TV channel + 600 speech channels	4 miles
Single wire transmission line		About 100 to 1,000 Mc/s	Probably a few TV channels	About 2 to 10 miles
Microwave links		Below 500 Mc/s	Maximum of 60	40 to 50 miles
		500 to 1,000 Mc/s	Up to 120	40 to 50 miles
		2,000 Mc/s	240 × 6 or 1 TV × 6	30 to 40 miles
		4,000 Mc/s	600 × 6 or 1 TV × 6	25 to 30 miles
		6,000 to 8,000 Mc/s	600 × 6 or 1 TV × 6 Maximum 2 TV × 6	25 to 30 miles
		11,000 Mc/s	Less than 600	Less than 20 miles
Long haul waveguide (H_{01})		30,000 Mc/s up to about 100,000 Mc/s	1,000 super channels ≡ several hundreds of TV channels ≡ several hundred thousands of speech channels	20 to 40 miles (attenuation 2 to 4 db/mile)

derive the advantage of regeneration. Regeneration is a necessary requirement because of the large signal distortion, even with waveguides of moderate length (say 10 miles). It has been established beyond any doubt that for long-distance communication purposes only modulation systems capable of regeneration can be used, and of these PCM has definite technological advantages.

This paper is not an attempt at a balanced summary of the subject matter, but is a presentation of the opinions of the authors.

2. Summary of Properties of Waveguides

There are four principal factors influencing the performance of a waveguide: (1) Its geometry both in shape and size (in terms of the wavelength), (2) its mode of operation, (3) the value of the surface impedance of its walls, and (4) the nature and magnitude of the tolerances on the cross section.

For long-distance communication waveguides of circular cross section operating in the H_{01} mode have been chosen. The choice is chiefly a matter of technological preferences based on a number of considerations. Such waveguides have relatively low dispersion and low attenuation and can be constructed to discriminate against unwanted modes, and the requirements on the tolerances on the cross section are less exacting than for other waveguides and modes.

The exact waveguide properties and construction is a matter of compromise between a number of conflicting factors such as cost of terminal equipment and repeaters, permissible signal distortion, service reliability, etc. And, since these factors can be traded for each other it is impossible to give a specification for a waveguide under any given conditions except in the light of accumulated experimental experience. But, to fix orders of magnitude a waveguide operating in the 4- to 8-mm band would be about 2 to 3 in. in diameter.

With waveguides there are two principal sources of signal distortion: (1) Delay distortion [6], and (2) mode conversion-reconversion phenomena [1, 4]. Delay distortion arises (like with most communication media) because of the nonlinearity of the phase characteristic, $\beta(\omega)$. This leads to the undesirable feature that the high frequency components of the signal travel faster than the low frequency components, a phenomenon known as dispersion. A corresponding distortion due to the variation in the attenuation characteristic $\alpha(\omega)$ is, with waveguides, negligible [6].

The actual bandwidth limitation due to delay distortion depends to a large extent on the modulation method and is particularly troublesome with FM. PCM, on the other hand, is rather immune, but even here 10-mμsec modulation pulses would be unrecognizable after a journey down a typical waveguide, say, 30 miles long; regeneration is, therefore, called for. In addition, certain amount of equalization of the $\beta(\omega)$ characteristic may be a necessity.

Mode conversion-reconversion is a new phenomenon, peculiar to waveguide transmission systems. It arises because a typical waveguide suitable for long distance transmission can support a large number of modes apart from the desired one (H_{01}), and because of the irregularities in the waveguide (small dents, changes in diameter and cross sectional shape, small bends and kinks, etc.). In consequence, at each minute irregularity the preferred transmission mode (H_{01}) becomes scattered and partially transformed into the parasite modes. The process is known as mode conversion and leads to a gradual diffusion of energy into the parasite modes and, therefore, increased attenuation. With some exceptions this process of mode conversion is actually not particularly harmful. It cannot, however, exist on its own but, by reciprocity, it is accompanied by the complementary process of "reconversion." In this process, the energy now partially carried in the unwanted modes becomes reconverted (by being scattered by subsequent irregularities) back to the H_{01} mode. But since the group velocities of the parasite modes differ from that of the H_{01} mode, the reconversion is not in phase with the signal carried in the H_{01} mode. Further, since the degree of the distortion is phase dependent and the phase of the reconverted signal is related to the distance between the conversion and reconversion points in terms of the wavelength, the whole process of mode conversion-reconversion is frequency sensitive. The overall frequency attenuation curve is, therefore, very irregular, leading to considerable signal distortion. Because of the nature of mode conversion-reconversion phenomena it is inconceivable that suitable terminal equipment could be constructed to counteract its effects. Mode conversion-reconversion effects are conveniently minimized by suitable waveguide design.

There is one particular aspect of mode conversion-reconversion that calls for special attention: this arises through bending of the waveguide. The circular waveguide carrying the H_{01} mode can support simultaneously the E_{11} mode, having identical velocity.[3] In a straight waveguide this is of no direct consequence, but if the waveguide is bent in an arc of a circle then the two modes become coupled with subsequent exchange of energy between the modes. This leads to large attenuation and signal distortion. Once again the effect is counteracted by judicious waveguide design.

It is possible to design a whole series of components [1, 5] such as specially tailored bends and corners, tapers, mode transducers, etc. But the design is not as straightforward as with components for conventional single mode rectangular waveguide. The waveguide can support a large number of modes and, therefore, any changes of the waveguide geometry must be made with great care bearing in mind mode conversion-reconversion phenomena. This requires a detailed study of wave transmission

[3] Such modes are termed degenerate.

in multimode waveguides and the coupling effects due to irregularities; a field relatively unexploited in its analytical and experimental aspects.

Despite all the planning difficulties, a waveguide when properly designed will give satisfactory service and will handle successfully a bandwidth well in excess of 20 kMc/s, which is equivalent to an intelligence bandwidth of about 1,000 Mc/s, a capacity not offered by any other existing communication medium.

3. Delay Distortion in Uniform Waveguides

As is well known, with waveguides both $\alpha(\omega)$ and $\beta(\omega)$ are functions of frequency. It can be shown [6], however, that the effect of $\alpha(\omega)$ on signal distortion is negligible in comparison with $\beta(\omega)$. Here, therefore, only the effect of the $\beta(\omega)$ characteristic will be examined.

The phase propagation coefficient $\beta(\omega)$ is given by

$$\beta=\sqrt{(\omega^2-\omega_c^2)}/c, \tag{1}$$

where c is the velocity of light, and ω_c the cutoff frequency of the waveguide, which is a geometrical parameter. These relations are illustrated in figure 2.

The phase (v_{ph}) and group velocities (v_g) are defined by

$$\frac{v_{ph}}{c}=\frac{\omega_o}{\sqrt{(\omega_o^2-\omega_c^2)}}=\frac{c}{v_g}. \tag{2}$$

These quantities are frequency dependent.

If the signal is composed of several frequencies then, naturally, the signal will be distorted because the high frequency components will travel faster than the low frequency ones. The differential phase delay between the extreme components of the modulating envelope is a measure of signal distortion: it is the delay distortion term. For a waveguide operated at a frequency substantially above cutoff the bandwidth (in Mc/s) can be expressed as follows [6]:

$$\mathrm{f}=(19/F)(f_o/l)^{1/2}(\delta\phi)^{1/2} \tag{3}$$

where

F = cutoff frequency/carrier frequency
l = length of waveguide in kilometers
f_o = carrier frequency in kilomegacycles per second
$\delta\phi$ = permissible phase delay between the carrier and the sideband in radians.

It has been assumed that f is a small proportion of carrier frequency.

For example, for a typical rectangular waveguide $F=0.6$, and therefore at the carrier frequency of 10 kMc/s (and length 30 km) we get

$$f=9.4\ (1\ \mathrm{rad})^{1/2}\mathrm{Mc/s}.$$

The permissible amount of delay distortion ($\delta\phi$) is a function of modulation method. Clearly, with AM if $(\delta\phi)=\pi/2$ then inversion of sidebands takes place: a condition of severe distortion. For AM, FM, and many other modulation methods the maximum possible value of $\delta\phi$ is only a small fraction of 1 rad. For PCM, however, ($\delta\phi$) can take quite substantial values; once again, therefore, PCM is superior to the more common modulation methods.

For wideband application the modulation methods must be analyzed individually. For example, with pulse transmission systems, the energy contained in a pulse of finite duration gradually becomes spread out on the time scale. For a given waveguide length the degree of pulse distortion is a function of pulse duration. But up to a certain minimum pulse duration the pulse is quite recognizable and most of the energy is contained in the time interval equal to the duration of the transmitted pulse. For pulses of shorter duration the pulse distortion becomes quite severe and increases as pulsed duration decreases [6]; simultaneously the energy becomes diffused over a longer and longer time interval. The actual pulse width for which this happens is related to the geometry of the waveguide cross section and waveguide lengths (fig. 3).

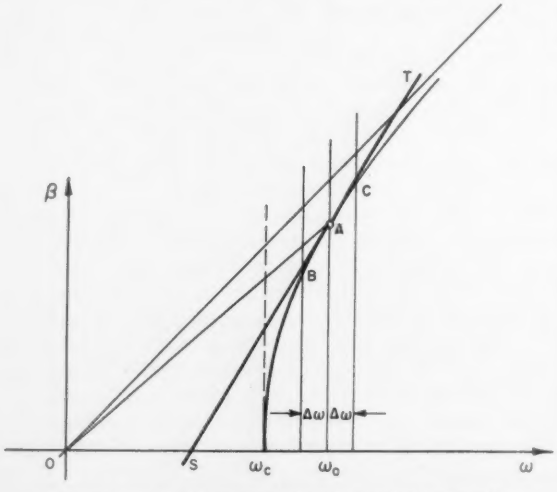

FIGURE 2. *β–ω characteristic of a perfect waveguide.*

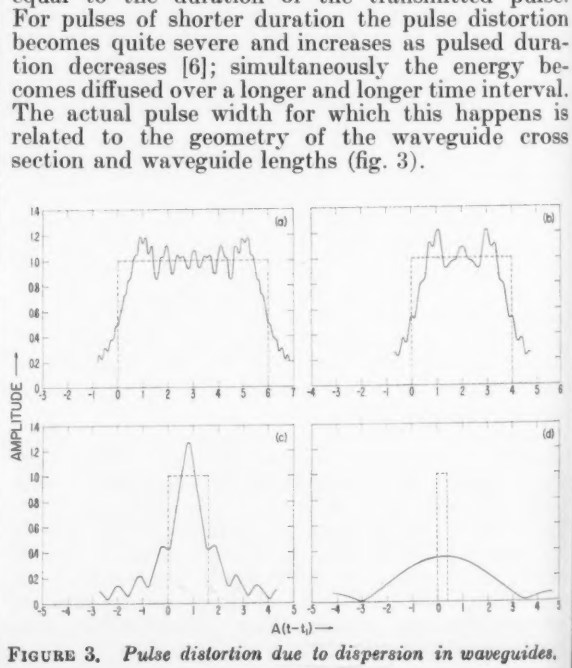

FIGURE 3. *Pulse distortion due to dispersion in waveguides.*

Typical waveguides for long-distance transmission have $F=0.15$, then at a frequency of 35 kMc/s pulses as short as 10 mμsec can be transmitted without significant distortion over a distance of some 30 km. Such performance is sufficient for many applications, but if it were required to transmit even shorter pulses some equalization of waveguide characteristic would then be necessary. Such equalization is best carried out at the terminal equipment.

4. Properties of Uniform Waveguides and Their Uses

4.1. Simple Waveguides

The reasons for choosing for long-distance transmission the circular waveguide operated in the circular electric mode (H_{01}) have been explained in section 2. Such waveguides can support, apart from the desired (H_{01}) mode a multitude of other modes all of which are undesirable. The total number of modes that can possibly propagate in a waveguide with diameter D is known as the modulus of overmoding, M. This is approximately given by

$$M=2.55(D/\lambda_0)^2. \tag{4}$$

The larger the modulus of overmoding, the larger the number of possible modes and, consequently, the greater the engineering difficulties in preventing mode conversion-reconversion phenomena. Yet, a large ratio D/λ_0 is necessary to have low attenuation and dispersion. Of necessity, therefore, the proportions of a waveguide are a compromise. Typically, D/λ_0 is of the order of 10 or more and the modulus of overmoding is, therefore, at least about 200 to 400.

Each of the modes propagates with a characteristic group velocity given by

$$v_g/c=c/v_{ph}=\sqrt{(1-F^2)}. \tag{5}$$

The commonest type of waveguide is a plain metallic pipe. With such waveguides the wall of the waveguide presents a surface resistance R_s given by [7]

$$R_s=\sqrt{(\pi f\mu/\sigma)}\div\sqrt{(\mu_o/\epsilon_o)}=R_m \tag{6}$$

where σ is the conductivity of the metal, μ its permittivity, and $\sqrt{(\mu_o/\epsilon_o)}=377$ ohms, is the free space impedance. This surface resistance gives rise to attenuation which for E_{mn} modes is given by [7]

$$\alpha_{mn}^{(e)}=\frac{8.686}{D/2}\cdot\frac{R_s}{\sqrt{(1-F^2)}}, \tag{7}$$

and for H_{mn} modes by

$$\alpha_{mn}^{(h)}=\frac{8.686}{D/2}\cdot\frac{F^2}{\sqrt{(1-F^2)}}\left[1+\frac{1}{F^2}\frac{(m/\chi_{mn}^{(h)})^2}{1-(m/\chi_{mn}^{(h)})^2}\right]R_s. \tag{8}$$

These attenuations are given in decibels per meter if D, the diameter of the waveguide, is measured in meters.

The attenuation of the H_{01} mode (the wanted mode) is given by [7]

$$\alpha_0=\frac{8.686}{D/2}\cdot\frac{F^2}{\sqrt{(1-F^2)}}R_m \tag{9}$$

Thus for a copper waveguide at the free space wavelength of 8.7 mm, it is 1.2 db/mile.

Most of the unwanted modes have attenuation and group velocities differing substantially from the H_{01} mode. Thus attenuations of 10 to 50 times that of the H_{01} mode is common and group velocities of most modes differ from the H_{01} mode by as much as 10 percent or more. A few of the modes, however, have properties similar to those of the H_{01} mode. For example, the E_{11} mode has group velocity almost equal to that of the H_{01} mode and a few of the modes, notably the H_{02}, H_{03}, H_{12}, H_{13}, H_{22}, and H_{23}, have attenuations only 3 to 10 times as much as the H_{01} mode. These modes, therefore, tend to be particularly troublesome and the only way to deal with them satisfactorily is through judicious use of special waveguides.

4.2. Special Waveguides

Waveguides of special construction are necessary, as explained in the earlier sections, principally to combat or at least to minimize the mode conversion-reconversion effects. For such applications, disk waveguides were first to be suggested and various elliptic, corrugated, and more complex structures were tried for negotiating bends. After many years of research it is now clear that only helical, and dielectric coated waveguides are likely to be of any extensive use. Such waveguides behave as if their surface impedance were anisotropic.

The theory of propagation in anisotropic waveguides can be quite involved, but since waveguides for long distance transmission have, in general, small surface impedance an approximate treatment is adequate, and this will be given here [8, 9].

The propagation coefficient in such waveguides is given by

$$\gamma=\gamma_o+\delta\gamma=j\beta_o+(\alpha+j\delta\beta)=\alpha+j\beta, \tag{10}$$

where the quantity $\delta\gamma(=\alpha+j\delta\beta)$ is composed of the attenuation coefficient (α) and a quantity $\delta\beta$ modifying the phase change coefficient (β_o) of the waveguide with zero surface impedance. The coefficient α is proportional to surface resistance (R_s) and $\delta\beta$ to surface reactance (X_s), these being respectively the real and imaginary parts of surface impedance, Z_s.

With anisotropic waveguides the quantity Z_s may be described in terms of the matrix of its components; most simply in terms of its two principal components Z_η and Z_ξ which are surface impedance components along the two principal axes. The sum of the projection of these components along the ϕ and z directions define the circumferential (Z_ϕ) and axial (Z_z) components of the surface impedance; and it is these components that are used in the subsequent formulas. Z_ϕ can be regarded as the surface impedance presented to the currents flowing in the waveguide wall in the circumferential direction and Z_z a corresponding quantity for currents flowing in the axial direction.

In such waveguides the attenuation of E-waves is given by [9]

$$\alpha^{(e)}=2R_z/D\sqrt{(1-F^2)} \qquad \text{nepers} \tag{11}$$

and for H-waves by

$$\alpha_{mn}^{(h)}=\frac{2}{D}\frac{F^2}{\sqrt{(1-F^2)}}\left[R_\phi+R_z\frac{1-F^2}{F^4}\left(\frac{m}{\pi}\frac{\lambda_o}{D}\right)\right]\times\left[1-\left(\frac{m}{\pi}\frac{\lambda_o}{D}\right)^2\right]^{-1} \text{nepers} \tag{12}$$

where the meaning of symbols is as before.

In the above formulas if X_z, X_ϕ are substituted for R_z and R_ϕ, respectively, then $\delta\beta$ will be obtained.

4.3. Dielectric Coated Waveguides

A metallic surface exhibits a surface impedance given by [8]

$$Z_m=(1+j)R_m \tag{13}$$

where R_m is given by (6). The surface of a copper tube ($\sigma=5.8\times10^7$ mho/m), therefore, presents at $\lambda_o=8.7$ mm a surface impedance of $(1+j)\times1.28\times10^{-4}$, relative to free space (about 0.048 ohms).

If, now, the metallic tube is coated with a thin layer of dielectric then its surface impedance will be enhanced as given in table 2, where t is the thickness of the dielectric layer, $k_o=2\pi/\lambda_o$, ϵ_r relative permittivity, and δ the loss angle of the dielectric. Clearly, by choosing suitable materials and the thickness of the dielectric layer, it is possible to obtain within wide limits any required surface impedance components and, consequently, the attenuation and phase velocity of the E and H modes can be varied relative to the H_{on} modes. By way of illustration, at the free space wavelength of 8.7 mm, for $\epsilon_r=2$, $\tan\delta=0.15$, and $t=0.046$ mm, the surface impedance components become $Z_z=2.5\times10^{-3}+j\ 1.7\times10^{-2}$ and $Z_\phi=3.7\times10^{-6}+j\ 3.3\times10^{-4}$ over and above the value of Z_m. If we substitute these values in eqs (11) and (12) we find that for a waveguide of 7-cm diam, there is a 20-fold increase in attenuation of E and H modes (other than H_{on}) relative to the H_{01} at the expense of only a 3 percent increase in attenuation of the H_{01} mode. The surface reactance X_z is, at the same time, increased by a factor of 140 leading to a substantial change in phase velocity of most modes.

The increase in relative attenuation is necessary to cope with mode conversion-reconversion, due to irregularities in the waveguide, while the increase in the surface reactance, X_z, is necessary so that the waveguide can cope with bends.

TABLE 2. *The surface impedance of a dielectric coated metal surface*

These value must be augmented by $Z_m=R_m+jX_m$ ($Rm=Xm=\sqrt{\pi f\mu/\sigma}\sqrt{\epsilon_o/\mu_o}$) the surface impedance of the metal.

Surface impedance	Re part	Im part
$Z_z=R_z+jX_z$	$R_z=tk_o(\tan\delta/\epsilon_r)$	$X_z=tk_o(1-1/\epsilon_r)$
$Z_\phi=R_\phi+jX_\phi$	$R_\phi=\frac{1}{3}(tk_o)^3(\epsilon_r\tan\delta)$	$X_\phi=\frac{1}{3}(tk_o)^3(\epsilon_r-1)$

4.4. Ring or Disk Structures

Any periodic array of coaxial disks or rings of different surface impedances falls into this class. If the pitch of such a structure is small in comparison with the wavelength then a simple approximate treatment is possible, as follows:

Let Z_1 and Z_2 be the surface impedance of the individual elements, thickness t_1 and t_2, respectively, then the anisotropic components of the effective surface impedance are given by

$$\left.\begin{aligned} Z_z&=\frac{Z_1t_1+Z_2t_2}{t_1+t_2}\\ Z_\phi&=\frac{Z_1Z_2(t_1+t_2)}{Z_2t_1+Z_1t_2}\end{aligned}\right\}. \tag{14}$$

Since in most applications $|Z_2|>|Z_1|$ and $t_2<<t_1$ these expressions can be further simplified to

$$\left.\begin{aligned} Z_z&=Z_2t_1/(t_1+t_2)\\ Z_\phi&=Z_1(t_1+t_2)/t_1\end{aligned}\right\}. \tag{15}$$

Thus given Z_1, Z_2, t_1, and t_2 the surface impedance components Z_z and Z_ϕ can be calculated. In turn, the attenuation and phase propagation coefficients can be obtained from (11) and (12).

The quantities Z_1 and Z_2 are determined from the knowledge of the actual physical structure. This can be a lengthy calculation, but since in practical applications only an estimate of the value of the surface impedance is needed, it is permissible to make a number of rather drastic approximations. For example, for a corrugated waveguide (fig. 4), Z_1 is the copper intrinsic impedance and Z_2 is the input impedance to a parallel plane transmission line,

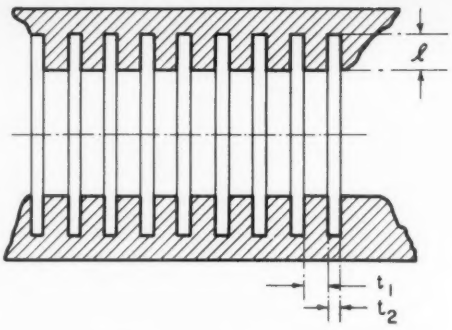

FIGURE 4. *Corrugated waveguide.*

length l, and separation between plates t_2. Thus

$$\left.\begin{aligned} Z_z &= R_m[1+l/(t_1+t_2)]+j2\pi\,\frac{l}{\lambda_0}\,t_2/(t_1+t_2) \\ Z_\phi &= Z_m(t_1+t_2)/t_1 \end{aligned}\right\} \quad (16)$$

where Z_m is the surface impedance of the metal (e.g., eq (13)).

It will be observed that Z_ϕ has been increased a little, in proportion of $(t_1+t_2)/t_1$, but that Z_z is highly reactive. Such waveguides are particularly suitable for negotiating bends.

Clearly, other structures can be calculated in an analogous manner.

4.5. Helical Waveguides

It will be observed from eqs (15) that Z_z and Z_ϕ can be adjusted within very wide limits to any desirable values provided that the proportions of the microstructure of the waveguide surface are suitably chosen. This feature makes the disk waveguides, and their variants, extremely attractive. But, unfortunately, such waveguides are difficult if not impossible to manufacture in quantity. It is for this reason that helical waveguides are preferred.

It can be shown that if the pitch of the helical waveguide is very small, as would be with waveguides wound with a fine wire, and the surface impedance not too large (say less than 10^{-1}, i.e., some 40 ohms), then the helical waveguide behaves as a corresponding ring structure.

A particularly important structure is shown in figure 5; this shows a helix of insulated (copper) wire set in a suitable resin and backed by a resistive layer of surface impedance R, the whole structure is enclosed in a suitable protective jacket. If the wire diameter is t_1 and the gap between the wires t_2, then provided that t_2 is not too small, the structure behaves approximately as a corresponding disk structure (fig. 6) with $l=t_1$.

Using the procedure as outlined before, eqs (15) can be used where $Z_1=Z_m=$copper intrinsic impedance and Z_2 is taken equal to the input impedance of a transmission line length l, terminated in a

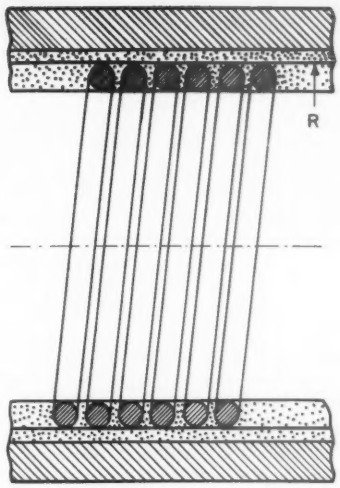

FIGURE 5. *A helical waveguide.*

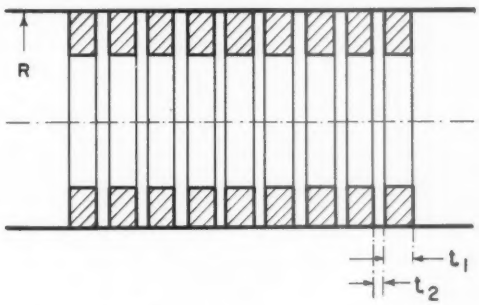

FIGURE 6. *Ring structure with a resistive layer.*

resistive impedance R. Clearly, therefore,

$$\left.\begin{aligned} Z_z &= R\,\frac{t_2}{t_1+t_2}+j2\pi(l/\lambda_0)\,\frac{t_2}{t_1+t_2} \\ Z_\phi &= Z_m\,\frac{t_1+t_2}{t_1} \end{aligned}\right\}. \quad (17)$$

As a numerical example consider a helical waveguide with following constants: $t_1=l=\lambda_0/10$, $t_2=\frac{1}{2}t_1$, $R_m=10^{-4}$ (approximately copper impedance), $R=10^{-2}$ (approximately 4 ohms) then, neglecting the lay angle of the helix, at a free space wavelength of 8.7 mm the surface impedance components become

$$Z_z=0.003+j0.021$$

$$Z_\phi=1.5(1+j)\times10^{-4}.$$

The propagation coefficients follow from eqs (7) and (8). Thus for a waveguide 7 cm in diam there is a 50 percent increase in the attentuation of the H_{01}

mode, and a 30-fold increase in the attenuation of most E-modes. The attenuation of the lower order H-modes has also been increased by a factor of 30, while the surface reactance is increased 200 times.

5. Basic Theory of Nonuniform Waveguides

Theory of nonuniform waveguides is fundamental for thorough understanding of transmission aspects as well as design of many waveguide components peculiar to long distance transmission by waveguide. Thus, commonly, waves are conveyed from an oscillator *via* a single mode rectangular waveguide through a transducer to a circular waveguide then through a taper to the main waveguide run.

We shall see that a mode transducer, a bent waveguide, as well as a taper are particular embodiments of nonuniform transmission lines. The main waveguide run is also a nonuniform transmission line in the sense that it can carry a large number of modes and all minute irregularities act as coupling elements between the lines; each line representing one particular mode.

In general, we represent a nonuniform waveguide by its equivalent circuit: n coupled transmission lines, where n is the number of possible modes of propagation (see fig. 7).

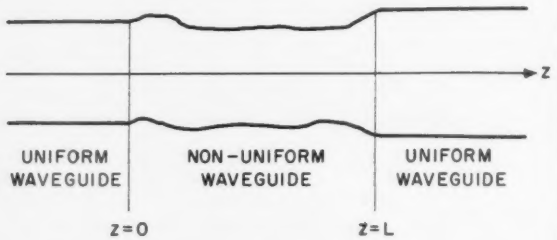

FIGURE 7. *Schematic of a nonuniform waveguide.*

For convenience in analysis, nonuniform waveguides can be subdivided into (1) straight waveguides, and (2) bent waveguides.

5.1. Straight Waveguides

The first general solution to transmission in nonuniform waveguides was obtained by Stevenson [10] in terms of a series of transverse wave functions. Through such an approach it is possible to obtain equivalent generalized telegraphist's equations [11] of the waveguide. Adopting Reiter's approach [12, 13], it can be shown [17] that for the forward and backward traveling waves the following equations hold

$$\frac{dA_i^+}{dz}=-j\beta_i A_i^+-\frac{1}{2}\frac{d(\ln K_i)}{dz}A_i^-+\sum_p (S_{ip}^+A_p^++S_{ip}^-A_p^-),$$

$$\frac{dA_i^-}{dz}=-\frac{1}{2}\frac{d(\ln K_i)}{dz}A_i^++j\beta_i A_i^-+\sum_p (S_{ip}^-A_p^++S_{ip}^+A_p^-) \tag{18}$$

where z is the coordinate along the waveguide axis.

$A_i^\pm$ are amplitude coefficients of the forward (+) and backward (−) traveling waves on the ith line (corresponding to the ith mode).
$S_{ip}^\pm$ are the corresponding coupling coefficients between the waves on lines i and p (a parameter related to the geometry of the waveguide).
K_i is the wave impedance of the ith line.
β_i the propagation coefficient.

The above are exact equations for a set of lossless nonuniform transmission lines where S, K, and β are, in general, functions of z. These equations are exact representation of transmission in a nonuniform waveguide. In principle, therefore, given the functional dependence of the waveguide geometry on the coordinate z, the propagation problem can be solved, but the computational difficulties are in most cases formidable. With practical waveguides, however, it is possible to proceed with a number of simplifying assumptions leading in many cases to rather simple solutions [14, 15, 16, 17].

In the first place, we assume that the waveguide geometry changes slowly and consequently S, K, and β are slowly varying functions of z. The coupling between the lines per unit length will therefore be small. If now the input at one end of the waveguide is a pure mode, amplitude A_o, then the boundary conditions are simply

$$\left.\begin{aligned} &A_m^+(0)=A_o \qquad A_m^-(L)=0 \\ &A_i^+(0)=0 \qquad A_i^-(L)=0 \qquad (i\neq m)\end{aligned}\right\}. \tag{19}$$

With these assumptions only the coupling between the line m and the remaining lines need be considered; the cross coupling between the lines can be neglected and so can the reflected waves. We then obtain a simplified solution in the form [17]

$$A_m^+(z)=A_o\exp\left[-j\int_0^z \beta_m dz\right]. \tag{20}$$

The amplitude of the remaining waves are given by

$$\left.\begin{aligned} A_m^-(0)&=-\exp\left[-j\int_0^L \beta_m dz\right]\int_0^L\left(S_{mm}^- -\frac{1}{2}\frac{d(\ln K_m)}{dz}\right)\exp\left[-j2\int_0^z \beta_m dz\right]dz \\ \frac{A_i^+(L)}{A_i^-(0)}&=\pm\exp\left[-j\int_0^L \beta_i dz\right]\int_0^L S_{im}^\pm \exp\left[-j\int_0^z (\beta_m\mp\beta_i)dz\right]dz\end{aligned}\right\} \tag{21}$$

In the derivation of these expressions it has been assumed that none of the modes are at the cutoff. When dealing with components, such as tapers for example, some modes are of necessity at the cutoff at some cross section along the taper, and it would appear that (20) and (21) are not a sound basis for design. Nevertheless, it appears that the use of (20) and (21) is usually justified [18].

It is to be observed that usually it is only the lower order modes that need to be at all considered (typically H_{02}, H_{03}, H_{12}, H_{13}, H_{22}, H_{23}; cf., section 4.1.).

The β coefficients of these modes differ but very little from that of the H_{01} and consequently (eq (21)) only the coefficients of the forward traveling waves (A^+) need be considered; the coefficients A^- are very much smaller and can, therefore, be neglected.

Using eqs (21) an interesting proposition can be proven. In general, a pure mode at the input to a waveguide will produce at the output a combination of modes. For a good transducer the output consists of an almost pure mode of the desired kind. The purity of this mode can now be made as high as desired merely by increasing the length of the transducer: the longer and more gradual the transducer the purer is the mode at the output.

5.2. Propagation in Bent Waveguides

The general coupled transmission line equations for a bent waveguide of arbitrary cross section were given by Shimizu [19] from which the relations for a circular waveguide follow. The particular case of a bent circular waveguide was analyzed earlier by Jouguet [20], who analyzed the field in a curved waveguide by means of perturbation calculus and obtained the field in terms of an expansion in powers of $1/R$, where R is the radius of curvature of the waveguide.

It can be shown that if a curved section of waveguide is interposed between two straight waveguides (fig. 8) and a pure H_{01} mode is incident at one end of the curved waveguide, then the wave appearing at the other end is composed of the H_{01}, E_{11}, and a series of H_{1n} modes [19, 20, 21], but the exact proportion

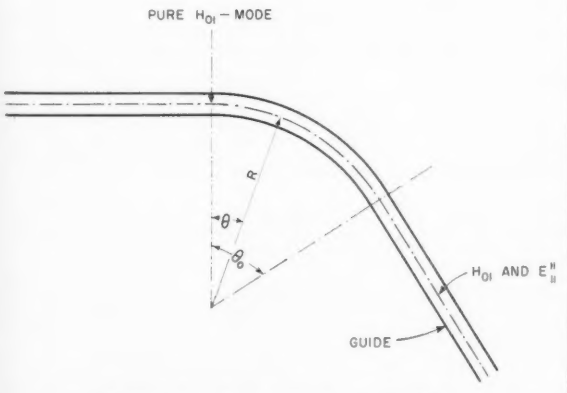

FIGURE 8. *Curved circular waveguide.*

of each of the modes depends on the geometry of the bend. The equivalent circuit of the bend is therefore $n+2$ coupled transmission lines: one for the H_{01}, one for the E_{11}, and n lines one for each of the H_{1n} modes. The coefficients of the coupling matrix are constants related to the geometry of the bend. But it can be shown, further, that if the radius of curvature is large, the series of the H_{1n} modes may be neglected, since these are of $1/R^2$ or higher order, and therefore only the H_{01} and E_{11} modes need be considered. The equivalent circuit is then, simply two coupled transmission lines.

Jouguet's analysis can be further extended to waveguides of arbitrary surface impedance [2]. It transpires that provided the radius of bend is not too small, the field inside a curved waveguide can be represented by [4]

$$\Psi = A(\mathscr{H}_{01} + \tau \mathscr{E}_{11}) e^{-\gamma l} \tag{22}$$

that is the field is a linear combination of the H_{01} and E_{11} modes in a definite proportion. The proportionality factor can take two possible values given by

$$\tau^2 - 2p\tau - 2 = 0, \tag{23}$$

where

$$p = \frac{h_0 \beta_0}{k_0^2} \frac{R}{s} jZ_s. \tag{24}$$

If the surface impedance and the radius of curvature are small then p is small and τ is approximately given by $\sqrt{2}$; therefore, the expression for the field [2] can be put into the form

$$\Psi = \mathscr{H}_{01} \cos \delta\beta_R l + j\sqrt{2}\mathscr{E}_{11} \sin \delta\beta_R l e^{-\gamma_0 l}, \tag{25}$$

where

$$\left.\begin{aligned} \delta\beta_R &= \frac{k_0}{h_0 R\sqrt{2}} \\ \text{and} \qquad \gamma_1 &= j(\beta_0 \pm \delta\beta_R) + \frac{1}{2}(\alpha_E + \alpha_H) \end{aligned}\right\} \tag{26}$$

with β_0 the phase propagation coefficient of the straight waveguide, α_E and α_H the attenuation coefficients of the E_{11} and H_{01} modes in the straight waveguide.

Two important conclusions must be made: (1) The energy is carried alternately in the H_{01} and E_{11} modes, and (2) the mean attenuation of the complete normal mode (25) is equal to the mean of those for the E_{11} and H_{01} modes.

Evidently, the waveguide is unsuitable for the transmission of the H_{01} mode around the bends. However, the examination of the above equations shows that if p is a large real number a different situation arises. Large real values of p are obtained for highly reactive surfaces (X_s a large number), and in such waveguides the two modes H_{01} and E_{11}

[4] $\mathscr{H}_{01}$ stands for the field of the H_{01} mode, and $\mathscr{E}_{11}$ stands for the field of the E_{11} mode.

propagate almost independently of each other, but the attenuation of H_{01} mode is slightly increased. In such a waveguide, the attenuation of the H_{01} mode is given by [2]

$$\alpha_1=\alpha_0+\alpha_R \tag{27}$$

where α_0 is the attenuation in the straight waveguide and is given by (eq (12))

$$\alpha_0=\frac{2}{D}\frac{F^2}{\sqrt{(1-F^2)}}R_\phi. \tag{28}$$

The additional attenuation due to the bend is given by

$$\alpha_R=\frac{D}{4R^2}\frac{R_s/|Z_s|^2}{F^2\sqrt{(1-F^2)}}. \tag{29}$$

Clearly, by choosing a sufficiently large surface reactance it is possible to bring this increase in attenuation below any predetermined level. Such values of surface reactance can be conveniently obtained either by coating the waveguide surface with a layer of dielectric or by corrugating the waveguide surface in a suitable manner.

The ratio $\alpha_R/\alpha_0=\nu_R(R_z/R_\phi)$ defines a quality factor of the bent waveguide. With the help of figure 9 it is possible to determine the required value of surface reactance for a given value of radius of curvature and quality factor ν_R. Clearly, helical waveguides of appropriate proportions (sec. 4) can be designed for the purpose of negotiating bends.

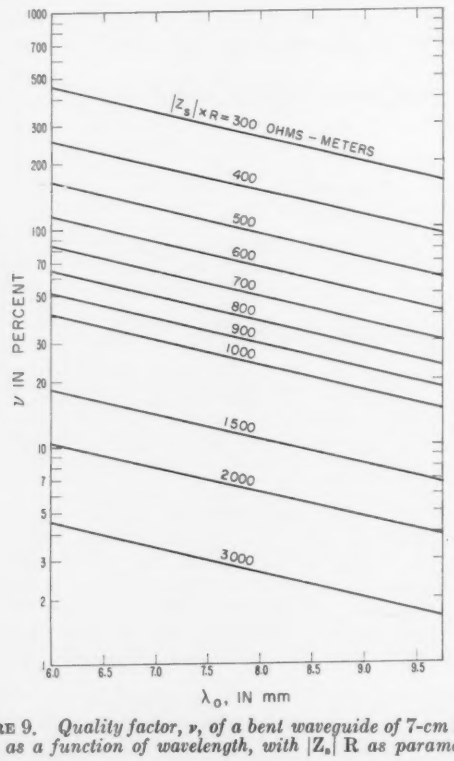

FIGURE 9. *Quality factor, ν, of a bent waveguide of 7-cm diameter as a function of wavelength, with* $|Z_s|$ R *as parameter.*

With suitably designed waveguides, bends even of a few hundred feet in radius can be negotiated quite successfully. A further improvement can be achieved by increasing gradually the radius of bend by means of a suitable transition curve [22] (a "tapered transition"). This is yet another embodiment of a set of nonuniform coupled transmission lines.

6. Transducers

A transducer is a waveguide configuration which achieves a required change of mode pattern and/or pattern size.

6.1. Tapers

A taper is the simplest illustration: it achieves a change in waveguide diameter and, if properly designed, leaves the mode pattern unaltered yet changed in size.

The rigorous theory [23, 24] of tapers can be very involved indeed but for our applications a number of approximations are permissible resulting in an adequate and simple design procedure.

Consider two coaxial waveguides joined by a conical taper and suppose that the larger waveguide (radius a) is operated substantially above cutoff (overmoded waveguide) and the smaller waveguide (radius b) carries a pure H_{01} mode. The taper will, evidently, give rise to a series of unwanted modes besides the H_{01} mode, but because of the symmetry of the structure only the H_{on} modes will be present. If, now, the diameter of the smaller waveguide is sufficiently small to permit only the H_{01} mode to propagate, the amplitudes of the H_{on} modes in the larger waveguide will be a simple function of the parameter σ given by

$$\sigma=\pi\frac{a}{\lambda}\frac{a-b}{L} \tag{30}$$

where L is the length of the taper and λ the free space wavelength.

These relations are obtained from simple analytical considerations [25] by expanding the fields in the circular waveguides in cylindrical harmonics and the field in the conical region in spherical harmonics and equating the fields in the cross sections radius a and b, respectively.

It can be shown that out of the modes produced by the taper the H_{02} mode is largest in amplitude. Considering, therefore, the conversion into the H_{02} mode only we get for the taper length

$$L\simeq\frac{0.57}{\sqrt{p}}\frac{a}{\lambda}(a-b) \tag{31}$$

where p is power conversion coefficient, which is the ratio of the permitted power in the H_{02} mode to that in the H_{01} mode.

For some applications the length of such a taper may be excessive, but a further improvement is possible by using a two-section conical taper (fig. 10).

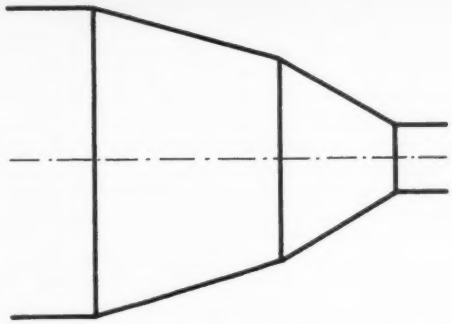

FIGURE 10. *Schematic of a two-section conical taper.*

For such a taper [26] by choosing correctly the proportions of the two cones the performance of the taper can be considerably improved. Optimum performance is possible only at one frequency, but by correct design it is possible to keep the sum of the energy carried in the H_{02} and H_{03} modes below any required level, over a substantial bandwidth [26].

More elaborate design procedures have been devised by several investigators [18, 24, 27]. But it appears [28] from results on antenna theory that provided the taper contour is "smooth and gradual" and that the derivatives at the taper ends are zero, there will be very little mode conversion even over a wide bandwidth.

6.2. Mode Transducers

With the exception of a few isolated instances there is no general design procedure for mode transducers. In a few simple cases it is possible to predict from the changes in the waveguide geometry the type of mode produced and with a little engineering intuition to design sometimes a reasonably satisfactory transducer. In most cases, however, even the intuitive approach is of no avail. Recently a satisfactory design procedure has been proposed [29] and confirmed experimentally. This is explained below.

Consider a mode transducer connecting two uniform waveguides A and B. According to an established theorem, if the change from waveguide A to waveguide B is effected very gradually then a pure mode in waveguide A will produce a substantially pure mode in waveguide B: the purity of the mode in waveguide B will be the higher the longer the transducer.

To determine the modes present at the ends of the transducer, it is necessary to choose several cross sections along its length and to determine the eigen functions in each. If the number of cross sections chosen is sufficient, then from the similarity between the successive field patterns of field distribution it is possible to examine the passage of any given mode along the whole length of the transducer, in detail.

To design a mode transducer, the desired modes in the uniform waveguides are given, and it is then required to determine the surface of the transducer for reasonable mode purity. We then choose a cross-sectional wave function Ψ (as a continuous function of z) such that it becomes the desired mode at each end of the transducer (at $z=0$ and $z=L$, where L is the length of the transducer). This wave function determines the surface of the transducer; and, provided that the function Ψ is a slowly varying function, the modes involved will be substantially pure. The design procedure is essentially numerical or graphical.

As an illustration consider the H_{01} circular to H_{01} rectangular mode transducer. For convenience and better illustration we propose to design the transducer in two parts: (1) H_{01} circular to H_{02} rectangular, and (2) H_{02} rectangular to H_{01} rectangular.

For the first transducer a convenient choice for the wave function is

$$\Psi_m = g_1(z) J_0\left(\frac{\pi}{w}\sqrt{x^2+y^2}\right) + g_2(z) \cos\frac{\pi}{w} x \qquad (32)$$

where to satisfy the requirements at each end of the transducer, the conditions are

$$\begin{aligned} g_1(0)&=1 \qquad g_1(L_1)=0, \\ g_2(0)&=0 \qquad g_2(L_1)=1, \end{aligned} \qquad (33)$$

with L_1=the length of the transducer and x,y= Cartesian coordinates in the transverse plane.

The diameter, d, of the circular waveguide and the width $2w$ of the rectangular waveguide are adjusted so that their cutoff numbers are equal ($d/w=2.44$).

Evidently the function Ψ_m reduces at the ends of the waveguide to the eigenfunctions of the circular and rectangular waveguides respectively. The surface of the transducer for any intermediate values of z is most easily determined graphically as follows. For any required value of z, curves of Ψ_m=a constant are plotted: these represent the lines of electric field. But a permissible boundary must be normal to such lines and, therefore, the cross-sectional contour can be mapped. Figure 11 shows four contours of such a transducer, and since we know that the transducer must be gradual, in most cases four contours are sufficient to determine the surface of the transducer.

Since the wave functions of the H_{02} and H_{01} modes have the same mathematical formula the obvious choice for the wave function of the second transducer is [30]

$$\Psi_m = \cos\frac{\pi}{w} x.$$

The curves Ψ_m=a constant are simply straight lines and, therefore, the transducer has the shape shown in figures 12 and 13; the dimension δ changes slowly from $\delta=0$ to $\delta=h$.

Since h is not equal to the diameter of the circular waveguide a further taper is necessary to connect the two transducers. Thus the complete H_{01} circular to H_{02} rectangular transducer is made up from the above three parts.

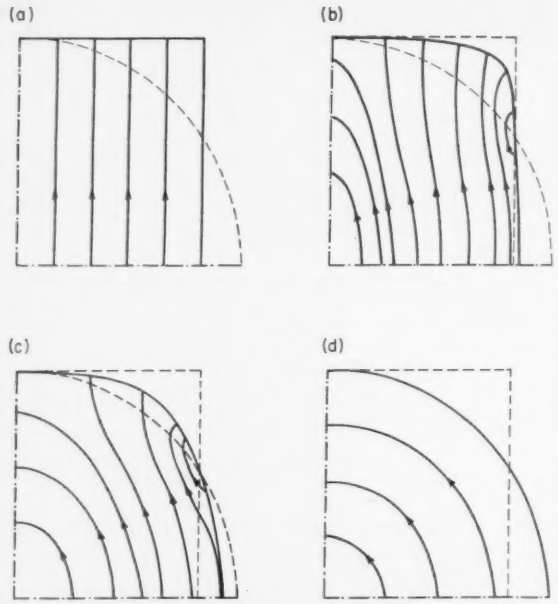

FIGURE 11. *Schematic showing a gradual mode transformation from the* H_{01} *circular to the* H_{02} *rectangular (only one quadrant showing).*

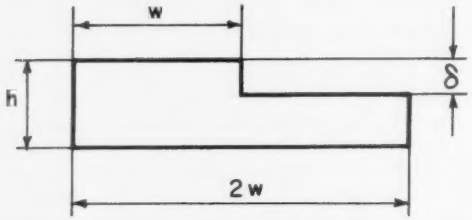

FIGURE 12. *Cross section of an* H_{01} *to* H_{02} *rectangular transducer.*

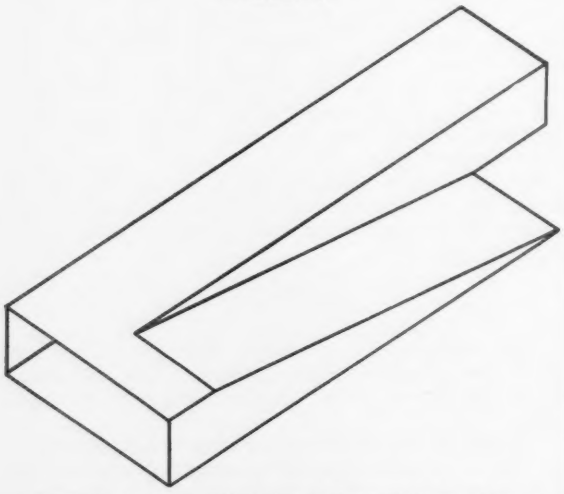

FIGURE 13. *Perspective view of the complete* H_{01} *to* H_{02} *rectangular transducer.*

7. Slightly Irregular Waveguides

The general problem of propagation in slightly nonuniform waveguides was investigated by Katzenelenbaum [31] and in a number of specific cases by Morgan [32] and Iiguchi [33].

In the case of a waveguide carrying an H_{01} mode at a frequency substantially above cutoff, a quasi-optical approach [34] can be adopted leading to simple derivation of relevant formulas. The problem can be stated with reference to figure 13. The cross section of waveguide A is circular and that of B differs a little but in an arbitrary manner. By assuming that the field in the aperture is substantially the field as produced by the H_{01} mode in the waveguide A according to geometrical optics, simple integral relations can be derived for the intensity of the modes produced in waveguide B. There are only H-modes produced and the amplitude of the H_j mode is given by [34]

$$A_j = \int_{S_0} \nabla_t \Psi_j \nabla_t \Psi_{01} dS \tag{35}$$

where S_o is the aperture, ∇_t is the gradient operator in the transverse plane, Ψ_j is the wave function of the H_j mode in waveguide B, and Ψ_{01} is the wave function of the H_{01} mode in waveguide A.

In the case of a junction formed by two offset circular waveguides of identical diameters only H_{1n} modes will be generated if the exciting mode is a pure H_{01} mode. If there is a small change in waveguide diameter and the waveguides are coaixal then only H_{on} modes are produced. Similar deductions can be made for other discontinuities without actually solving the expression (35).

For the two coaxial waveguides of slightly different diameter (see fig. 14) eq (35) leads to particularly simple relations. In this case the amplitude (A_{on}) of the H_{on} mode produced by the incident H_{01} mode is given by

$$\frac{A_{on}}{A_{01}} = \frac{2\chi_1\chi_n}{\chi_1^2 - \chi_n^2}\left(\frac{r_2 - r_1}{r_1}\right) \tag{36}$$

where χ_i is the ith root of $J_1(x)=0$.

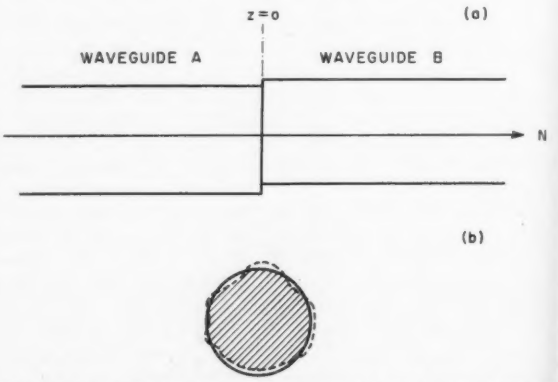

FIGURE 14. *The junction of two waveguides of slightly different cross section.*

Consider now two such steps in tandem. Clearly the contributions from the conversions must be combined taking the correct phases into account. It can then be shown that if the inserted length of the waveguide is one-half beat wavelength (of H_{01} and H_{02}) long and its diameter the mean of the two extreme waveguides, then the mode conversion is minimized [35]. The same procedure can be applied to other H_{on} modes and a suitable transition between two waveguides of different diameters designed.

8. Mode Conversion-Reconversion

As mentioned in section 2 mode conversion-reconversion is a phenomenon existing in any over moded waveguide, such as would be used for long-distance transmission. The level of mode conversion or reconversion on their own is a function of waveguide tolerances, but the combined effect of mode conversion-reconversion, which determines the signal distortion is also a function of waveguide design or more precisely it is related to the surface impedance of the waveguide.

For technological reasons one cannot reduce the mode conversion process beyond a certain limit, related to the waveguide tolerances. For given tolerances, however, the mode conversion-reconversion process can be reduced, in principle, below any predetermined level by choosing suitable surface impedance. [5] The remaining problem then is a technological one, of realizing such surface impedance. The actual design is a compromise between what is desirable from the mode conversion-reconversion point of view and what is practicable or at all possible to achieve using existing methods.

Briefly, for good performance on bends, waveguides must have high surface reactance in the axial direction (X_z components) while the circumferential component (X_ϕ) remains small. For good discrimination against unwanted modes produced by typical small irregularities, large attenuation for unwanted modes and small attenuation for the H_{01} mode is called for: that is large R_z and small R_ϕ.

Due to waveguide irregularities a large number of modes become coupled together. If the coupling coefficients representing the aggregate effect of waveguide irregularities contain a periodic component, considerable signal distortion takes place [4]: in effect the $\beta(\omega)$ characteristic becomes broken up by regularly spaced absorption bands. But if the irregularities are spaced in a random manner no such extreme signal distortion will take place; but on the other hand, the α and β characteristics become irregular in a random manner with a root mean square value proportional to $(c/\Delta\beta)^2$ (c is the rms value of the coupling coefficient c, and $\Delta\beta$ the difference between the phase propagation coefficients of the H_{01} mode and the parasitic mode) leading to effective crosstalk between the components of the coded signal. In general, the signal distortion due to mode conversion-reconversion is a function of the quantity $(c/\Delta\beta)^2/\Delta\alpha$ where $\Delta\alpha$ is the difference between the attenuations of the parasitic mode and the H_{01} mode. For this reason the more the group velocities of the parasitic modes differ from that of the H_{01} mode and the greater the attenuation of the parasitic modes, the smaller the signal distortion due to mode conversion-reconversion. As discussed in section 4, special waveguides can bring about such changes and hence their significance.

[5] The conversion to H_{on} modes has been neglected, since this is not usually troublesome.

9. Conclusions

Waveguides for long distance communications already form a wide specialized subject, too wide to be discussed adequately in an article of this size. But we have discussed the main constituents of a waveguide communication system pointing out the necessity of regenerative modulation method, such as PCM.

Special waveguides have been discussed in some detail because, in the light of present knowledge, such waveguides—either of the helical type or dielectric coated—are the only types likely to succeed.

Mode conversion phenomena are intimately connected with overmoded waveguides, of the type used for long distance transmission. Deep understanding of mode conversion processes is essential for successful designs and accordingly a theory has been outlined. The design of such components as tapers, mode transducers, and bends rest on mode conversion theory.

Various sources of signal distortion have been analyzed in some detail, but it has been stressed that if PCM modulation is used and regenerative repeaters, as well as special waveguides, a most advanced system of unequalled capacity will result.

Most of the work described in this paper was carried out as part of a research program of Standard Telecommunication Laboratories Ltd. The authors have benefited from discussions with a number of their colleagues: such discussions helped to crystalize many of the more involved ideas.

Acknowledgment is also made to Standard Telecommunication Laboratories Ltd., for permission to publish the paper.

10. References

[1] S. E. Miller, Waveguide as a communication medium, Bell System Tech. J. **33,** 1209 (1954).

[2] A. E. Karbowiak, Microwave aspects of waveguides for long distance transmission, Proc. Inst. Elec. Engrs. (London), Monograph No. 287R (Feb. 1958).

[3] H. M. Barlow, The exploration of waveguide for trunk waveguide multiple channel communications, J. Brit. Inst. Radio Engrs. **7,** 251 (Oct. 1947).

[4] A. E. Karbowiak, Distortion of information in non-uniform multimode waveguides, Conv. on Long Distance Transmission by Waveguide, London (Jan. 1959).

[5] A. E. Karbowiak and H. Knight, An experimental investigation of waveguides for long distance transmission, Conv. on Long Distance Transmission by Waveguide, London (Jan. 1959).
[6] A. E. Karbowiak, Propagation of transients in waveguides, Proc. Inst. Elec. Engrs. (London), Monograph No. 224R **105C** (Feb. 1957).
[7] A. E. Karbowiak, Waveguide characteristics, Electron. and Radio Engr. **34,** 379 (Oct. 1957).
[8] A. E. Karbowiak, Theory of imperfect guides—The effect of wall impedance, Proc. Inst. Elec. Engrs. (London) **102B,** 698 (Sept. 1955).
[9] A. E. Karbowiak, Microwave propagation in anisotropic waveguides, Proc. Inst. Elec. Engrs. (London), Monograph No. 147R **103C,** 139 (Aug. 1955).
[10] A. F. Stevenson, General theory of electromagnetic horns, J. Appl. Phys. **22,** 1447 (Dec. 1951).
[11] S. A. Schelkunoff, Conversion of Maxwell's equations into generalised telegraphist's equations, Bell System Tech. J. **34,** 995 (Sept. 1955).
[12] G. Reiter, Connection of two waveguides by a waveguide of variable cross-section (in Hungarian), Thesis from Appl. Math., Univ. Eotvos Lorand, Budapest (June 1955).
[13] G. Reiter, Generalised telegraphist's equation for waveguides of varying cross-section, Proc. Inst. Elec. Engrs. (London), pt. B Suppl. No. 13, p. 54 (Jan. 1959).
[14] B. Z. Katzenelenbaum, Non-uniform waveguides with slowly changing parameters (in Russian), Doklady Akad. Nauk. S.S.R. **12,** 711 (1955).
[15] B. Z. Katzenelenbaum, On the general theory of non-uniform waveguides (in Russian), Dokl. Akad. Nauk. S.S.R. **116,** 203 (1957).
[16] B. Z. Katzenelenbaum, On the theory of non-uniform waveguides with slowly changing parameters, Intern. Conf. Ultrahigh Frequency Circuits and Antennas, Paris (Oct. 1957).
[17] L. Solymar, Spurious mode generation in non-uniform waveguide, IRE Trans. **MTT–7,** 379 (July 1959).
[18] H. G. Unger, Circular waveguide taper of improved design, Bell System Tech. J. **37,** 899 (July 1958).
[19] Y. Shimizu, Theory of transmitting circular electric wave around bends, presented at Intern. Conf. Ultrahigh Frequency Circuits and Antennas, Paris (Oct. 1957).
[20] M. Jouguet, Effect of curvature on the propagation of electromagnetic waves in guides of circular cross-section, Cables et Transmission **1,** 133 (1947).
[21] W. J. Albersheim, Propagation of TE_{01} waves in curved waveguides, Bell System Tech. J. **28,** 1 (1949).
[22] H. G. Unger, Normal mode bends for circular electric waves, Bell System Tech. J. **36,** 1292 (1957).
[23] K. Tanaka, Mode conversion through the tapered section of circular waveguide system, Intern. Conf. Ultrahigh Frequency Circuits and Antennas, Paris (Oct. 1957).
[24] B. Z. Katzenelenbaum, Long symmetrical waveguide taper for H_{01} wave (in Russian), Radiotekh. Elektron. **2**[1], 531 (1957).
[25] L. Solymar, Design of a conical taper in circular waveguide system supporting H_{01} mode, Proc. IRE **46,** 618 (1958).
[26] L. Solymar, Design of a two-section conical taper in circular waveguide system supporting the H_{01} mode, Proc. Inst. Elec. Engrs. (London), pt. B. Suppl. No. 13, p. 119 (Jan. 1959).
[27] L. Solymar, Monotonic multi-section tapers for overmoded circular waveguides, Proc. Inst. Elec. Engrs. (London), pt. B. Suppl. No. 13, p. 121 (Jan. 1959).
[28] L. Solymar, Discussion on "Special microwave equipment," Proc. Inst. Elec. Engrs. (London), pt. B. Suppl. No. 13, p. 147 (Jan. 1959).
[29] L. Solymar and C. C. Eaglesfield, Design of mode transducers, IRE Trans. **MTT–8,** 61 (Jan. 1960).
[30] C. C. Eaglesfield, Y. Klinger, and L. Solymar, A new H_{10} to H_{20} mode transducer (to be published in Proc. Inst. Elec. Engrs. (London)).
[31] B. Z. Katzenelenbaum, Imperfect waveguide in boundary and geometry, Izvest. Akad. Nauk., p. 9 (1955).
[32] S. P. Morgan, Mode conversion losses in transmission of circular electric waves through slightly non-circular guides, J. Appl. Phys. **21,** 329 (1950).
[33] S. Iiguchi, Mode conversion in the transmission of TE_{01} wave through a slight tilt and a slight off-set of waveguide, Intern. Conf. Ultrahigh Frequency Circuits and Antennas, Paris (Oct. 1957).
[34] L. Solymar, Overmoded waveguides, optical approach to mode conversion, Electron. and Radio Engr. **36,** 426 (Nov. 1959).
[35] L. Solymar, Step transducer between overmoded circular waveguides, Proc. Inst. Elec. Engrs. (London), pt. B. Suppl. No. 13, p. 129 (Jan. 1959).

(Paper 65D1–105)

JOURNAL OF RESEARCH of the National Bureau of Standards—D. Radio Propagation
Vol. 65D, No. 1, January–February 1961

Useful Radiation From an Underground Antenna [1,2]

Harold A. Wheeler

(February 26, 1960)

An underground antenna delivers power to the surrounding conductive medium, and a fraction of the power goes out as radiation above the surface. This fraction is denoted the "radiation efficiency." It is expressed in simple terms for two types of underground antennas. The first and simplest is a vertical loop in a submerged spherical radome. The second is a submerged horizontal insulated wire with each end connected to a ground electrode. In each case, the efficiency is the product of three simple factors: The first depending on the index of refraction between air and ground; the second proportional to the size (radius of the radome or length of the wire); the third giving the attenuation with depth. An example for 1 megacycle per second gives an efficiency of 0.0014 for an underground wire of specified dimensions. The radiation efficiency is applicable to sender or receiver.

For protection from hazards above the ground, an underground antenna may be considered for some purposes, such as communication over a moderate distance. In a sender, such an antenna radiates a small part of its power out of the ground into free space. In a receiver, it intercepts a small part of the wave power that penetrates into the ground. Usually the most favorable path between two antennas is in the space above ground, even if both of the antennas are underground.

It is the purpose of this note to give some simple formulas for the radiation efficiency and some other properties of underground antennas of two simple forms. These are based on previous publications of R. K. Moore [1] [3], J. R. Wait [1a], and the writer [2 to 6], which were directed to underwater antennas presenting essentially the same problems.

By formulating the efficiency of radiation out of the ground, separate from other losses in the antenna and in propagation, the formulas are simplified and the contributing factors are made apparent. These formulas are used in computing the performance of an underground antenna to be described by L. E. Rawls [7]. They are also applicable to the transmission formulas for computing system performance, as proposed by C. R. Burrows [8], H. T. Friis [9,10], and K. A. Norton [11]. This "separation of the variables" is usually helpful in understanding the respective factors in performance.

The radiation pattern of the cases here to be considered is that of a small vertical loop just above ground. The reference for evaluating radiation efficiency is a perfect small loop just above a perfect ground plane, as shown in figure 1(a). The power supplied to the loop is all radiated; this useful radiated power is symbolized by P_r. In a sender, the loop image doubles the far field. In a receiver,

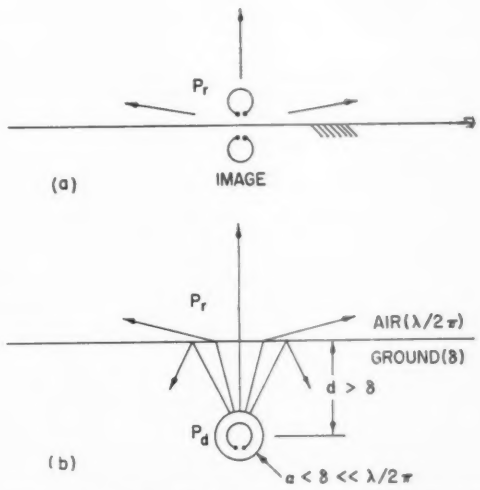

FIGURE 1. *A perfect small loop as a basis for expressing the radiation efficiency of an underground antenna.*

a. Loop over perfect ground plane.
b. Loop in submerged radome.

the total interception area (3/2 radiancircle) is only half associated with the actual loop above ground, so it has an interception area of only ¾ radiancircle, as referred to the power density in a plane wave along the ground.

The simplest case of an underground antenna is a small loop in a small spherical radome located underground at a certain depth, as shown in figure 1(b). The radome, of radius a, is filled with perfect insulating material (such as air), and its center is submerged to the depth d below the surface.

The relative properties of the ground and the space above (air) are indicated by the radianlengths in the respective mediums, δ and $\lambda/2\pi$. Assuming that the ground behaves mainly as a conductor rather than a dielectric, the former (δ) is equal to

[1] Contribution from Wheeler Laboratories, Great Neck, N.Y., and Development Engineering Corp., Leesburg, Va.
[2] Paper presented at Conference on the Propagation of ELF Radio Waves, Boulder, Colo., Jan. 26, 1960.
[3] Figures in brackets indicate the literature references at the end of this paper.

the well-known skin depth. All properties are to be expressed simply in terms of ratios of the several "length" dimensions.

The "index of refraction" may be defined as

$$n=\lambda/2\pi\delta>>1 \tag{1}$$

which is the ratio of phase velocities in the respective mediums. It is assumed to be very great, which is conducive to propagation of a wave along the ground with little "wave tilt."

Assuming a perfect loop as the radiator in figure 1(b), the power out of the loop (P_d) goes into the ground, and a small part of it (P_r) is radiated above ground. The ratio of these two quantities is the radiation efficiency:

$$\frac{P_r}{P_d}=\left(\frac{2\pi\delta}{\lambda}\right)^3 \quad \left(\frac{a}{\delta}\right) \quad \left(\exp-\frac{2d}{\delta}\right) \tag{2}$$

immersion ($1/n^3$) | size (loss) | depth (atten.)

The three factors have the indicated significance. The middle factor is peculiar to this type, reflecting the excess dissipation in the near magnetic field if the size of the radome is much less than the radiansphere in the ground.

The same value of efficiency is applicable in a receiver by reciprocity. In fact, the efficiency is more easily derived for a receiver, since plane waves may be assumed above and below the surface. It is then necessary also to compute the resistance appearing in the loop as a result of the surrounding ground, and this is easily done for the small spherical radome. In a receiver, the "noise temperature" of atmospheric radio noise above the surface may be multiplied by this efficiency to give the apparent temperature of such noise reaching the radome interior. This apparent temperature may be added to the actual temperature in the ground around the radome.

Figure 2 shows another type of underground antenna, for which the radiation efficiency and some other properties will be evaluated. The radiator is a long insulated wire buried in the ground in a horizontal position. Each end is connected to a ground electrode. In a sender, the current in the wire is provided by a generator connected in series.

For simplification, it is assumed that the wire has a small radius ($r<<\delta$) and a length (l) much greater than the skin depth but much less than the wavelength in air ($3\pi\delta<l<\lambda/\pi$); also that the depth (d) is

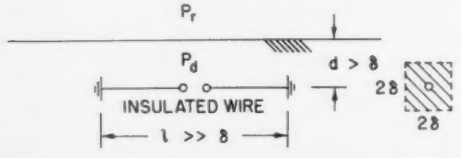

FIGURE 2. *A horizontal wire as an underground antenna.*

greater than the skin depth (as indicated). Each ground electrode is assumed to be "perfect," approximating a large plane perpendicular to the wire.

On the same basis as the preceding loop antenna, the long wire has the radiation efficiency:

$$\frac{P_r}{P_d}=\left(\frac{2\pi\delta}{\lambda}\right)^3 \quad \left(\frac{l}{3\pi\delta}\right) \quad \left(\exp-\frac{2d}{\delta}\right) \tag{3}$$

size (gain)

As before, the middle factor is peculiar to this type, but here there is a gain instead of a loss, in proportion to the length of the wire.

The resistance and reactance (R and X) of the underground wire, as derived by R. K. Moore [1], are expressed as follows:

$$R=\frac{1}{8}\omega\mu_0 l=\frac{1}{8}R_c\frac{2\pi l}{\lambda}=47.1\frac{2\pi l}{\lambda}=296\frac{l}{\lambda}\text{ ohms} \tag{4}$$

$$Q=1/p=X/R=\frac{4}{\pi}\left[\ln\frac{\sqrt{2}\,\delta}{r}-0.577\right]=\frac{4}{\pi}\ln\frac{0.794\,\delta}{r}. \tag{5}$$

The wave resistance of free space is represented by $R_c=377$ ohms.

The resistance is that of the ground return circuit. It is equal to the resistance of a cross section $2\delta\times2\delta$ of ground conductivity, on the basis of uniform current density, as indicated in the diagram. This resistance is involved in evaluating the efficiency. If the wire depth is less than the skin depth, the resistance changes very little. In fact, an older derivation by J. R. Carson [12] shows that the resistance has the same value for the special case of a wire located on the surface.

The reactance is that of a coaxial line comprising the wire in a circular shield of radius about 0.8 δ. The reactance is given for a wire of perfect conductivity and complete skin effect. For an actual wire small enough to neglect the skin effect, add ¼ in the brackets in (5). If the depth is less than the skin depth, the reactance increases slightly; if on the surface, add ½ in the brackets in (5) for this change.

Implicit in the radiation efficiency is the effective height of the loop formed by the wire and the ground return. The radiation above ground is the same as if there were a loop of the following effective height, with its center at the depth of the wire:

$$h=\delta/\sqrt{8}. \tag{6}$$

It is remarkable that this is valid for any depth of the wire below the surface.

An example of the long wire underground is described by the following dimensions and computed properties:

Frequency	$f=1$ Mc/s,
wavelength	$\lambda=300$ m,
ground conductivity	$\sigma=0.01$ mho/m,
skin depth	$\delta=5$ m,
depth	$d=1$ m,
length	$l=100$ m,
radius	$r=3$ mm,
index of refraction	$n=10$,
effective height	$h=1.8$ m,
resistance	$R=99$ ohms,
reactance	$X=900$ ohms,
power factor	$p=0.11$,
radiation efficiency	$P_r/P_a=0.0014=-28.5$ db.

In this example, for each 1 kw of power into the ground, only 1.4 w will end up in useful radiation above the surface.

The efficiency can be increased by locating a number of wires (N) in parallel in a grid, and supplying all with equal currents to form a sort of "current sheet." If the wires are spaced more than the skin depth (or more than twice the skin depth if near the surface) the efficiency is multiplied by the number (N) approximately.

Two practical problems have been ignored in the above. One is the power loss in the end connections. The other is the current variation along the wire.

The ground electrode for each end connection should have enough surface to reduce its resistance much below the irreducible value of the ground return (given above).

Some current variation along the wire is caused by the voltage applied to the capacitance to ground through the insulation. The voltage developed by the resistance is inevitable. However, the voltage developed by the reactance can be reduced by inserting series capacitors along the length. In the present case, for example, a capacitor of 50-ohms reactance (about $\frac{1}{2}$ R) may be inserted at intervals of 50-ohms wire reactance to tune out this reactance at one frequency. This would require 18 series capacitors in the wire.

The straight long wire does not have the highest efficiency possible for its length. A narrow loop of the same length, enclosed in a cylindrical radome, has greater efficiency by virtue of its wire return instead of a ground return. However, this loop has a much smaller power factor, so it must be critically tuned and has a relatively narrow bandwidth.

These formulas for radiation efficiency and other properties are intended to indicate the behavior of certain types of underground (or underwater) antennas. They are expressed in simple terms, and they fit into the usual computations of terminal circuits and point-to-point transmission.

The earlier work of Carson [12] and Moore [1] has contributed much to this subject, as mentioned in the text. The recent studies have been made as an aid to practical designs being proposed by Developmental Engineering Corp.

References

[1] R. K. Moore, The theory of radio communication between submerged submarines, Cornell Univ., thesis (June 1951).

[1a] J. R. Wait, The magnetic dipole antenna immersed in a conducting medium, Proc. IRE **40,** 1244 (1952).

[2] H. A. Wheeler, Radio wave propagation formulas, Hazeltine Rept. 1301W (May 11, 1942). (Transmission formula as a power ratio, interception area, radiancircle.)

[3] H. A. Wheeler, Universal skin-effect chart for conducting materials, Electronics **25,** 152 (1952). (Formulas and chart, including land and water, all frequencies.)

[4] H. A. Wheeler, Fundamental limitations of a small VLF antenna for submarines, IRE Trans. **AP–6,** 123 (1958). (Coil in spherical radome submerged in water, power interception area, power factor.)

[5] H. A. Wheeler, The spherical coil as an inductor, shield or antenna, Proc. IRE **46,** 1595 (1958). (Coil in spherical radome submerged in water.)

[6] H. A. Wheeler, The radiansphere around a small antenna, Proc. IRE **47,** 1325 (1959).

[7] L. E. Rawls, A practical underground transmitting antenna, topic presented by Developmental Engineering Corp. in meeting on Jan. 26, 1960, at the NBS, Boulder, Colo.

[8] C. R. Burrows, Radio propagation over plane earth—field strength curves, Bell System Tech. J. **16,** 45 (1937). (Transmission formula as a power ratio.)

[9] H. T. Friis, A note on a simple transmission formula, Proc. IRE **19,** 254 (1946). (Transmission formula as a power ratio in terms of interception area.)

[10] S. A. Schelkunoff and H. T. Friis, Antennas—Theory and practice (John Wiley & Sons, Inc., New York, N.Y., 1952). (Transmission formula as a power ratio, problems, pp. 300–1.)

[11] K. A. Norton, Transmission loss in radio propagation—II, NBS Tech. Note 12 (June 1959). (Power ratios.)

[12] J. R. Carson, Wave propagation in overhead wires with ground return, Bell System Tech. J. **5,** 539 (1926).

(Paper 65D1–106)

JOURNAL OF RESEARCH of the National Bureau of Standards—D. Radio Propagation,
Vol. 65D, No. 1, January–February 1961

Observation of *F*-Layer and Sporadic-*E* Scatter at VHF in the Far East[1]

K. Miya, T. Sasaki, and M. Ishikawa

(April 26, 1960)

This paper describes properties of sporadic-*E* scatter and *F*-layer scatter observed over the Okinawa-to-Tokyo path (1480 kilometers) and the Philippines-to-Tokyo path (2850 kilometers) operating at frequencies of about 50 megacycles per second.

Sporadic-*E* scatter is often observed on the Okinawa signal in the evening hours and has the closest correlation (0.94 in correlation ratio) with the occurrence of sporadic *E* characterized by the descriptive symbol "M" of all ionospheric factors. Bearing of the *Es* scatter shows a regular diurnal variation similar to that of the normal *E*-layer scatter.

F-layer scatter generally appears on the Philippine signal in autumn when the *F*-layer at the path midpoint displays an anomaly denoted by the symbol "R" or "S" having a top frequency of higher than 14 megacycles per second. A pulse test exhibited a pattern of multipath signals extending over more than 1 millisecond. Bearing of the *F*-layer scatter, an evening phenomenon, gradually deviates westwards from the great-circle path with the lapse of time.

1. Introduction

Great progress has been made in the study of transmission by way of inhomogenities in the ionosphere, commonly termed scattering in the *E*-layer. In addition, *F*-layer scatter in the Far East has been pointed out by R. Bateman and others [1][2] and a peculiar signal enhancement has been reported recently by the authors [2] as a kind of scatter associated closely with sporadic *E*. Continuous measurements of signal strength, bearing, and angle of elevation at about 50 Mc/s have been carried out in Tokyo on Okinawa and Philippine signals transmitted until the end of October 1959 as the continuation of a part of the United States program for the IGY.

Aside from characteristics of *Es* propagation which will be reported as an interest in the field of communications engineering, the following will mainly describe the types of scatter mentioned above.

2. Scope of Observation

2.1. Signals Measured and Experimental Circuits

An outline of the experimental circuits is shown in figure 1. Continuous waves of 2-kw output were emitted towards the middle part of Japan at 49.68 Mc/s from Okuma, Okinawa, and at 49.84 Mc/s from Poro, the Philippines. Each of the transmitting antennas was a horizontal 5-element Yagi, having a gain of 7 db relative to a dipole, a height of 12 m above the ground, and a half-power beamwidth of 54°. The measurements were conducted at Fukuoka receiving station, near Tokyo, from October 1958 through October 1959. Pulse signals, from Poro, were observed in autumn 1959.

The orientations of both paths were almost from southwest to northeast. The transmitting antenna used at Okuma was beamed to 35°13′ E of N deviating northwards by 8.5° off the great-circle path to Tokyo. Surface path length between Okuma and Tokyo is 1480 km, and Poro and Tokyo is 2850 km. So one-hop *Es* propagation may exist over the former circuit and two-hop *Es* or one-hop *F*2 propagation over the latter.

The Yamagawa and Okinawa ionosphere stations are located 330 km and 160 km from the path midpoints, respectively, as seen in figure 1.

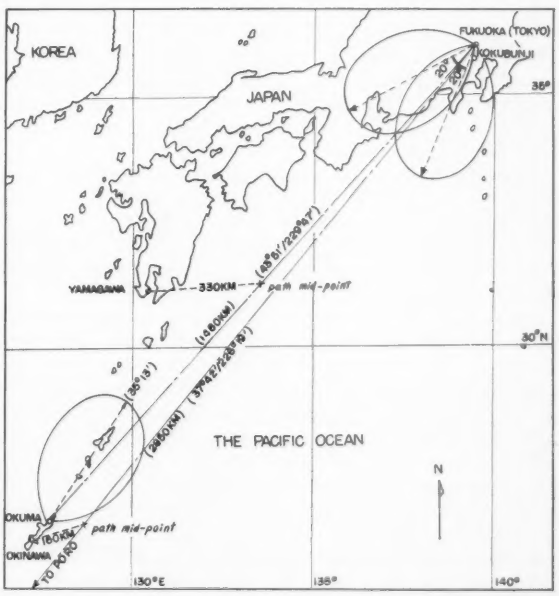

FIGURE 1. *Map of the Far East, showing the forward scatter paths and the ionosphere stations.*

[1] Contribution from Kokusai Denshin Denwa Co., Tokyo, Japan.
[2] Figures in brackets indicate the literature references at the end of this paper.

2.2. Method of Observation

Three 5-element Yagis A, B, and C of same construction as the transmitting antenna were used for the measurements. Yagis A and B were mounted 30.6 m high on two iron poles separated by 105 m, directivities being shifted by 20° westwards and southwards from the true bearing of Okuma respectively. Yagi C was mounted at a height of 12.6 m, being beamed to the same direction as Yagi A. Bearing and angle of elevation were obtained from the ratios of voltages induced on Yagis A and B and on Yagis A and C, respectively.

The ratio of voltages was continuously recorded using two sets of voltage ratio meters [2] which are capable of measuring angles of arrival accurately even on a low level of the signal strength. The output voltage of the meter was logarithmically compressed and indicated by a pen recorded as open-circuit voltage measured at 75 Ω impedance in decibels above 1 μv.

3. Observational Results

3.1. Okuma-to-Tokyo Transmission

Figures 2 and 3 show typical results observed on the Okuma signal in winter and summer months, respectively. Figure 4 exhibits an example of appearance of the pen records during a period including all types of scatter.

In winter, the signal received is mainly the normal *E*-layer scatter including meteoric bursts throughout the day. Attenuation of the scatter in the ionosphere is estimated to be between 72 and 82 db in the median value, showing the maximum at about 1800 J.s.t. and the minimum around midday.

As seen in figure 4, the signal strength sometimes rises to a maximum of 30 db above the level of the normal value, late in the evening. This phenomenon will be referred to as *Es* scatter and its characteristics will be discussed later.

Hourly median angles of arrival are indicated by dots, and ranges between upper and lower quartiles are shown by lengthwise lines in figures 2 and 3. Bearing data explicitly show a diurnal variation which deviates westwards off the true bearing during the period of 1800 to 1000 J.s.t. and slightly southwards early in the afternoon. Seasonal and diurnal distributions of hourly median bearings are exhibited in figure 5 representing contours of equal bearings. The figure shows a feature of regular diurnal variation with a tendency of deviating westwards a few degrees off the true bearing on the average throughout a year. The fact that the main lobe of the transmitting antenna is beamed northwards off the great-circle path may be one of the causes of the average deviation of bearing. However, attention must be drawn to the fact that the diurnal variation including the average deviation is quite similar to W. R. Vincent and others' results of best antenna angle for meteoric bursts [3]. The seasonal variation of bearing showed a complicated but periodic behavior.

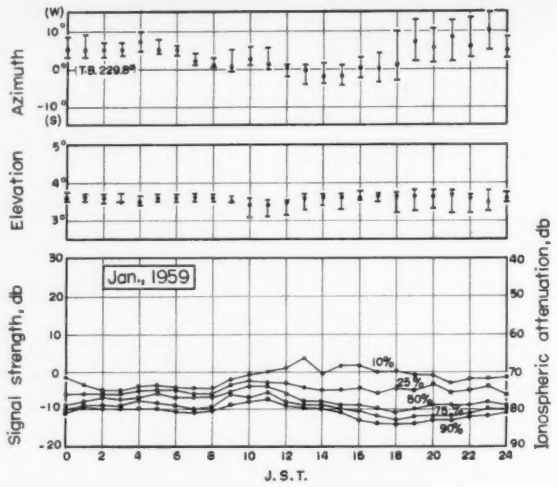

FIGURE 2. *Diurnal curves of signal strength, angles of arrival.* Okuma-Tokyo, 49.68 Mc/s, January 1959.

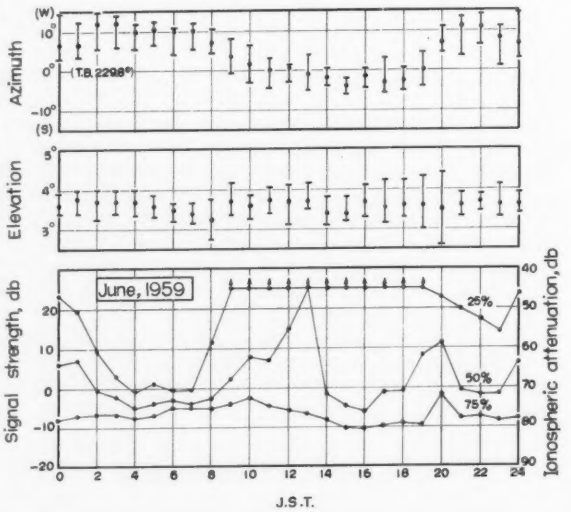

FIGURE 3. *Diurnal curves of signal strength, angles of arrival.* Okuma-Tokyo, 49.68 Mc/s, June 1959.

No noticeable variation of angle of incidence was observed in the median value. The minimum, however, was clearly observed during a period of 1100 to 1200 J.s.t. during all the months except summer, when the normal *E*-layer scatter was mainly received.

In summer when *Es* reflections are most common, and produce an increase of many times the normal signal level, hourly values of angles of arrival are distributed in a wider range than those observed in winter as seen in figures 2 and 3.

The range of quartiles of signal strength, bearing, and angle of elevation shows the minimum excursion at about 0600 J.s.t. early in the morning.

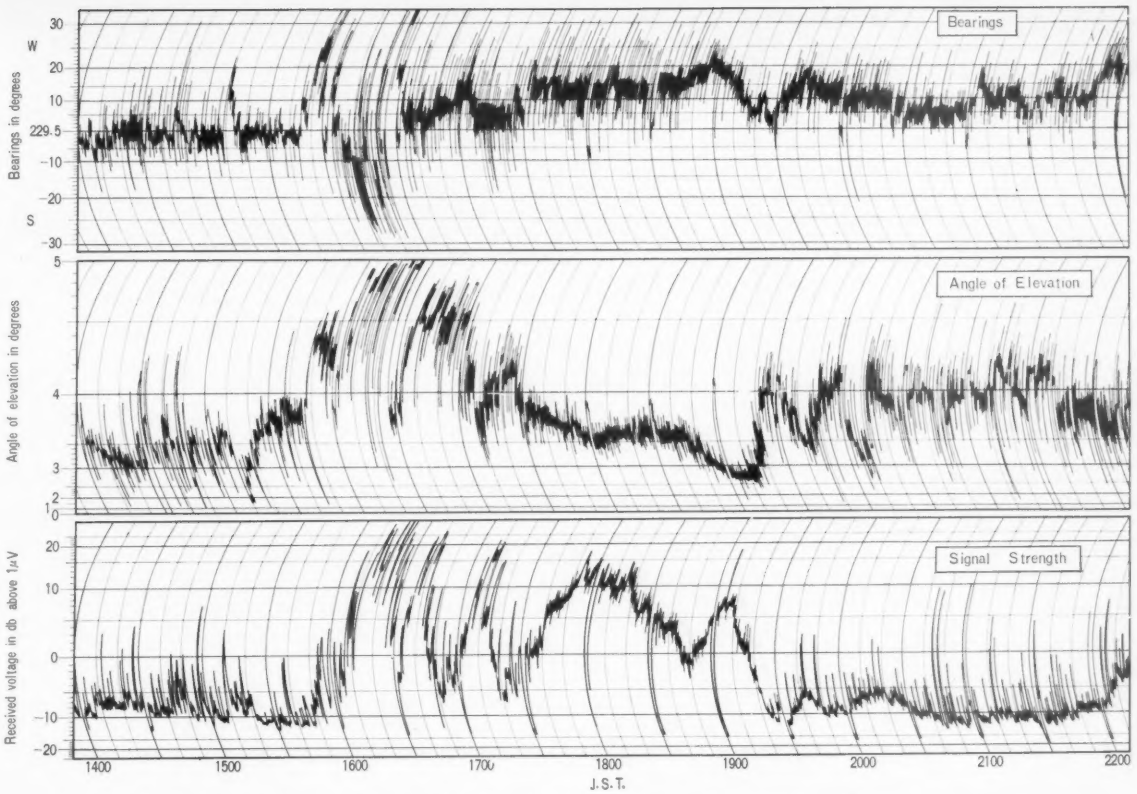

FIGURE 4. *A typical record of angles of arrival and signal strength observed on January 12, 1959.*

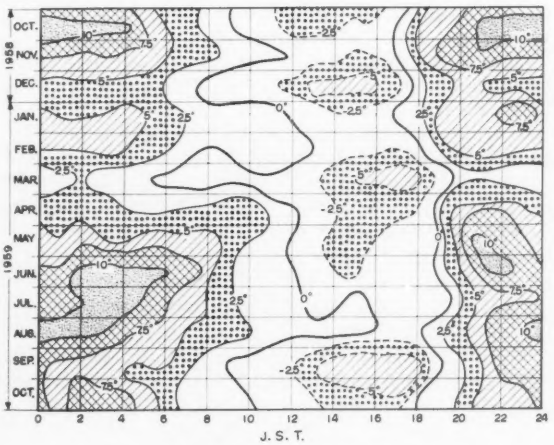

FIGURE 5. *Contours of equal bearing.*
Okuma-Tokyo, 49.68 Mc/s, October 1958–October 1959.

3.2. Poro-to-Tokyo Transmission

The signal from Poro was received only a small part of the time, except in summer and autumn. Judging from the characteristic appearance of sporadic E, most of the signals received in summer are inferred to be two-hop propagation by way of the Es specular reflection. Most hourly median bearings observed in summer were nearly the true bearing. Hourly median angles of elevation were between 3.5° and 3.9° and they showed lower values in the daytime. These angles observed are slightly lower than the calculated by estimating height of sporadic E to be 90 km.

On the other hand, it is obvious that the signal received in autumn was propagated via the F-region. Behavior of this signal will be described in the later chapter.

4. Sporadic-E Scatter

4.1. General

As mentioned above, a remarkable signal enhancement is nightly observed on Okuma signal, sometimes attaining a level 30 db higher than that of the normal E-layer scatter. The authors called the event "Es evening enhancement" [2], because it is closely associated with sporadic E and it is likely to occur late in the evening. The enhancement appears to represent sporadic E scatter because of the following features. The Es scatter does not undergo as rapid a change in signal strength as sporadic E propagation and shows a gradual variation over an hour to several hours.

When this takes place, variations of bearing and angle of elevation are always observed. These variations are quite different from that of *Es* propagation as shown in figure 4. The *Es* scatter closely correlates with some type of sporadic *E* at the path midpoint rather than the magnitude of the *foEs* itself. The relationship is now explored.

4.2. Rate of Occurrence

Judging from a statistical study of *foEs* and attenuation in the ionosphere, Γ, the signal of $\Gamma \leqq 45$ db is assumed to be reflected by sporadic *E* and the signal of $\Gamma > 70$ db as the normal *E*-layer scatter. An analysis was made of the signal of 45 db $< \Gamma \leqq 70$ db, the range in which most of the *Es* scatter is included.

Seasonal and diurnal distributions of signals of 45 db $< \Gamma \leqq 70$ db are shown in figure 6(a) indicating contours, of equal occurrence rates of reception in percentage, N_Γ. One of the most distinctive features in the figure is that the maximum rate appears late in the evening. The authors tried to find some ionospheric factor which had a close correlation with the distribution in figure 7(a). This was found to be the occurrence of the descriptive symbol "M" [3] associated with the "critical frequency" of sporadic *E* (*foEs*). Figure 6(b) indicates contours of equal occurrence of such sporadic *E*, N_M, observed at the Yamagawa ionosphere station. Comparing the temporal distributions of figure 6(a) and figure 6(b), it is seen that there is a reasonably good correlation between the two sets of data.

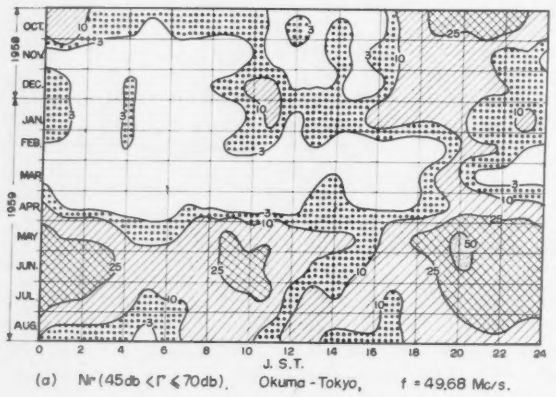

(a) N_Γ (45db $< \Gamma \leqq$ 70db), Okuma - Tokyo, f = 49.68 Mc/s.

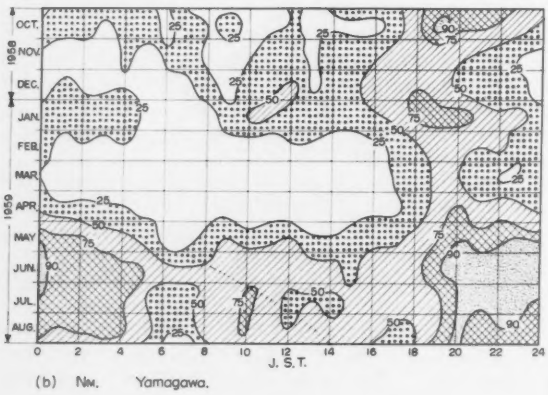

(b) N_M, Yamagawa.

FIGURE 6. *Contours of equal rates in percentage of* N_Γ *and* N_M.

N_Γ: rate of occurrence of *Es* scatter, and N_M: rate of occurrence of *Es* affixed by symbol "M" at the path midpoint.

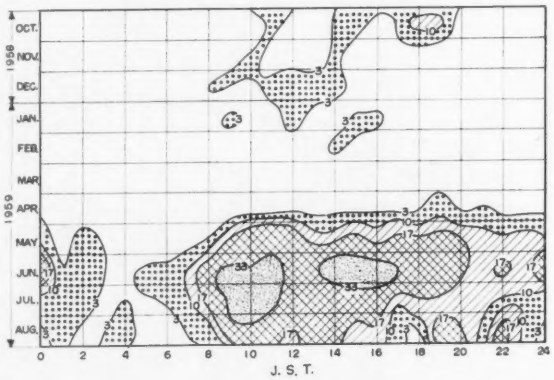

FIGURE 7. *Contours of equal rate in percentage of foEs above 7.5 Mc/s at Yamagawa.*

N_F (*foEs* $\geq$ 7.5 Mc/s).

For reference, the occurrence of sporadic *E* with *foEs* above 7 Mc/s, N_F, is shown in figure 7. This figure is pertinent enough for the purpose of investigating correlation because N_F for any value of *foEs* gives a similar distribution to that of figure 7. Figures 6(a) and 7 have a resemblance to each other in seasonal variation, but not always in diurnal variation.

In order to obtain quantative relationship between N_Γ and N_M, hourly mean values of N_Γ and N_M for 3 months every season are plotted as a correlation diagram shown in figure 8. From the figure, the following relation is calculated:

$$N_\Gamma = 0.42\, N_M^2,$$

where correlation coefficient between them is 0.9 and correlation ratio is 0.94.

An analysis using data observed at the Kokubunji ionosphere station, which is located 750 km from the path-midpoint, did not result in as good an association as the above. This may be because the station is too far away to give a good correlation.

4.3. Angles of Arrival

Needless to say, the measured angles of arrival are influenced by the signals from all the modes of propagation present. The data were, therefore,

[3] M, Measurement questionable because the ordinary and extraordinary components are not distinguishable.

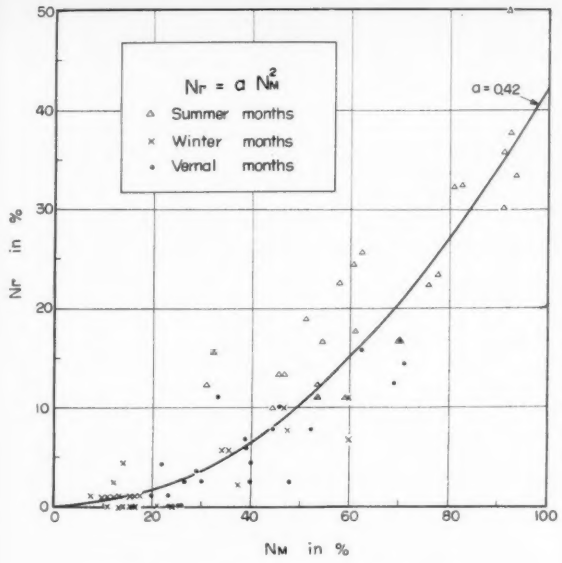

FIGURE 8. *Correlation between* N_Γ *and* N_M.
N_Γ: rate of occurrence of *Es* scatter, and N_M: rate of occurrence of *Es* affixed by symbol "M".

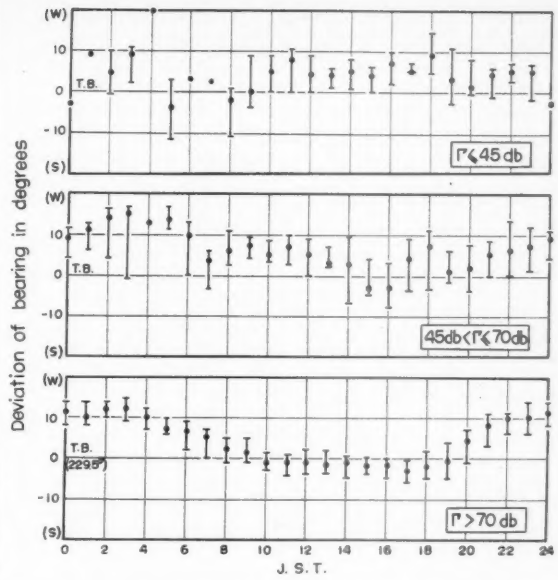

FIGURE 9. *Bearing in each range of* $\Gamma \leq 45$ *db,* $45 \text{ db} < \Gamma \leq 70$ *db and* $\Gamma > 70$ *db.*
Okuma-Tokyo, 49.68 Mc/s, July 22–August 21, 1959.

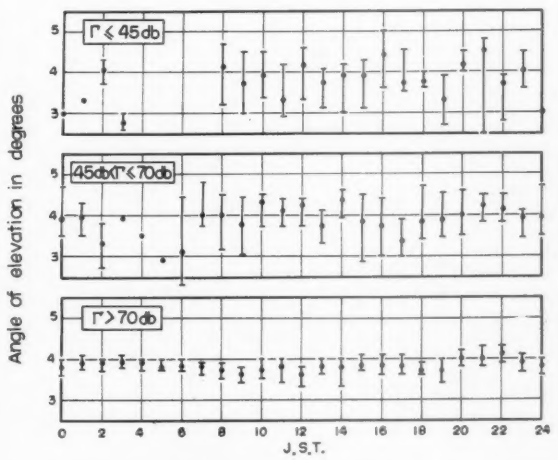

FIGURE 10. *Angle of elevation in each range of* $\Gamma \leq 45$ *db,* $45 \text{ db} < \Gamma \leq 70$ *db and* $\Gamma > 70$ *db.*
Okuma-Tokyo, 49.68 Mc/s, July 22–August 21, 1959.

arranged into three groups according to the previous classification of ionospheric attenuation, namely: $\Gamma > 70$ db, 45 db $< \Gamma \leq 70$ db, and $\Gamma \leq 45$ db. Arrangement was made, in this manner, of the data obtained during a period in July and August 1959, for which wide dynamic range recordings were available. Figures 9 and 10 are the results of measurements.

From these figures the following features are noted: The normal *E*-layer scatter of $\Gamma > 70$ db showed a regular diurnal variation of angle of arrival with a narrow range of quartile distributions; on the contrary, the *Es*-reflected signal of $\Gamma \leq 45$ db displayed a wide distribution of angles of arrival with no clear diurnal variation and a westerly deviation of bearing of several degrees on the average. On the other hand, the bearings of the *Es* scatter of 45 db $< \Gamma \leq 70$ db exhibited a diurnal variation similar to that of the normal scatter, being accompanied with a wider distribution than that of the normal scatter.

From the results mentioned above, it is inferred that the *Es* evening enhancement or *Es* scatter is not caused by the normal reflection from sporadic-*E* clouds but by an irregularity of sporadic *E*, and that the diurnal variation of bearing of the *Es* scatter may be related to the same mechanism as that of the normal *E*-layer scatter.

5. *F*-Layer Scatter

F-layer scatter was pointed out by R. Bateman and others [1] as an evening enhancement observed in the Far East in autumn. The event frequently occurred over the Poro-to-Tokyo path in the evening hours in September and October. When this took place, *F*-layer measurements at the Okinawa ionosphere station quite near the path midpoint always indicated either of the following conditions:

(a) *F*2 critical frequency higher than the 18 Mc/s required for the normal reflection in oblique incidence propagation at the used frequency, or

(b) *F*2-layer critical frequency qualified by the

symbol "R" or "S",[4] where the top frequency was higher than about 14 Mc/s.

Figure 11 is a typical example illustrating such a correspondence of the signal strength with the "*f*-plot" of ionospheric data. There is no doubt that the signal received in autumn is closely associated with the *F*2-layer. It is also obvious that ionosperic layers other than the *F*2-layer did not take part in the propagation during the period of autumnal observation where especially sporadic *E* was inactive. Figure 12 shows diurnal curves of reception of signal, N_R, and N_I, the occurrence of the two ionospheric conditions, "R" and "S", observed in October 1959. Fair agreement can be seen between N_R and N_I. The spread-*F* condition was rarely observed at Okinawa which is quite near the path midpoint, during the observational period.

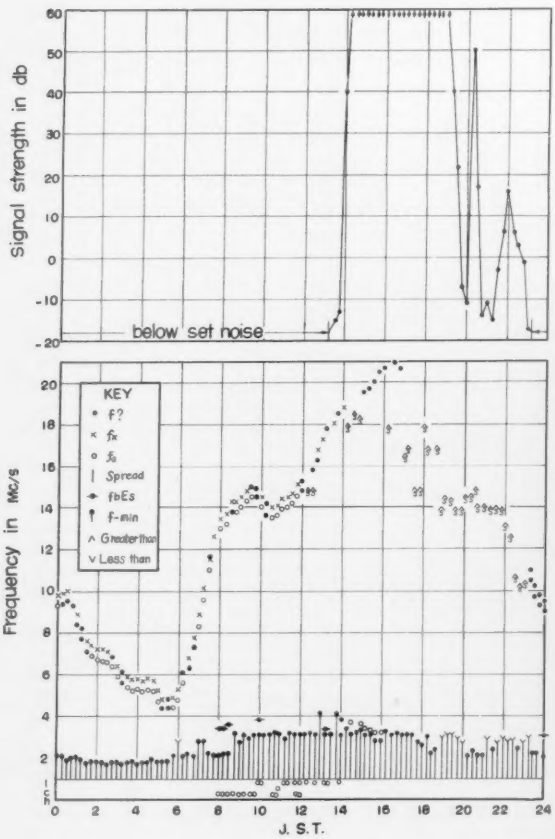

FIGURE 11. *Diurnal curves of signal strength and f-plot of ionospheric data observed at the Okinawa ionosphere station.*

Poro, the Philippines—Tokyo, 49.84 Mc/s, October 7, 1959.

[4] R, Measurement influenced by, or impossible because of, absorption in the vicinity of a critical frequency.
S, Measurement influenced by, or impossible because of, interference or atmospherics.

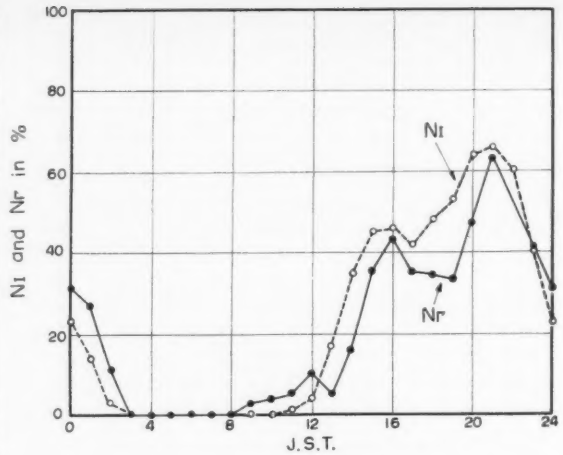

FIGURE 12. *Comparison of* N_R *and* N_I.

N_R: rate of reception of *F*-layer scatter.
Poro, the Philippines-Tokyo, 49.84 Mc/s, October 1959.
N_I: rate of occurrence of the ionospheric anomalies at Okinawa.

Pulse signal of 50 microseconds duration was observed at Tokyo on September 23, 1959. Figure 13 exhibits the typical A-display of the received pulse. It is composed of a number of components corresponding to various propagation paths spreading over a range of more than 1 msec. The maxi-

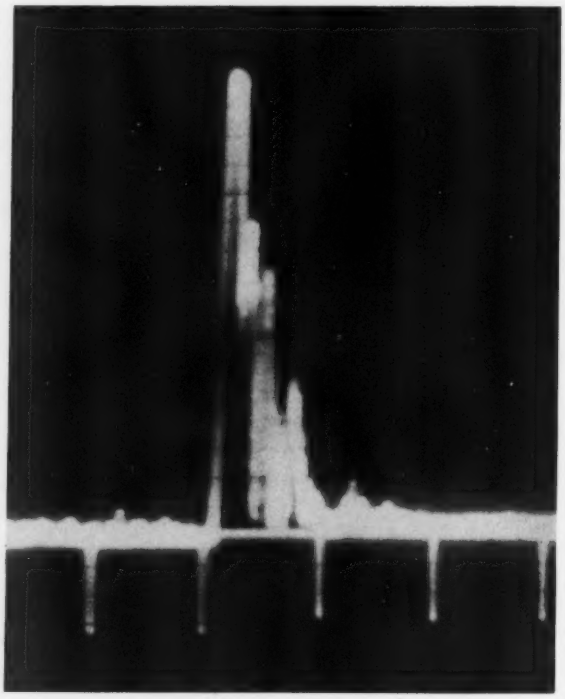

FIGURE 13. *A typical A-display of the received pulse.*

Poro, the Philippines-Tokyo, 49.84 Mc/s, 2203 J.s.t., September 23, 1959, time mark of 1 msec.

mum delay time is of the same order as that observed by R. Bateman and others [1] for the Poro-to-Onna, Okinawa, path (1347 km). The ionospheric condition when the picture was taken corresponded to the case (b) above. From these observations, it is inferred that the received signal is propagated by way of scattering from an anomaly in the $F2$-layer peculiar to a region in the low latitude in addition to the normal $F2$-propagation.

Figure 14 shows the results observed in October 1959. The signals generally arrive from the true bearing early in the evening, but their bearings gradually deviate westwards with the lapse of time. It is one of the future problems to clarify whether the westerly deviation is caused by movement of the anomaly or by such mechanism as scattering from field-alined blobs of ionization in the F region as suggested already [1].

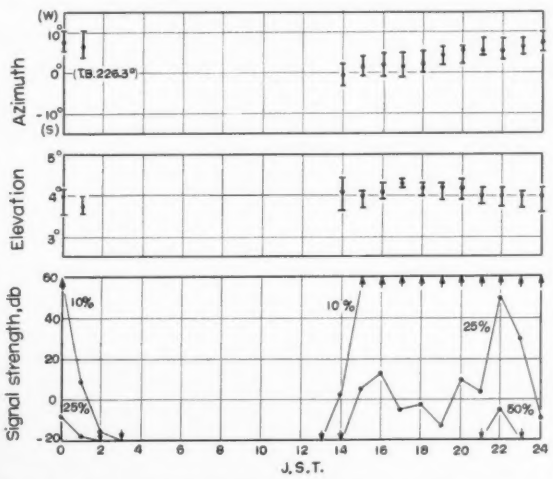

FIGURE 14. *Diurnal curves of signal strength, angles of arrival.*

Poro, the Philippines-Tokyo, 49.84 Mc/s, October 1959.

The authors express their thanks to Dr. S. Namba, Chief of Research Laboratory, K.D.D., for his encouragement in the study, to CRPL and The Voice of America in the United States Government, and the Radio Research Laboratories, Japan, for their cooperation and assistance in the continuation of transmissions and in the data arrangement.

6. References

[1] R. Bateman, J. W. Finney, E. K. Smith, L. H. Tveten and J. M. Watts, IGY observation of F-layer scatter in the Far East, J. Geophys. Research **64,** 403 (1959).

[2] K. Miya, T. Sasaki, and M. Ishikawa, Angles of arrival of a VHF signal in ionospheric forward propagation, Rep. Ionosphere and Space Research, Japan **8,** 187 (1959).

[3] W. R. Vincent, R. T. Wolfram, B. M. Sifford, W. E. Jaye, and A. M. Peterson, Analysis of oblique path meteor-propagation data from the communications viewpoint, Proc. I.R.E. **45,** 1706 (1957).

(Paper 65D1–107)

JOURNAL OF RESEARCH of the National Bureau of Standards—D. Radio Propagation

Vol. 65D, No. 1, January–February 1961

A High-Resolution Rapid-Scan Antenna[1]

H. V. Cottony and A. C. Wilson

(August 11, 1960)

An electronically scanned antenna array is described. It consists of a broadside array of seven Yagi elements spaced 1.4 wavelengths apart. Each element antenna is connected to a preamplifier-converter. Each converter is connected to a local oscillator differing by 20 c/s from that connected to the converter for the adjacent element. All oscillators are locked in phase. The converter outputs are connected to a common IF amplifier. This arrangement produces a 5.8-degree-wide beam swept over a 41.8-degree azimuth sector at a rate of 20 scans per second. The system operates at 40.92 Mc/s. The output of the system is displayed on an oscilloscope, and data on the direction of arrival and character of a distant VHF signal are presented visually.

Sample records of signal components propagated by ionospheric scatter, meteor trail reflections, and sporadic-E layer are cited.

1. Introduction

An antenna having a very narrow width of main lobe is a useful tool in the field of propagation studies. It can enable an investigator to resolve the modes of propagation arriving from different directions. Many of the important propagation phenomena are, however, subject to rapid variation with time. It is important, therefore, that, in addition to high resolving property, the antenna be capable of being scanned over the desired sector at a rate more rapid than the change of the propagation phenomena being studied. A project for the design and construction of an antenna system demonstrating this principle was authorized in July 1959. This paper describes the accomplishments on the project to date.

The application of an antenna is essential in selecting its parameters. This particular antenna had as its object the measurement of the direction of arrival of a VHF signal (40.92 Mc/s) transmitted from a point 1295 km (805 mi) away, and propagated variously by ionospheric scatter, meteor trail reflections, and sporadic E-layer reflections. It was anticipated that the direction of arrival might depart by 10 and more degrees off the great-circle route. It was not, however, anticipated to be further than about 20 deg off because the reflection points had to be visible optically from both the transmitting and receiving points. The signal scattered by the ionosphere is known to be fluctuating rapidly. The duration of the meteor trail reflection varies, but is likely to be of the order of 1 or 2 sec. For this reason the duration of the scan had to be of the order of 0.1 sec or shorter. In addition, the maximum acceptable rate of scan was, in this application, limited by considerations of pulse transmission and beamwidth.

In order to measure the path delay, it was planned to utilize pulse transmissions for some of the measurements. Earlier work by Carpenter and Ochs [1][2] showed that relative path delays greater than 0.5 msec were rare, but that reasonably numerous delays in the time of arrival up to that value could be expected. This would restrict the pulse repetition rate to 2000 pps. A pulse repetition rate of 500 pps was decided upon. The pulse repetition rate and the beamwidth of the main lobe set a limit on the maximum rate of scan. Thus, if the beamwidth were 1 deg and the pulse repetition rate —500 pps, for complete sector coverage without gaps the maximum scan speed should be limited to 500 deg/sec. For a 2-deg beamwidth it could be 1000 deg/sec. If the sector of scan were restricted to 40 deg, 20 deg to each side of the great-circle path, the maximum permissible scanning rate would, for the two cases, be 12 and 25 scans per second. This is the limit on the maximum rate of scan.

The conventional means of obtaining a radiation pattern narrow in one plane is to make an antenna wide in that plane. While there are available methods for reducing the beamwidth of an antenna of a given dimension, these methods have limitations. The array described here was designed and employed conventionally. It consists of 7 horizontally polarized 5-element Yagi antennas in a broadside array. The spacing was made as large as possible without introducing harmful directional ambiguities. The spacing settled upon was 1.4 wavelengths. This resulted in ambiguities at an angle of 20.9 degrees off the great-circle path. For any other point within the 20.9°-0°-20.9° sector, the other point of ambiguity lies outside the sector and may be presumed to be very improbable. Five-element Yagis were selected because their half-power beamwidth in the E-plane, 56 deg, permitted operation within the 40-deg sector without introducing serious inequality of

[1] Contribution from Central Radio Propagation Laboratory, National Bureau of Standards, Boulder, Colo.

[2] Figures in brackets indicate the literature references at the end of this paper.

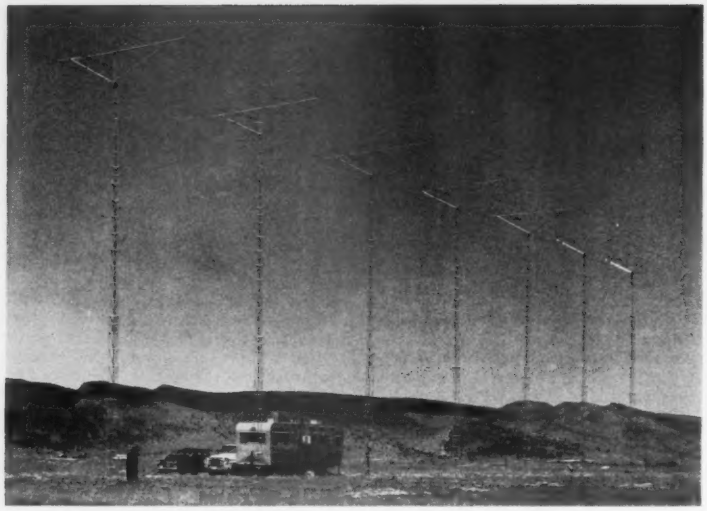

FIGURE 1. *A view of the antenna system.*

response. At the same time they were effective in discriminating against the signals outside the sector. The gain of the individual Yagi antenna was approximately 11.3 db relative to an isotropic radiator. The beamwidth of the array, when directed straight ahead, was computed to be 5.8 deg for 20-db sidelobe suppression.

Figure 1 is a view of the array. It is located on the Table Mesa near Boulder, Colo. It is directed at a bearing of 84.66° pointing along the great-circle path, towards the transmitter at Long Branch, Ill., field station 1295 km away.

2. Principle of the Electronic Scan

Because the method of electronic scan introduced with this antenna is the important contribution to the project, it is believed desirable to describe it in some detail.

Figure 2 is a diagram of a 7-element stationary array in which the directivity is obtained by proper phasing of the element currents. If the elements are equispaced with a separation d and the beam is to be directed at an angle β to the right, it is necessary to advance the phase of the current in elements 3_I, 2_I, and 1_I by phase angles 3δ, 2δ, and δ where $\delta=2\pi(d/\lambda)\sin\beta$. The phases of the currents in the elements on the right side have to be retarded by corresponding angles. Such phasing can be accomplished either mechanically, electrically, or electronically. Many ingenious methods of doing this have been tried [2]. All of them have some drawbacks. With this antenna, a method of phasing in a mixer circuit is introduced.

It is known that when two voltages, $e_1=A\sin 2\pi f_1$ and $e_2=B\sin(2\pi f_2+\delta)$, are connected to the inputs of a nonilnear network, the outputs will contain the sum and difference of frequency voltages, $e_s=C\cos[2\pi(f_1+f_2)+\delta]$ and $e_d=\mathrm{C}\cos[2\pi(f_1-f_2)-\delta]$, in which the phase relationship of the original voltages is not lost. If e_2 is the local oscillator voltage, the phase of the signal contributed by an element antenna is controllable by varying the phase of the local oscillator. The practical means of doing it is by varying δ continuously in one direction so that in a time interval, t_s, it changes from 0 to 2π. Such a continuous phase change is equivalent to an incremented frequency change, $\Delta f=(1/t_s)$. To obtain proper scan of the antenna, it is necessary to connect each to its own converter with the local heterodyne voltages differing in frequency by frequency increment Δf. If the local heterodyne voltage for antenna

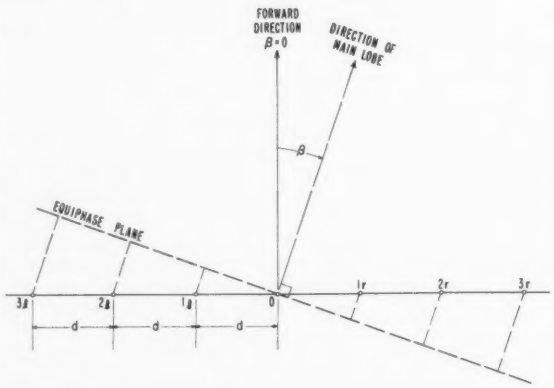

FIGURE 2. *A diagram of a seven-element broadside array illustrating the steering of the main beam by phasing.*

0 is $e_0=A \sin 2\pi f_0$ the local heterodyne voltages for antennas 3_l, 2_l, and 1_l will be e_3, e_2, and e_1, equal respectively to $A \sin 2\pi(f_0-3\Delta f)$, $A \sin 2\pi(f_0-2\Delta f)$ and $A \sin 2\pi(f_0-\Delta f)$. The element antennas on the right side of the array should have local heterodyne frequencies increased by the same increments. The beam of such antenna will rotate unidirectionally from left to right with a scan frequency equal to Δf. It should be noted that the range of scan is from one main lobe to another. If the element spacing, d, were equal to $\lambda/2$, for $\delta=\pm\pi$ there would be two main lobes, at $\beta=-90°$ and $+90°$, respectively. Thus, the scan would begin at $\beta=-90°$ and sweep to $+90°$. If the spacing, d, were less than $\lambda/2$, the main beam would form in the imaginery region of $\sin\beta<-1$, sweep through the real sector $-90°$ to $0°$ to $+90°$, and disappear into the imaginary region of $\sin\beta>+1$. If d were greater than $\lambda/2$, several main beams might be present at all times and the entire ensemble of main beams would rotate clockwise. For $d=1.4\lambda$ and $\delta=\pi$, there is a main lobe in the imaginary region, $\beta=\sin^{-1}-1.07$, two real lobes at $-20.9°$ and $+20.9°$, respectively, and another lobe in the imaginary region, $\beta=\sin^{-1}+1.07$. In one cycle the beams sweep through one interval between lobes. In this discussion, the fact that the radiation pattern has mirror-image symmetry about the line of the array has been ignored. In physical construction, a reflecting screen or unidirectional elements would normally be employed.

The proper operation of this scanning technique is very dependent upon finding a successful solution to the problem of generating an ensemble of local heterodyne voltages. These have to differ in frequency by the increment Δf, but must be locked in phase. It is possible to accomplish this in a number of ways. The method selected here was to pulse the oscillator having a fundamental frequency f_0 at a pulse rate corresponding to Δf. If the length of the pulse is short, a spectrum of frequencies is generated with the center frequency at f_0 and other frequencies at increments of Δf up and down the frequency scale, all of these voltages will be in phase or 180 deg out of phase. If the length of the pulse is short compared to $2/(n\Delta f)$, the amplitudes of different frequency voltages will be approximately the same and the phases the same. n is the number of elements in the array. The frequencies can then be separated by crystal filters. In practice, it was found desirable to generate and separate the frequency ensemble in the 20 kc/s band, and to step up the frequencies after separation, by heterodyning against a common oscillator in two steps. The 20-c/s frequency separation produced a corresponding sweep rate. This was rapid enough to observe the propagational variations with time. It was also sufficiently slow to observe pulse transmission without gaps in the sector coverage.

3. Details of Construction

The design for the five-element Yagi antenna had been worked out in detail a number of years previously for another application. Its gain was measured to be 11.3 db relative to an isotropic radiator. The approximate half-power width of the main lobe was measured to be 50 deg. Within the sector of interest, 21°-0°-21°, the gain varied within ±1 db of the mean. The secondary lobe level was below −24 db. Each Yagi was matched to have a coaxial terminal impedance of 50.0 ohms.

The Yagi antennas were separated by 33.65 ft (1.4 wavelengths). From earlier measurements, it is known that, at this separation, the effect of one of these antennas on the radiation pattern of the adjacent one is negligible.

For communication over a 1295 km path via ionospheric scatter mode, the optimum angle of departure is computed to be approximately 6.7 deg and the height of the antenna, 2.15 wavelengths (approximately 52 ft). All of the antennas were connected to the equipment by equal lengths of RG–9B/U coaxial cable. It was contemplated that the antenna would be adjusted to have a Dolph-Chebyshev current distribution for a −20-db side-lobe level. On that basis, the beamwidth of the array was computed to be 5.84 deg.

Figure 3 presents the computed radiation pattern of the array. The curve in dashed line is the radiation pattern of the single Yagi antenna. In computing this pattern, the antennas were assumed to be in phase; this produced the main lobe in the straight-ahead position. Other main lobes are at the 45°, 135°, and 180° positions.

The frequency of 10.70 Mc/s was selected for IF amplification; therefore, for 40.92-Mc/s reception, the local oscillator frequencies had to be centered on 30.22 Mc/s. With the present state of filtering techniques, it would be difficult to separate component voltages spaced 20 c/s apart at this frequency. To avoid lengthy experimentation, the frequency of 18 kc/s was selected as being the highest at which ready separation of frequencies could be carried out.

Figure 4 presents a block diagram of the electronic circuitry involved in the production of beam scan. An 18-kc/s crystal-controlled oscillator is pulsed at a rate of $\Delta f=20$ pps. The length of the pulse is 4 msec; a short pulse is required in order that the amplitudes of the required sidebands remain in phase and reasonably constant. The output of the pulsed oscillator contains frequencies of 18 kc/s, 18 kc/s$+\Delta f$, 18 kc/s$+2\Delta f$, . . . 18 kc/s$-\Delta f$, 18 kc/s$-2\Delta f$, . . . etc. The output is connected to seven filters in parallel, each adjusted to one of the desired frequencies. The passband of each crystal filter is essentially flat for 6 cycles, centered at the individual crystal filter design frequency. The rejection of the unwanted sidebands by each crystal filter is at least 30 db. Each selected frequency, 18 kc/s$+r\Delta f$, is stepped up by beating against a 2-Mc/s oscillator to 1.982 Mc/s$-r\Delta f$. This frequency, in turn, is filtered from 2 Mc/s and 2.018 Mc/s$+r\Delta f$ frequencies.

The 1.982 Mc/s$-r\Delta f$ frequency is again stepped up to 30.22 Mc/s$-r\Delta f$ by heterodyning with a 28.238 Mc/s oscillator, and separated from 28.238 Mc/s and

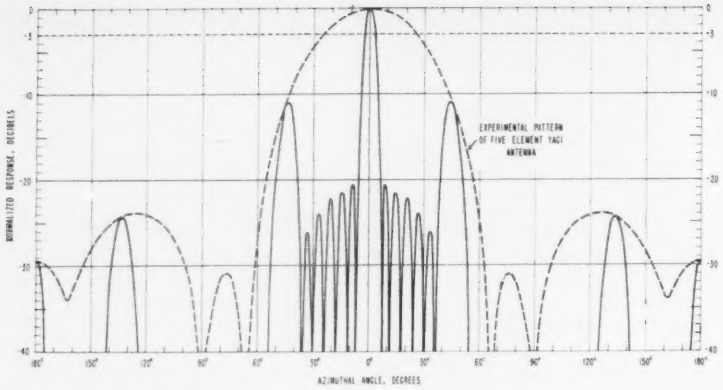

FIGURE 3. *Computed radiation pattern in E-plane of an array of 7 Yagi antennas.*
Currents adjusted to Dolph-Chebyshev distribution for -20-db side-lobe level.

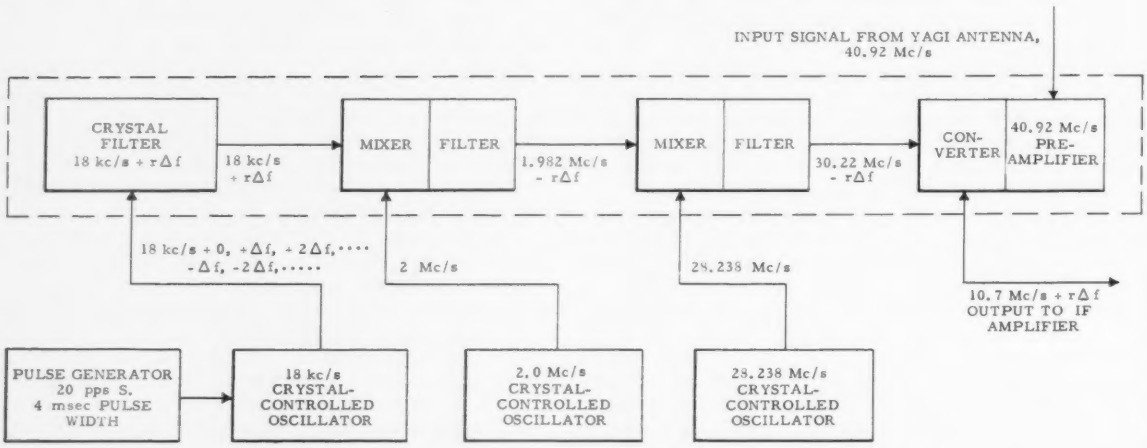
INPUT SIGNAL FROM YAGI ANTENNA, 40.92 Mc/s
CRYSTAL FILTER 18 kc/s + rΔf
18 kc/s + rΔf
MIXER
FILTER
1.982 Mc/s - rΔf
MIXER
FILTER
30.22 Mc/s - rΔf
CON-VERTER
40.92 Mc/s PRE-AMPLIFIER
18 kc/s + 0, +Δf, + 2Δf, ···· -Δf, -2Δf, ·····
2 Mc/s
28.238 Mc/s
10.7 Mc/s + rΔf OUTPUT TO IF AMPLIFIER
PULSE GENERATOR 20 pps S. 4 msec PULSE WIDTH
18 kc/s CRYSTAL-CONTROLLED OSCILLATOR
2.0 Mc/s CRYSTAL-CONTROLLED OSCILLATOR
28.238 Mc/s CRYSTAL-CONTROLLED OSCILLATOR

FIGURE 4. *Block diagram of one filter-mixer and preamplifier-converter channel*

26.256 Mc/s+$r\Delta f$ frequencies by filtering. From there it is connected to its appropriate, rth, converter. The seven crystal filters for the 18-kc/s frequency ensemble are the only critically adjusted items of the circuitry. Other filters and components are readily interchangeable with components of other channels because frequency separation is reasonable. In order not to introduce phase differences, care was exercised in adjusting antennas to have identical characteristics, to cut all transmission lines to be equal in length, and to construct all equipment pertaining to the seven channels to be as nearly identical electrically as possible. This avoided gross differences in phases or amplitudes. Provisions were incorporated in the frequency-generating circuits for compensating for small unavoidable discrepancies in phase. Provisions were also incorporated for adjustments in amplitude over a range of several decibels. This was to provide for tapering the current distribution of the array. Figure 5 shows a view of the equipment mounted in the rack.

4. Adjustment of the Antenna

Before the antenna was placed in operation, it was expected that difficulties would be encountered with unequal phase and amplitude variations in the seven channels. It was also felt that the adjustments of the electronic equipment could not be expected to remain sufficiently stable for very long periods of time. Practical experience with the equipment, however, dispelled these apprehensions. Phase and amplitude differences were small and easily compensated for; the stability was such that adjustments remained satisfactory from one day to another, even after equipment shutdown. The process of adjust-

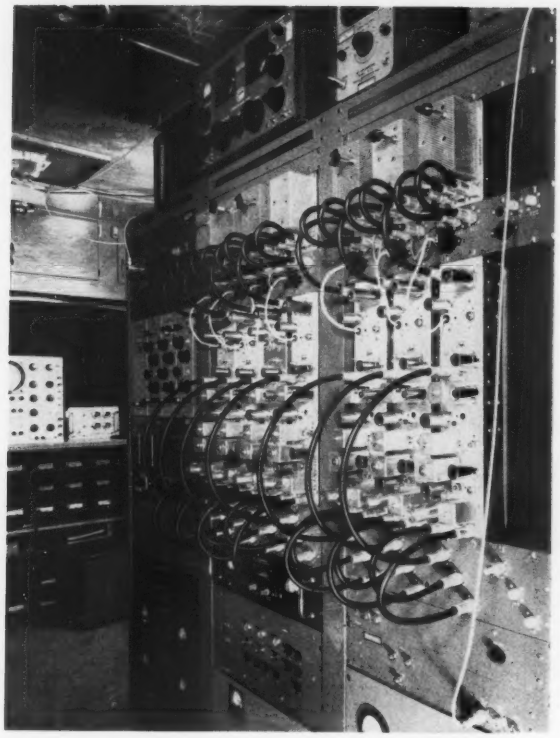

FIGURE 5. *A view of the electronic equipment for production of rapid scan.*

ment itself proved to be easier than with a non-scanning array because the effect of each adjustment was visible immediately on the oscilloscope display.

After some experimentation, a procedure for adjustment was evolved. The phases and amplitudes of each channel were adjusted, one at a time, with reference to the center element as follows: A precision coaxial attenuator with insertion loss equal to the level of the rth element for Dolph-Chebyshev distribution is inserted in the coaxial line leading to the 0th (center) element. The rth element is connected through its circuitry with an insertion of 180-deg delay (half-wavelength coaxial line). The outputs of the 0th and rth converters are then combined in the IF amplifier and displayed on the oscilloscope. The amplitude of the rth element is adjusted to obtain a null (or a series of nulls, depending on the value of r). The phase is adjusted to move the null into the center of the display. This is the complete adjustment routine for one, rth, element. After all elements are adjusted, they are connected together through their respective converters to the IF amplifier. It is desirable to check the pattern by a distant target transmitter. Minor adjustment can then be made to improve the secondary lobe level. A mobile target transmitter was also found to provide a convincing demonstration that the equipment really operated as intended.

In lieu of a distant target transmitter a signal generator can be, and has been, employed. The antennas are disconnected. Each pre-amplifier is then connected through an individual, 20-db, precision, coaxial attenuator to the signal generator. The distant target transmitter is thus simulated in the zero-degree position. If the combined input impedance of the seven circuits in parallel is matched back to the 50-ohm value, a means of quantitative calibration is provided. The equipment described is provided with solenoidally operated switches to provide means for rapid check and calibration.

5. Results

Since the output of the antenna is cyclic with a 20 c/s repetition rate, it lends itself readily to oscilloscope presentation. The horizontal sweep is triggered by the pulse, and the output of the receiver is connected to the vertical deflection plates. The display shows the signal amplitude as ordinate, with the direction of arrival as azimuth. Since a distant VHF signal arriving by ionospheric scatter mode is distributed in the direction of arrival, the display pattern is a convolution of the antenna radiation pattern and the true signal or signal pattern distribution. The phenomenon is familiar in radio astronomy and has been discussed at length by

Bracewell and Roberts [3]. When the signal arrives from a point source, as from a target transmitter, the display shows the true radiation pattern with the response maximum in the direction of the signal source. Figure 6 presents three displays recorded while a local target transmitter, mounted on a vehicle, moved in front of the antenna from left to right. It is useful for demonstrating the proper functioning of the system.

Since this system was put in operation, 2 months ago, a variety of propagational phenomena have been observed on the frequencies of 40.88 and 40.92 Mc/s. During the greater proportion of the time, the observed signal arrives by a regular ionospheric scatter mode. Occasionally, strong meteor-trail reflections have been observed and recorded. These exceed the scattered signal by several orders in magnitude, but last only a second or two at a time. Signals propagated by sporadic-*E* layer have also been observed. These are very steady, high in amplitude, and usually arrive along the great-circle path. Figures 7 through 10 illustrate the phenomena as observed using this antenna system. It should be noted that the recording camera was not synchronized with the sweep of the oscilloscope. In order to get at least one complete sweep, the shutter speed was set at 0.1 sec. Therefore, most records show two almost complete scans. These are not believed to be objectionable; in fact, they convey the transient nature of the phenomena. The interval between sweeps is 50 msec.

Figure 7 presents photographic records illustrating propagation by ionospheric scatter. While the maximum signal is generally at, or close to, the great-circle path (0-deg azimuth), it fluctuates, both in amplitude and in direction. Occasionally, it deviates by more than 10 deg. from the great-circle path. The convolution of the radiation and the signal patterns is noticeably broader than the radiation pattern by itself. This is clear evidence that the signal pattern is dispersed. A higher resolution antenna is highly desirable for more detailed examination of the fine structure of the signal.

Figure 8 is a record of several meteors. Although some are observed at zero azimuth, most are to one side or the other of the great-circle path. Because the duration of the meteor is very brief, it is not possible to adjust the sensitivity of the receivers to obtain a good full-scale deflection. Experiments are underway to adopt magnetic tape recording techniques for this application. The display pattern is very close to the radiation pattern of the antenna, indicating that the signal comes from a source which is virtually a point.

Figure 9 shows a record observed while sporadic *E*-layer propagation was taking place. The display pattern appears to be identical to the radiation pattern. This is to be expected from a specular reflection by a smooth surface. The signal is likely to remain steady for a considerable length of time and is usually along the great-circle path.

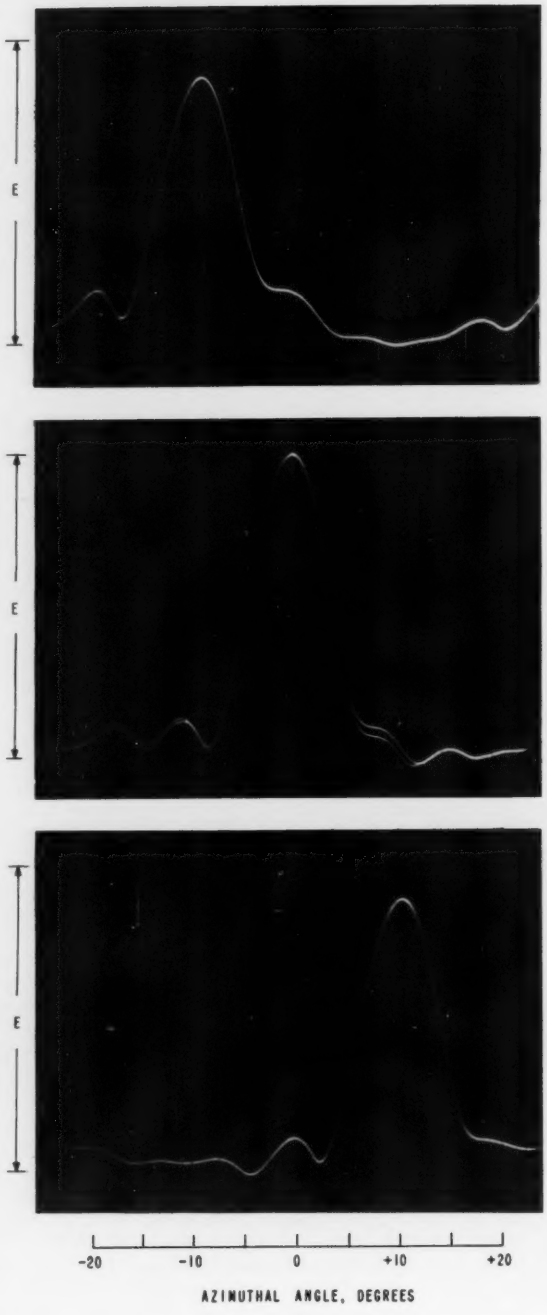

FIGURE 6. *Display of responses obtained with a target transmitter in far zone moving from left to right.*

The response to a point source of radiation is the radiation pattern of the antenna.

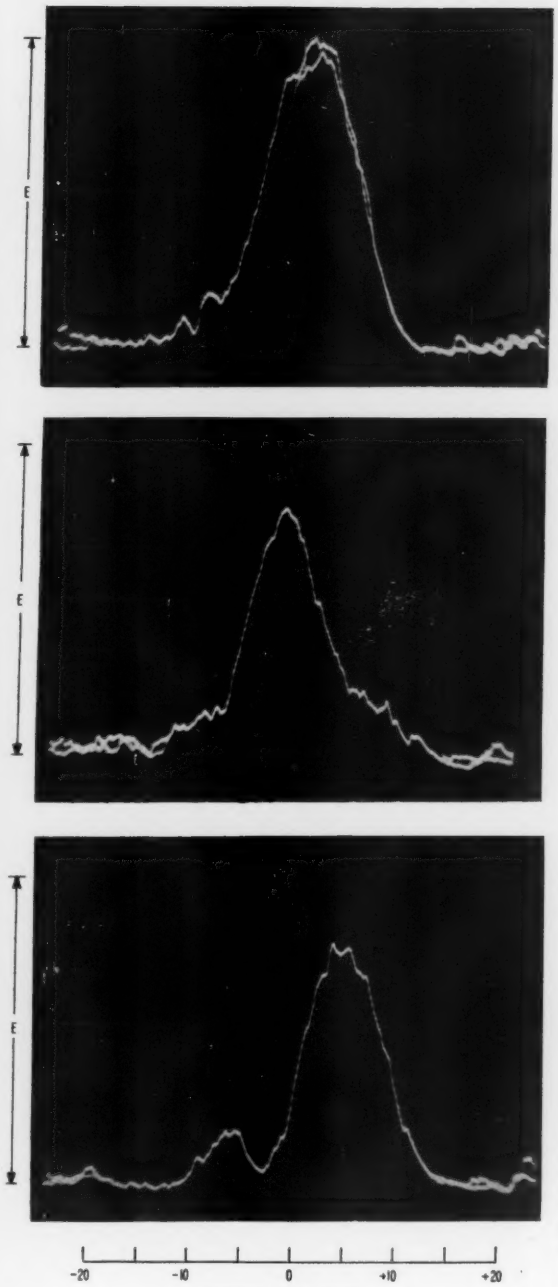

FIGURE 7. *Display of responses with signal arriving via normal ionospheric scatter mode.*

The response is a convolution of the antenna radiation pattern and the angular distribution of the signal components.

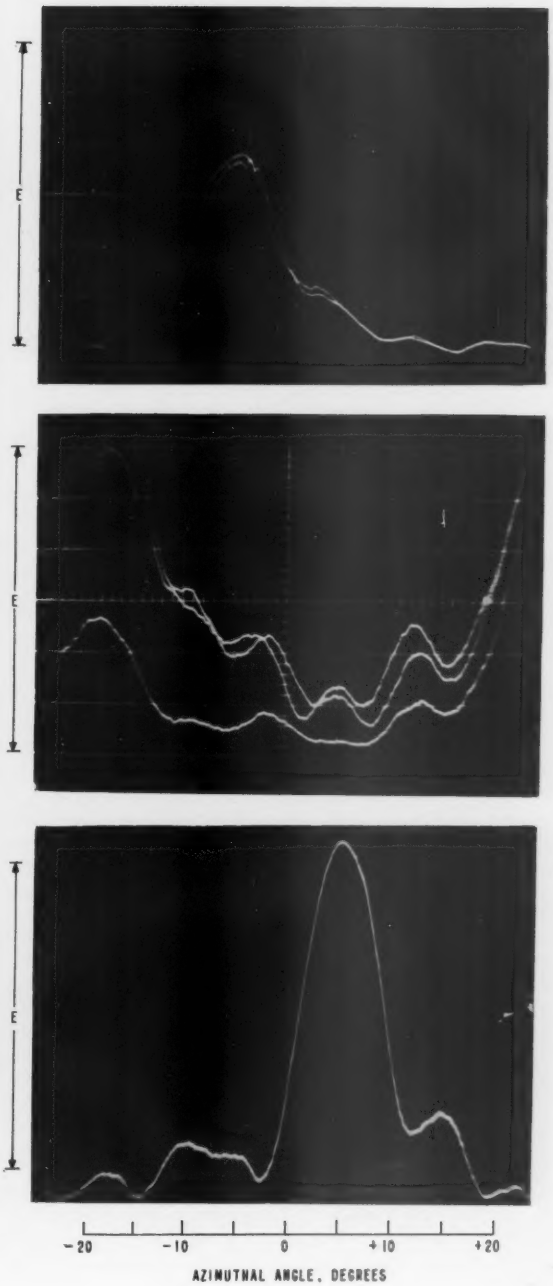

FIGURE 8. *Display of responses with signal arriving via meteor trail reflection.*

The propagation mode identifiable by enhanced signal strength, duration of the order of a second, and off-great-circle direction of arrival.
The similarity between the response pattern and the antenna radiation pattern indicates that the reflection is a point source.

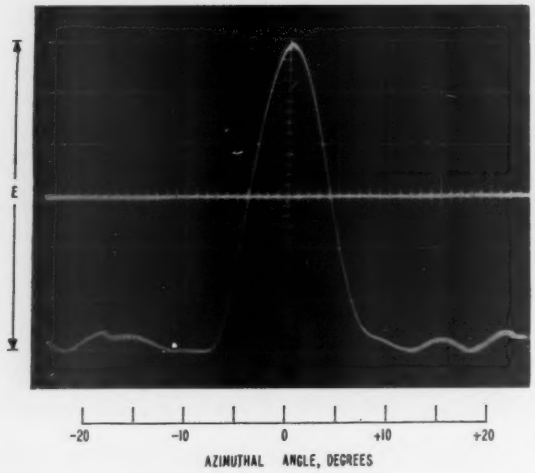

FIGURE 9. *Display of responses with signal arriving via sporadic-E layer reflection.*

The sensitivity of the system is greatly reduced relative to that used with scatter reception (of the order of 90 db).
Besides high intensity, this mode is characterized by great-circle path direction of arrival and stability over a period of an hour or greater.

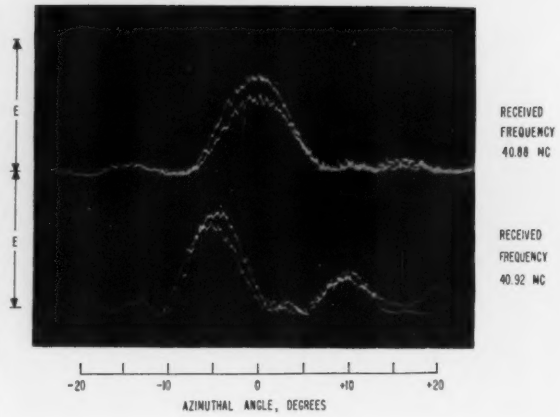

FIGURE 10. *Display of simultaneous responses to signal at 40.88 and 40.92 Mc /s.*

In addition to frequency difference, the 40.88-Mc/s transmission was characterized by narrow (5-deg) beamwidth. 40.92-Mc/s transmission used 50-deg-wide antenna beam; 10-db difference in transmitted power maintained intensity of illumination at approximately equal level.

Simultaneously with the 20-kw signal at 40.92 Mc/s, used for the above experiments, there was a 2-kw transmission at 40.88 Mc/s. Both originated at Long Branch, Ill. The 40.92 Mc/s signal was radiated by a corner-reflector antenna with a half-power beamwidth of approximately 50 deg. The 40.88 Mc/s signal was radiated by a rhombic antenna with a beamwidth of about 5 deg. Because the area of the ionosphere illuminated by one was so much greater than that illuminated by the other, it was considered desirable to compare signals received simultaneously on two frequencies. Two IF receivers tuned to10.70 and 10.66 Mc/s were connected to the output of the antenna system at the same time. The outputs of the two receivers were connected to sections A and B of a dual-trace oscilloscope. Figure 10 illustrates the comparison between the two signals. While the study of propagational phenomena is beyond the scope of this paper, the application illustrates the versatility of the scanning principle. The principal limit on bandwidth of operation was, in this case, presented by the Yagi antennas comprising the antenna system.

In the earlier discussion of the principles of the scan, it was mentioned that measurements using pulse transmissions were contemplated. In 1958 and 1959, Carpenter and Ochs [1], using pulsed 40.92 Mc/s transmissions, with 3-μsec pulse, at 250 pps and 700 kw peak power, measured relative delay time for meteor reflections. Delays of over 1 msec relative to the normal scatter signal were observed. By recording the distribution, they were able to deduce the direction of arrival of reflected signals. The equipment employed by Carpenter and Ochs has been, to a large extent, incorporated in this project. It is planned to modify the display so as to present the direction of arrival as azimuth (as it is now) but to show the relative delay in microseconds as ordinate and with intensity modulation amplitude. The display is similar to that familiar in television. Figure 11 shows the raster

FIGURE 11. *Scan "Raster" for reception of pulses.*

Two-millisecond scan corresponds to pulsing period (500 pps).

form of the display. It should be noted that the line separation is 2 deg; this illustrates the discussion of the interrelations of minimum beamwidth and the maximum scanning rate earlier in this paper. Figure 12 presents a record of a signal arriving by a

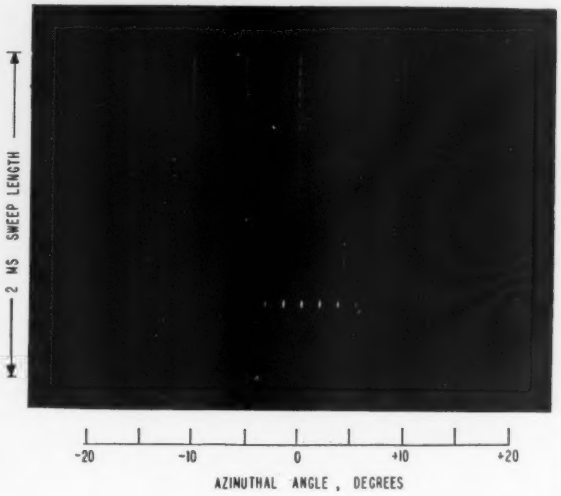

FIGURE 12. *Display of response to pulse transmission using intensity modulation of oscilloscope and vertical sweep sychronized with pulsing rate.*

sporadic-*E* mode. Because of lack of power in the pulse transmitter, reception of regular ionospheric scatter has been unsatisfactory.

Work is under way to overhaul the transmitter for high-power pulse transmission. Work is also under way to increase the size of the array to 25 elements. This would permit a beamwidth of 1.5 deg with the present 20-db side-lobe level. A more detailed study of propagation phenomena can then be possible.

6. Applications

The significant characteristic of this antenna is the ease of obtaining very rapid rates of scan. The 20 c/s rate was the slowest which was deemed readily realizable, without experimentation. As the scan rate is increased, the problem of separating the spectral frequencies of the pulse becomes easier. Scanning rates in the order of kilocycles, and even megacycles, appear realizable.

The availability of very rapid scanning rates opens up an opportunity for use of sampling technique for both measurement and communication. If the period of scan is shorter than the Nyquist interval for the message received, the information is fully preserved, even though the antenna is directed at the source only a fraction of the time. By proper gating, the information arriving from different sources can be directed into appropriate channels. The technique is analagous to that familiar in other applications.

The antenna described in this paper scans in a single dimension. With a minor modification, the principle is equally applicable to a two-dimensional scan. Figure 13 illustrates this application. A

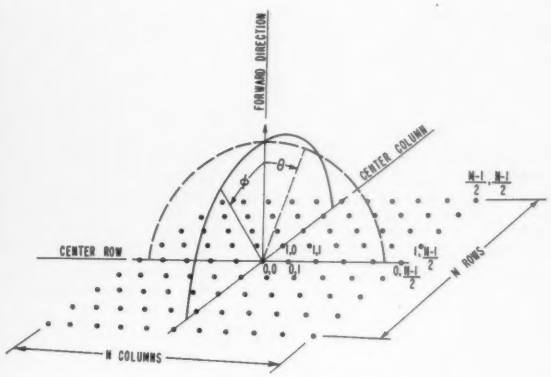

FIGURE 13. *Application of electronic sweep to scanning in two dimensions.*

rectangular array of $m \times n$ elements is shown. These are arranged in m rows and n columns, $n[(m-1)/2]$ elements to each side of the center row, and $m[(n-1)/2]$ elements to each side of the center column. The elements may be identified by their position in the array, by row and column.

The center element (0,0) is connected to a converter with a heterodyne frequency f_0. The array can then be scanned in the θ-plane at a scanning rate Δf if each converter receives its proper heterodyne voltage frequencies. For element (r,q), it should be $f_{rq}=f_0 \pm q\Delta f$. To obtain scan in the ϕ-plane, at a scanning rate δf, the heterodyne voltage frequency for the same element should be $f_{rq}=f_0 \pm r\delta f$. To scan in both planes simultaneously, $f_{rq}=f_0 \pm r\delta f \pm q\Delta f$. The scanning operation itself would be analogous to the scan in the television picture. The ratio $\Delta f/\delta f$ would determine the number of "lines" in the scan. It should be equal to, or greater than, the ratio of $\Phi/W\phi$ where Φ is the width of the sector scanned in the ϕ-plane and W_ϕ is the half-power beamwidth in that plane. Since W_ϕ varies roughly inversely as the aperture, $(m-1)d$, the ratio $\Delta f/\delta f$ should equal approximately the number of rows, m.

A special case of interest above is a possible application of Mills' cross array. In this application, the rectangular array reduces to the central row and the central column with a common center element (0,0). The multiplicative process essential to the operation of Mills' cross can be added in addition to the scanning. A complete picture of a phenomenon varying with time over an area can then be obtained instantaneously. This might be of interest, for example, in radio astronomy in the study of solar eruptions.

All of the above applications are from the standpoint of receiving antennas. The principle is applicable to transmission, but the techniques have to be modified considerably.

7. Conclusions

The 2 months of operation of this antenna system provide adequate evidence of the practical value of the scanning principle described here. In the particular application detailed here, it provided a visual view of rapid variations in amplitude and direction of arrival with time. The information value of such a display is considerably greater than that of single-dimensional variation of amplitude with time.

The stability of the system with time, temperature changes, etc., appears to be satisfactory. It should be noted that, in many respects, the equipment as it is at present may be termed "breadboard." With some refinements, a very high order of dependability should be realizable. The adjustment of the array is actually much easier than that of a conventional array without scan. Since the pattern can be displayed on an oscilloscope, the effect of changing individual adjustment controls is instantly visible. The process of adjustment, therefore, becomes greatly expedited.

The 5.8 deg beamwidth of the seven-element, 8.4 wavelength-wide array is barely adequate to demonstrate the possibilities of the system. Reduction in beamwidth is, however, a matter of adding to the array. Work is under way to increase the number of elements to 25, and the overall array width to 33.6 wavelengths. The beamwidth of the main lobe can then be reduced to 1.5 deg with 20-db side-lobe level.

The generation of a phase-locked ensemble of frequencies for heterodyne use may be accomplished in a number of ways other than that described here. Phase-lock oscillators can be employed. A single oscillator at a frequency Δf may be used to generate harmonics which can be amplified and stepped up in frequency by beating against a common oscillator.

Application to two-dimensional scan appears to be straightforward but, of course, remains to be tried.

8. References

[1] Carpenter, R. J. and Ochs, G. R., High resolution pulse measurements of oblique radio reflections from meteor trails at 41 Mc/s. (A paper delivered at URSI–IRE meeting Oct. 20, 1959, San Diego, Calif.)

[2] Electronic Scanning Symposium, Apr. 29–May 1, 1958. USAF Cambridge Research Center, Bedford, Mass. AFCRL–TR–58–145 (I), ASTIA Document No. AD 152409.

[3] Bracewell, R. N. and Roberts, J. A., Aerial smoothing in radio stronomy. Australian J. Phys. **7**, No. 4, 615 (Dec. 1954).

(Paper 65D1–108)

Publications of the National Bureau of Standards*

Selected Abstracts

Amplitude and phase of the low- and very-low-radiofrequency ground wave, J. R. Johler, L. C. Walters, and C. M. Lilley, *NBS Tech. Note 60* (*PB161561*) (*1960*) *$0.75.*

Graphs and tables of the low- and very-low-radiofrequency ground wave are presented as a function of frequency, 100 c/s to 1000 kc.

On the excitation of electromagnetic surface waves on a curved surface, J. R. Wait, *IRE Trans. Ant. Prop.* **AP–8,** *446* (*1960*).

The excitation and propagation of surface waves on a spherical inductive boundary is considered. The source is taken to be a vertical electric dipole. The circumferential attenuation rate of the various modes are discussed where it is indicated that the dominant mode is very similar to the trapped surface wave for a plane inductive boundary. The results appear to conflict with those of Barlow, but are in sympathy with some numerical data of Elliott for the circumferential attenuation rate of the dominant mode.

Carrier-frequency dependence of the basic transmission loss in tropospheric forward scatter propagation, K. A. Norton, *J. Geophys. Research* **65,** *2029* (*1960*).

A further interpretation is given of certain Lincoln Laboratory data obtained in an experiment using scaled antennas as published by Bolgiano [1959]. This paper has three objectives: (1) to consider the significance of these data as regards the theory of radio propagation through a turbulent atmosphere; (2) to describe a suitable method for the measurement of the meteorological parameters entering the theory; (3) to apply a further statistical analysis to these data. On the basis of this analysis of the Lincoln Laboratory data, it is concluded (1) that the

$$\{2/\Gamma(\mu)\}(\rho/2)^{\mu}K_{\mu}(\rho)$$

correlation model provides a description of tropospheric turbulence adequate for the description of these data with μ assigned the fixed value 1, and (2) that the variation of the carrier-frequency dependence of the basic transmission loss from hour to hour arises simply from a lack of correlation in the hourly median losses on widely separated carrier frequencies rather than from changes of μ in this correlation model.

The use of geostationary satellites for the study of ionospheric electron content and ionospheric radio-wave propagation, O. K. Garriott and C. G. Little, *J. Geophys. Research* **65,** *2025* (*1960*).

This paper describes a proposed radio propagation experiment utilizing a geostationary satellite. The experimental methods for determining the total electron content of the ionosphere are discussed, and the advantages and capabilities of the methods are summarized. Other possible studies utilizing the satellite transmissions are also outlined.

Photochemical rates in the equatorial F_2 region from the 1958 eclipse, T. E. Van Zandt, R. B. Norton, and G. H. Stonehocker, *J. Geophys. Research* **65,** *2003* (*1960*).

The F_2-region electron-density data from the eclipse on October 12, 1958, at Danger Islands has been analyzed with a new method. It is shown that (1) temperature changes and transport of electrons were probably negligible during the eclipse, and (2) the rate of photoionization $q(h)$ and the linear recombination coefficient ('attachment coefficient') $\beta(h)$ can be approximated between 290 km and 400 km by

$$q(h)=880\exp[-(h-300)/186]\text{ electrons cm}^{-3}\text{sec}^{-1}$$

$$\beta(h)=6.8\times10^{-4}\exp[-(h-300)/103]\text{ sec}^{-1}$$

where the height h is measured in kilometers. The rate of formation of ion pairs between 290 and 400 km is $(.76)10^{10}$ ion pairs/cm² sec, or about (0.25) ergs/cm² sec. This implies a total rate of energy absorption in the F region of at least 2 ergs/cm² sec.

On the theory of the slow-tail portion of atmospheric waveforms, J. R. Wait, *J. Geophys. Research* **65,** *1939* (*1960*).

The propagation of the slow-tail portion of atmospherics is considered from the waveguide-mode viewpoint. The source, which is a lightning discharge, is represented by a vertical dipole. The transient response of the distant electric field is then computed for various forms of the source current waveform. The results are then employed to reinterpret the experimental data of Hepburn. As suggested by the present theory it is found that the observed separation t_s between the oscillatory head of the atmospheric and the maximum of the slow-tail amplitude varies with distance ρ to the source according to a law of the form

$$(t_s)^{1/2}=A+B\rho.$$

The constant A is related to the pulse width of the source, and the constant B depends on ionospheric parameters. Values of effective ionospheric conductivities deduced from the theory are consistent with earlier results for the VLF band. The influence of nonvertical currents in the discharge channel is also briefly discussed.

VLF attenuation for east-west and west-east daytime propagation using atmospherics, W. L. Taylor, *J. Geophys. Research* **65,** *1933* (*1960*).

Daytime attenuation characteristics have been computed by comparing the amplitude spectra of atmospheric waveforms recorded at four widely separated stations. The results of these attenuation measurements are presented for the band of frequencies from 3 to 30 kc/s and involving distances of 1000 to 10,000 km. Nonreciprocity is evident from this study. Attenuation rates over sea water for east-to-west propagation were about 3 db/1000 km greater for frequencies below 8 kc/s, and about 1 db/1000 km greater for frequencies above 10 kc/s, than for west-to-east propagation. East-to-west attenuation rates over land were about 1 db/1000 greater than for over sea water.

Influence of earth curvature and the terrestrial magnetic field on VLF propagation, J. R. Wait and K. Spies, *J. Geophys. Research* **65,** *2325* (*1960*).

An account is given of some recent work on the mode theory of VLF ionospheric propagation. Attention is confined to the behavior of the attenuation coefficient of the dominant mode. The ionosphere is assumed to be a sharply bounded and homogeneous ionized medium. It is indicated that earth curvature increases the attenuation rate by as much as a factor of 2 as compared with the corresponding attenuation for a flat earth. The influence of the earth's magnetic field is also shown to be important. In fact, east-to-west propagation paths suffer much greater attenuation than west-to-east paths. The theoretical results in the present paper appear to agree well with the experimental data of W. L. Taylor.

Rapid frequency analysis of fading radio signals, J. M. Watts and K. Davies, *J. Geophys. Research* **65,** *2295* (*1960*).

Examples of frequency analysis of fading radio signals for long periods of time are demonstrated, and the method of obtaining them is explained. They include both regular HF propagation and VHF ionospheric forward-scatter samples. The procedure is also useful for the analysis of other natural phenomena having long time scales and slow variations.

A study of 2-Mc/s ionospheric absorption measurements at high latitudes, K. Davies, *J. Geophys. Research* **65**, *2285 (1960).*

Ionospheric absorption (L) at high latitudes is studied using the published data on 2.0 Mc/s at five Canadian stations during 1957 and 1958. The seasonal and diurnal variations are considered, and it is found that a pronounced winter anomaly in noon absorption occurs at Churchill but not at Resolute Bay. The diurnal variations indicate that the dependence of absorption on solar zenith angle decreases with increase of latitude. The distribution of midnight absorption with latitude shows that, although the maximum occurs in the auroral zone, high absorption is also encountered over the polar cap. A study of the duration of long-lasting blackouts shows that in summer the duration is longer as the latitude increases.

On the excitation of electromagnetic surface waves on a curved surface, J. R. Wait, *IRE Trans. Ant. Prop.* **AP-8**, *445 (1960).*

The excitation and propagation of surface waves on a spherical inductive boundary are considered. The source is taken to be a vertical electric dipole. The circumferential attenuation rates of the various modes are discussed where it is indicated that the dominant mode is very similar to the trapped surface wave for a plane inductive boundary. The results appear to conflict with those of Barlow, but are in sympathy with some numerical data of Elliott for the circumferential attenuation rate of the dominant mode.

Diffractive corrections to the geometrical optics of low frequency propagation, J. R. Wait, *Electromagnetic Wave Propagation (International Conference Sponsored by the Postal and Telecommunications Group of the Brussels Universal Exhibition), edited by M. Desirant and J. L. Michiels, p. 87–101 (Academic Press, New York, N.Y., 1960).*

The radiation fields are computed for an axial slot on a cylinder whose surface is regularly corrugated. The mathematical idealization is a magnetic line source on a cylindrical surface whose boundary impedance is specified. Special attention is given to surfaces whose radii of curvature are large compared to the wave-length.

Radiation from a slot on a large corrugated cylinder, J. R. Wait and A. M. Conda, *Electromagnetic Wave Propagation (International Conference Sponsored by the Postal and Telecommunications Group of the Brussels Universal Exhibition), edited by M. Desirant and J. L. Michiels, p. 103–109 (Academic Press, New York, N.Y., 1960).*

The radiation fields are computed for an axial slot on a cylinder whose surface is regularly corrugated. The mathematical idealization is a magnetic line source on a cylindrical surface whose boundary impedance is specified. Special attention is given to surfaces whose radii of curvature are large compared to the wave-length.

Atmospheric bending of radio waves, B. R. Bean, *Electromagnetic Wave Propagation (International Conference Sponsored by the Postal and Telecommunications Group of the Brussels Universal Exhibition), edited by M. Desirant and J. L. Michiels, p. 163–181 (Academic Press, New York, N.Y., 1960).*

Meteorological data from many diverse climates and seasons indicate that the refractive index gradient over the first kilometer above the earth's surface is highly correlated with the surface value of the refractive index. Further, 60% of the bending of radio rays passing completely through the earth's atmosphere is accomplished in the first kilometer above the earth's surface. These observations have led to the development of several models of the height distribution of the refractive index that yield more realistic values of radio ray bending than the effective earth's radius approach and have the further advantage of being adjustable for any season or location for which standard surface weather observations are available.

Low and medium frequency radio propagation, K. A. Norton, *Electromagnetic Wave Propagation (International Conference Sponsored by the Postal and Telecommunications Group of the Brussels Universal Exhibition), edited by M. Desirant and J. L. Michiels, p. 375–444 (Academic Press, New York, N.Y., 1960).*

During recent years, extensive progress has been made in understanding the nature of ionospheric propagation in the frequency range from 30 to 1000 kc. In particular, Wait and Conda have developed suitable methods for determining the effect of the curvature of the earth on the illumination of the ionosphere by antennas radiating at angles near and below grazing incidence, Belrose has developed empirical formulas for ionospheric absorption in the range 70 to 250 kc, Watt has analyzed data which makes possible the extension of these formulas to still lower frequencies, and Bean has developed a radio standard tropospheric atmosphere which makes possible good estimates of the bending of the radio waves in propagation to and from the ionosphere. Making use of these results, together with earlier studies made by the author of the absorption of radio waves in the band 540 to 1600 kc and some new results on focusing by the curved surface of a rough ionosphere, predictions are made of the propagation loss expected in ionospheric propagation between short vertical electric dipoles for waves propagated by m reflections at the ionosphere. The predictions appear to be in general agreement with the available experimental data, although the paper clearly points up the desirability of more definitive studies of the influence of absorption and polarization, particularly as regards the larger distances which involve propagation by more than one ionospheric reflection. The methods in this paper indicate that the propagation loss increases only very slowly as the angle of departure approaches and goes well below grazing incidence with the earth; this provides an explanation for recent experimental data obtained with a pulse system as reported by Doherty which indicates very large intensities for one-hop sky waves on 100 kc both day and night at ranges up to 1800 miles.

On the computation of diffraction fields for grazing angles, J. R. Wait and A. M. Conda, *Electromagnetic Wave Propagation (International Conference Sponsored by the Postal and Telecommunications Group of the Brussels Universal Exhibition), edited by M. Desirant and J. L. Michiels, p. 661–670 (Academic Press, New York, N.Y., 1960).*

The diffraction of electromagnetic waves by a convex cylindrical surface is considered. Attention is confined primarily to the region near the light-shadow boundary. The complex-integral representation for the field is utilized to obtain a correction to the Kirchoff theory. Numerical results are presented which illustrate the influence of surface curvature and polarization on the diffraction pattern. Good agreement with the experimental results of Bachynski and Neugebauer is obtained.

The resonance excitation of a corrugated-cylinder antenna, J. R. Wait and A. M. Conda. *Inst. Elec. Engrs. Mono. 386E (June 1960).*

Radiation from an axial magnetic line or slot source on the surface of a corrugated cylinder is considered. It is indicated that the power radiated in a given mode for the structure depends critically on the surface reactance and the circumference of the cylinder. In fact, for certain values of these parameters, particular modes are strongly excited and contain most of the radiated power. Numerical results are presented for several interesting cases.
The analysis is extended to an elliptic cylinder whose surface also possesses an inductive reactance. In order to facilitate the solution it is necessary to assume a special azimuthal variation of the surface reactance. For the model as chosen, strong resonance characteristics are again obtained. This model may be adapted to study the problem of a corrugated panel on a flat metallic ground plane which is excited by a parallel slot source.

Other NBS Publications

Journal of Research, Vol. 64A, No. 6, November-December 1960. 70 cents.

The spectrum of singly ionized atomic iodine (I II). W. C. Martin and C. H. Corliss.
The third spestrum of gold (Au III). L. Iglesias.
Tolerances for layer thicknssses in dielectric multilayer coatings and interference filters. K. D. Mielenz.
Note on particle velocity in collisions between liquid drops and solids. O. G. Engel.
Resistance of white sapphire and hot-pressed alumina to collision with liquid drops. O. G. Engel.
Note on the thermal degradation of polytetrafluoroethylene as a first-order reaction. S. L. Madorsky and S. Straus.
Heat of formation of titanium trichloride. W. H. Johnson, A. A. Gilliland, and E. J. Prosen.
Heat of formation of decaborane. W. H. Johnson, M. V. Kilday, and E. J. Prosen.
Ultra low-conductivity water by electrophoretic ion exclusion. W. Haller and H. C. Duecker.
Spectrophotomeric determination of the ionization constant of dimethylpicric acid (2,4,6-trinitro-3,5-xylenol) in water at 25° C. M. M. Davis, M. Paabo, and R. A. Robinson.
Spestrophotometric determination of the ionization constant of 2,4,6-trinitro-*m*-cresol in water at 25° C. M. M. Davis and M. Paabo.
Method for the separation of titanium, zirconium, iron, and aluminum from one another and for their subsequent determination. T. J. Murphy, W. S. Clabaugh, and R. Gilchrist.

Journal of Research, Vol. 64B, No. 4, October-December 1960. 75 cents.

Magnetic polarizability of a short right circular conducting cylinder. T. T. Taylor.
Accuracy of Monte Carlo methods in computing finite Markov chains. N. W. Bazley and P. J. Davis.
Error bounds in the Rayleigh-Ritz approximation of eigenvectors. H. F. Weinberger.
Sequence transformations based on Tchebycheff approximations. J. R. Rice.
Numerical solution of the frequency equations for the flexural vibration of cylindrical rods. W. E. Tefft.

Journal of Research, Vol. 64C, No. 4, October-December 1960. 75 cents.

Error analysis of a standard microwave phase shifter. G. E. Schafer and R. W. Beatty.
A method of controlling the effect of resistance in the link circuit of the Thomson or Kelvin double bridge. D. Ramaley.
Automatic precise recording of temperature. G. S. Ross and H. D. Dixon.
Gimbal device to minimize the effects of off-center loading on balance pans. H. A. Bowman and L. B. Macurdy.
Response of microchemical balances to changes in relative humidity. H. E. Almer.
Chemical changes occurring during the weathering of two coating-grade asphalts. S. H. Greenfeld.
Characteristics of fifteen coating-grade asphalts. S. H. Greenfeld.

Stabilization of free radicals at low temperatures, edited by A. M. Bass and H. P. Broida. NBS Mono. 12 (1960) $1.50.
New description of thorium spectra, R. Zalubas. NBS Mono. 17 (1960) 65 cents.
Measurement of neutron flux and spectra for physical and biological applications. NBS Handb. 72 (1960) 35 cents.
Protection against radiations from sealed gamma sources. NBS Handb. 73 (1960) (Supersedes H54) 30 cents.
Standardization activities in the United States. A descriptive directory, S. F. Booth. NBS Misc. Publ. 230 (1960) (Supersedes M169) $1.75.
Hydraulic Research in the United States, 1960, H. K. Middleton. NBS Misc. Publ. 231 (1960) $1.00.
Alphabetical index to tables of chemical kinetics. Homogeneous reactions. Supplement 2 to NBS Circ. 510 (1960) 35 cents.
A survey and bibliography of recent research in the propagation of VLF radio waves, J. R. Wait. NBS Tech. Note 58 (PB161559) (1960) 75 cents.
Measurements and standards in plasma-physics and astrophysics at the National Bureau of Standards. NBS Tech. Note 59 (PB161560) (1960) $1.00.
Proceedings of the 1960 conference on the propagation of E.L.F. radio waves. NBS Tech. Note 61 (PB161562) (1960).
Single scattered neutrons from an isotropic point sourse, E. R. Mosburg, Jr., and W. M. Murphey. NBS Tech. Note 63 (PB161564) (1960) 50 cents.
An analysis of an absolute torsional pendulum viscometer, E. A. Kearsley, Trans. Soc. Rheology III, 69 (1959).
The black void reactor concept, C. O. Muehlhause, Nuclear Sci. and Engr. **7,** No. 6, 505 (1960).
Dewar system for low temperature experiments, C. T. Zahn, Rev. Sci. Instr. **31,** No. 3, 328 (1960).
Radio echoes from field-aligned ionization above the magnetic equator and their resemblance to auroral echoes, K. L. Bowles, R. Cohen, G. R. Ochs, and B. B. Balsley, Letter J. Geophys. Research **65,** 1853 (1960).
Measurement on the smoothness of paper, T. W. Lashof and M. Mandel, Tappi **43,** No. 5, 385 (1960).
Geomagnetic and solar data, J. V. Lincoln, J. Geophys. Research 65, 1639 (1960); J. Geophys. Research **65,** 1821 (1960).
The spark of originality, A. T. McPherson, The Chemist **37,** No. 7, 275 (1960).
Infrared emission spectra of gaseous B_2O_3 and B_2O_2, D. White, D. E. Mann, P. N. Walsh, and A. Sommer, J. Chem. Phys. **32,** No. 2, 481 (1960).
A demonstration of color perception with abridged color-projection systems, C. S. McCamy, Photographic Sci. and Engr. **4,** No. 3, 155 (1960).
Heat of formation of nitrogen trifluoride and the N–F bond energy, G. T. Armstrong, S. Marantz, and C. F. Coyle, Commun. to Editor, J. Am. Chem. Soc. **81,** 3798 (1959).
Elastic constants of synthetic single crystal corundum at room temperature, J. B. Wachtman, W. E. Tefft, D. G. Lam, R. P. Stinchfield, J. Am. Ceram. Soc. **43,** No. 6, 334 (1960).
A simple centering jig and goniometer for punching or drilling spheres for structural models, D. K. Smith, Am. Mineralogist **45,** No. 5–6, 273 (1960).
Propagation of electromagnetic pulses in a homogeneous conducting earth, J. R. Wait, Appl. Sci. Research **B8,** 213 (1960).
Shielded coaxial leads for low temperature electrical measurements, N. L. Brown and R. N. Barfield, Rev. Sci. Instr. **31,** No. 5, 517 (1960).
Rapid impact loading of textile yarns, J. C. Smith, Book "High Speed Testing", Vol. 1, p. 67 (Interscience Publ. Inc., New York, N.Y. 1960).
The absolute zenith intensity of [OI] 5577 at College, Alaska, F. E. Roach and M. H. Rees, J. Geophys. Research **65,** 1489 (1960).
Studies on sudden commencements of geomagnetic storms using IGY data from United States stations, S. Matsushita, J. Geophys. Research **65,** No. 5, 1423 (1960).
Photometric observations of the twilight glow [OI] 5577 and [OI] 6300, L. R. Megill, J. Atmospheric and Terrest. Phys. **17,** 276 (1960).
Microwave spectrum and internal rotation of ethyl cyanide, V. W. Laurie, J. Chem. Phys. **31,** No. 6, 1500 (1959).
A study of local geomagnetic influence on the [OI] 5577 nightglow emission at Fritz Peak, J. W. McCaully, F. E. Roach, and S. Matsushita, J. Geophys. Research **65,** No. 5, 1499 (1960).
Local standards laboratories, A. T. McPherson, Handbook of Electrical Measurements, 1960 Ed., p. 72 (1960).

Infrared emission spectrum of gaseous HBO_2, D. White, D. E. Mann, P. N. Walsh, and A. Sommer, J. Chem. Phys. **32,** No. 2, 488 (1960).

The Stokes flow problem for a class of axially symmetric bodies, L. E. Payne and W. H. Pell, J. Fluid Mech. **7,** Pt. 4, 529 (1960).

A further note on "sweepers," J. M. Watts, J. Atmospheric and Terrest. Phys. **18,** 81 (1960).

The incidence equation $AA^t=aA$, K. Goldberg, Am. Math. Mo. **67,** 367 (1960).

Analysis of two-factor classifications with respect to life tests, M. Zelen, Book "Contributions to Probability and Statistics," Paper 42, p. 508 (Stanford Univ. Press, Stanford, Calif., 1960).

Compressive properties of hard tooth tissues and some restorative materials, J. W. Stanford, K. V. Weigel, G. C. Paffenbarger, and W. T. Sweeney, J. Am. Dental Assoc. **60,** No. 6, 746 (1960).

OH emission in the earth's atmosphere, D. M. Gates and E. Jones, Proc. 2d Natl, Infrared Information Symp. **4,** 145 (1959).

Microwave spectrum of trans-crotononitrile, V. W. Laurie, J. Chem. Phys. **32,** No. 5, 1588 (1960).

Tropospheric fields and their long-term variability as reported by TASO, P. L. Rice, Proc. IRE **48,** 1021 (1960).

On the power of some rank-order two-sample tests, J. R. Rosenblatt. Book "Contributions to Probability and Statistics," Paper 32, p. 358 (Stanford Univ. Press, Stanford, Calif., 1960).

Disc distribution of flares associated with certain radio bursts, C. Warwick, Proc. Symp. Physical Processes in the Sun-Earth Environment, July 20–21, 1959 (Ottawa, Defence Research Telecommunications Establishment) DRTE Publ. No. 1025, 249 (1960).

Effect of tensile properties of reinforcement on the flexural characteristics of beams, R. G. Mathey and D. Watstein, J. Am. Concrete Inst. **31,** No. 12, 1253 (1960).

The ionization potential of fluorine, J. T. Herron and V. H. Dibeler, Jr., Chem. Phys. **32,** No. 6, 1885 (1960).

The intensity of [OI] 5577 in the subauroral region as a function of magnetic activity, F. E. Roach, J. Geophys. Research **65,** No. 5, 1495 (1960).

Valences of the elements in analytical procedures, J. I. Hoffman, Chem. Anal. **49,** No. 1, 30 (1960).

A comparative study of absolute zenith intensities of [OI] 5577, F. E. Roach, J. W. McCaulley, E. Marovich, and C. M. Purdy, J. Geophys. Research **65,** No. 5, 1503 (1960).

Clay mineral content of two domestic kaoline, W. C. Ormsby and J. M. Shartsis, J. Am. Ceram. Soc. **43,** No. 6, 335 (June 1960).

Some canons of sound experimentation, C. Eisenhart, Bull. Inst. Intern. Stat. **XXXVII,** No. 3, 339–350 (1960).

Thermodynamic properties of helium at low temperatures and high pressures, D. B. Mann and R. B. Stewart, Trans. Am. Soc. Mech. Engrs. J. Heat Transfer **81,** No. 4, 324–326 (November 1959).

Interpolation of platinum resistance thermometers, 20° to 273.15° K, R. J. Corruccini, Rev. Sci. Instr. **31,** No. 6, 637–640 (June 1960).

Low-temperature transport properties of commercial metals and alloys. IV. Reactor grade Be, Mo, and W, R. L. Powell, J. L. Harding, and E. F. Gibson, J. Appl. Phys. **31,** No. 7, 1221–1224 (July 1960).

A rating scale method for evaluating research positions, H. A. McKean, J. Mandel, and M. N. Steel, Personnel Admin. **23,** No. 4, 29–36 (July-Aug. 1960).

Post office mechanization, B. M. Levin, M. C. Stark, and P. C. Tosini, Proc. Information Processing and Retrieval, Am. Inst. Elec. Engrs. General Meeting, June 19–24, 1960, Atlantic City, New Jersey, Am. Inst. Elec. Engrs. Paper CP60–937 (1960).

Sensitive thermal conductivity gas analyzer, J. R. Purcell and R. N. Keeler, Rev. Sci. Instr. **31,** No. 3, 304–306 (March 1960).

A study of two water resistance testers for shoe upper leather, R. L. Hebert, J. Am. Leather Chemists Assoc. **LV,** No. 7, 388–405 (July 1960).

Transfer of liquid hydrogen through uninsulated lines, R. J. Richards, W. G. Steward, and R. B. Jacobs, Proc. 1959 Cryogenic Engr. Conf., Vol. 5, Advances in Cryogenic Engineering, p. 103 (Plenum Press, New York, N.Y., 1960).

Bounds on the dissipation of energy in steady flow of a viscous incompressible fluid around a body rotating within a finite region, E. A. Kearsley, Arch. Rational Mech. and Analysis **5,** No. 4, 347–354 (1960).

Cavity resonator dielectric measurements of rod samples, H. E. Bussey, Conf. Electrical Insulation (Annual Report of 1959), Natl. Acad. Sci., Natl. Research Council Publ. **756,** 15–20 (1960).

Analysis of fractionally replicated 2^m3^n designs, R. C. Bose and W. S. Connor, Bull. Inst. Intern. Stat. **XXXVII,** No. 3, 141–160 (1960).

Influence of source distance on the impedance characteristic of ELF radio waves, J. R. Wait, Proc. IRE Letter to Editor **48,** 1338 (1960).

**Publications for which a price is indicated (except for Technical Notes) are available only from the Superintendent of Documents, U.S. Government Printing Office, Washington 25, D.C. (foreign postage, one-fourth additional). The Technical News Bulletin and Basic Radio Propagation Predictions are available on a 1-, 2-, or 3-year subscription basis, although no reduction in rates can be made. Reprints from outside journals and the NBS Journal of Research may often be obtained directly from the authors.*

U.S. GOVERNMENT PRINTING OFFICE: 1960

Notice

The papers listed below will appear in early issues of RADIO PROPAGATION, Section D of the JOURNAL OF RESEARCH of the National Bureau of Standards:

Initial results of a new technique for investigating sferic activity. Gifford Hefley, Robert H. Doherty, and Robert F. Linfield.

Fresnel region fields of circular aperture antennas. Ming-Kuei Hu.

Free-balloon borne meteorological refractometer. John F. Theisen and Earl E. Gossard.

Effect of antenna radiation angles upon HF radio signals propagated over long distances. W. F. Utlaut.

Relationship between red auroral arcs and ionospheric recombination. G. A. M. King and F. E. Roach.

Graphical determination of radio ray bending in an exponential atmosphere. C. F. Pappas, L. E. Vogler, and P. L. Rice.

Weather and reception level on a troposphere link—annual and short-term correlations. L. G. Abraham, Jr. and J. A. Bradshaw.

A formula for radio ray refraction in an exponential atmosphere. G. D. Thayer.

The impedance of a monopole antenna with a circular conducting-disk ground system on the surface of a lossy half-space. S. W. Maley and R. J. King.

Ionospheric motions observed with high-frequency backscatter sounders. Lowell H. Tveten.

Radio-wave propagation in the earth's crust. Harold A. Wheeler.

ANNOUNCEMENT

of

CRPL Summer Courses on

RADIO PROPAGATION

Two courses will be given: a two-week course on *Ionospheric Propagation,* and a one-week course on *Tropospheric Propagation.* Emphasis will be on the fundamental characteristics of propagation and their application to telecommunications.

Details, including fees, will be covered in a subsequent announcement.

Place: NBS, Boulder Laboratories
Tentative Dates: July 31 to August 18, 1961

UNITED STATES
GOVERNMENT PRINTING OFFICE
DIVISION OF PUBLIC DOCUMENTS
WASHINGTON 25, D.C.

OFFICIAL BUSINESS

PENALTY FOR PRIVATE USE TO AVOID
PAYMENT OF POSTAGE, $300
(GPO)

JOURNAL OF RESEARCH of the National Bureau of Standards Vol. 65D, No. 1 January–February 1961
D. Radio Propagation

Contents

	Page
Incoherent scattering by free electrons as a technique for studying the ionosphere and exosphere: some observations and theoretical considerations. Kenneth L. Bowles.	1
Radio wave absorption of several gases in the 100 to 117 kMc/s frequency range. C. O. Britt, C. W. Tolbert, and A. W. Straiton.	15
On the theory of diffraction by a composite cylinder. Ralph D. Kodis.	19
An atlas of oblique-incidence ionograms (a digest). Vaughn Agy, Kenneth Davies, and Roger Salaman.	35
A new approach to the mode theory of VLF propagation. James R. Wait.	37
East-west effect on VLF mode transmission across the earth's magnetic field. D. Dobrott and A. Ishimaru.	47
Magneto-ionic propagation phenomena in low- and very-low-radiofrequency waves reflected by the ionosphere. J. Ralph Johler.	53
Correlation of monthly median transmission loss and refractive index profile characteristics. B. R. Bean and B. A. Cahoon.	67
Characteristics of waveguides for long-distance transmission. A. E. Karbowiak and L. Solymar.	75
Useful radiation from an underground antenna. Harold A. Wheeler.	89
Observation of *F*-layer and sporadic-*E* scatter at VHF in the Far East. K. Miya, T. Sasaki, and M. Ishikawa.	93
A high-resolution rapid-scan antenna. H. V. Cottony and A. C. Wilson.	101
Publications of the National Bureau of Standards.	111
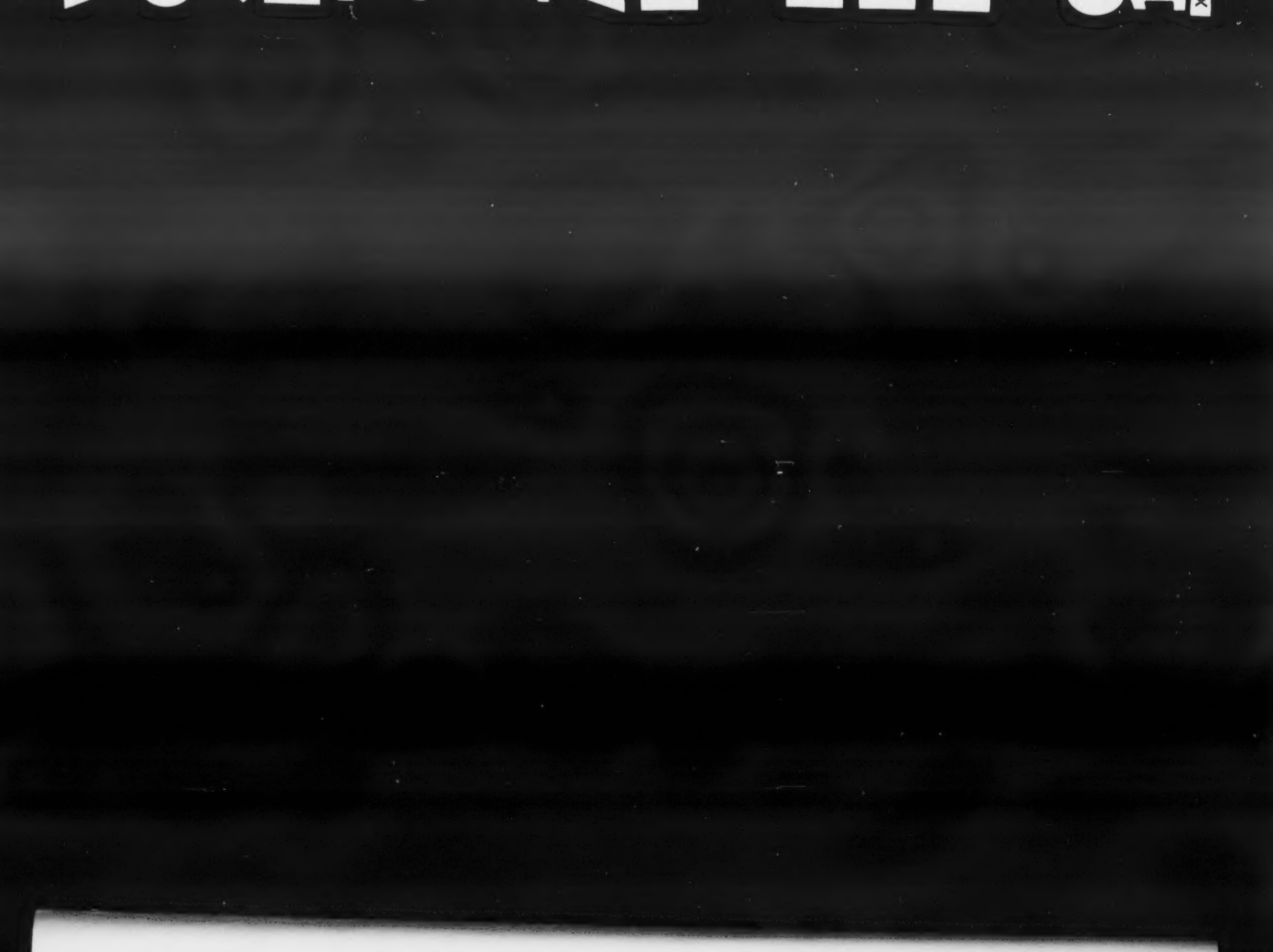
For sale by the Superintendent of Documents, U.S. Government Printing Office, Washington 25, D.C. Price 70 cents (single copy)
Subscription price: $4.00 a year; $0.75 additional for foreign mailing.
UNITED STATES GOVERNMENT PRINTING OFFICE, WASHINGTON : 1961